UNIVERSITÄT
DUISBURG
ESSEN

Offen im Denken

1,1‘-Binaphthyl based catenanes for asymmetric organocatalysis

Dissertation

zur Erlangung des akademischen Grades eines

Doktors der Naturwissenschaften

-Dr. rer. nat. -

Dennis Jansen

geboren in Oberhausen, Deutschland

Fakultät für Chemie

Universität Duisburg-Essen

2021

Declaration of authorship
I declare that I completed this work on my own and did not use any other source than stated.

_____

Dennis Jansen, June 2021

DOI: 10.17185/duepublico/74773
URN: urn:nbn:de:hbz:465-20230731-101825-8

The work presented in this thesis was accomplished in a period between October 2017 and April 2021 under the supervision of Prof. Dr. Jochen Niemeyer at the Faculty of Chemistry at the University of Duisburg-Essen.

First Reviewer: Prof. Dr. Jochen Niemeyer

Second Reviewer: Prof. Dr. Stephen Goldup

Chair: Prof. Dr. Matthias Epple

Date of oral examination: 23.08.2021

A part of this work has already been published and presented:

D. Jansen, J. Gramüller, F. Niemeyer, T. Schaller, M. C. Letzel, S. Grimme, H. Zhu, R. M. Gschwind J. Niemeyer, *Chem. Sci.* **2020**, *11*, 4381-4390.

Further publications:

C. Gerke, M.F. Ebbesen, D. Jansen, S. Boden, T. Freichel, L. Hartmann, *Biomacromolecules* **2017**, *18*, 787-796.

D. Jansen, M. Kohlhaas, J. Niemeyer, *Nachrichten aus der Chemie* **2018**, *66*, 15-18.

S. Thölke, H. Zhu, D. Jansen, F. Octa-Smolin, M. Thiele, K. Kaupmees, I. Leito, S. Grimme, J. Niemeyer, *Eur. J. Org. Chem.* **2019**, *55*, 5190-5195.

N. Pairault, H. Zhu, D. Jansen, A. Huber, C. G. Daniliuc, S. Grimme, J. Niemeyer*, *Angew. Chem. Int. Ed.* **2020**, *59*, 5102-5107.

Poster presentations:

09/2019 *Asymmetric organocatalysis with chiral [2]catenanes*, 3rd CRC1093 International Symposium, University of Duisburg-Essen.

02/2019 *Asymmetric organocatalysis with chiral [2]catenanes*, SupraChem 2019, Würzburg.

03/2018 *Asymmetric organocatalysis with chiral [2]catenanes*, 9th MS_CEC Symposium, Münster

Table of contents

1. Introduction

1.1 Mechanically interlocked molecules

In the early 20th century Linus Pauling defined the different forces which hold atoms or groups of atoms together. He differentiated between electrostatic, covalent and metallic bonds.[1] In addition to that he stated that "we shall say that there is a chemical bond between two atoms or groups of atoms in case that the forces acting between them are such as to lead to the formation of an aggregate with sufficient stability to make it convenient for the chemist to consider it as an independent molecular species."[2] Even though supramolecular interactions were not explicitly meant by this, in many cases aggregates of molecules that are held together by supramolecular interactions fulfil these criteria and are considered as an independent chemical species today.

About half a century from this, the idea of aggregates through intermolecular interaction found its application in the pioneering works of the Nobel laureates *Jean-Marie Lehn*, *Donald Cram* and *Charles Pederson*. With their crown ethers[3], carcerand complexes[4] and cryptands[5] which can selectively bind molecules or atoms, supramolecular chemistry was established as a new research field. Even though this type of lock and key principle was already known for biological systems,[6] it was the first time that non-biological molecules were used to selectively bind guests by non-covalent, intermolecular interactions (***Figure 1***).

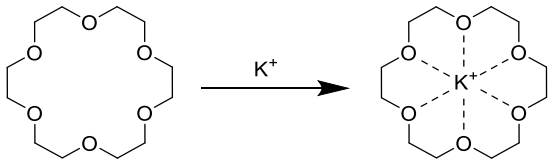

Figure 1: 18-crown-6 as an example for the selective binding of potassium ions by formation of an synthetic host-guest system.[3]

One step further, association of molecules can not only be achieved by intermolecular attractive forces between the subcomponents, but also by interlocking them. This type of bond, which also does not rely on covalent bonds, is called mechanical bond[7] and its formation is closely related to supramolecular chemistry. The most prominent molecules featuring this mechanical bond are catenanes and rotaxanes (***Figure 2***).

[1] J. F. Stoddart, *Angew. Chem., Int. Ed.* **2017**, *56*, 11094–11125.
[2] *The Nature of the Chemical Bond and the Structure of Molecules and Crystals: An Introduction to Modern Structural Chemistry*, L. Pauling, Cornell University Press, New York, **1939**.
[3] C. J. Pedersen, *J. Am. Chem. Soc.* **1967**, *89*, 7017–7036.
[4] D. J. Cram, S. Karbach, Y. H. Kim, L. Baczynskyj, G. W. Kallemeyn, *J. Am. Chem. Soc.* **1985**, *107*, 2575–2576.
[5] J.-P. Behr, C. J. Burrows, R. Heng, J.-M. Lehn, *Tetrahedron Lett.* **1985**, *26*, 215–218.
[6] E. Fischer, *Ber. Dtsch. Chem. Ges.* **1894**, *27*, 2985–2993.
[7] a) *The Nature of the Mechanical Bond: From Molecules to Machines*, C. J. Bruns, J. F. Stoddart **2017**, John Wiley & Sons,G. Barin, R. S. Forgan, J. F. Stoddart, *Proc. Math. Phys. Eng. Sci.* **2012**, *468*, 2849–2880.

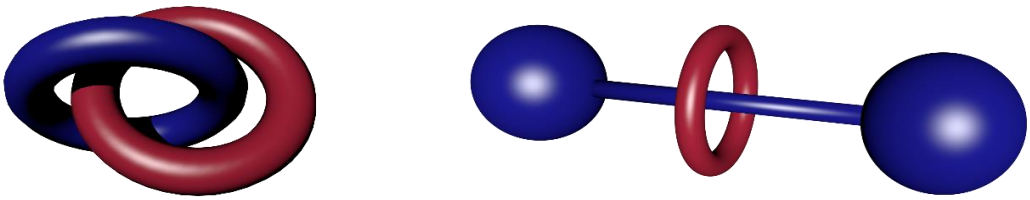

Figure 2: Schematic representation of the most prominent types of mechanically interlocked molecules, a [2]catenane (left) and a [2]rotaxane (right).

To condense the wide research field of mechanically interlocked molecules and its development,[8] it can be separated into six categories (***Figure 3***).[9]

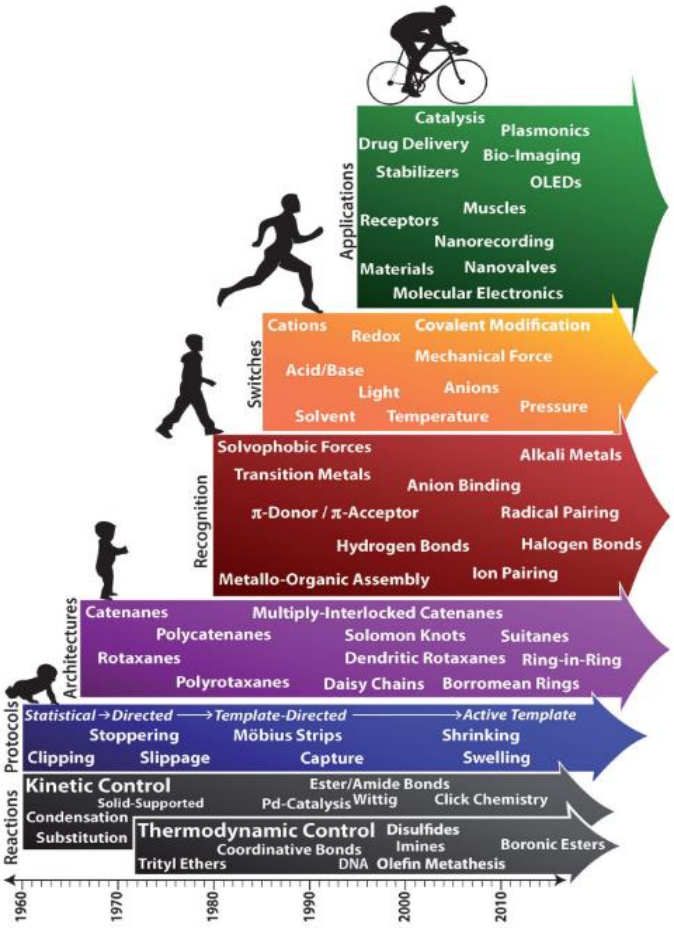

Figure 3: Overview of the development of the research field of mechanically interlocked molecules.[10]

Even though the probability of the existence of catenanes was most likely already discussed in the early 20th century,[11] it was not earlier than 1960 when the field of mechanically interlocked molecules was

[8] D. Sluysmans, J. F. Stoddart, *Trends Chem.* **2019**, *1*, 185–197.
[9] J. F. Stoddart, *Angew. Chem. Int. Ed.* **2014**, *53*, 11102–11104.
[10] Figure taken from reference 9. Reused with permission from John Wiley and Sons (license number: 5077160989759).
[11] H. L. Frisch, E. Wasserman, *J. Am. Chem. Soc.* **1961**, *83*, 3789–3795.

established with the first catenane synthesis.[12] From this on, not only more and more reactions were employed in the synthesis of MIMs (***Figure 3***, black arrow), but also new synthetic approaches were established (***Figure 3***, blue arrow). Most notably templated MIM synthesis (see chapter 4.1) starting from the 1980s gave this research field a tremendous boost also opening the way for other architectures such as molecular knots,[13] Borromean rings,[14] suitanes,[15] polycatenanes and polyrotaxanes,[16] which, however, are often based on catenanes and rotaxanes (***Figure 3***, purple arrow). Strongly connected with the upcoming techniques of templated synthesis is the use of those MIMs for recognition. Here, often the driving force for the template is later exploited to bind a suitable guest inside of the MIM (***Figure 3***, red arrow).[17] Another topic inside of the broad MIM research field is about molecular switches which have been extensively studied starting from the mid of the 1980s (***Figure 3***, orange arrow).[18] Those molecular switches represent one subcategory of molecular machines.[19] In 2016 *Jean-Pierre Sauvage*, *J. Fraser Stoddart* and *Ben L. Feringa* were awarded with the Nobel prize for their work on the design and synthesis of molecular machines,[20] a topic which is closely related to the field of mechanically interlocked molecules. The latest category, application of MIMs (***Figure 3***, green arrow), arose from the easier availability of MIMs through the ever increasing synthesis techniques in the last decades.[21] This opened the way to apply MIMs in many sophisticated fields such as drug delivery systems, molecular electronic and catalysis (see chapter 1.4).

1.1.1 Rotaxanes

Rotaxanes are the most common interlocked molecules. They consist of at least one linear section, a thread, onto which at least one macrocycle is threaded. Dissociation of the macrocycle is prevented by introducing stoppers at both ends of the thread, which are big enough to be unpassable for the macrocycle.[22]

The first rotaxane was reported in 1967 by *Harrison* et al.[23] This rotaxane consists of an acyloin macrocycle on a C10-thread which was stoppered by triphenylmethyl stoppers at each end. The biggest drawback in the early era of rotaxanes and catenanes was the low yield in the synthesis of the interlocked molecules. Chemists relied on a statistical formation or covalent-directed synthesis resulting in poor overall yields. In the 1980's *Sauvage* and coworkers established the template synthesis of catenanes[24] using a metal ion to

[12] E. Wasserman, *J. Am. Chem. Soc.* **1960**, *82*, 4433–4434.
[13] S. D. P. Fielden, D. A. Leigh, S. L. Woltering, *Angew. Chem. Int. Ed.* **2017**, *56*, 11166–11194.
[14] P. R. Ashton, O. A. Matthews, S. Menzer, F. M. Raymo, N. Spencer, J. F. Stoddart, D. J. Williams, *Liebigs Ann. Chem.* **1997**, *1997*, 2485–2494.
[15] A. R. Williams, B. H. Northrop, T. Chang, J. F. Stoddart, A. J. P. White, D. J. Williams, *Angew. Chem.* **2006**, *118*, 6817–6821.
[16] S. Mena-Hernando, E. M. Pérez, *Chem. Soc. Rev.* **2019**, *48*, 5016–5032.
[17] a) K. M. Bąk, K. Porfyrakis, J. J. Davis, P. D. Beer, *Mater. Chem. Front.* **2020**, *4*, 1052–1073,M. J. Chmielewski, J. J. Davis, P. D. Beer, *Org. Biomol. Chem.* **2009**, *7*, 415–424,A. Docker, P. D. Beer **2021**, 83–120,H. M. Tay, P. Beer, *Org. Biomol. Chem.* **2021**.
[18] R. Klajn, J. F. Stoddart, B. A. Grzybowski, *Chem. Soc. Rev.* **2010**, *39*, 2203–2237.
[19] J. Berná, D. A. Leigh, M. Lubomska, S. M. Mendoza, E. M. Pérez, P. Rudolf, G. Teobaldi, F. Zerbetto, *Nat. Mater* **2005**, *4*, 704–710.
[20] a) J. F. Stoddart, *Angew. Chem., Int. Ed.* **2017**, *56*, 11094–11125,B. L. Feringa, *Angew. Chem. Int. Ed.* **2017**, *56*, 11060–11078,J.-P. Sauvage, *Angew. Chem. Int. Ed.* **2017**, *56*, 11080–11093.
[21] a) N. H. Evans, *Chem. Eur. J.* **2018**, *24*, 3101–3112,J. E. M. Lewis, M. Galli, S. M. Goldup, *Chem. Commun.* **2016**, *53*, 298–312,S. F. M. van Dongen, S. Cantekin, J. A. A. W. Elemans, A. E. Rowan, R. J. M. Nolte, *Chem. Soc. Rev.* **2014**, *43*, 99–122.
[22] A. Yerin, E. S. Wilks, G. P. Moss, A. Harada, *Pure Appl. Chem.* **2008**, *80*, 2041–2068.
[23] I. T. Harrison, S. Harrison, *J. Am. Chem. Soc.* **1967**, *89*, 5723–5724.
[24] C. Dietrich-Buchecker, J. Sauvage, J. Kintzinger, *Tetrahedron Lett.* **1983**, *24*, 5095–5098.

prearrange the subcomponents of the MIM (for a detailed description of these works see chapter 4.1). About 10 years later the same concept was also applied in the synthesis of rotaxanes.[25] The resulting increase in yield and the resulting availability of MIMs changed them from a mere curiosity to a research field with growing interest. In the case of rotaxanes this has led to a plethora of application such as molecular motors[26], artificial molecular rotors,[27] shuttles and molecular muscles,[28] drug delivery systems,[18] chemical sensors[29] and catalysts.[30] In each case the application of the rotaxane arises from its unique properties created by the mechanical bond.

One specific property of rotaxanes arises from the circumstance that a cavity can be created in-between macrocycle and thread, which can be exploited to enhance the binding affinity, chemo- or stereoselectivity of guest-binding when compared to the non-interlocked counterparts.[31] Another central feature of a rotaxane, that makes it an interesting candidate of the aforementioned applications, is the possibility of a large-amplitude motion of the interlocked parts without separation of the individual parts. The relative positioning of the subcomponents (i.e. the co-conformation of the MIM) can even be controlled by carefully choosing the functional groups of the macrocycle and the thread. This way, different resting stations for the macrocycle can be created and the thermodynamically preferred station can be switched by different external stimuli. Building up on this, the ring can also be "wrapped around" a functional moiety of the thread and thus act as an inhibitor, blocking the functional group of the thread. If another resting station for the macrocycle is available, switching of the macrocycles position can be possible thus exposing the functional group and "activating" the thread. One example of a rotaxane where the macrocycle can be switched by external stimuli was shown by *Sauvage* in 1994.

[25] C. Wu, P. R. Lecavalier, Y. X. Shen, H. W. Gibson, *Chem. Mater.* **1991**, *3*, 569–572.
[26] C. A. Schalley, K. Beizai, F. Vögtle, *Acc. Chem. Res.* **2001**, *34*, 465–476.
[27] G. S. Kottas, L. I. Clarke, D. Horinek, J. Michl, *Chem. Rev.* **2005**, *105*, 1281–1376.
[28] J. P. Collin, C. Dietrich-Buchecker, P. Gaviña, M. C. Jimenez-Molero, J. P. Sauvage, *Acc. Chem. Res.* **2001**, *34*, 477–487.
[29] a) N. H. Evans, C. J. Serpell, P. D. Beer, *Chem. Commun.* **2011**, 8775–8777,Q. Li, Y. Wu, Y. Liu, L. Shangguan, B. Shi, H. Zhu, *Org. Lett.* **2020**, 6662–6666,M. J. Langton, P. D. Beer, *Acc. Chem. Res.* **2014**, *47*, 1935–1949.
[30] a) C. Kwamen, J. Niemeyer, *Chem. Eur. J.* **2021**, 175–186,N. Pairault, J. Niemeyer, *Synlett* **2018**, *29*, 689–698,A. Martinez-Cuezva, A. Saura-Sanmartin, M. Alajarin, J. Berna, *ACS Catal.* **2020**, *10*, 7719–7733.
[31] a) N. L. Kilah, M. D. Wise, C. J. Serpell, A. L. Thompson, N. G. White, K. E. Christensen, P. D. Beer, *J. Am. Chem. Soc.* **2010**, *132*, 11893–11895,J. Y. C. Lim, I. Marques, V. Félix, P. D. Beer, *Angew. Chem., Int. Ed.* **2018**, *57*, 584–588,G. T. Spence, P. D. Beer, *Acc. Chem. Res.* **2013**, *46*, 571–586.

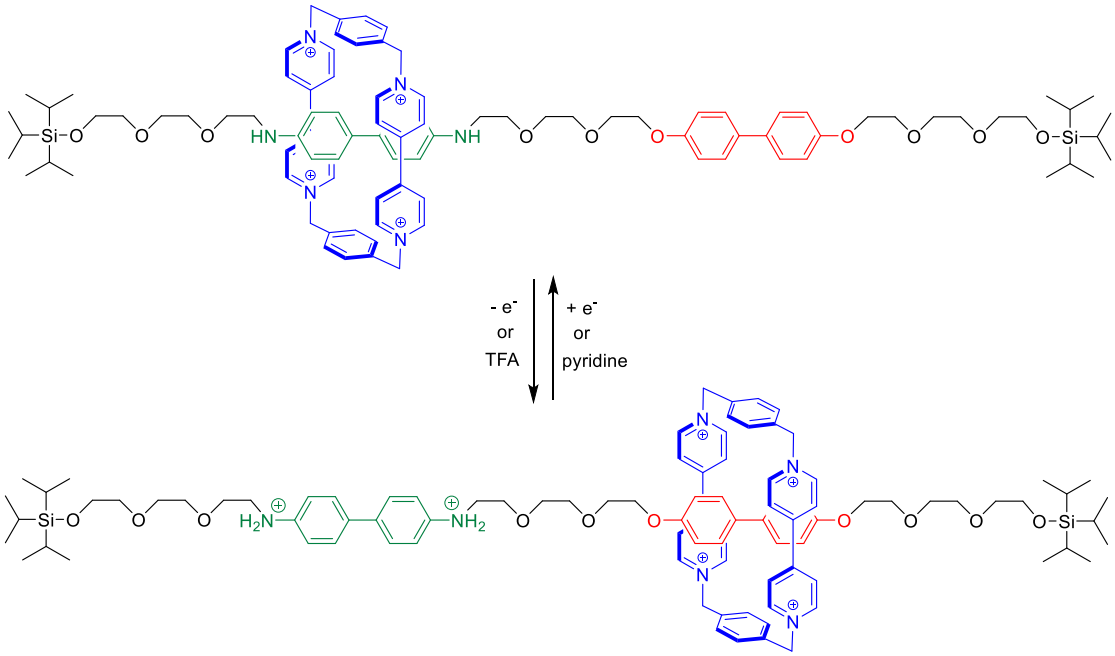

Figure 4: Example of a rotaxane which can be switched chemically and electrochemically.

The rotaxane consists of an ethylene glycol based axle which contains a benzidine based (***Figure 4***, green) and biphenol based (***Figure 4***, red) π-electron donor station and a π-electron acceptor macrocycle containing two bipyridinium moieties. At room temperature the macrocycle moves along the axle fast, however, at lower temperatures two co-conformers, where the macrocycle rests either at the benzidine or at the biphenol station are discernible in ^{1}H-NMR. In this state 84% of the overall molecules consist of the rotaxane where the macrocycle rests at the benzidine station while only 16% consists of the rotaxane where the biphenol is occupied by the macrocycle. Upon treating the rotaxane with trifluoroacetic acid or by oxidation, a cationic benzidine moiety is created which induces the movement of the macrocycle to the biphenol station by electrostatic repulsion. This state can be reversed by either reduction or neutralisation of the acid by pyridine, thus yielding the original state where the benzidine station is occupied by the macrocycle.

1.1.2 Catenanes

Another class of mechanically interlocked molecules are catenanes. They consist of at least two macrocycles which are intertwined in a fashion, that does not allow dissociation of one macrocycle from another without breaking a covalent bond. If the catenane consists of identical macrocycles it is called a homocatenane (or homocircuit catenane) while a catenane consisting of different macrocycles is called a heterocatenane (or heterocircuit catenane). The number of interlocked macrocycles in a catenane is given in square brackets, so a catenane with two macrocycles is called [2]catenane, a catenane with three macrocycles [3]catenane etc. (***Figure 5***)

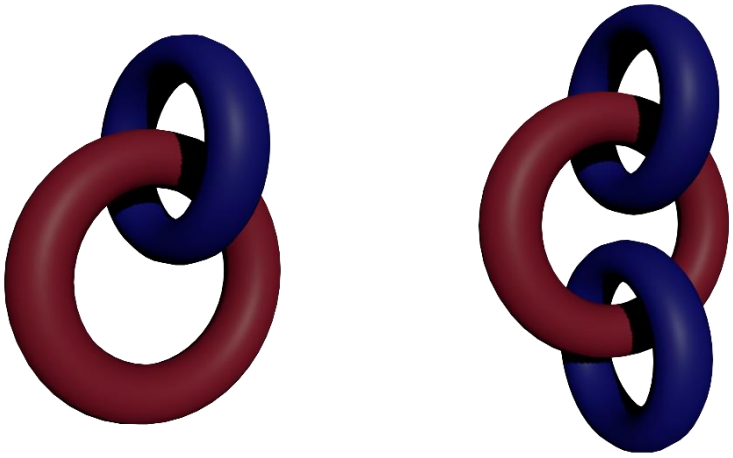

Figure 5: Schematic representation of a hetero-[2]catenane and a hetero-[3]catenane.

The synthesis of catenanes is usually realised by a ring closing reaction, e.g. ring closing metathesis[32], imine-bond formation[33] or Copper(I)-catalysed Azide-Alkyne Cycloaddition (CuAAC).[34] The catenane formation can be realised by a single ring closing reaction, called monocyclisation, or by a twofold ring closing reaction, called double-cyclisation.

The first catenane was reported by *Wassermann* in 1960 using statistical methods.[12] Just like in the case of the statistical approach for rotaxanes the yield was exceptionally low (> 1%). Nowadays the most common strategy for synthesis of catenanes are templated preorganization of the precursors prior to ring closing (see chapter 4.1.).

When it comes to the application of catenanes, three different ways of exploiting its interlocked structure can be described. Firstly, functional groups which are present in different macrocycles can be held in close proximity. Through the mechanical link, dissociation of these functionalities can be prevented thus increasing the local molarity of the functional groups. Certainly, this can also easily be achieved by just integrating the functionalities into one, non-interlocked molecule. However, the advantage of using a catenane for this is the co-conformational freedom of the subcomponents, which easily allows the functionalities to adaptively adopt different co-conformations that are energetically similar, e.g. for accommodation of a guest molecule or substrate in catalysis. This point is especially interesting for such functional groups that have only a weak interaction between each other. One example of this was shown by *Niemeyer* et al. in 2017 where they used a homocatenane consisting of two phosphoric acid groups. The catenation allowed for asymmetric catalysis via a dimeric phosphoric acid pathway leading to higher stereoselectivities compared to non-interlocked catalysts (more detailed description in chapter 3.1).[35]

A second way to make use of the specific three-dimensional structure of a catenane is used in host-guest chemistry. Upon catenation, a cavity is created in-between the two macrocycles, that can be filled by an

[32] D. Quaglio, G. Zappia, E. de Paolis, S. Balducci, B. Botta, F. Ghirga, *Org. Chem. Front.* **2018**, *5*, 3022–3055.
[33] X. Han, G. Liu, S. H. Liu, J. Yin, *Org. Biomol. Chem.* **2016**, *14*, 10331–10351.
[34] K. D. Hänni, D. A. Leigh, *Chem. Soc. Rev.* **2010**, *39*, 1240–1251.
[35] R. Mitra, H. Zhu, S. Grimme, J. Niemeyer, *Angew. Chem. Int. Ed.* **2017**, *56*, 11456–11459.

appropriate guest. In some cases, the binding constant and/or the kinetic stability of a complex is higher when using catenanes in contrast to using the non-interlocked counterpart.[36]

Lastly, the mechanical bond of a catenane can be exploited in a similar fashion as in a rotaxane.[37] While the macrocycle in a rotaxane is able to move along or can rotate around the thread, these types of movements can also be found in a catenane. The controlled movement of one macrocycle along the other is a promising feature, allowing applications as molecular machines. A sophistical molecular motor based on a catenane was shown by *Leigh* and coworkers in 2017 (**Figure 6**).[38]

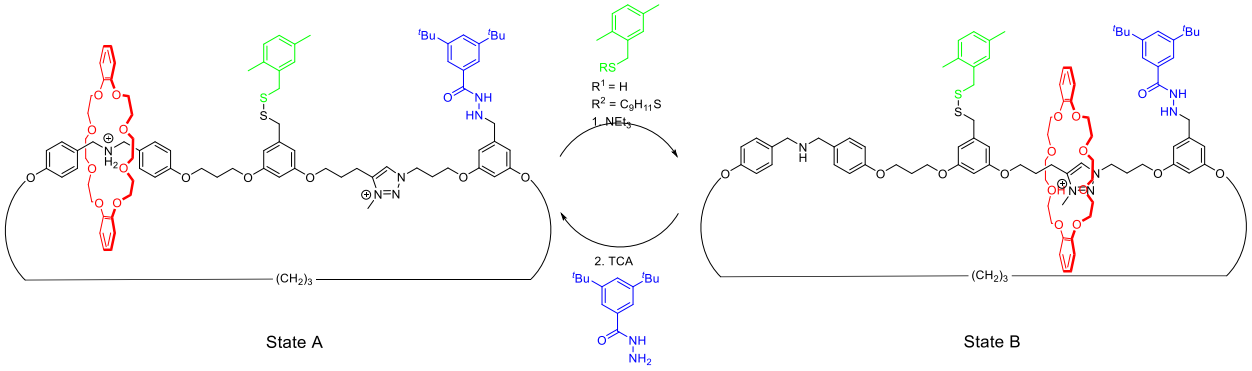

Figure 6*:* Application of a catenane as a molecular machine.

Similar to the rotaxane described in chapter 1.1.1, this catenane also possesses two binding sites based on a secondary amine/ammonium and a methylated triazolium, also showing pH-dependent change in affinity of the crown ether macrocycle. In addition, two stoppers are introduced (green and blue) which do not allow movement of the macrocycle beyond them. However, these stoppers are base-labile (green) and acid-labile (blue). Starting from the catenane in state A (see **Figure 6**), addition of base (triethylamine) not only removes the green stopper, but also induces deprotonation of the ammonium groups and thus translocation of the macrocycle from the secondary amine towards the triazolium site. Since the blue stopper is still present this movement can only proceed in one direction (i.e. clockwise in Figure 6). Addition of trichloroacetic acid (TCA) creates an acidic environment, where the now stable disulfide bond of the green stopper is formed again, while the blue stopper is cleaved off and the secondary amine is protonated. This induces movement of the macrocycle from the triazolium site towards the protonated secondary amine in the same direction. Thus, a 360° movement of the crown ether along the other macrocycle is finished within one pulse of fuel (base and acid) addition.

In addition to the application as a molecular motors as shown above, catenanes have also been used as molecular switches and chemical sensors.[39] Another interesting application for catenanes that has not attracted as much attention as the other applications yet is catalysis. In 2008 *Hagiwara* and coworkers

[36] A. M. Albrecht-Gary, Z. Saad, C. O. Dietrich-Buchecker, J. P. Sauvage, *J. Am. Chem. Soc.* **1985**, *107*, 3205–3209.
[37] a) D. Cao, M. Amelia, L. M. Klivansky, G. Koshkakaryan, S. I. Khan, M. Semeraro, S. Silvi, M. Venturi, A. Credi, Y. Liu, *J. Am. Chem. Soc.* **2010**, *132*, 1110–1122,V. Zanichelli, L. Dallacasagrande, A. Arduini, A. Secchi, G. Ragazzon, S. Silvi, A. Credi, *Molecules* **2018**, *23*.
[38] S. Erbas-Cakmak, S. D. P. Fielden, U. Karaca, D. A. Leigh, C. T. McTernan, D. J. Tetlow, M. R. Wilson, *Science* **2017**, *358*, 340–343.
[39] a) Collier, Mattersteig, Wong, Luo, Beverly, Sampaio, Raymo, Stoddart, Heath, *Science* **2000**, *289*, 1172–1175,G. Gil-Ramírez, D. A. Leigh, A. J. Stephens, *Angew. Chem. Int. Ed.* **2015**, *54*, 6110–6150,Z. Zhu, A. C. Fahrenbach, H. Li, J. C. Barnes, Z. Liu, S. M. Dyar, H. Zhang, J. Lei, R. Carmieli, A. A. Sarjeant et al., *J. Am. Chem. Soc.* **2012**, *134*, 11709–11720.

reported a catenane which contains phosphine groups on each of the macrocycles and which was applied as a ligand in the palladium catalysed *Suzuki* coupling of bromobenzene and phenylboronic acid.[40]

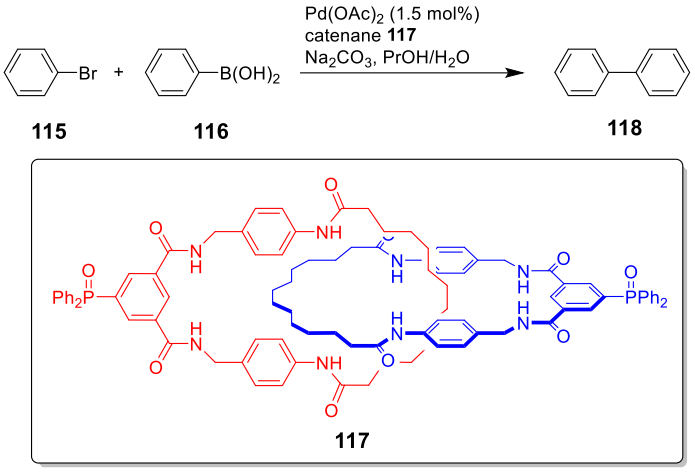

Figure 7: *Suzuki* coupling using a bisphosphine catenane and $Pd(OAc)_2$ as palladium source.

It has to be noted, however, that the group did not investigate on the formation of a possible catenane-palladium species and did not report any comparative reactions without the catenane. Thus the influence of the catenane in this reaction remains unknown.

Another example of a catenane ligand was published recently by *Au-Yeung*.[41]

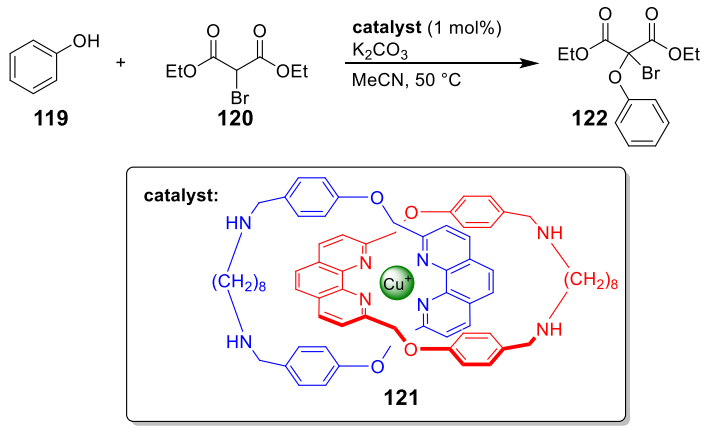

Figure 8: Cross dehydrogenative C-O coupling catalysed by Cu(I) ligated by a catenane.

Catenane **121** consists of phenanthroline derived macrocycles which form Cu(I) complexes to catalyse the cross dehydrogenative C-O coupling of phenol and bromodicarbonyl **120**. In contrast to non-interlocked phenanthroline ligands, the reaction with the catenated ligand afforded a slightly higher yield (92% for the catenated ligand and 71% for non-interlocked ligands), which was explained by a stable, coordinatively saturated complex which only transiently reveals the active site during substrate transformation.

The bisphosphoric acid catenane of *Niemeyer* remains the only example of a catenane as an asymmetric organocatalyst (see chapter 3.2 for a detailed description).[35]

[40] M. Yamazaki, T. Hagiwara, M. Sekiguchi, T. Sawaguchi, S. Yano, *Synth. Commun.* **2008**, *38*, 553–558.
[41] L. Zhu, J. Li, J. Yang, H. Y. Au-Yeung, *Chem. Sci.* **2020**, *11*, 13008–13014.

1.2 Chirality in MIMs

Chirality is a type of isomerism where two molecules consist of the same atoms, which are connected the same way, however, the molecules cannot be aligned, but are mirror images of one another. These chiral molecules, which resemble our left and right hand, are called enantiomers. Enantiomers have the same physical properties and behave the same chemically in an achiral environment, but can be differentiated in a chiral environment. This chiral environment is the basic principle of asymmetric catalysis (see chapter 1.3).

The part that creates this difference between the enantiomers is called stereogenic element. There are three types of stereogenic elements that are most commonly found in chiral molecules (***Figure 9***).

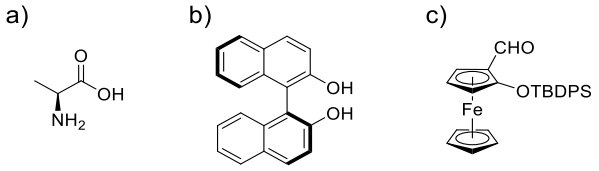

Figure 9*:* Examples for covalent chiral molecules: a) Point chiral (*S*)-alanine, b) axially chiral (*S*)-BINOL and c) planar chiral silyl-protected (*p*-*S*)-2-hydroxyferrocene-aldimine.[42]

Chirality that results from these elements are called point chirality, axial chirality and planar chirality and they belong to a category which is called covalent chirality.

These types of covalent chirality can also be implemented in mechanically interlocked molecules. Especially point chirality and axial chirality is often used to enable the MIM to be applied in enantioselective sensing or asymmetric catalysis.[43] In addition to that, there are also other, non-covalent types of chirality which can be the result of the mechanical bond of a MIM which are called chirotopic mechanical stereogenic elements. A selection of these elements will be shortly presented in this subchapter. For a much more detailed view on chirality as a result of the mechanical bond the review by *Goldup* et al.[44] is recommended. Naming of the chiral elements is based on this review.[45]

Mechanical planar chiral stereogenic units are found in rotaxanes, where a macrocycle which does not possess rotational symmetry (i.e. C_{1h} symmetry) is threaded onto a non-centrosymmetric axle. (***Figure 10***).

[42] J. Niemeyer, G. Kehr, R. Fröhlich, G. Erker, *Dalton Trans.* **2009**, 3716–3730.
[43] A. Martinez-Cuezva, A. Saura-Sanmartin, M. Alajarin, J. Berna, *ACS Catal.* **2020**, *10*, 7719–7733.
[44] E. M. G. Jamieson, F. Modicom, S. M. Goldup, *Chem. Soc. Rev.* **2018**, *47*, 5266–5311.
[45] Other authors may use different words to describe the same chirality.

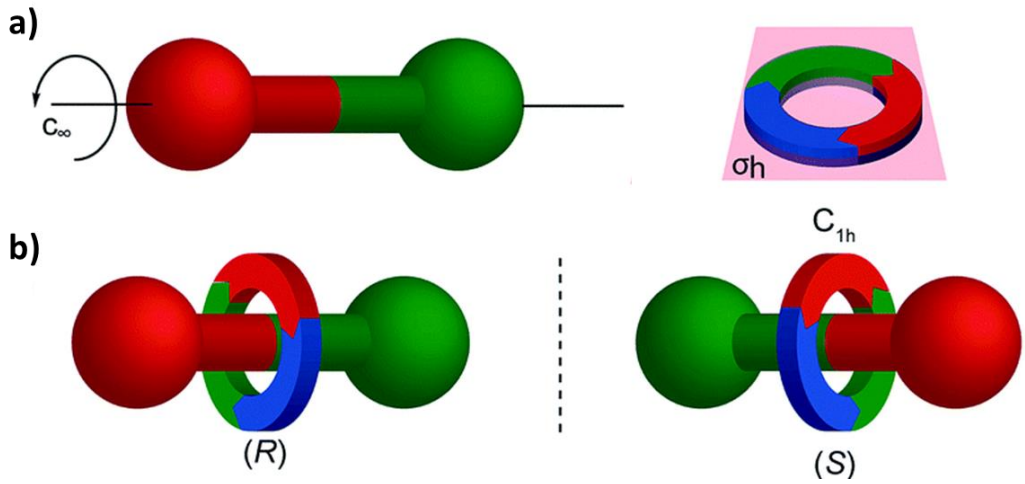

Figure 10: Schematic representation of a) Non-centrosymmetric axle and macrocycle with C_{1h} symmetry and b) the resulting enantiomers of the mechanically planar [2]rotaxane.[46]

Several groups have published the synthesis of such mechanical planar chiral rotaxanes. Enantiomerically pure compounds are usually obtained by separation of the enantiomers using chiral liquid chromatography,[47] by kinetic resolution[48] or stereoselective synthesis.[49]

Catenanes can also possess mechanical chirality when they are based on two dissymmetric (also called non-rotational symmetric) (*vide supra*) macrocycles (***Figure 11***).

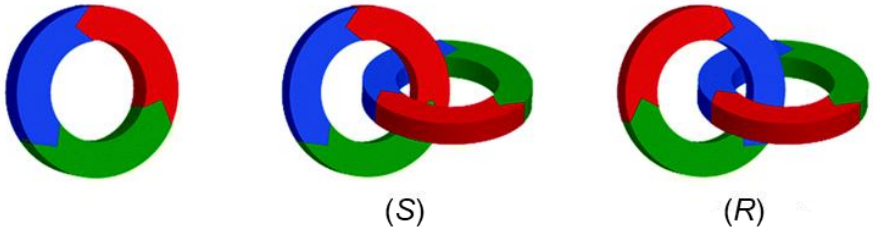

Figure 11: Macrocycle without rotational symmetry and the possible two enantiomeric homo[2]catenanes consisting of this macrocycle.[44]

These chiral catenanes are called topologically chiral catenanes. While the synthesis of such catenanes was already carried out in the early stages of the MIM research field, chemists usually rely on isolation of enantiomerically pure catenanes by chiral liquid chromatography methods.[50] Recently *Goldup* et al. published a very sophisticated approach to improve the separation by using a chiral auxiliary during the catenane synthesis. The resulting diastereomeric catenanes could be separated using standard organic

[46] Reproduced with permission from E. M. G. Jamieson, F. Modicom, S. M. Goldup, *Chem. Soc. Rev. 47*, **2018**, pp. 5266–5311- published by The Royal Society of Chemistry.
[47] R. Jäger, M. Händel, J. Harren, F. Vögtle, K. Rissanen, *Liebigs Ann. Chem.* **1996**, *1996*, 1201–1207.
[48] A. Imayoshi, B. V. Lakshmi, Y. Ueda, T. Yoshimura, A. Matayoshi, T. Furuta, T. Kawabata, *Nat. Commun.* **2021**, *12*, p. 404.
[49] M. A. Jinks, A. de Juan, M. Denis, C. J. Fletcher, M. Galli, E. M. G. Jamieson, F. Modicom, Z. Zhang, S. M. Goldup, *Angew. Chem. Int. Ed.* **2018**, *57*, 14806–14810.
[50] a) Y. Kaida, Y. Okamoto, J.-C. Chambron, D. K. Mitchell, J.-P. Sauvage, *Tetrahedron Lett.* **1993**, *34*, 1019–1022,C. Yamamoto, Y. Okamoto, T. Schmidt, R. Jäger, F. Vögtle, *J. Am. Chem. Soc.* **1997**, *119*, 10547–10548.

chemistry separation techniques. The chiral auxiliary is then cleaved off to yield the enantiomerically pure topologically chiral catenane.[51]

As described in chapter 1, one subcomponent of a MIM can perform a high amplitude motion along the other sub-component (e.g. movement of the macrocycle alone the axle in a rotaxane). If a covalent chiral element is located in the centre of the axle and can block the macrocycles movement over this element two enantiomers are possible, depending on which side the macrocycle is located (***Figure 12***). As this kind of chirality arises from the relative position (i.e. conformations) inside the rotaxane, it is called co-conformational covalent chirality.

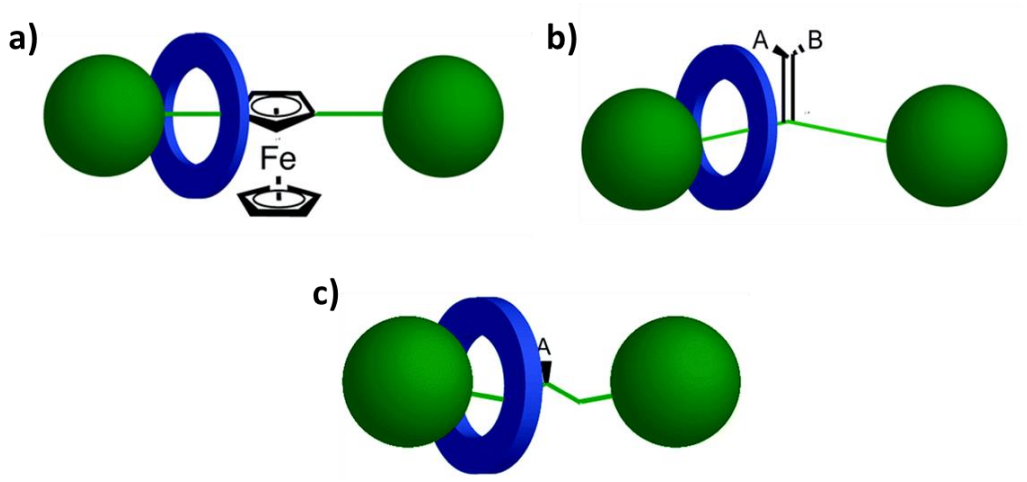

Figure 12: Three schematic examples of co-conformational covalent chirality. a) Co-conformational planar chiral [2]rotaxane, b) Co-conformational axial chiral [2]rotaxane and c) Co-conformational point chiral [2]rotaxane.[44]

[51] M. Denis, J. E. M. Lewis, F. Modicom, S. M. Goldup, *Chem* **2019**, *5*, 1512–1520.

1.3 Asymmetric organocatalysis

Optically pure compounds are of high interest especially for the agricultural and pharmaceutical industry.[52] There are different synthetic pathways towards optically pure compounds: Starting from a non-enantioselective synthesis which produces the desired compound as a racemic mixture, desired enantiomers can be separated, e.g. by co-crystallisation with a chiral additive, by covalent modification with a chiral auxiliary and subsequent separation of the diastereoisomers or by chromatography with a chiral stationary phase.[53] In addition to costs and time which accompany the separation of the enantiomers, half of the synthesized product consists of the undesired enantiomer, which limits the theoretical yield to a maximum of 50%. Thus, a more efficient way to get hands on enantiomerically pure products is of high desire.

A more convenient way towards an optically pure product can be achieved by asymmetric catalysis, often circumventing the need to separate enantiomers afterwards.[54] In enantioselective catalysis a prochiral molecule is converted into a chiral product, where one enantiomer is produced solely or at least in great excess, by using a chiral catalyst. This chiral catalyst creates a difference in energy of the corresponding transition states towards the formation of each enantiomer, thus the kinetically favoured formation of one enantiomer can be achieved.

There are three main subcategories of asymmetric catalysts which can be distinguished.[55]

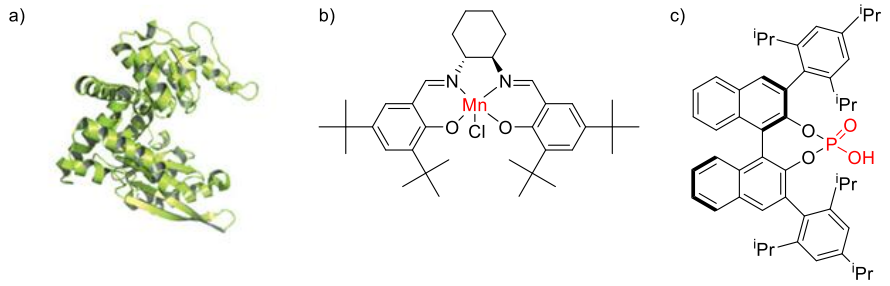

Figure 13: Illustration of representatives of each category of asymmetric catalysts: a) Biomolecule (enzyme)[56] b) metal complex c) organocatalyst.

Firstly, biomolecules like enzymes often catalyse reactions in a stereoselective fashion. The chiral information of the enzyme stems from the amino acids as well as the protein secondary and tertiary structure around the catalytic centre. The second type of enantioselective catalysts are transition metals, which are ligated by chiral ligands. While the catalytic activity mainly comes from the metal, the chiral ligands create an environment in which substrates are bound to the metal in a fashion that allows energetic differentiation of the diastereomeric transition states towards each enantiomer. Another way to undergo asymmetric catalysis has gained a lot of attention since the early 21st century.[55] Asymmetric organocatalysis allows stereoselective transformation of a molecule without the help of a transition metal or an enzyme. Rather, the catalyst consists of a synthetic and in many cases purely organic molecule, which, however, is often inspired by natural bio-catalytic processes.[57] While some systems use immobilised organocatalysts in

[52] B.-F. Sun, *Tetrahedron Lett.* **2015**, *56*, 2133–2140.
[53] V. A. Davankov, *Chromatographia* **1989**, *27*, 475–482.
[54] J. Merad, C. Lalli, G. Bernadat, J. Maury, G. Masson, *Chem. Eur. J.* **2018**, *24*, 3925–3943.
[55] B. List, *Chem. Rev.* **2007**, *107*, 5413–5415.
[56] Reproduced from Y.-P. Xue, C.-H. Cao, Y.-G. Zheng, *Chem. Soc. Rev.* **2018**, *47*, 1516–1561. With permission from The Royal Society of Chemistry.
[57] L. Bernardi, M. Fochi, M. Comes Franchini, A. Ricci, *Org. Biomol. Chem.* **2012**, *10*, 2911–2922.

heterogeneous organocatalysis[58], homogenous organocatalysis where the organocatalyst in the same phase as the substrate remains the predominant application. Thus this chapter will focus on asymmetric homogenous organocatalysis.

One way to classify different types of organocatalysts is the differentiation between Lewis bases, Lewis acids, Brønsted bases and Brønsted acids (***Figure 14***).[59]

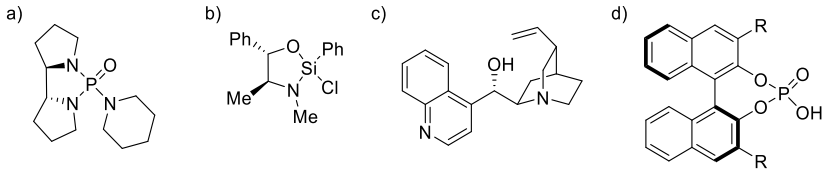

Figure 14 Selected examples of the four different types of organocatalysts: a) Phosphoramide-based Lewis base catalyst b) Chiral silane as Lewis acid catalyst[60] c) Cinchona alkaloid as Brønsted base catalyst d) Chiral phosphoric acid (CPA) as Brønsted acid catalyst

A Lewis base organocatalyst is characterized by its ability to act as an electron pair donor to the substrate or reagent and increase its rate of conversion.[61] Prominent Lewis bases used in organocatalysis are *N*-heterocyclic carbenes[62], various phosphoramides[63] and other nitrogen containing catalysts[64] as well as chalcogens in general.[65]

In Lewis acid catalysis the most obvious Lewis acid is a metal which, together with its ligands, forms a catalytically active complex. Especially transition metals have shown to catalyze a wide range of reactions.[66] In contrast to this, asymmetric Lewis acid organocatalysis is still in its very early stages, with only a few examples compared to the other fields of organocatalysis.[67] Non-metal Lewis acids that were successfully used in asymmetric organocatalysis include chiral silyl-ethers that can transfer a silylium-ion[68] and phosphonium salts.[69]

The other two types, Brønsted bases and acids, rely on deprotonation/protonation of the substrate and formation of an ionic catalyst-substrate adduct. However, it must be noted that the differentiation between Brønsted acids/bases and hydrogen bonding catalysts is not always unambiguous, because usually there is not a strict cutoff but rather a smooth transition between intermolecular interactions such as hydrogen bonding and protonation/deprotonation.[70]

---

[58] a) P. C. Bulman Page, A. Mace, D. Arquier, D. Bethell, B. R. Buckley, D. J. Willock, G. J. Hutchings, *Catal. Sci. Technol.* **2013**, *3*, 2330–2339,P. H. R. Oliveira, B. M. S. Santos, R. A. C. Leão, L. S. M. Miranda, R. A. S. San Gil, R. O. M. A. Souza, F. G. Finelli, *ChemCatChem* **2019**, *11*, 5553–5561,P. Riente, J. Yadav, M. A. Pericàs, *Org. Lett.* **2012**, *14*, 3668–3671,A. Savateev, M. Antonietti, *ACS Catal.* **2018**, *8*, 9790–9808.
[59] J. Seayad, B. List, *Org. Biomol. Chem.* **2005**, *3*, 719–724.
[60] S. Shirakawa, R. Berger, J. L. Leighton, *J. Am. Chem. Soc.* **2005**, *127*, 2858–2859.
[61] S. E. Denmark, G. L. Beutner, *Angew. Chem. Int. Ed.* **2008**, *47*, 1560–1638.
[62] D. Enders, O. Niemeier, A. Henseler, *Chem. Rev.* **2007**, *107*, 5606–5655.
[63] a) S. E. Denmark, X. Su, Y. Nishigaichi, D. M. Coe, K.-T. Wong, S. B. D. Winter, J. Y. Choi, *J. Org. Chem.* **1999**, *64*, 1958–1967,S. E. Denmark, H. M. Chi, *J. Am. Chem. Soc.* **2014**, *136*, 8915–8918,V. Kozma, F. Fülöp, G. Szőllősi, *Adv. Synth. Catal.* **2020**, *362*, 2444–2458.
[64] A. Erkkilä, I. Majander, P. M. Pihko, *Chem. Rev.* **2007**, *107*, 5416–5470,S. Mukherjee, J. W. Yang, S. Hoffmann, B. List, *Chem. Rev.* **2007**, *107*, 5471–5569.
[65] E. M. McGarrigle, E. L. Myers, O. Illa, M. A. Shaw, S. L. Riches, V. K. Aggarwal, *Chem. Rev.* **2007**, *107*, 5841–5883.
[66] J. Wen, F. Wang, X. Zhang, *Chem. Soc. Rev.* **2021**, *50*, 3211–3237.
[67] O. Sereda, S. Tabassum, R. Wilhelm, *Top. Curr. Chem.* **2010**, *291*, 349–393.
[68] a) A. D. Dilman, S. L. Ioffe, *Chem. Rev.* **2003**, *103*, 733–772,T. Gatzenmeier, M. van Gemmeren, Y. Xie, D. Höfler, M. Leutzsch, B. List, *Science* **2016**, *351*, 949–952.
[69] T. Werner, *Adv. Synth. Catal.* **2009**, *351*, 1469–1481.
[70] K. Rothermel, M. Melikian, J. Hioe, J. Greindl, J. Gramüller, M. Žabka, N. Sorgenfrei, T. Hausler, F. Morana, R. M. Gschwind, *Chem. Sci.* **2019**, *114*, p. 1929.

Brønsted bases are mostly nitrogen-bases such as chiral secondary and tertiary amines,[71] especially cinchona alkaloids,[72] ureates[73] and guanidines.[74] Brønsted acid organocatalysis is dominated by carboxylic or phosphoric acids. Especially phosphoric acids combined with axial chiral backbones, called chiral phosphoric acids (CPA), became of high interest since the first example by *Terada* in 2004[75] (***Figure 15***) and one year later by *List*.[76]

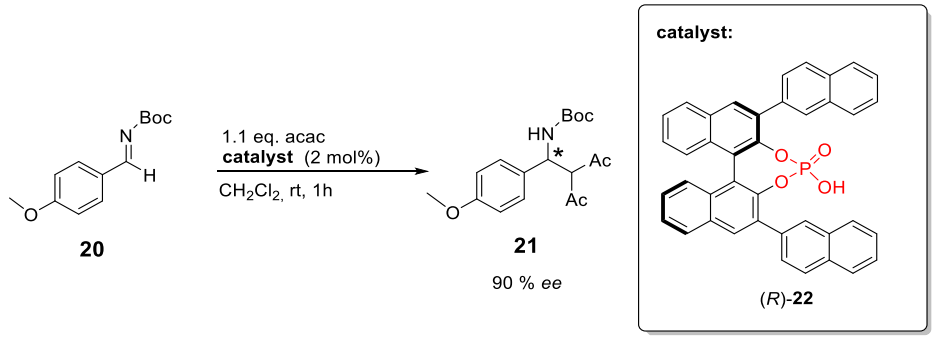

Figure 15: Teradas first example of CPA in Brønsted acid organocatalysis: Direct Mannich reaction of acetylacetone and an imine **20**.

Terada applied catalyst (*R*)-**22** based on a phosphoric acid functionalized 1,1'-binaphthyl (BINOL) backbone. To further increase the stereoinduction of this axially chiral catalyst, bulky substituents were introduced in 3,3'-positions, mostly aryl- or alkyl(aryl)-groups. Using the naphthyl-substituted catalyst (*R*)-**22**, a stereoselectivity of 90% *ee* was observed in the direct Mannich reaction of imine **20** with acetylacetone. In the reaction, the acidic catalyst protonated the imine substrate and forms a phosphate-iminium ion pair. This activates the imine for the nucleophilic attack of acetylacetone and at the same time creates the chiral environment needed for the reaction to proceed with high stereoselectivity.

The CPA in the previous example activated the substrate by formation of an ion pair. In general, the phosphoric acid group is capable of catalysing a reaction via three different activation modes, called mono activation, dual activation and bifunctional activation (***Figure 16***).[77]

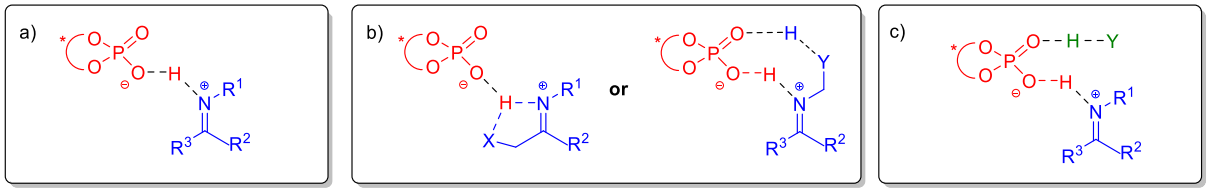

Figure 16: Modes of activation in phosphoric acid catalysis: a) Mono activation b) Dual activation of one molecule with two h-bond acceptors (imine + X) or one h-bond acceptor (imine) and one h-bond donor (HY) c) Bifunctional activation of an electrophile (blue) and nucleophile (green).

When the catalysis proceeds via mono activation the phosphoric acid protonates the substrate to form an ionic aggregate or a hydrogen bonded catalyst-substrate complex, depending on substrate, solvent and catalyst acidity. If the substrate has a functional group in close proximity, it can establish a secondary

[71] C. Palomo, M. Oiarbide, R. López, *Chem. Soc. Rev.* **2009**, *38*, 632–653.
[72] T. Marcelli, H. Hiemstra, *Synthesis* **2010**, *2010*, 1229–1279.
[73] A. Kondoh, S. Ishikawa, M. Terada, *J. Am. Chem. Soc.* **2020**, *142*, 3724–3728.
[74] D. Leow, C.-H. Tan, *Chem. Asian J.* **2009**, *4*, 488–507.
[75] D. Uraguchi, M. Terada, *J. Am. Chem. Soc.* **2004**, *126*, 5356–5357.
[76] S. Hoffmann, A. M. Seayad, B. List, *Angew. Chem. Int. Ed.* **2005**, *44*, 7424–7427.
[77] D. Parmar, E. Sugiono, S. Raja, M. Rueping, *Chem. Rev.* **2014**, *114*, 9047–9153.

interaction with the phosphoric acids which is called dual activation. Depending on the nature of the second functionality it shares the hydrogen bond with the first functional group (in case the second functionality is a second hydrogen bond acceptor) or forms another hydrogen bond with the P=O unit. This shows that the POOH-group can not only act as a hydrogen bond donor or Brønsted acid, but also as a Lewis base with its second oxygen atom. This feature can be used for bifunctional activation by the phosphoric acid in the reaction of a nucleophile with an electrophile. The electrophile is activated via the OH-group similarly as in the mono activation mode, while the nucleophile interacts with the P=O moiety. The reactants are therefore not only activated by their primary interactions with the catalyst, but are also brought into close proximity, leading to the desired reaction.

Another way chiral phosphoric acids (or its phosphates) can be used as catalysts is called asymmetric counterion-directed catalysis (ACDC). In ACDC, induction of stereoselectivity is achieved by ion pairing of a chiral anion provided by the catalyst molecule with a cationic intermediate. In order to distinguish ACDC from mono activation of CPAs, the anionic species in ACDC is not necessarily generated in situ (e.g. by deprotonation) but can be directly applied as the anion.[78] An example of this method was shown by *List* et al. in 2006 (Figure 17).[79]

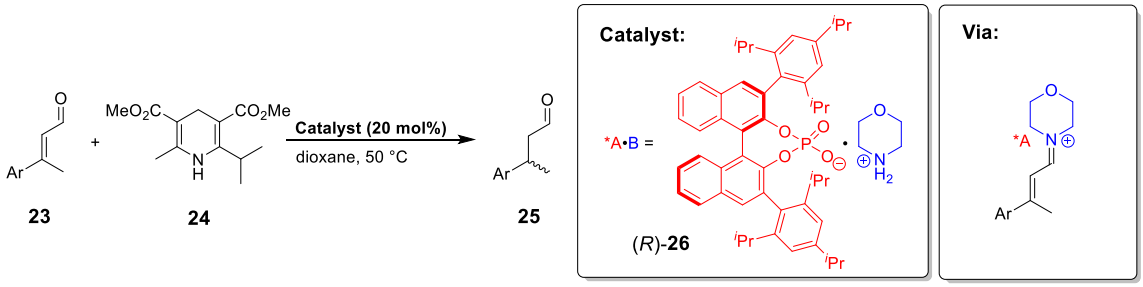

Figure 17: Transfer hydrogenation of α-β-unsaturated aldehydes with Hantzsch ester and a CPA•morpholinium salt catalyst.

In this example α-β-unsaturated aldehydes were transformed into the corresponding saturated derivatives by transfer hydrogenation (see chapter 3.1) with Hantzsch ester **24**. Activation of the aldehyde was achieved by formation of the corresponding iminium species by reaction with morpholine (blue) from the catalyst salt (*R*)-**26**. As typical for ACDC, stereoinduction is reached by ion pairing of the chiral phosphate (red) to the intermediate iminium species. High enantiomeric excesses that were obtained in this reaction (96 - 98% *ee*), underlining that ACDC can be a powerful strategy in asymmetric organocatalysis.

[78] M. Mahlau, B. List, *Angew. Chem. Int. Ed.* **2013**, *52*, 518–533.
[79] S. Mayer, B. List, *Angew. Chem., Int. Ed.* **2006**, *45*, 4193–4195.

1.4 MIMs in asymmetric catalysis

As already mentioned in chapter 1.1 mechanically interlocked molecules have some interesting applications due to their unique properties which are the result of the mechanical bond. One sophisticated application of MIMs is their use in catalysis. In this context the mechanical bond can be exploited in many ways (***Figure 18***), of which some are presented in this chapter.

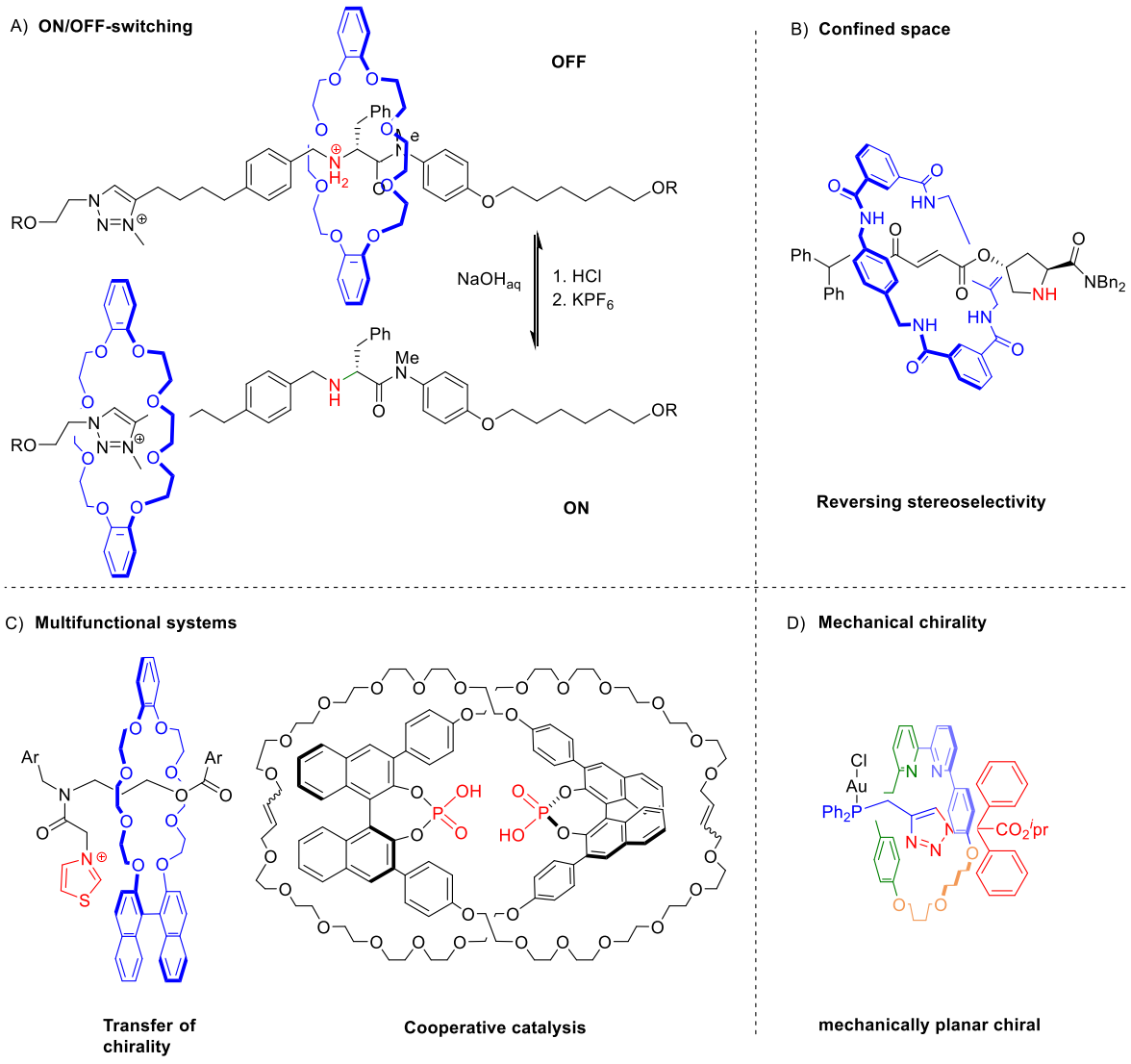

Figure 18: Selected examples of how the mechanical bond can be used in catalysis.

In rotaxanes the macrocycle can be used to be wrapped around a catalytic centre on the axle causing the rotaxane catalyst to be inactive. If another resting station is present on the axle, the macrocycle can be switched by external stimuli, thus exposing the catalytic centre and activating the catalyst. One example of this principle was shown by *Leigh* in 2014.[80]

[80] V. Blanco, D. A. Leigh, V. Marcos, J. A. Morales-Serna, A. L. Nussbaumer, *J. Am. Chem. Soc.* **2014**, *136*, 4905–4908.

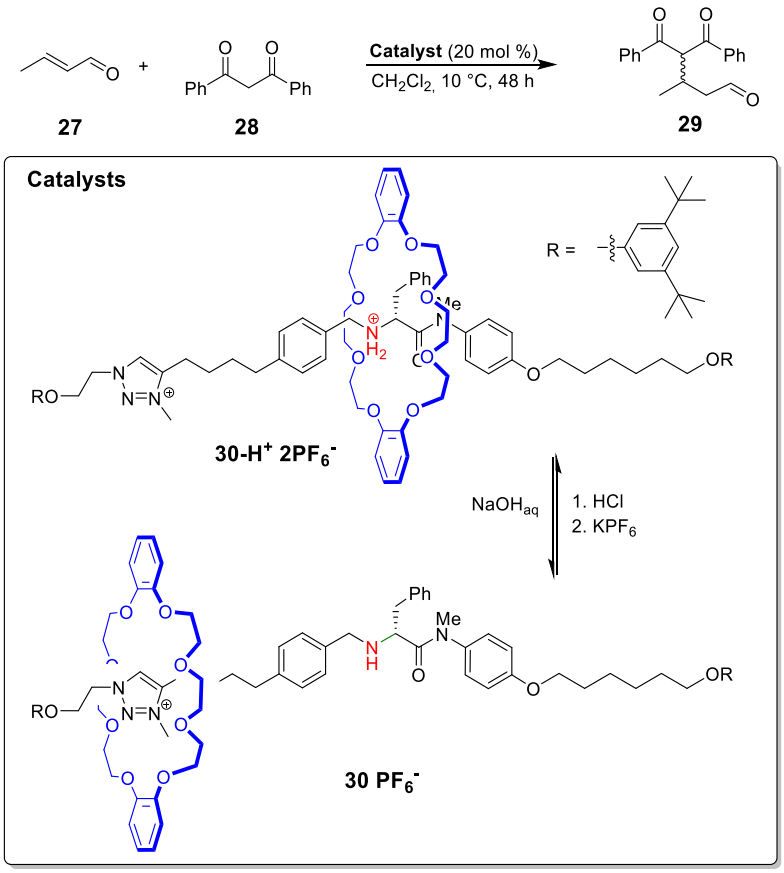

Figure 19: Asymmetric Michael addition catalysed by an acid-base switchable rotaxane.

The asymmetric Michael addition of 1,3-diphenyl-1,3-propanedione **28** to *E*-crotonaldehyde **27** is catalysed by a secondary amine, which is incorporated into the axle of the rotaxane catalyst. The rotaxane used in this example features two resting stations for the crown ether macrocycle, a triazolium station and the secondary ammonium station (highlighted in green). The position of the macrocycle is controlled by addition of acid or base. In the first case the secondary amine is protonated and the macrocycle moves towards this position, because the affinity to the ammonium moiety is higher than to the triazolium. The catalytic activity of the rotaxane is completely supressed in this state, since the macrocycle blocks the catalytic centre. After addition of sodium hydroxide, the ammonium is deprotonated to the secondary amine and the macrocycle moves to the triazolium group, turning on the catalytic activity of the rotaxane by exposing the secondary amine. Notably, the shutdown of the catalytic activity by addition of acid is not possible for the non-interlocked thread. Enantiomeric excesses obtained with this catalyst were similar to those of commercially available cyclic amine organocatalysts (80 % *ee* for **30** PF_6^-).

Recently *Berna* showed that the confined space in a rotaxane can lead to interesting behavior in asymmetric catalysis when compared to the non-interlocked thread.[81]

[81] A. Martinez-Cuezva, M. Marin-Luna, D. A. Alonso, D. Ros-Ñiguez, M. Alajarin, J. Berna, *Org. Lett.* **2019**, *21*, 5192–5196.

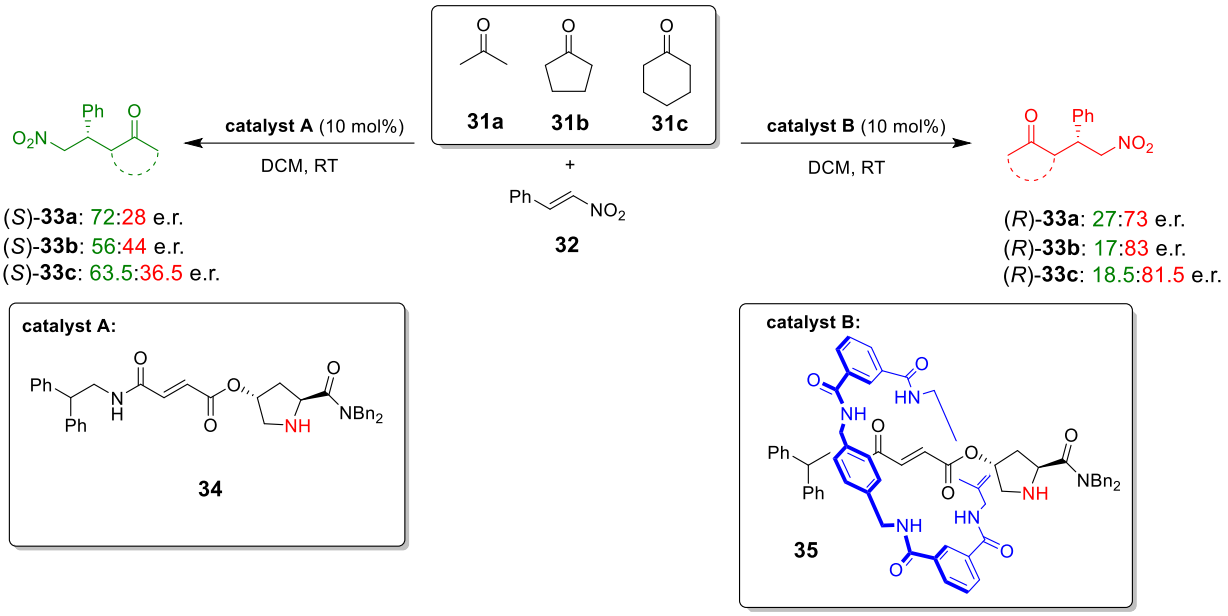

Figure 20: Asymmetric *Michael* reaction catalysed by the sole thread **34** (left) or rotaxane **35** (right).

In this example the *Michael* addition of different ketones to β-nitrostyrene catalysed by a prolinamide derivative was examined. Using rotaxane **35** as a catalyst, an excess of the (*R*)-product was observed in all three cases (46 – 66% *ee*), while an excess of the (*S*)-product was observed when using the sole thread **34** as a catalyst (27 – 44% *ee*). Calculation revealed that the close proximity of the macrocycle to the catalytic centre is the reason for the different stereoselectivity. By establishing a hydrogen bond with the electrophile, the macrocycle promotes the attack of the nucleophile to the *Si* face of the β-nitrostyrene, leading to the (*R*)-product. A

Another application of a rotaxane where the interaction of the two subcomponents is crucial for the stereoselectivity in asymmetric organocatalysis was reported by *Takata* in the early 2000s (Figure 21).[82]

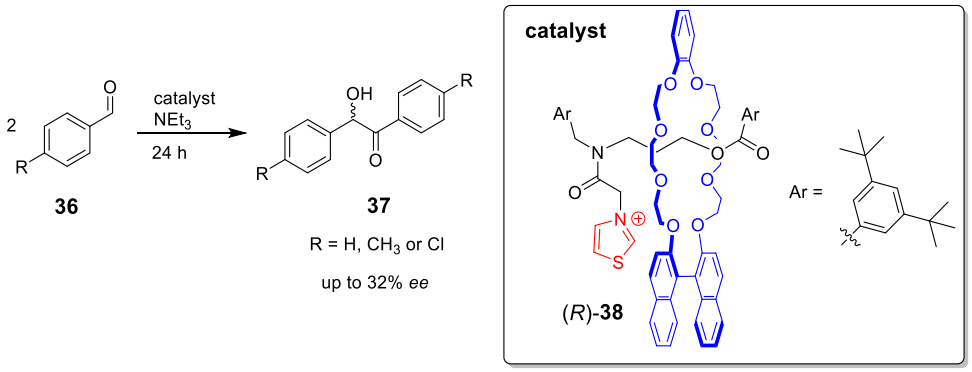

Figure 21*:* Benzoin condensation catalysed by chiral rotaxane (*R*)-**38**.

In this example different aldehydes were converted to the corresponding hydroxyketones in a benzoin condensation. The rotaxane catalyst consisted of a thread which bears a catalytically active thiazolium moiety and a chiral BINOL based crown ether macrocycle, which results in an axially covalent chiral

[82] Y. Tachibana, N. Kihara, T. Takata, *J. Am. Chem. Soc.* **2004**, *126*, 3438–3439
* The authors call the rotaxane mechanically point-chiral.

rotaxane. Interestingly, this rotaxane is able to transfer the chirality from one subunit onto the catalytically active subunit. Conversions of up to 90% and enantiomeric excesses up to 32% were obtained.

One of the most interesting results that arise from the mechanical bond are the new types of chiral elements, that are not accessible by covalent chemistry (chapter 1.2). Thus, it is not surprising that MIMs containing these new chiral elements were applied in asymmetric catalysis. One example of a co-conformationally covalently chiral rotaxane was published by *Leigh* et al. in 2016.[83]

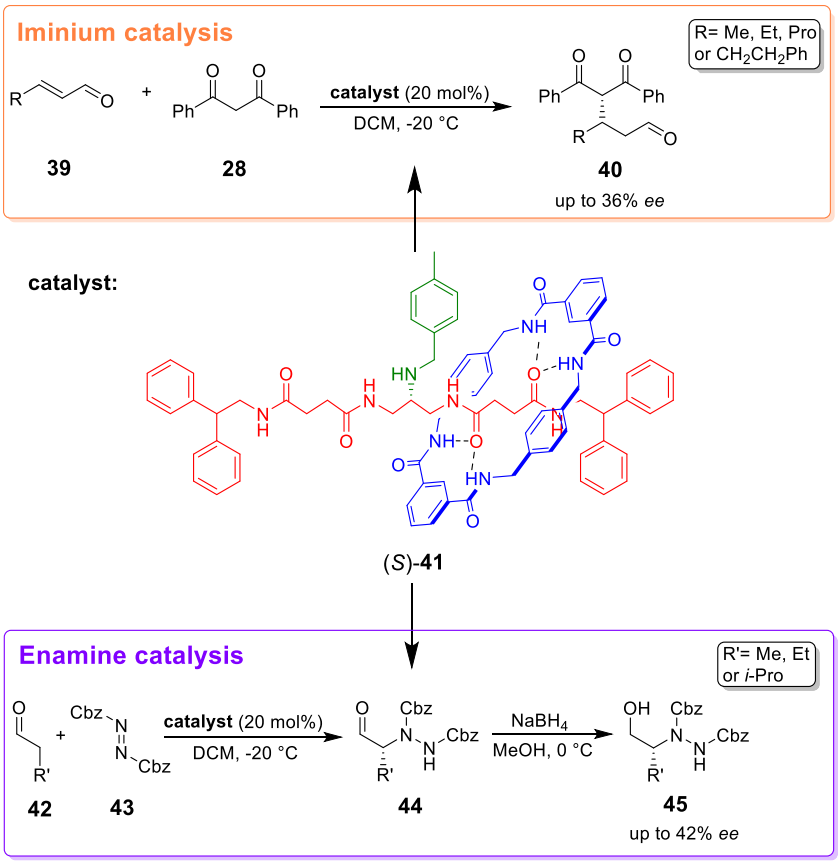

Figure 22: Asymmetric iminium and enamine catalysis by the co-conformational point chiral rotaxane (*S*)-**41**.

The rotaxane catalyst is composed of a symmetrical amide-based axle (red) bearing a prochiral secondary amine (green). Since the secondary amine is big enough to prevent movement of the macrocycle beyond it, the macrocycle is locked on one side of the thread. This leads to desymmetrization of the axle and thus turning the prochiral secondary amine into a chiral group. Since the chirality in this rotaxane stems from the two conformations of the macrocycle, it is called a co-conformationally chiral rotaxane (***Figure 12*** c)). This stereogenic element which is directly based on the mechanical bond, was able to induce stereoselectivity in the Michael addition of 1,3-diphenyl-1,3-propanedione to different unsaturated aldehydes via iminium catalysis and in the addition of dibenzyl azodicarboxylate to various aldehydes in an amination via enamine catalysis. For the iminium catalysis a stereoselectivity of up 36% *ee* was achieved, while the enamine catalysis yielded an enantiomeric excess of 42%. It has to be noted that the catalyst only had an optical purity of 84% *ee*.

[83] Y. Cakmak, S. Erbas-Cakmak, D. A. Leigh, *J. Am. Chem. Soc.* **2016**, *138*, 1749–1751.

Another type of chirality as a result of a mechanical bond has been exploited in asymmetric catalysis as well. *Goldup* et al. recently used a mechanical planar chiral rotaxane as a ligand in an asymmetric Au(I)-meditated cyclopropanation reaction.[84]

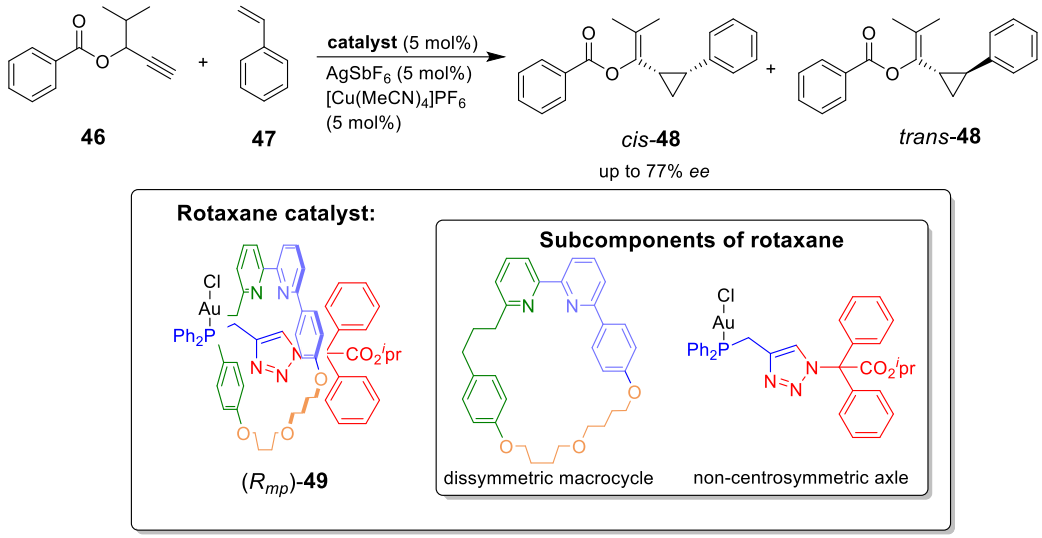

Figure 23: Au(I)-mediated cyclopropanation using mechanically planar chiral rotaxane (R_{mp})-**49** as the stereoinducing ligand.

In contrast to the previous example of a co-conformational point chiral rotaxane, this mechanical planar chiral (MPC) rotaxane does not contain any point chiral or prochiral unit, but creates its chirality solely through the mechanical bond. MPC rotaxane (R_{mp})-**49** was applied as a chiral ligand for the gold catalysed cyclopropanation inspired by *Uemura* [85] which converts propargylic esters with styrene to *cis* and *trans* cyclopropane derivatives. Rotaxane (R_{mp})-**49** was capable of achieving high enantiomeric excess of up to 77 % and diastereomeric excesses typically above 90% for various aromatic propargylic esters.

[84] A. W. Heard, S. M. Goldup, *Chem* **2020**, *6*, 994–1006.
[85] K. Miki, K. Ohe, S. Uemura, *Tetrahedron Lett.* **2003**, *44*, 2019–2022.

2. Objective

Application of mechanically interlocked molecules in asymmetric catalysis is dominated by chiral rotaxanes while chiral catenanes are still underexplored. This is rather surprising as they have several interesting properties that could be exploited in this field as well. Therefore, application of catenanes as chiral catalysts will be investigated in this work.

The first part of this thesis deals with the application of catenated and non-catenated chiral phosphoric acids in asymmetric organocatalysis. In more detail, an acyclic and macrocyclic phosphoric acid as well as a bisphosphoric acid catenane are applied as catalysts for the transfer hydrogenation of 2-phenylquinoline. DFT calculations suggested that this catalytic reaction can proceed via two different pathways, a monomeric phosphoric acid pathway and a dimeric phosphoric acid pathway. This hypothesis is tested within this work experimentally by analysing and interpreting kinetic and stereoselectivity data. Special focus lies on the concentration dependent behaviour of the acyclic phosphoric acid (*S*)-**3**.

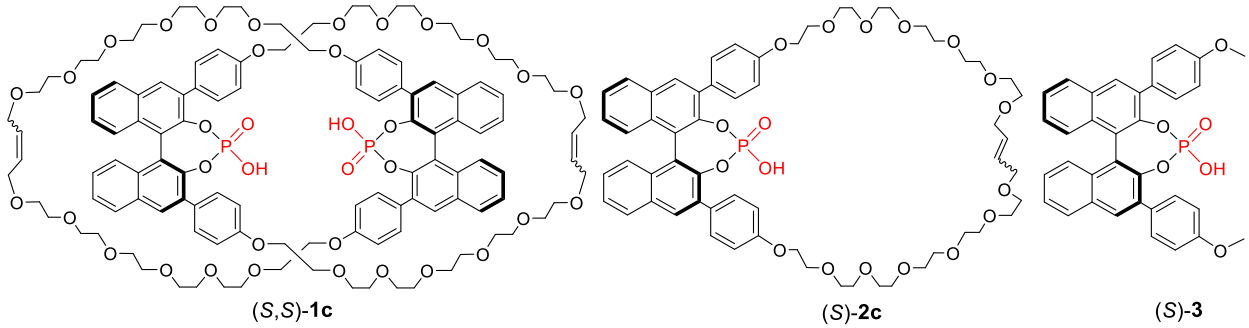

=> Application for the Brønsted acid catalyzed transfer hydrogenation

Figure 24: Chiral phosphoric acid catalysts which are investigated in the first part of this work.

In the second part a hetero-[2]catenane and a hetero[3]catenane are synthesized using an active metal template method. After further functionalisation, the catenanes are applied in different asymmetric catalytic reactions. Here, two modes of action which exploit the mechanical bond of the catenanes are investigated.

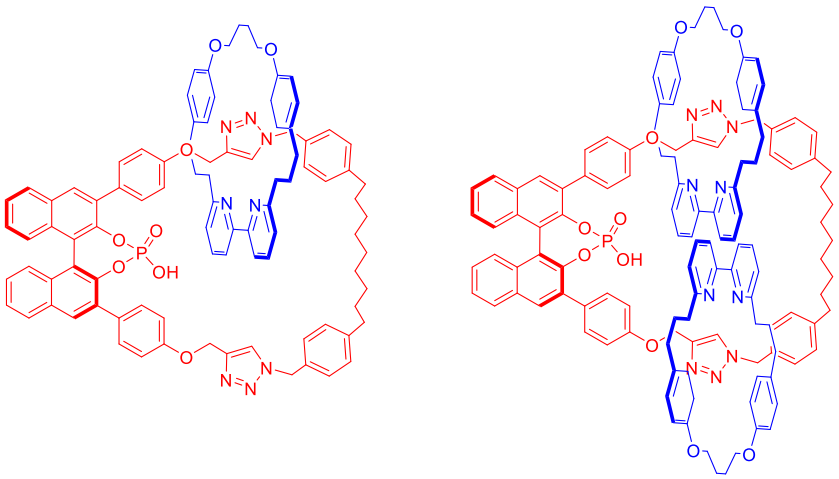

=> Application for Brønsted acid catalysis and as ligands in metal catalysis

Figure 25: [2]- and [3]catenane that are synthesized and applied in catalysis in the second part of this work.

3. Acid-acid interactions in Brønsted acid organocatalysis

This chapter will deal with catalyst-catalyst interactions and how the influence of such interactions in asymmetric catalysis can be investigated by chemical kinetic analysis and analysis of the stereoselectivity. For this an introduction into supramolecular catalyst interactions (chapter 3.1) as well as a general introduction into transfer hydrogenations (chapter 3.2.) and how kinetic analysis can be used to unveil reaction mechanisms (chapter 3.3) is described.

3.1 Theoretical background – Supramolecular catalyst interactions

Organocatalysts possess functional groups which are necessary to interact with substrates in catalytic reactions. However, due to relatively high catalyst loadings in some asymmetric organocatalytic reactions,[86] it is conceivable that these functional groups of the catalyst also interact with each other. When it comes to the effect of such catalyst-catalyst interactions it strongly depends on the nature of the catalyst and the examined reaction if an interplay between two catalyst molecules is beneficial for the catalytic outcome or not. For example, catalyst aggregation led to decreased catalyst efficiency and stereoselectivity for some cinchona-alkaloid based catalysts.[87] In another example the interaction of two catalyst molecules was examined by *Jacobsen* in 2016 where a thiourea hydrogen bonding catalyst was employed in the enantioselective alkylation of α-chloroethers (***Figure 26***).[88]

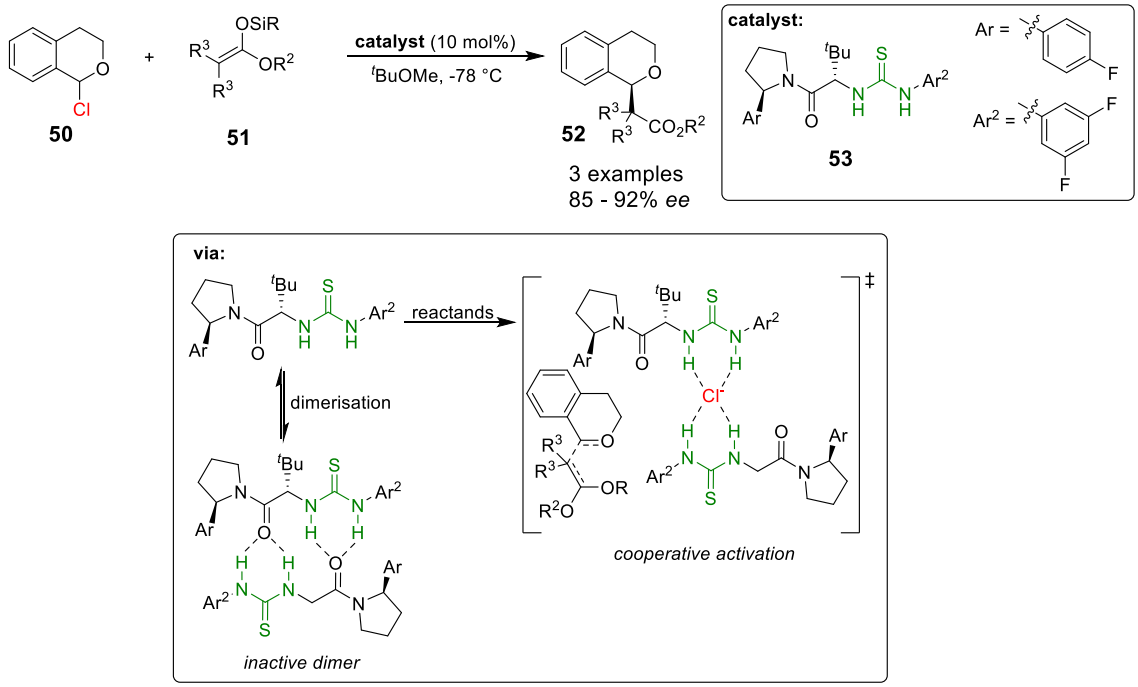

Figure 26: Enantioselective alkylation of α-chloroisochroman via dual H-bond activation by a thiourea catalyst.

[86] a) B. List, R. A. Lerner, C. F. Barbas, *J. Am. Chem. Soc.* **2000**, *122*, 2395–2396,M. Rueping, A. P. Antonchick, T. Theissmann, *Angew. Chem. Int. Ed.* **2006**, *45*, 3683–3686.
[87] a) H. B. Jang, H. S. Rho, J. S. Oh, E. H. Nam, S. E. Park, H. Y. Bae, C. E. Song, *Org. Biomol. Chem.* **2010**, *8*, 3918–3922,S. H. Oh, H. S. Rho, J. W. Lee, J. E. Lee, S. H. Youk, J. Chin, C. E. Song, *Angew. Chem. Int. Ed.* **2008**, *47*, 7872–7875,H. S. Rho, S. H. Oh, J. W. Lee, J. Y. Lee, J. Chin, C. E. Song, *Chem. Commun.* **2008**, 1208–1210,R. Salvio, L. Massaro, A. Puglisi, L. Angelini, A. Antenucci, S. Placidi, F. Sciubba, L. Galantini, M. Bella, *Org. Biomol. Chem.* **2018**, *16*, 7041–7049,G. Tárkányi, P. Király, T. Soós, S. Varga, *Chemistry* **2012**, *18*, 1918–1922.
[88] D. D. Ford, D. Lehnherr, C. R. Kennedy, E. N. Jacobsen, *J. Am. Chem. Soc.* **2016**, *138*, 7860–7863.

The reaction proceeds via cooperative anion-binding of chloride from the *α*-chloroisochroman by two catalyst molecules **53**. For this, a catalyst monomer has to bind the substrate first, followed by binding of the chloride by a second catalyst molecule. In contrast to this, dimerization of catalyst molecules by hydrogen bonding leads to formation of an aggregate that is inactive in this reaction. As this dimerization is concentration dependent, the catalyst primarily rests in the inactive dimeric state at high catalyst loadings, while at low catalyst loadings the probability of formation of the active catalyst-substrate-catalyst complex is decreased, ultimately leading to inefficiency of this thiourea catalyst in the examined reaction.

In further studies *Jacobsen* was able to show that the formation of the inactive catalyst dimer can be prevented by implementing two urea moieties into one molecule which, however, are still able to catalyse the reaction cooperatively.[89]

Aggregation of catalysts was not only observed for the nitrogen based catalysts mentioned before. Especially BINOL based phosphoric acids, which are widely applied in asymmetric organocatalysis (see chapter 1.3) can have a relatively strong interaction by formation of hydrogen bonds between two phosphoric acid moieties (***Figure 27***). Consequently, *Limbach* was able to show that dimethylphosphoric acid is able to form dimers and trimers[90] and *Hunger* identified a trimeric complex which consisted of two diphenylphosphoric acids which cooperatively bind 2-methylquinoline.[91]

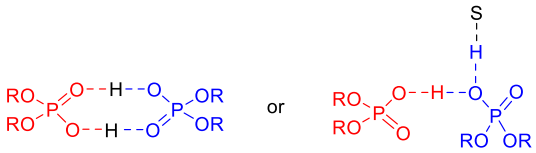

Figure 27: Hydrogen bonding between two phosphoric acids and possible hydrogen bonding of a phosphoric acid-dimer with a substrate.

Attractive forces can not only occur between the phosphoric acids. BINOL based CPAs with large substituents in 3,3'-positions were able to form dimeric phosphoric acid-imine complexes by additional weak non-covalent interactions.[92]

Similar to the example of *Jacobsen* where two catalytically active units were placed in one molecule, *Gong* also showed that bisphosphoric acids can be used to cooperatively catalyse reactions via Brønsted-acid assisted Brønsted-acid catalysis (BBA) (***Figure 28***).[93]

[89] a) C. R. Kennedy, D. Lehnherr, N. S. Rajapaksa, D. D. Ford, Y. Park, E. N. Jacobsen, *J. Am. Chem. Soc.* **2016**, *138*, 13525–13528,Y. Park, K. C. Harper, N. Kuhl, E. E. Kwan, R. Y. Liu, E. N. Jacobsen, *Science* **2017**, *355*, 162–166.
[90] C. Detering, P. M. Tolstoy, N. S. Golubev, G. S. Denisov, H.-H. Limbach, *Doklady Physical Chemistry* **2001**, *379*, 191–193.
[91] C. Malm, H. Kim, M. Wagner, J. Hunger, *Chem. Eur. J.* **2017**, *23*, 10853–10860.
[92] M. Melikian, J. Gramüller, J. Hioe, J. Greindl, R. M. Gschwind, *Chem. Sci.* **2019**, *10*, 5226–5234.
[93] L. He, X.-H. Chen, D.-N. Wang, S.-W. Luo, W.-Q. Zhang, J. Yu, L. Ren, L.-Z. Gong, *J. Am. Chem. Soc.* **2011**, *133*, 13504–13518.

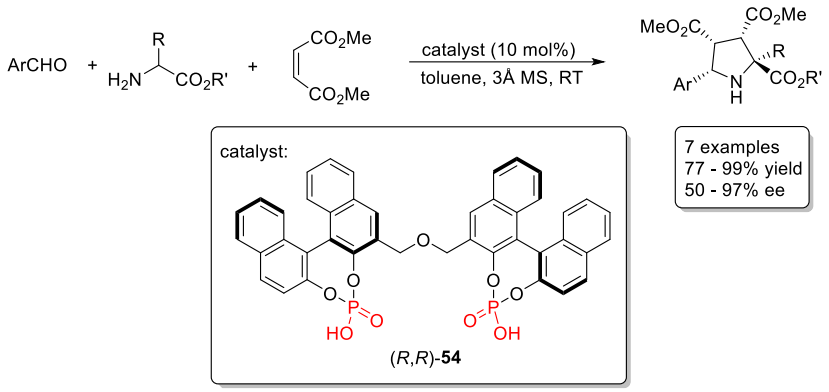

Figure 28: 1,3-dipolar cycloaddition of aldehydes with aminoesters and dimethyl maleate catalyzed by a chiral bisphosphoric acid.

For this two BINOL based phosphoric acids were connected covalently by different linkers, of which the oxapropylene linked catalyst (*R*,*R*)-**54** showed the best results in the 1,3-dipolar cycloaddition of aldehydes with aminoesters and dimethyl maleate. High yields (77 – 99%) and high enantiomeric excesses (50 – 97%, with 6 out of 7 examples > 90% *ee*) were obtained. Interestingly, the bisphosphoric acid is able to activate the nucleophile and the electrophile cooperatively with both phosphoric acids through hydrogen bonding.

Another aspect in BBA with multiple chiral phosphoric acids that are covalently linked is the correct positioning of the phosphoric acid units. If the phosphoric acid units in rigid molecules are not in close proximity, cooperative catalysis can be prevented, which can lead to lower stereoselectivities.[94] Therefore, it is generally useful to incorporate multiple phosphoric acids for BBA into a flexible molecule as it was shown for example by *Gong*[93] or *Niemeyer*.[35]

[94] S. Thölke, H. Zhu, D. Jansen, F. Octa-Smolin, M. Thiele, K. Kaupmees, I. Leito, S. Grimme, J. Niemeyer, *Eur. J. Org. Chem.* **2019**, *2019*, 5190–5195.

3.2 Theoretical background - Transfer hydrogenation

One important class of reduction reactions is hydrogenation, where hydrogen is added to a substrate. To achieve this, two different methods can be distinguished. In the first method dihydrogen gas is used to reduce various functional groups such as esters, alkenes and alkynes.[95] Due to a strong covalent bond in H_2 (104.2 kJ/mol)[96] a catalyst has to be used in order to pre-activate the dihydrogen. Here, different homogeneous and heterogeneous metal catalysts proved to be very active, making this a large area of research.[97] The second method is called transfer hydrogenation (TH). In TH hydrogen gas is substituted by compound which are able to deliver hydride ions and protons to other molecules, thus effectively leading to a reduction by transfer of two hydrogen atoms. The big advantage is that no flammable H_2 gas has to be used. Additionally, hydrogen donors used in TH are readily commercially available, robust and easy to handle.[98] Hydride donors that are frequently used in transfer hydrogenations include formic acid,[99] various alcohols in the Meerwein-Ponndorf-Verley (MPV) reduction[100], benzothiazolines[101] and 1,4-dihydropyridines (Hantzsch esters).[102] In order to get a better overview over the plethora of transfer hydrogenation reactions, the reactions can be classified by the type of catalyst that is used. The field of transfer hydrogenation is dominated by transition metal catalysed reactions.[97] Beside this, other metals which act as Lewis acids (usually $AlCl_3$) in MPV-type reduction,[103] enzymatic catalysis[104] or uncatalysed transfer hydrogenations[105] are commonly used as well. Since organocatalysis in general started booming in the early 2000s, transfer hydrogenations catalysed by small organic molecules has gained a lot of attention since then. Especially 1,4-dihydropyridines have become prominent reducing agents in organocatalytic transfer hydrogenation. The first organocatalytic metal-free transfer hydrogenation was demonstrated by *List* et al. in 2004 (**Figure 29**).[106]

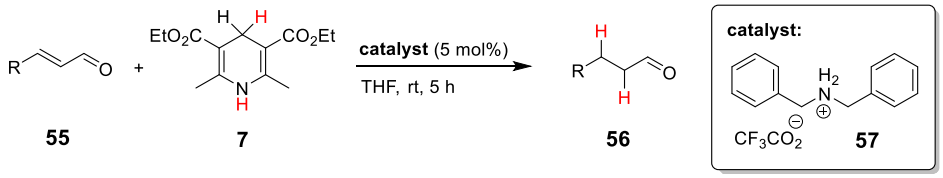

Figure 29: *Lists* first example of a transfer hydrogenation using the Hantzsch ester as a hydrogen source and a dibenzylammonium catalyst.

In this example different α-β-unsaturated aldehydes **55** were applied as Michael-acceptor systems and were reduced to their corresponding saturated derivatives using Hantzsch ester **7** as the hydrogen source. The reaction was catalysed by a dibenzylammonium organocatalyst. This catalyst forms the corresponding

[95] a) S. Werkmeister, K. Junge, M. Beller, *Org. Process Res. Dev.* **2014**, *18*, 289–302,Árpád Molnár George A. Olah G. K. Surya Prakash **2018**, 863–957.
[96] J. E. Bartmess, J. A. Scott, R. T. McIver, *J. Am. Chem. Soc.* **1979**, *101*, 6046–6056.
[97] P. A. Chaloner, M. A. Esteruelas, F. Joó, L. A. Oro *Catalysis by Metal Complexes* **1994**, Springer Netherlands.
[98] D. Wang, D. Astruc, *Chem. Rev.* **2015**, *115*, 6621–6686.
[99] a) J. Eppinger, K.-W. Huang, *ACS Energy Lett.* **2016**, *2*, 188–195,K. M. Shamsuddin, M. Zobairi, M. Musharraf, *Tetrahedron Lett.* **1998**, *39*, 8153–8154,R. Nie, Y. Tao, Y. Nie, T. Lu, J. Wang, Y. Zhang, X. Lu, C. C. Xu, *ACS Catal.* **2021**, *11*, 1071–1095.
[100] W. N. Moulton, R. E. van Atta, R. R. Ruch, *J. Org. Chem.* **1961**, *26*, 290–292.
[101] Y. Shibata, M. Yamanaka, *J. Org. Chem.* **2013**, *78*, 3731–3736.
[102] D. Richter, H. Mayr, *Angew. Chem. Int. Ed.* **2009**, *48*, 1958–1961.
[103] D. Klomp, U. Hanefeld, J. A. Peters **2006**, 585–630.
[104] S. Banerjee, P. J. Sadler, *RSC Chem. Biol.* **2021**, *2*, 12–29.
[105] B. Chan, L. Radom, *J. Phys. Chem. A* **2007**, *111*, 6456–6467.
[106] J. W. Yang, M. T. Hechavarria Fonseca, B. List, *Angew. Chem. Int. Ed.* **2004**, *43*, 6660–6662.

iminium species of the former carbonyl, thus activating it for the nucleophilic attack of the hydride from Hantzsch ester (red H^- in 4-position), followed by proton transfer of the H^+ bound to the nitrogen of the Hantzsch ester. Hydrolysis yields the saturated aldehyde and recovers the free catalyst. The yield was good for all aldehydes applied in this screening, including aromatic as well as alkyl substituents (81-96 %).

Building on these successful results of application of Hantzsch ester in the metal free transfer hydrogenation and the evolving use of chiral phosphoric acids (CPA) as Brønsted acid organocatalysts at this time (see chapter 1.3), *Rueping* and co-workers showed that the transfer hydrogenation of imines by Hantzsch ester can be catalysed by acids and even proceeds stereoselectively when chiral acids such as CPAs are used (***Figure 30***).[107]

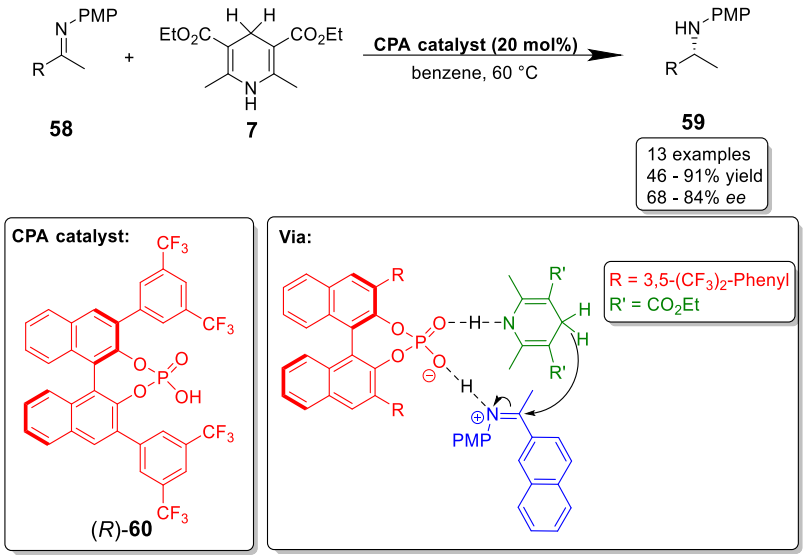

Figure 30: Asymmetric transfer hydrogenation of imine **58** using Hantzsch ester **7** catalysed by CPA (*R*)-**60**.

For this, different secondary ketimines were reduced to the corresponding secondary amines using Hantzsch ester **7**. The chiral phosphoric acid organocatalyst used in this reaction has two functions. It activates the substrates for the transfer hydrogenation and induces stereoselectivity by its bulky 3,5-(trifluoromethyl)phenyl substituents in then BINOLs 3,3'-position. The activation proceeds via the bifunctional activation mode through hydrogen bonding/protonation of the imine as well as hydrogen bonding to the Hantzsch ester through the lone pairs of the P=O unit, also bringing the two substrates in close proximity for the hydride attack on the imine. The yields using the catalyst depicted above were moderate or good for different ketimines (46% - 91%) and the stereoselectivity was between 68% and 84% *ee*, proving the good applicability of CPAs in transfer hydrogenations.

Beside imines and Michael acceptor systems shown above, other reactions with enamides[108], α-amino esters[109], olefins[110] as well as light-driven dehalogenation of α-haloketones[111] were successfully conducted with Hantzsch esters in transfer hydrogenations reactions. In addition to the iminium and CPA catalysts,

[107] M. Rueping, E. Sugiono, C. Azap, T. Theissmann, M. Bolte, *Org. Lett.* **2005**, *7*, 3781–3783.
[108] G. Li, J. C. Antilla, *Org. Lett.* **2009**, *11*, 1075–1078.
[109] G. Li, Y. Liang, J. C. Antilla, *J. Am. Chem. Soc.* **2007**, *129*, 5830–5831.
[110] N. J. A. Martin, L. Ozores, B. List, *J. Am. Chem. Soc.* **2007**, *129*, 8976–8977.
[111] Y.-Q. Yang, Z. Lu, *Synthesis* **2018**, *51*, 508–515.

different other organocatalysts were employed in TH as well. Those include e.g. thiourea[112] or benzyl isothiouronium chloride catalysts.[113]

CPAs have also been used to catalyse transfer hydrogenation of 2-substituted quinolines by *Rueping* in 2006 (***Figure 31***).[114]

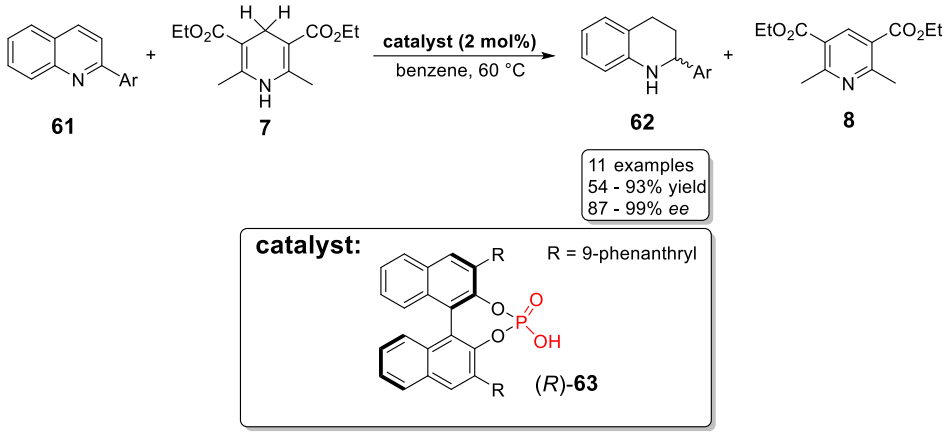

Figure 31: Transfer hydrogenation of 2-substituteted quinolines by a chiral phosphoric acid.

Similar to the transfer hydrogenation of imines, the CPA activates both substrates via the bifunctional activation mode by hydrogen bonding in this example as well. High enantiomeric excesses (87 – 99% *ee*) were obtained when the chiral phosphoric acid (*R*)-**63** with large substituents in 3,3'-position was employed as a catalyst.

The only example of a catenane in asymmetric organocatalysis is the bisphosphoric acid catenane by *Niemeyer* et al. which was used in the transfer hydrogenation of 2-substituted quinolines **61** by Hantzsch ester **7**.[35]

[112] Z. Zhang, P. Schreiner, *Synlett* **2007**, *2007*, 1455–1457.
[113] Q. Nguyen, T. Kim, *Synthesis* **2012**, *44*, 1977–1982.
[114] M. Rueping, A. P. Antonchick, T. Theissmann, *Angew. Chem. Int. Ed.* **2006**, *45*, 3683–3686.

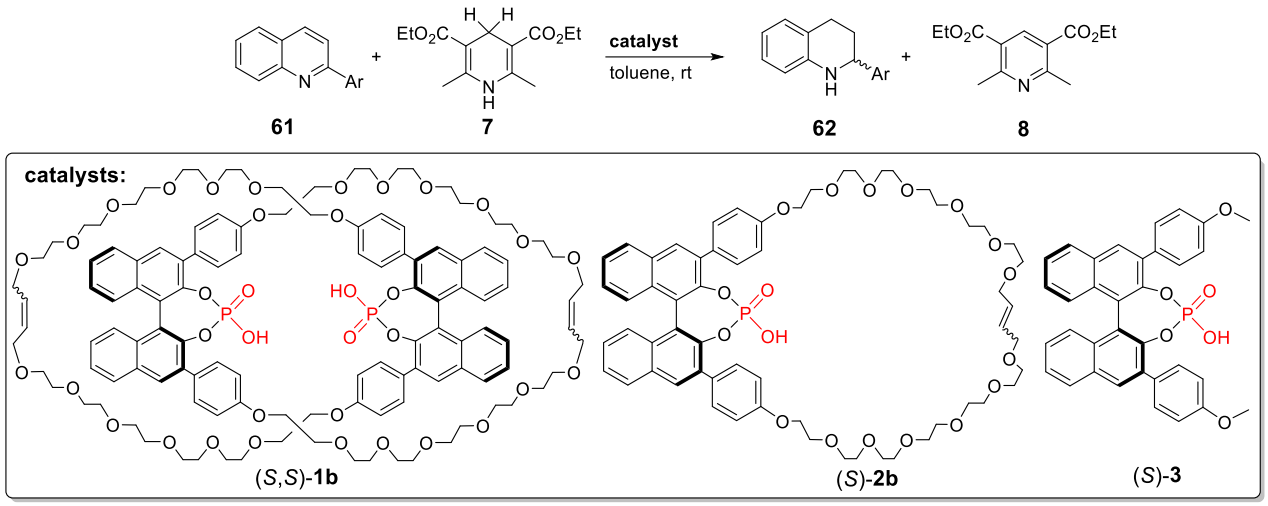

Figure 32: Asymmetric transfer hydrogenation of 2-substituted quinolines by a catenated CPA, a macrocyclic CPA and an acyclic CPA.

In this example stereoselectivities of three different CPAs were compared. These catalysts include the catenated chiral bisphosphoric acid (*S*,*S*)-**1b**, macrocyclic chiral phosphoric acid (*S*)-**2b** and acyclic chiral phosphoric acid (*S*)-**3**. Different stereoselectivities were found for these catalysts. While the catenated catalyst led to high enantiomeric excesses (82 - 98 % *ee*), the macrocycle (*S*)-**2b** produced much lower enantiomeric excesses with same substrates (-12 - 70 % *ee*). The excesses obtained with acyclic phosphoric acid (*S*)-**3** were just slightly above those using the macrocycle (9 - 84 % *ee*). In addition to varying the substrates, the influence of the catalyst loadings on the stereoselectivity for macrocycle (*S*)-**2b** and acyclic phosphoric acid (*S*)-**3** for the reaction with 2-phenylquinoline and Hantzsch ester were also investigated. While the stereoselectivities slightly changed for macrocycle (-12 to 10 % *ee*; 2.5 mol% to 10 mol%) the increase in stereoselectivity was much more pronounced in case of acyclic phosphoric acid (9 to 58 % *ee*; 2.5 mol% to 10 mol%). To shed light on the mechanistic differences between the catalysts, the experimental results were combined with DFT calculations, computing the transfer hydrogenation of 2-phenylquinoline using TPSS-D3/def2-SVP + DCOSMO-RS(toluene) optimized geometries. For this, energies of two catalytic pathways were determined, a monomeric pathway (***Figure 33***) and a dimeric pathway (***Figure 34***).[35]

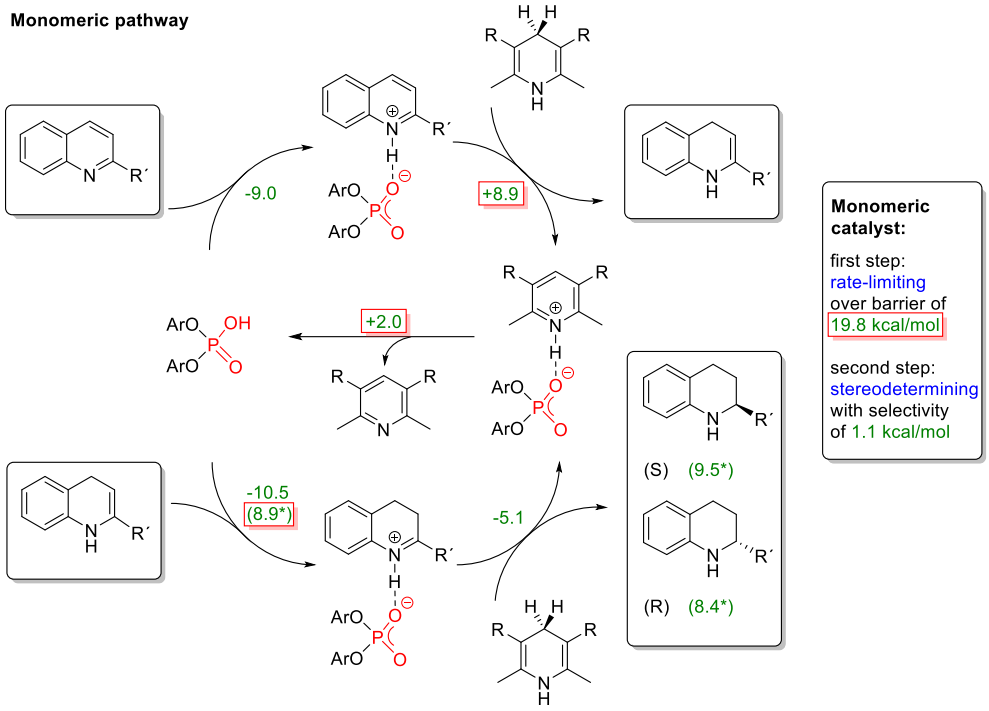

Figure 33: Calculated energies during the transfer hydrogenation of 2-phenylquinoline catalysed by a monomeric CPA.

The mechanism of the transfer hydrogenation is split into two overlapping catalytic cycles. In the first catalytic cycle the CPA binds to the quinoline via ion pairing. This exergonic step is followed by the combined endergonic steps including the hydride transfer from Hantzsch ester to form the corresponding pyridinium and 1,4-dihydroquinoline as well as dissociation of those to yield the free CPA (+ 10.9 kcal/mol). In the second cycle 1,4-dihydroquinoline binds to the CPA catalyst, which has a barrier of 8.9 kcal/mol, but is exergonic by -10.5 kcal/mol. This represents the rate-determining transition state and the overall barrier amounts to 19.8 kcal/mol when taking the two preceding endergonic steps (i.e. 8.9 + 2.0 +8.9 kcal/mol) into account. At this point two diastereomeric complexes are possible leading to the (*S*)-product or (*R*)-product after a second hydrogenation by Hantzsch ester. The energetic difference of the transition states towards the respective enantiomers is 1.1 kcal/mol, the energetically preferred product being the (*R*)-product.

The mechanism of the dimeric pathway contains the same steps as the monomeric pathway. However, dimerization of the CPA prior to substrate binding leads to different energies during the catalytic cycle. The overall barrier amounts to 21.1 kcal/mol, which includes the first hydrogenation and the pyridine dissociation, which is significantly more endergonic with 14.4 kcal/mol for the dimeric case in comparison to the monomeric case (2.0 kcal/mol, see ***Figure 33***). In the second cycle, which determines the stereoselectivity, a higher difference in energy for the transition states towards the respective enantiomers is found in the dimeric pathway (3.9 kcal/mol in favour of (*R*)-product).

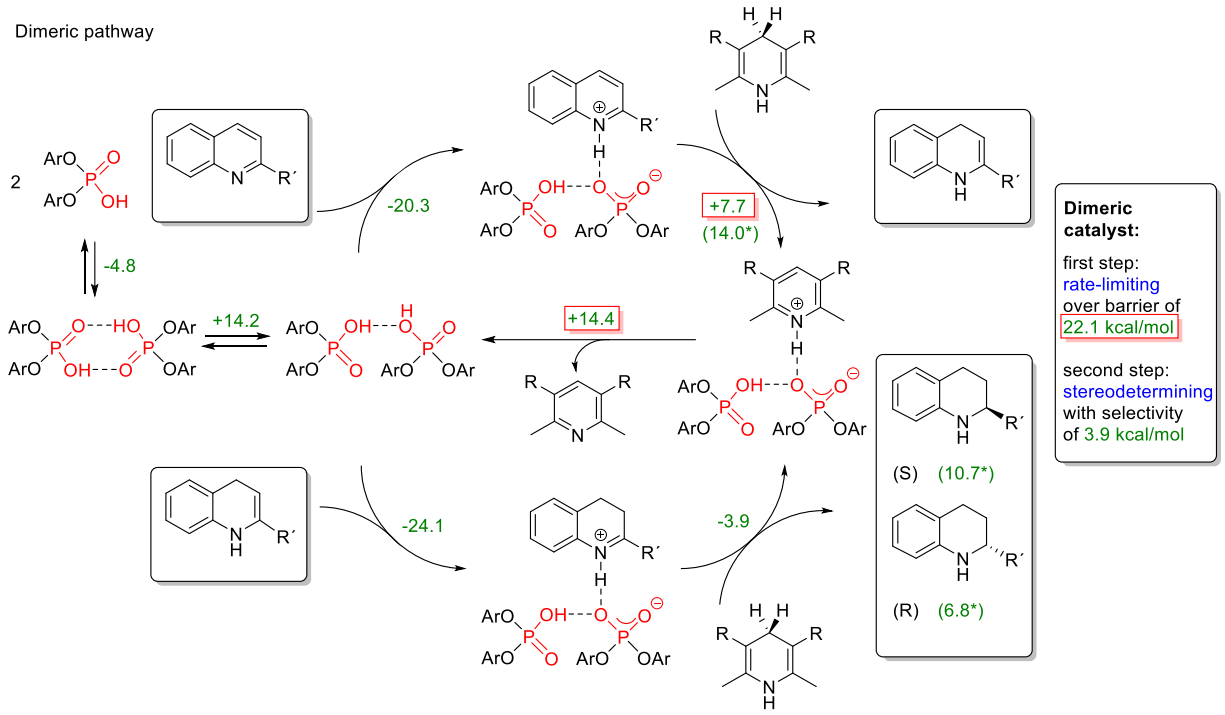

Figure 34: Calculated energies during the transfer hydrogenation of 2-phenylquinoline catalysed by a dimeric CPA.[35]

These energetic differences in the two pathways could help to explain the different stereoselectivities for the catenated catalyst compared to the other catalysts.

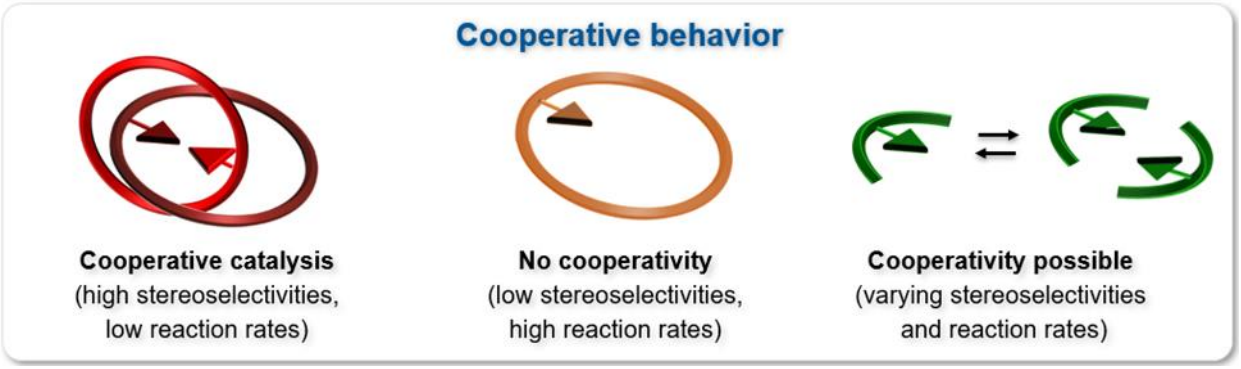

Figure 35: Schematic representation of the cooperative behaviour in catalysis of the catenane (left), macrocycle (middle) and acyclic phosphoric acid (right).

Based on the calculations, we propose that the mechanical bond of the catenane ensure a high local concentration of two phosphoric acid groups at all time. Therefore, this catalyst reacts mainly through the dimeric pathway. To catalyse via the same dimeric pathway, macrocyclic CPA (*S*)-**2b** and acyclic CPA (*S*)-**3** have to dimerize under the given reaction conditions. While this is indicated by the high concentration dependent stereoselectivity of the acyclic phosphoric acid, the macrocycles dimerization seems to be hindered, thus this catalyst mainly reacts via the monomeric pathway even at higher concentrations.

It has to be noted that these explanations are only based on the DFT calculations and a few data points. Thus an in depth investigation on the mechanisms using the three different catalyst is of high interest.

3.3 Theoretical Background - Kinetic investigation of chemical reactions

Understanding how a substrate is converted to a product is of utmost importance in fundamental research but can also be industrially relevant when it comes to improving the outcome of a reaction. For this, it is very useful to know the mechanism behind a reaction, because this allows for optimisation by variation of parameters in a more controlled fashion than in trial-and-error methods.

Different characteristics (e.g. enthalpy, entropy, activation energy, stoichiometry, kinetics) describe the nature of a given reaction. The characteristics can be unveiled by different techniques to learn about the mechanism of the reaction. These techniques include for example differential scanning calorimetry or differential thermal analysis which can be used to track the change of heat of a reaction and therefore allow determination of the enthalpy of a reaction.[115] Other methods that possibly give insight into the mechanism of a reaction are isotope labelling, which are used e.g. to identify where one functional group of the substrate ends up in the product,[116] or analysis of intermediates, which, in some cases, can be isolated and analysed by standard spectroscopic methods. For short lived intermediates techniques such as spectroscopic pump probe experiments[117] or trapping of the intermediates are known.[118] With the great progresses that have been made in computational chemistry in the last decades, quantum chemical calculations have made an immense contribution towards understanding reaction mechanisms. Today, experimental data is often combined with quantum chemical calculations to further back up hypotheses by calculating energies of transition states and even predict the stereoselectivity of a reaction.[119]

3.3.1 Classical approach to chemical kinetic analysis

One of the most commonly used methods to investigate reaction mechanisms, however, is chemical kinetic analysis. In chemical kinetic analysis the rate of conversion of the substrate or the rate of formation of product is followed. This was done for the first time by *Wilhelmy* in 1850 in the acid-catalysed conversion of saccharose to glucose and fructose.[120] He described the influence of the substrates concentration on the rate of conversion. Mathematically, this process can be described by a differential equation

$$v = -\frac{d[A]}{dt}$$

where v is the rate of reaction and [A] the concentration of the substrate.

[115] W. Parrish, *Fluid Ph. Equilibria* **1986**, *29*, 177–192.
[116] U. Maitra, J. Chandrasekhar, *Reson.* **1997**, *2*, 29–37.
[117] C. Hess, S. Funk, M. Bonn, D. N. Denzler, M. Wolf, G. Ertl, *Appl. Phys. A* **2000**, *71*, 477–483.
[118] a) T. Rosenau, A. Potthast, P. Kosma **2006**, *205*, 153–197,J. Ruiz, L. García, M. Vivanco, Á. Berros, J. F. van der Maelen, *Angew. Chem. Int. Ed.* **2015**, *54*, 4212–4216.
[119] Q. Peng, F. Duarte, R. S. Paton, *Chem. Soc. Rev.* **2016**, *45*, 6093–6107.
[120] L. Wilhelmy, *Ann. Phys. Chem.* **1850**, *157*, 499–526.

Usually the kinetics of a chemical reaction are expressed by a rate law. This rate law links the rate of a reaction with the concentration of its substrates. In the case of two substrates A and B that convert to a product, the rate can be expressed as:

$$v = k[A]^m[B]^n$$

In this, k is the reaction rate constant and the exponents m and n describe the fractional order of reaction for A/B. The sum of the exponents is called the overall reaction order. The fractional reaction orders m and n must not be confused with the stoichiometric coefficient of the substrate. Even though they are identical for elementary reactions, they may differ for non-elementary reactions e.g. for multi-step processes or when using a catalyst. Here, the stoichiometric coefficient is the amount of molecules that react, the fractional reaction order of a substrate, however, describes the contribution of a substrates concentration to the reaction rate. Thus, fractional orders are not necessarily equal to the stoichiometric coefficients and can even be fractional numbers. Thus, determination of reaction orders is, next to determination of initial reaction rates and rate constants, an important step in elucidating reaction mechanisms in kinetic analysis.

3.3.1.1 Determination of reaction rate constants – Graphical approach

For elementary reactions, rate constants can be easily obtained by integration and linearization of the differential equation and plotting it.[121] In the following table the differential rate equations, integrated and linearized equations for the case of a reaction orders of 0, 1 and 2 for a substrate A are displayed.

Table 1: Rate laws for reactions with different orders.

Order in A	**0th order**	**1st order**	**2nd order**
Differential rate equation	$-\frac{d[A]}{dt} = k$	$-\frac{d[A]}{dt} = k[A]$	$-\frac{d[A]}{dt} = k[A]^2$
Integrated equation	$[A] = [A]_0 - kt$	$[A] = [A]_0 e^{-kt}$	$\frac{1}{[A]} = \frac{1}{[A]_0} + kt$
Linearized equation	$[A] = [A]_0 - kt$	$ln[A] = ln[A]_0 - kt$	$\frac{1}{[A]} = \frac{1}{[A]_0} + kt$

For non-elementary reactions the same approach can be used, however, reaction orders have to be guessed beforehand. Correctness of the guessed reaction order is verified when plotting the experimental data according to the linearized equation yields a straight line. Alternatively, the reaction rate constant can also be obtained by applying a non-linear fit to the experimental data.

[121] a) H. Pessen, *Science* **1961**, *134*, 676–677,J. H. Wright, J. H. Black, J. Coull, *J. Chem. Educ.* **1956**, *33*, p. 542.

3.3.1.2 Determination of substrate orders – Initial rates method

Different methods to determine the order of a substrate are known in classical kinetic analysis. As described before, the graphical approach can be used to determine the substrate order by guessing it and checking if the plotted experimental data yields a straight line in the linearized rate law. This can result in elaborated mathematical treatments when multiple substrates with higher orders are present.

Another prominent method for the determination of substrate orders, that is especially useful when the rate is dependent on more than one substrate, is called initial rates method.[122] This method is exemplified in the following by a reaction where the rate depends on two concentrations (e.g. in a A + B -> P reaction):

$$-\frac{d[A]}{dt} = v_0 = k[A_0]^n[B_0]^m$$

Multiple experiments are conducted where the initial concentration of one substrate (in this case B_0) is held constant, while the initial concentration of the other substrate is varied. This allows the elimination of the influence of substrate B on the initial rate v_0. Together with k it can be written as a constant k':

$$v_0 = k'[A_0]^n$$

Taking the logarithm on both sides transforms the equation into a linear form:

$$\ln(v_0) = \ln(k') + \ln([A_0]) * n$$

By plotting the logarithm of initial rates of the different experiments against the logarithm of initial concentrations, the substrate order *n* is obtained by measuring the slope of the line. This procedure can be repeated for any other component taking part in the reaction (other reagents and catalysts). Although the order in one substrate can be obtained from just two experiments with differing initial concentrations, this will result in a great amount of uncertainty due to the small sample size (***Figure 36***).

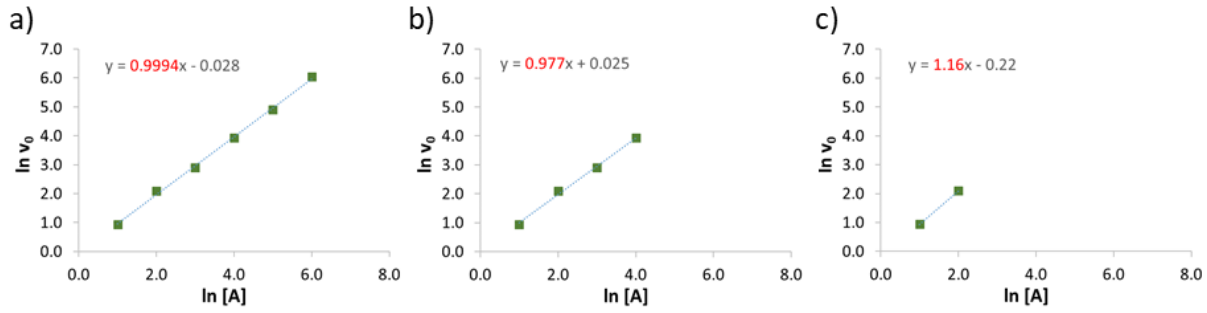

Figure 36: ln(v_0) vs. ln(A_0) plots using model initial rates and concentrations. The reaction order of substrate A is 1. A random error of up to 8% was generated using EXCEL rand() function. Different reaction orders (red) obtained when using a) all six initial rates, b) four out of six initial rates c) only two out of six initial rates.

[122] J. Casado, M. A. Lopez-Quintela, F. M. Lorenzo-Barral, *J. Chem. Educ.* **1986**, *63*, 450–452.

3.3.2 Visual kinetic analysis

In contrast to the tedious work that accompanies the kinetic investigation by classical kinetic analysis, visual kinetic analysis provides a set of methods that allow for the determination of the most important kinetically relevant data with only a few experiments.[123] These include product inhibition/catalyst deactivation and determination of substrate and catalyst orders.[124]

The key point to visual kinetic analysis is to modify experimental data in a way that allows for the data to be analyzed by naked eye. Other advantages are that only minimal mathematical treatments are necessary, all data points of a reaction are used (in the initial rates method only initial rates are extracted from the curve of conversion, while the other data points are neglected) and the results are presented in a graphically appealing way. Additionally, reactions can be carried out under kinetically relevant conditions (and not under pseudo first-order conditions).[125] One disadvantage is that the precision of visual kinetic analysis is low compared to other methods. However, often high precision is not necessary in kinetic analyses.[123] Visual kinetic analysis consists of two different techniques, reaction progress kinetic analysis (RPKA) and variable time normalization analysis (VTNA), which will be explained in this chapter.

3.3.2.1 Reaction progress kinetic analysis

Reaction progress kinetic analysis (RPKA) was introduced by *Blackmond* in 2005.[126] Since rate laws describe the correlation of reaction rates and concentrations, this method grants access to kinetic relevant data using rate vs. substrate-concentration-plots. For this, analytical methods which directly measure the rate of a reaction instead of a change in concentration is preferred. Reaction calorimetry is a commonly used analytic method which allows for the direct correlation of the observed heat flow to the reaction rate. As stated above, these reaction profiles are treated mathematically to allow a readout of kinetically relevant data by naked eye. For this, a set of methods is introduced which rely on same and different excess experiments. This excess describes the difference in initial concentrations in reactions with two substrates A and B:

$$excess = [B]_0 - [A]_0$$

The excess allows to express the rate law dependent on one variable only, by writing the time dependent concentration of one substrate (e.g. [B]) as:

$$[B] = [B]_0 - ([A]_0 - [A])$$

$$v = k * [A]^n * (excess + [A])$$

[123] C. D.-T. Nielsen, J. Burés, *Chem. Sci.* **2019**, *10*, 348–353.
[124] R. H. Crabtree, *Chem. Rev.* **2015**, *115*, 127–150.
[125] J. S. Mathew, M. Klussmann, H. Iwamura, F. Valera, A. Futran, E. A. C. Emanuelsson, D. G. Blackmond, *J. Org. Chem.* **2006**, *71*, 4711–4722.
[126] D. G. Blackmond, *Angew. Chem. Int. Ed.* **2005**, *44*, 4302–4320.

Catalyst deactivation and product inhibition (same excess experiments)

Product inhibition and catalyst deactivation can be investigated by same excess experiments. For a reaction between substrate A and B that is catalysed by catalyst C at least two experiments have to be conducted, where the initial concentrations are different, but the excess is the same. This allows to "jump into" the reaction at different times, because the concentrations of the substrate meet at some point during the course of the reaction, the only difference being the concentration of product that has formed as well as the turn over number of the catalyst (***Figure 37***). Overlaying of both reaction profiles reveals if there is an influence of product inhibition or catalyst deactivation on the reaction rate.

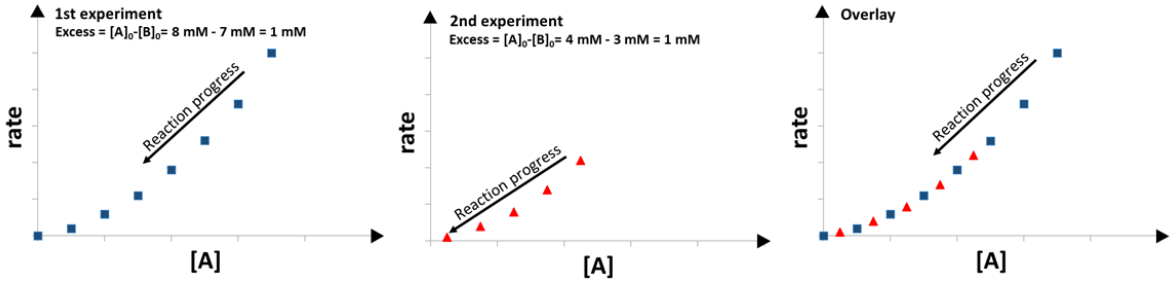

Figure 37: Schematic representation of same excess experiments to check for product inhibition/catalyst deactivation.[123] The experiment with the smaller initial concentration (red) allows to "jump into" the other reaction (blue) at time "t". Note that rate vs [substrate] profiles are read from right to left.

If the reaction profiles overlay, no product inhibition or catalyst deactivation exists. If the profiles do not overlay, the reason for this has to be distinguished in a third experiment, where the amount of product $[P]_t$ is added to the experiment with the lower initial concentrations (red). Like this, the only remaining difference is the turn over number of the catalyst. If the profiles now overlay the reaction exhibits product inhibition, if they do not overlay catalyst deactivation is present.

Determination of reaction orders (different excess experiments)

Similar to the initial rates method of classical kinetic analysis, determination of reaction orders is carried out by doing experiments at different initial concentrations. In RPKA, these experiments are called different excess experiments. Assuming a reaction consisting of substrate A and B that are converted with the help of catalyst C to form product P, two different excess experiments have to be conducted to determine the order in one substrate.

$$A + B \xrightarrow{C} P \qquad v = k[A]^n[B]^m[C]^p$$

For example, to determine the order m in B, two experiments have to be set up, where the only difference is the initial concentration $[B]_0$. Now, the experimental data of both experiments are plotted. For the y-axis the reaction rate divided by B to the power of m is plotted while for the x-axis the concentration of substrate A is plotted. Since m is the order in substrate B, it is not known. However, by guessing different values of x the shapes of the reaction profiles change. When the best overlap of both reaction profiles is obtained, the value of m is equal to the order in substrate B (***Figure 38***).

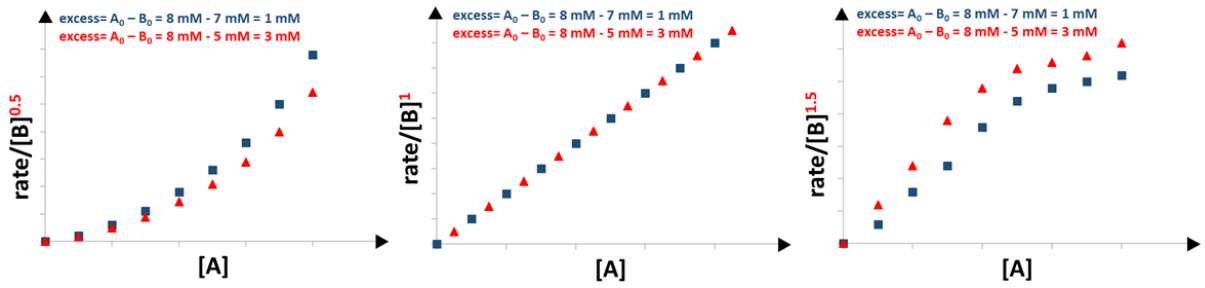

Figure 38: Schematic representation of the determination of orders using RPKA. If the order is guessed correctly, the reaction profiles overlay.

The same concept can be applied to other substrates as well as to the catalyst to determine their orders. By carefully choosing the conditions, determination of the second (and any additional) orders only requires one more experiment as one experiment has already been carried. Even though two reaction profiles are sufficient to determine the order, one may use more reaction profiles to increase the accuracy of this method.

3.3.2.2 Variable time normalization analysis

Variable time normalization analysis (VTNA) was introduced in 2016 by *Burés* as a second type of visual kinetic analysis. RPKA requires rate data that is directly obtained by only a few techniques such as isothermal calorimetry or must be calculated by converting concentrations into reaction rates mathematically which can lead to increase of noise in the data profile.[127] In contrast to this, VTNA allows visual analysis of concentration vs. time profiles, which directly are obtained by analytical methods that measure a signal which directly corresponds to a concentration. Those analytical methods include NMR, FTIR, UV/VIS spectroscopy or different chromatographic methods (GC, HPLC) combined with a suitable detector and possibly in combination with an internal standard. Due to the high availability of these analytical techniques, VTNA allows easier application of visual kinetic analysis and also to a broader spectrum of reactions that may not be followed by reaction calorimetry.

Product inhibition and catalyst deactivation (same excess experiments)

Similar to RPKA, product inhibition and catalyst deactivation in VTNA is investigated by same excess experiments. The only difference is, that the time axis for one experiment has to be altered. For example, the time axis of the experiment with the lower initial concentrations is shifted to the right by adding a value S to the time, so that the initial concentration of this experiments ends up on the curve of the other experiment (***Figure 39***).

[127] R. D. Baxter, D. Sale, K. M. Engle, J.-Q. Yu, D. G. Blackmond, *J. Am. Chem. Soc.* **2012**, *134*, 4600–4606.

Figure 39: Same excess experiments to check for catalyst deactivation/product inhibition. Addition of a value S to the time axis of the red curve results in overlay of both conversion curves.

If the both curves overlap, no product inhibition or catalyst deactivation is present. If the curves do not overlay a third experiment has to be conducted, where the amount of product formed in the first experiment as the time t = S is added to the second experiment. If the curves now overlay, product inhibition is present in the reaction, while no overlay indicates catalyst deactivation.

Determination of reaction orders (different excess experiments)

To determine the orders of substrates and catalyst visually by using concentration vs. time plots in VTNA, at least two different excess experiments have to be conducted, where the time axis has to be modified later on. For example, to determine the order in substrate B, the time axis has to be swapped by a normalized time axis which is calculated by the following equation.

$$\sum[B]^m \Delta t = \sum_{i=1}^{n} \left(\frac{[B]_i + [B]_{i-1}}{2}\right)^m (t_i - t_{i-1})$$

To obtain the order in substrate B, data of both experiments are plotted according to the normalized time axis and m is varied until both curves overlay (***Figure 40***).

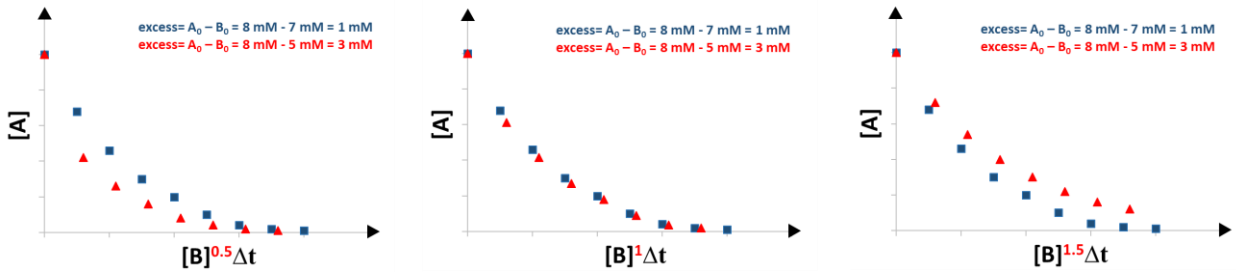

Figure 40: Visual kinetic analysis plot of [A] against normalized time scales $[B]^m\Delta t$. Variation of m until curve overlay allows determination of the order in B. Best overlap for m = 1.

The value of m then represents the order in substrate B. In the same way the orders of other substrates as well as the order in catalyst can be determined. A special case is present if the catalyst concentration stays constant throughout the reaction. Then the normalized time axis can be created easily by dividing each time data point t_i by the initial concentration of the catalyst to the power of the order p in catalyst.

$$[Cat]^p \Delta t = \frac{t_i}{[Cat]^p}$$

In summary, RPKA and especially VTNA provide powerful tools to obtain important kinetic information by naked-eye analysis of easily accessible reaction profiles. In contrast to classical kinetic analysis, fewer experiments have to be conducted. Additionally, only a few mathematical treatments allow presentation of the results in a visually appealing way.

3.4 Synthesis

The synthesis was carried out as previously during the master thesis[128] and was published recently.[129] Therefore, the synthetic steps are only briefly presented. Synthesis of the hexaethylene glycol based catenane as well as the synthesis from (*S*)-**67a** to (*S*)-**69** were only carried out in the master thesis (***Figure 41***).

Starting from commercially available (*S*)-BINOL (*S*)-**63** firstly the hydroxyl groups were protected using chloromethyl methyl ether (MOM-Cl) to avoid reactions at these phenolic positions in later steps. The MOM-protecting group also serves as an *ortho*-directing group in the next step, where a doubly lithiated species is formed at 3,3'-position after reaction with *n*-butyllithium, followed by lithium-halogen exchange with iodine to form diiodo-derivative (*S*)-**65**. In the next step a twofold *Suzuki* coupling was used to attach 4-hydroxyphenyl substituents at the 3,3'-positions to yield bisphenol (*S*)-**66.** To enable the subsequent ring closing reaction, which is needed for catenation, a twofold *Williamson* ether coupling is conducted by reaction of bisphenol (*S*)-**66** and allylated ethylene glycol tosylate **42a/c** under basic conditions to yield the derivate (*S*)-**67**. Successive removal of the MOM-protecting group under acidic conditions and phosphorylation of the diol (*S*)-**68** yielded the phosphoric acid derivative (*S*)-**69**. To prepare the catenation step, two phosphoric acid derivatives were pre-coordinated by reaction with $Ca(OMe)_2$ to obtain a passive metal template. The double cyclisation step was carried out under high dilution conditions using Grubbs II in a twofold ring closing metathesis. Isolation of the catenane and macrocycle was achieved by medium performance liquid chromatography on RP-18 silica gel. A systematic study by *Thorsten Marochow* to examine the influence of different parameters (concentration of the template, different catalysts and catalyst loadings, solvents and reaction time) revealed that a conversion of up to 40% towards the desired catenane can be achieved (under conditions stated in ***Figure 41***), however, most of the catenane is lost during the work-up.[130]

[128] D. Jansen *Synthesis of [2]catenanes based on 1,1'-binaphthpyl-phosphoric acids* **2017**, *Master Thesis*, Universität Duisburg-Essen.
[129] a) R. Mitra, M. Thiele, F. Octa-Smolin, M. C. Letzel, J. Niemeyer, *Chem. Commun.* **2016**, *52*, 5977–5980,D. Jansen, J. Gramüller, F. Niemeyer, T. Schaller, M. C. Letzel, S. Grimme, H. Zhu, R. M. Gschwind, J. Niemeyer, *Chem. Sci.* **2020**, *11*, 4381–4390.
[130] T. Marochow *Optimierung der Ringschlussmetathese zur Darstellung von [2]Catenanen* **2019**, *Bachelor Thesis*, Universität Duisburg-Essen.

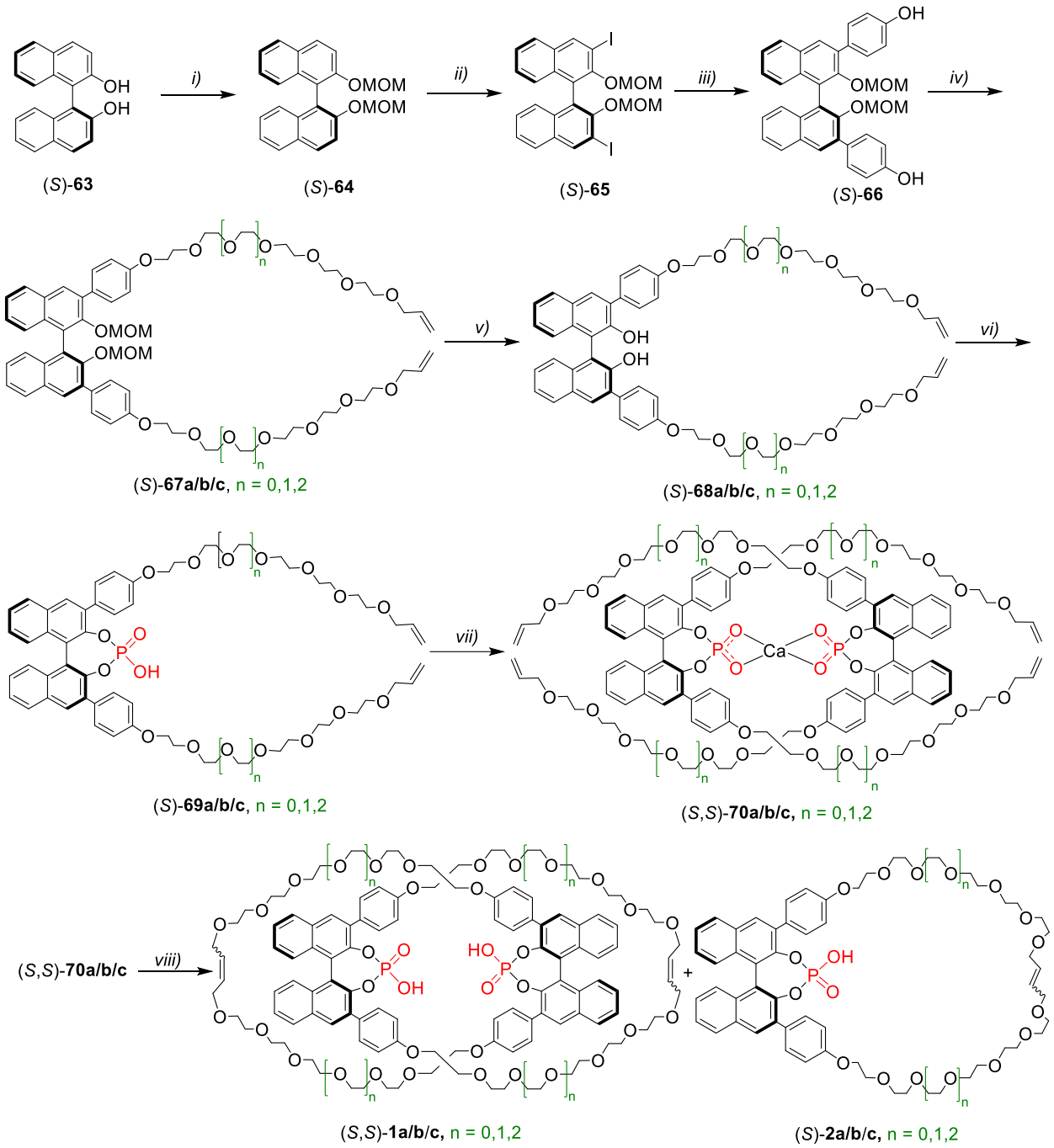

Figure 41: Synthesis of catenanes (*S*,*S*)-**1a/b/c** and macrocycles (*S*)-**2-a/b/c**. Reagents and conditions: *i*) 2.2 equiv. MOM-Cl, 2.2 equiv. NaH, tetrahydrofuran 96%; *ii*) 3 equiv. *n*-buthyllithium, 3 equiv. iodine, tetrahydrofuran 70%; *iii*) 4 equiv. 4-hydroxyphenylboronic acid, $Pd(Ph_3)_4$, Na_2CO_3 (2M), dimethoxyethane 74%; *iv*) 2.5 equiv. *O*-allyl-pentaethylene glycol tosylate, *O*-allyl-hexaethylene glycol tosylate, *O*-allyl-heptaethylene glycol tosylate, 5 equiv. K_2CO_3, 80 °C, acetonitrile 64/51/67% ; v) Amberlyst 15, reflux, tetrahydrofuran/methanol 92%; v*i*) $POCl_3$, pyridine, 60 °C, then H_2O, 93%; *vii*) 0.5 equiv. $Ca(OMe)_2$, toluene 88/99%; *viii*) Grubbs-II catalyst, dichloromethane, purification on RP-18, then washing with HCl (2M) (3%/10% for **1a**/**c** and 10%/16% for **2a**/**c**).

3.5 Methods for the kinetic investigation of the transfer hydrogenation of 2-phenylquinoline

3.5.1 Preliminary remarks

This chapter aims to elucidate the reaction mechanism of the transfer hydrogenation of 2-phenylquinoline catalysed by different phosphoric acid catalysts through kinetic investigations.

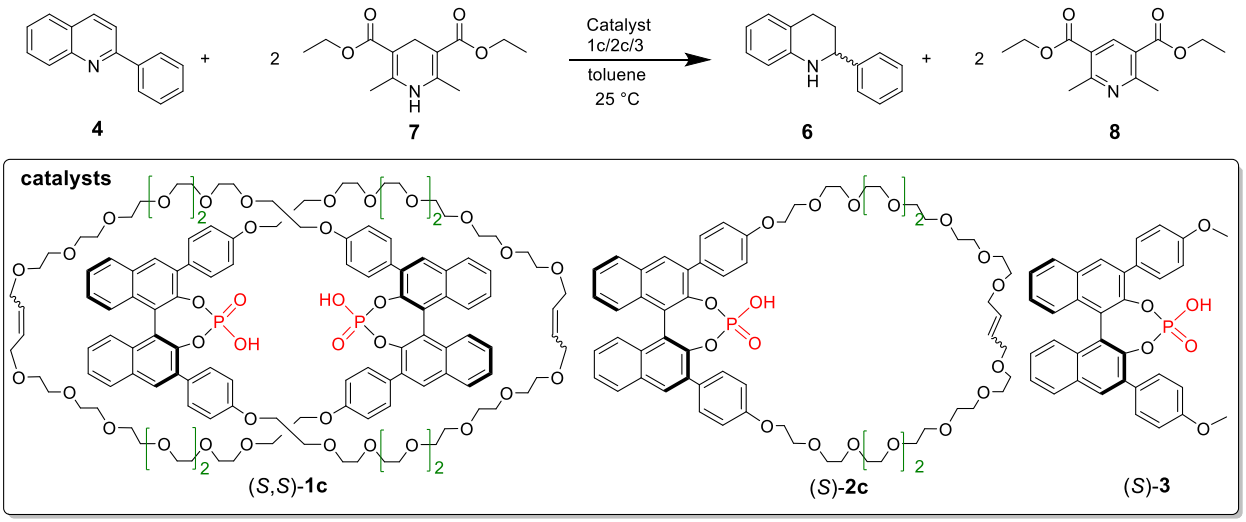

Figure 42: Focus of investigations in this chapter: Transfer hydrogenation of 2-phenylquinoline with Hantzsch ester catalysed by catenated catalyst **1c**, macrocyclic catalyst **2c** or acyclic catalyst **3**.

Special focus lays on intramolecular and intermolecular acid-acid interactions of the catalysts and their impact on reaction rates.

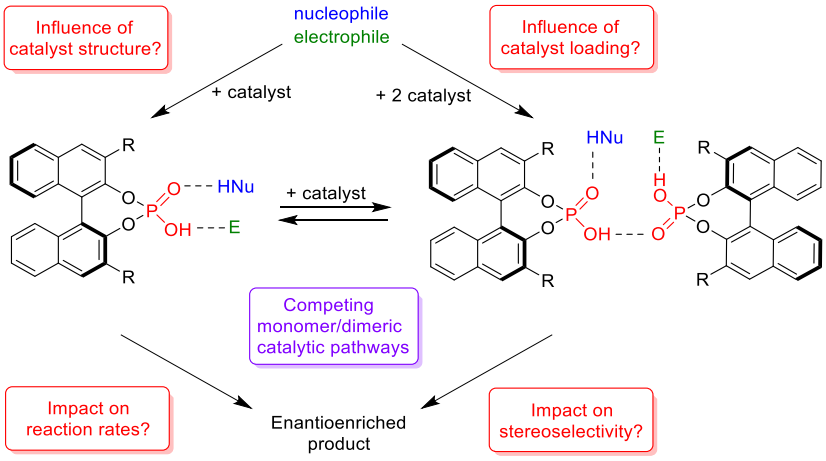

Figure 43: Overview of the key points of investigation.

As proposed in previous DFT calculations[35] this reaction can proceed via two different pathways, one containing a monomeric phosphoric acid and one containing a dimeric phosphoric acid. These calculations can explain the different stereoselectivities for the different catalysts and also propose that the two pathways have different activation energies, which ultimately lead to different reaction rates.

Therefore, classical kinetic analyses (graphical approach and initial rates method) are applied to obtain reaction rate constants, initial reaction rates and substrate/catalyst orders as well as variable time normalization analysis (VTNA) to check for product inhibition/catalyst deactivation. Substrate and catalyst orders are also acquired by VTNA. This allows the comparison of classical kinetic analysis with VTNA.

In addition to the three catalyst (acyclic phosphoric acid **3**, macrocyclic phosphoric acid **2c** and catenane **1c**) which are compared among each other, different sized catenanes (*S*,*S*)-**1a**/**b**/**c** will also be compared.

3.5.2 Method development

To conduct the kinetic measurements an appropriate method has to be established first. To reduce the mathematical treatment needed to apply the kinetic analysis methods mentioned before, an integral method is more favourable than a differential method. One major problem in following the reaction is that five different aromatic compounds are present in the reaction mixture at the same time. Due to high similarity of their spectra and therefore overlapping of signals, FTIR and UV/VIS measurements were ruled out as analytical methods. High performance liquid chromatography (HPLC) in combination with a UV/VIS detector is able to separate each of the compounds within the mixture and can be conducted with very little material. However, withdrawing samples and preparing them for HPLC analysis is an effortful procedure (note: to stop the reaction after withdrawal, the catalyst has to be removed from the reaction mixture chromatographically) and leads to the circumstance that a data point is acquired only every few minutes. This is especially impractical when the reaction proceeds very quickly.

^{1}H-NMR spectroscopy allows for acquisition of one data point about every 1 minute, depending on the settings. Comparing the spectra of all components, including the catalyst, revealed a clearly distinguished signal at 8.24 ppm that corresponds to two protons of the 2-phenylquinoline. Thus, the decrease in this substrate can be observed.

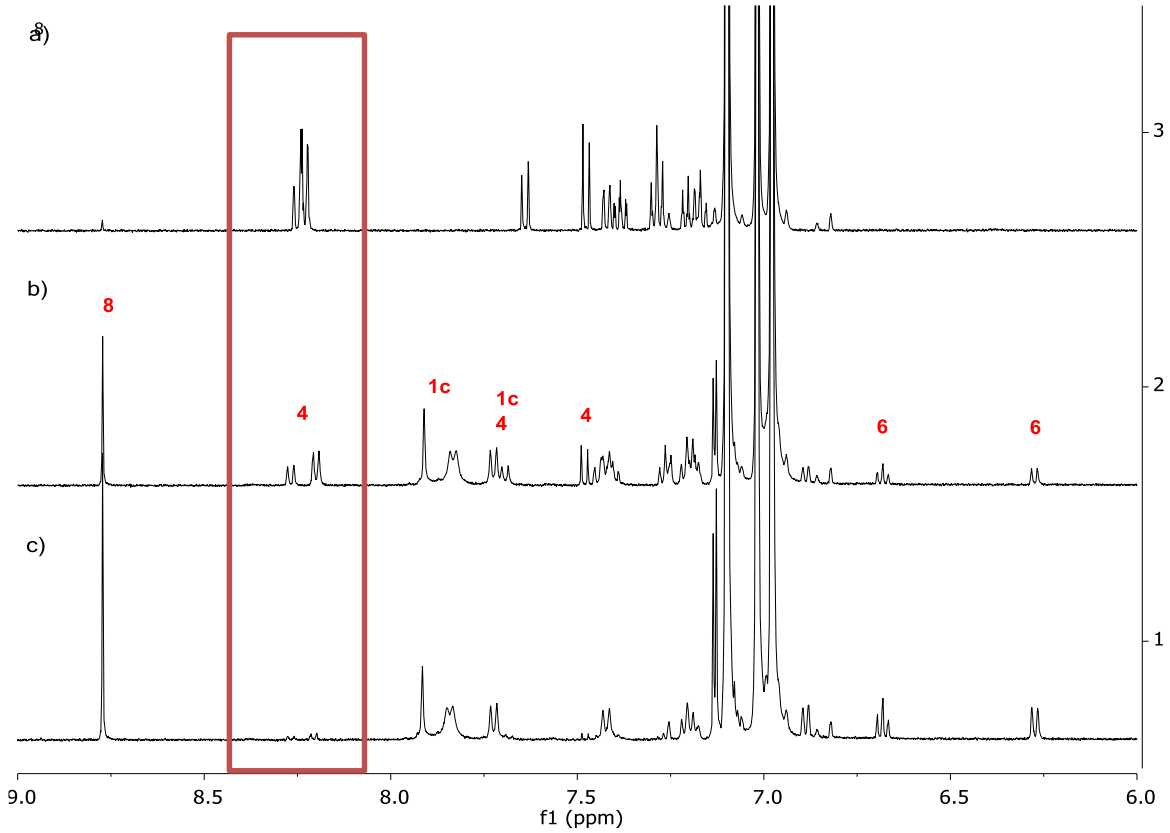

Figure 44: Aromatic region of a ^{1}H-NMR spectrum of a representative reaction mixture (34 mol% of 1-c as catalyst) at different times: a) Before catalyst addition, b) 49 % conversion, c) 94 % conversion. The highlighted signal at 8.30 - 8.14 ppm corresponds to three protons of **4**.

There are, however, some disadvantages that accompany the analysis by ^{1}H-NMR spectroscopy. Deuterated toluene is very expensive and Hantzsch ester **7** is slowly oxidized by air, which makes it more difficult to reuse stock solutions for further reactions. In addition, Hantzsch ester **7** is not well soluble in toluene (ca. 5 mM). While this is usually no problem in catalysis (the mixture can be slightly inhomogeneous in the beginning), measuring inhomogeneous solutions in NMR spectroscopy can lead to bad quality of the spectra.

Despite these problems, ^{1}H-NMR proved to be a suitable method. The concentrations were lowered compared to the conditions used in previous experiments[35] (1.66 mM vs 5 mM quinoline) to ensure full homogeneity of the reaction mixture. The quality of the spectra (i.e. signal-to-noise ratio) was sufficient even at these low concentrations.

As already stated above, the speed in which data points are acquired can be adjusted by carefully choosing the settings. For this, trials with different settings were carried out. The best trade-off between spectrum quality and speed of measurement was achieved by only shimming the sample before addition of the catalyst instead of before every measurement (note: This spectrum also served as the starting point of the concentration vs. time curve; referred to as t_0), leaving out dummy scans and lowering the relaxation delay to 2 seconds. For very fast reactions the number of scans was reduced to 10. These modifications allowed to take data points by ^{1}H-NMR about once every minute, which is especially important for reactions that are finished within only a few dozens of minutes.

3.5.3 Data processing and further analysis

With the optimised settings in hand, acquisition of a series of ^{1}H-NMR spectra was conducted to follow the transfer hydrogenation of 2-phenylquinoline with Hantzsch ester catalysed by either the acyclic phosphoric acid **3**, macrocyclic catalyst **2c** or catenated catalysts **1a/b/c**.

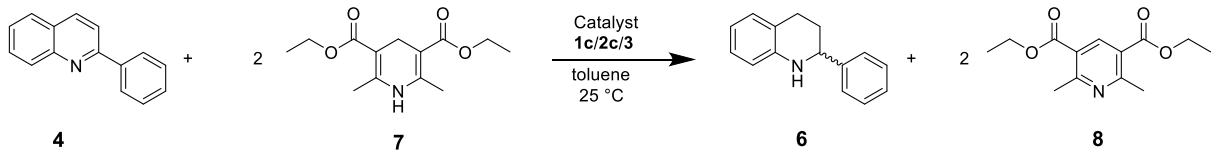

Figure 45: Transfer hydrogenation of 2-phenylquinoline **4** with Hantzsch ester **7**.

To ensure reproducibility and comparability amongst the different catalysts, raw data from the series of NMR spectra were strictly handled following a protocol, which included Fourier transformation, baseline correction and phase correction. This protocol was carried out using TopSpin version 4.0.6 for all raw data obtained in this kinetic investigation. A representative spectrum of a reaction mixture, that was treated according to this protocol is shown below. Some of the signals are assigned to the respective molecule.

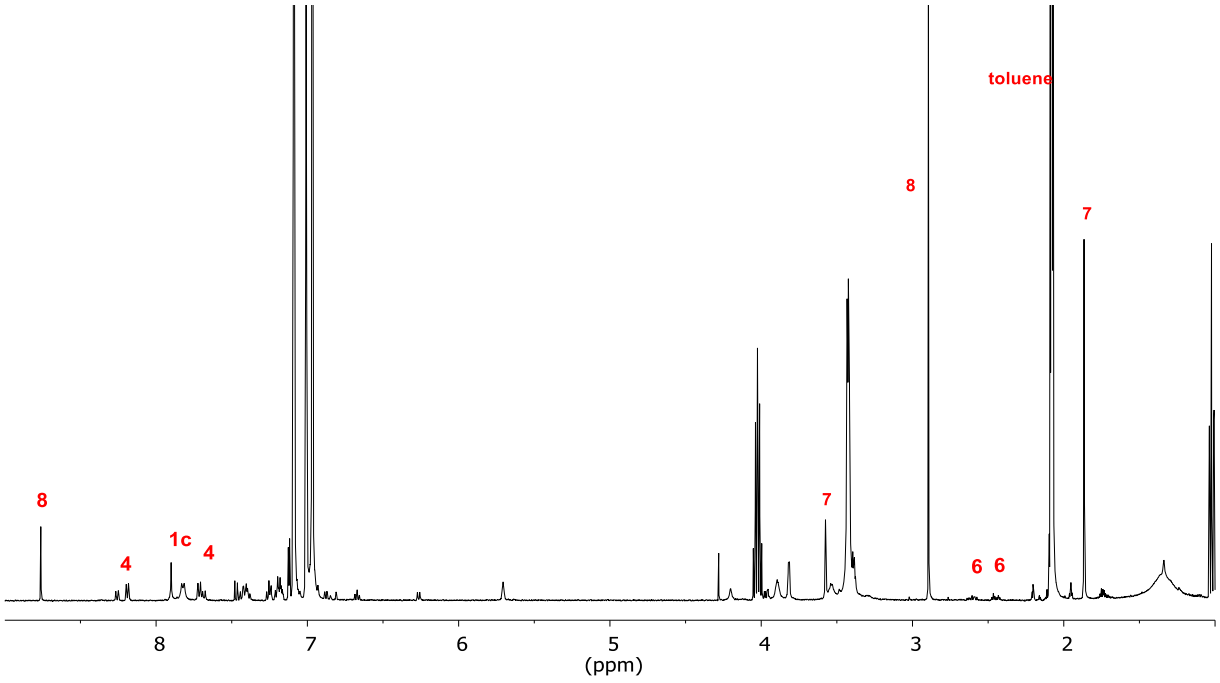

Figure 46: Representative ^{1}H-NMR spectrum of a reaction mixture showing signals for the starting materials **4** and **7**, the catalyst **1c** and products **6** and **8** ([D_8]-toluene, 500 MHz, 298 K).

In the spectrum several indicative signals for the different species present in the reaction mixture are labelled. Next to the assignment of these signals it is very important to determine the integral of each signal to properly convert the change in integral to a change in concentration. The assigned signals as well as their integral region and the number of protons that correspond to each signal are list below. It has to be to noted that the order of signals is different for the acyclic phosphoric acid **3**, because it lacks the distinct signals

in that region for protons at 4,4'-positions of the binaphthyl backbone. For the acyclic phosphoric acid **3** the signal for the methyl groups was used instead. Therefore, two tables, one for **2c** and **1c** and one for **3**, exist.

Table 2: Integrals of separate signal when using catenane **1c** or macrocycle **2c** as catalyst ([D_8]-toluene, 500 MHz, 298 K).

No. of Signal	Integral region	Compound	Number of protons
0	8.80 – 8.74	**8**	1H
1	8.30 – 8.14	**4**	3H
2	7.96 – 7.78	**1c/2c**	12H/6H
3	7.75 – 7.61	**4**	1H
4	3.61 – 3.56	**7**	2H
5	2.93 – 2.86	**8**	6H
6	2.66 – 2.55	**6**	1H
7	2.50 – 2.41	**6**	1H
8	2.11 – 2.04	**toluene**	9H
9	1.89 – 1.84	**7**	6H

Table 3: Integrals of separate signal when using acyclic phosphoric acid **3** as catalyst ([D_8]-toluene, 500 MHz, 298 K).

No. of Signal	Integral region	Compound	Number of protons
0	8.80 – 8.74	**8**	1H
1	8.30 – 8.14	**4**	3H
2	7.75 – 7.61	**4**	1H
3	3.61 – 3.56	**7**	2H
4	3.42 – 3.30	**3**	6H
5	2.93 – 2.86	**8**	6H
6	2.66 – 2.55	**6**	1H
7	2.50 – 2.41	**6**	1H
8	2.11 – 2.04	**toluene**	9H
9	1.89 – 1.84	**7**	6H

When it comes to choosing which signal to trace to create the concentration vs. time curve, either the decrease in signal 1 (2-phenylquinoline) or the increase in signal 6 or 7 (2-phenyl-tetrahydroquinoline) can be followed. Due to the oxidation of Hantzsch ester by air, following of compound **7** or **8** were ruled out. The most important part of the conversion curve is the beginning, because initial rates are determined at these positions. Since the concentration of product (i.e. signal 6 and 7) is very low at the beginning, the signal to noise ratio is high resulting in a big uncertainty in initial rates. This is why signal 1 was chosen to be followed. The amount of 2-phenylquinoline was determined by the amount that was added to the NMR

tube. Stock solution were used to increase the accuracy of this method and were prepared freshly on each day of measurements. This was especially important for the stock solution of Hantzsch ester, since it can be oxidized significantly by air overnight. To further increase accuracy and reproducibility stock solutions were used for up to four different measurements on the same day.

After acquisition of processed data from the spectra, classical kinetic analysis as well as visual kinetic analysis was used to extract kinetic relevant data.

3.5.4. Classical kinetic analysis

In this subchapter two different classical methods, namely graphical approach and initial rates method (see chapter 3.3) are described. These methods were used to obtain catalyst dependent reaction rate constants k_{obs} as well as initial rates v_0. In addition, determination of reaction orders is carried out, which is later compared to the orders obtained by VTNA.

3.5.4.1 Classical kinetic analysis – graphical approach

This approach relies on linearizing the rate law, which then allows a read out of catalyst dependent reaction rate constants k_{obs} from the slope. To achieve linearization, the orders in Hantzsch ester and quinoline have to be obtained by guessing. The correctness is verified by the linear nature of the resulting linearization plot.

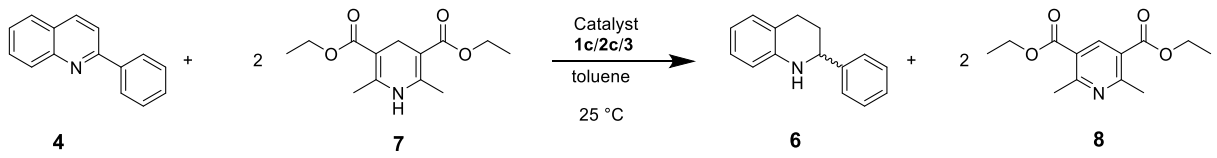

Figure 47: Transfer hydrogenation of 2-phenylquinoline **4** with Hantzsch ester **7**.

The rate law of this reaction can be written as:

$$-\frac{d[4]}{dt} = k_{obs} * [4]^m * [7]^n = k * [cat]^p * [4]^m * [7]^n$$

The following linearization was carried out assuming first order in both, Hantzsch ester and quinoline (m = n = 1). Therefore, the concentration of **7** can be expressed as:

$$[7] = [7]_0 - 2 * ([4]_0 - [4]) = [7]_0 - 2 * [4]_0 + 2 * [4]$$

This allows to write the initial concentrations ($[7]_0 - 2 * [4]_0$) as a constant c, so the equation now reads:

$$-\frac{d[4]}{dt} = k_{obs} * [4] * (c + 2 * [4])$$

$$\frac{d[4]}{[4] * (c + 2 * [4])} = -k_{obs} * dt$$

Partial fraction decomposition with x = [4] gives:

$$\int \frac{dx}{x*(c+2x)} = \frac{1}{c} * \int \frac{1}{x} - \int \frac{2}{2x+c} dx = \frac{1}{c}(\ln(x) - \ln(2x+c))$$

Integration from $[4]_0$ to [4] and $t_0 = 0$ to t gives:

$$\frac{1}{c}(\ln([4]) - \ln([4]_0) - \ln(2*[4]+c) + \ln(2*[4]_0+c)) = -k_{obs} * t$$

Bringing the equation into a linear form yields:

$$\frac{1}{c}\ln(\frac{[4]*(2*[4]_0+c}{[4]_0*(2*[4]+c)}) = -k_{obs} * t$$

$$\frac{1}{c}\ln(\frac{[4]*[7]_0}{[4]_0*(2*[4]+c)}) = -k_{obs} * t$$

This equation allows a plot which is in a linear form of y = mx + n. By plotting $\frac{1}{c}\ln(\frac{[4]*[7]_0}{[4]_0*(2*[4]+c)})$ against t, $-k_{obs}$ can be obtained from the slope. In addition to substrate orders of 1, two more linearizations were carried out (according to table 1, chapter 3.2), where each one of the substrates order is zero. The plots of all three cases are shown below (***Figure 48***). For graphical reasons in the first case the caption of the y-axis is changed to $y = \frac{1}{c}\ln(\frac{[4]*[7]_0}{[4]_0*(2*[4]+c)})$.

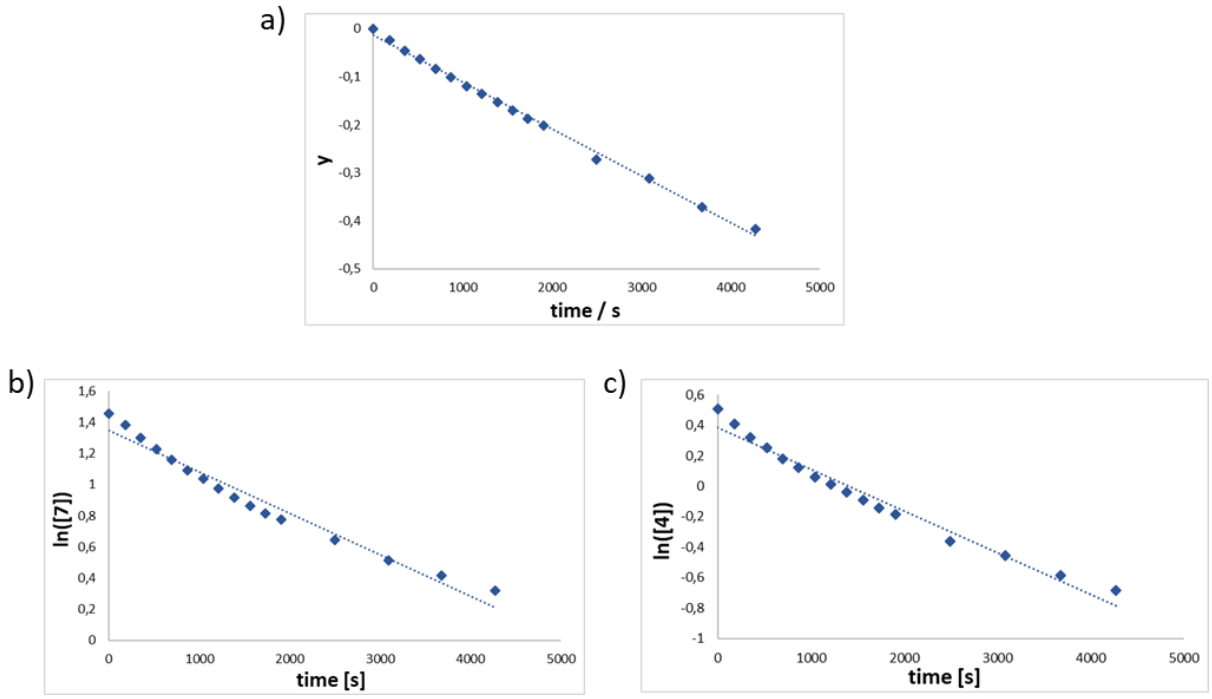

Figure 48: Linearization plots for different reaction order for quinoline 4 (m = order) and Hantzsch ester 7 (n = order). a) n=1 and m=1 b) n=1 and m=0 c) n=0 and m=1.

Both plots where the order in one substrate is zero do not show a linear behaviour, but a distinctive curvature. Good linearity is only obtained for orders of 1 for both substrates for this representative example. The slight deviation from the linear form can have several reasons, such as the oxidation of Hantzsch ester by air, relatively high deviations in the data points after linearization (i.e. heteroscedasticity) or that the true

order in substrate is a fractional value close to 1. Similar results were obtained for the other series of reactions.

3.5.4.2 Classical kinetic analysis – initial rates methods

The initial rates method was used to obtain initial rates v_0 as well as the catalyst dependent reaction rate constant k_{obs}. This allows comparison of the two classical kinetic methods, since with both methods k_{obs} is determined. In addition to that, determination of reaction orders was achieved by reading the slope of a $\ln(v_0)$ vs. ln(initial concentration) plot. Initial rates can be obtained from the original concentration vs. time plot as well, however, small deviations can lead to big errors, so a non-linear fit is used to increase the quality of the data. For this the rate law has to be solved for the concentration of quinoline [**4**]. Since the linearization of the rate law with reaction orders of 1 produced good results, this equation was used as a starting point.

$$\frac{1}{c}\ln\left(\frac{[4]*[7]_0}{[4]_0*(2*[4]+c)}\right) = -k_{obs}*t$$

$$\frac{[4]*[7]_0}{[4]_0*(2*[4]+c)} = e^{-k_{obs}*t*c}$$

$$\frac{[4]}{(2*[4]+c)} = \frac{[4]_0*e^{-k_{obs}*t*c}}{[7]_0}$$

$$\frac{1}{\left(2+\frac{c}{[4]}\right)} = \frac{[4]_0*e^{-k_{obs}*t*c}}{[7]_0}$$

$$\frac{c}{[4]} = \frac{[7]_0}{[4]_0*e^{-k_{obs}*t*c}} - 2$$

$$\frac{c}{[4]} = [7]_0 - \frac{2*[4]_0*e^{-k_{obs}*t*c}}{[4]_0*e^{-k_{obs}*t*c}}$$

$$\frac{c}{[4]} = -\frac{[7]_0*e^{-k_{obs}*t*c} - 2[4]_0}{[4]_0}$$

$$\frac{[4]}{c} = -\frac{[4]_0}{[7]_0*e^{-k_{obs}*t*c} - 2[4]_0}$$

$$[4] = -\frac{[4]_0*c}{[7]_0*e^{-k_{obs}*t*c} - 2[4]_0}$$

This equation was plotted using Microsoft Excel. The only variable in this is k_{obs} which can be varied to obtain the best fit to the experimental data. The best fit was defined via the sum of square residues for [**4**], which was minimized using the SOLVER plugin. Due to oxidation of Hantzsch ester which alters the conversion curve in later reaction times, it is necessary to define a maximum time (t_{max}) in which the fit is applied.

Table 4: The non-linear fit is applied from t_0 to t_{max} with different definitions for t_{max} based on conversion of **4** for the different catalyst.

Catalyst	t_{max}
Catenane **1c**	70 % conversion or maximum of 10 hours
Macrocycle **2c**	70 % conversion
3 ([**3**] < 0.2 mM)	70 % conversion
3 (0.2 mM < [**3**] < 0.8 mM)	90 % conversion
3 ([**3**] > 0.8 mM)	95 % conversion

With a protocol for the nonlinear fit in hand, the initial rates were determined by measuring the slope of the first three data points. K_{obs} from the non-linear fit gave almost identical results as the values obtained by linearization, which verifies that both methods are suited to obtain kinetic data for the transfer hydrogenation of 2-phenylquinoline by Hantzsch ester. Both methods are visualized in the following figure (***Figure 49***).

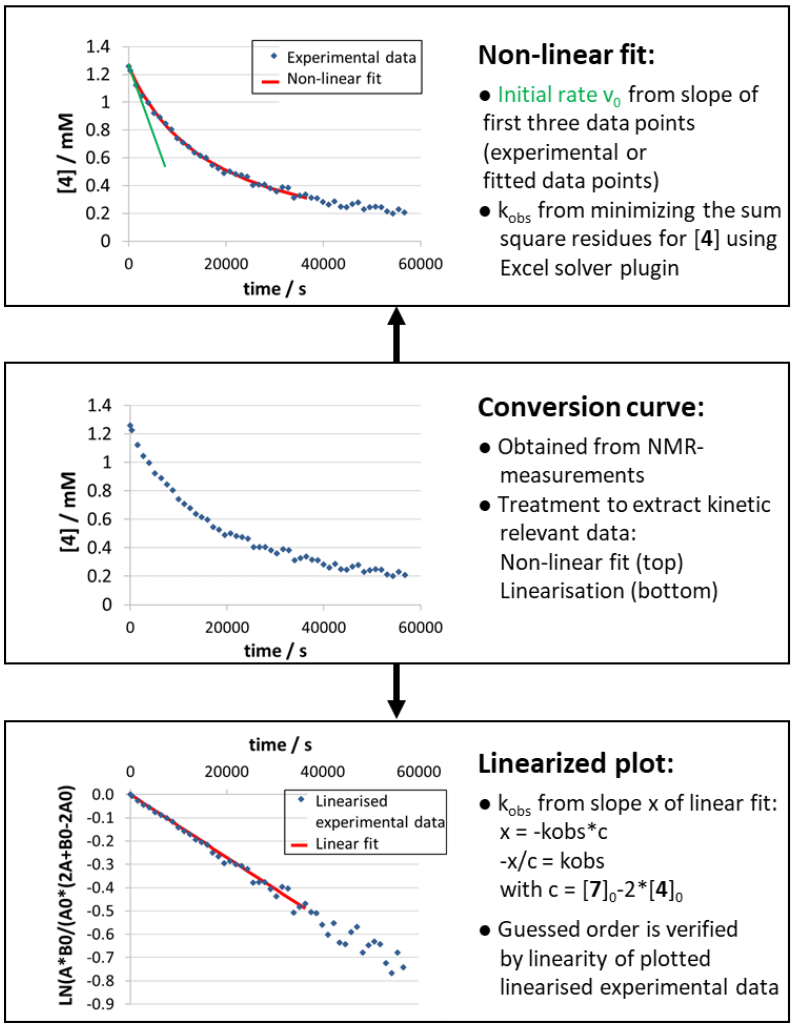

Figure 49: Overview of treatments of experimental data to obtain kinetically relevant data within classical kinetic analysis.

3.5.5 Variable time normalization analysis

As described in chapter 3.3.2, Variable time normalization analysis is relatively new and powerful tool to extract kinetic data out of the obtained curve of conversion with only little mathematical treatment. This method has been used in this work as well to determine orders and check for catalyst deactivation/product inhibition for the reaction investigated in this chapter.

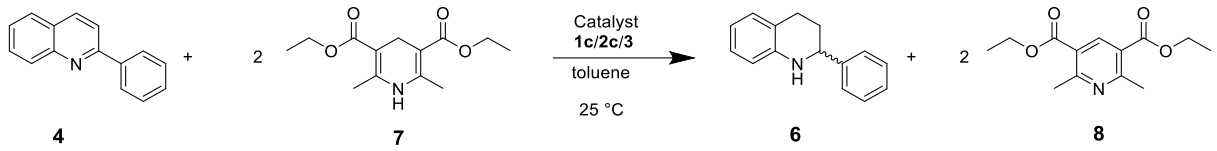

Figure 50: Transfer hydrogenation of 2-phenylquinoline **4** with Hantzsch ester **7**.

VTNA relies on same excess and different excess experiments. In case of the investigated reaction (***Figure 50***) two Hantzsch ester molecules are needed to convert one quinoline molecule. To take this stoichiometry into account, a factor of 0.5 for the Hantzsch ester applied when defining the excess:

$$excess = 0.5 * [7]_0 - [4]_0$$

Determination of substrate orders for 4/7

To determine the order in substrates **4** and **7** via VTNA, a normalized time axis t(norm) has to be calculated. This was done using the following equation.

$$t_{x+1}(norm) = t_x(norm) + (0.5 * ([A]_x + [A]_{x+1})^y * (t_{x+1} - t_x)$$

In this equation $[A]_x$ describes the concentration of **4** or **7** (depending on which order is determined) at time point x and $[A]_{x+1}$ the concentration at time x+1. Y is to substituted by the substrate order, that is being determined (m for **4**, n for **7**). Plotting of experimental data of different excess experiments according to the normalized time axis leads to determination of the respective substrate order by variation and checking for the best overlap for all reaction profiles.

Determination of catalyst orders

The order in catalyst was also determined using VTNA for all three catalysts. For this a series of experiments with varying catalyst concentrations was carried out. Each reaction was plotted as concentration in quinoline [**4**] vs. t(norm) which is defined as:

$$t_x(norm) = \frac{t_x}{[Cat]^p}$$

Again, the order is obtained by variation of the value (in this case p) until the best overlap of all plots is achieved.

Determination of product inhibition/catalyst deactivation

To check for product inhibition and catalyst deactivation series of same excess experiments with different initial concentrations for **4** for all three catalysts were carried out.

For this, concentration vs. time profiles were shifted in a way that every starting point lays on the curve of the reaction with the highest initial concentration (see ***Figure 39***).

$$t_x(norm) = t_x + \Delta t$$

3.6 Influence of catenane ring size on reaction rate and stereoselectivity

In catalysis the ring size of a catenated catalyst could potentially have an influence on the outcome of the reaction. Very small rings could decrease the co-conformational flexibility thus locking the catenane in a position that is unfavorable for cooperative catalysis. On the other hand, the rings of a catenane could potentially be so big that the influence of the mechanical bond on functional groups interactions between the two macrocycles becomes less significant.

To investigate this, catenanes with ten, twelve[131] and fourteen ethylene glycol units per macrocycle are being used to catalyze the transfer hydrogenation of 2-phenylquinoline.

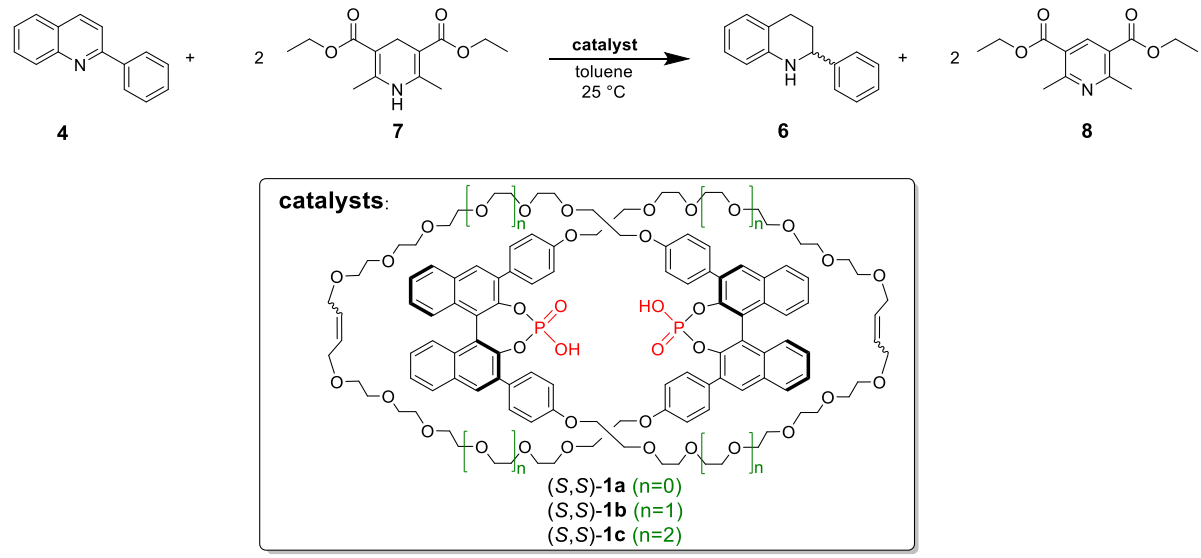

Figure 51: Transfer hydrogenation of 2-phenylquinoline using three different sized catenated catalysts.

Stereoselectivities using the different sized catenanes were already studied during the master thesis.[128] In these experiments no major difference in enantiomeric excesses was obtained (79% - 82 % *ee*).

Possible explanations are that the geometries of the transition states are not affected by adding or removing only two ethylene glycol units per macrocycle as the change in macrocycle size is relatively small or that the diastereomeric transition states are influenced in a similar fashion, so that kinetic selectivity is unaltered.

Effects on the initial reaction rates, however, were more pronounced for the reaction using the different sized catenanes.

[131] R. Mitra, M. Thiele, F. Octa-Smolin, M. C. Letzel, J. Niemeyer, *Chem. Commun.* **2016**, *52*, 5977–5980.

Table 5: Initial rate obtained from the nonlinear fit using the three different sized catenanes **1a/b/c** as catalysts.

Catalyst	v_0 (10^{-7} M s^{-1})	Enantiomeric excess (%)
1a	3.7	81
1b	3.1	79
1c	2.0	82

The results clearly show, that the reaction rate decreases with increasing numbers of ethylene glycol units.

One possible explanation for this is that the ethylene glycol units reduce catalyst activity through intramolecular hydrogen bonding of the phosphoric acid proton with the free lone pair of the oxygen of the ethylene glycol chain, as found a DFT-calculated structure of the macrocyclic catalyst.[35] Because this interaction is of multivalent nature, additional ethylene glycol units in larger rings therefore strengthen this effect, leading to a further decrease in reaction rate.

3.7 Kinetic analysis of the first reduction step

3.7.1 Product inhibition and catalyst deactivation

There is the possibility that the products that are formed during the transfer hydrogenation strongly bind to the catalyst and therefore act as inhibitors. This would have an influence on the reaction rate in the rate law that has to be considered. Another source that can alter the reaction rate is catalyst deactivation, which can happen if for example the catalyst degrades in the course of the reaction under the given conditions. To ensure the reaction rate is not influenced by these two phenomena, same excess experiments are carried out with each catalyst. The concentration profiles are plotted as explained in chapter 3.3.2 using VTNA.

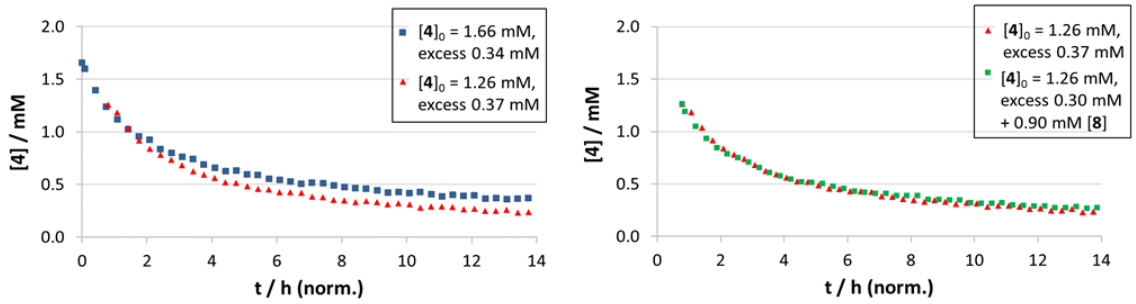

Figure 52: Plots obtained from same excess experiments using catenane **1c** without (left) and with added product (right).

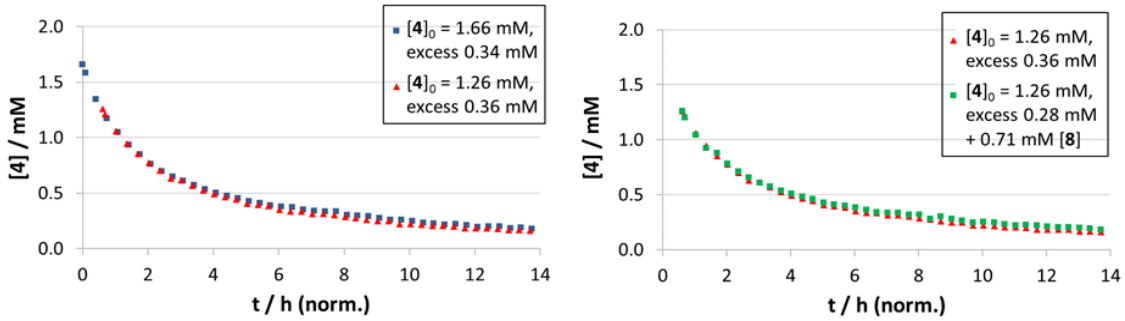

Figure 53: Plots obtained from same excess experiments using macrocycle **2c** without (left) and with added product (right).

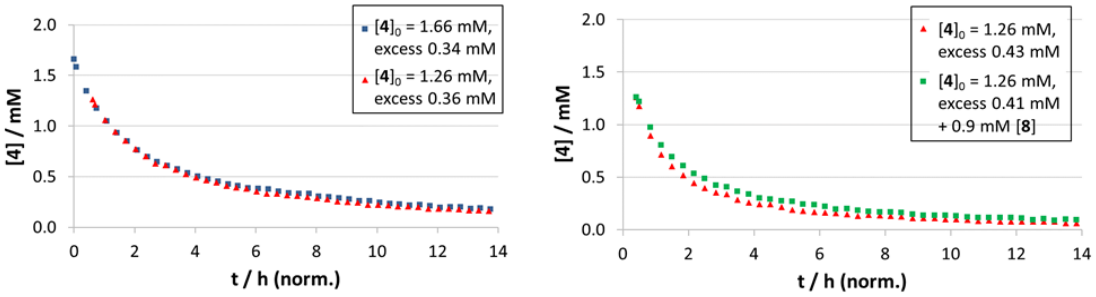

Figure 54: Plots obtained from same excess experiments using catalyst **3** without (left) and with added product (right).

In all three cases the plots overlay to an extend that it can be concluded that no product inhibition or catalyst deactivation is present. Small deviations (e.g. in catenane case) most likely stem from a small difference in catalyst loadings (6.8 mol% for blue curve vs 9.0 mol% for red curve) and are not significant enough to conclude that product inhibition or catalyst deactivation are present.

3.7.2 Substrate orders

In the following subchapter the substrate orders of quinoline **4** and Hantzsch ester **7** with each catalyst are determined by VTNA and partly by the initial rates method of classical kinetic analysis.

Substrate orders using catenane 1c as catalyst

To obtain the substrate order for quinoline **4**, experiments at four different initial concentrations of quinoline **4** (0.63 mM, 0.84 mM, 1.26 mM, 1.66 mM) and constant concentration of Hantzsch ester **7** (3.93 mM) were performed. To determine the substrate order for Hantzsch Ester **7** four different excess experiments were carried out, where the concentration of quinoline was kept constant (0.83 mM) and the concentration of Hantzsch ester **7** was varied (1.99 mM, 2.66 mM, 3.32 mM, 3.93 mM). The resulting ln(v_0) vs ln([substrate]) plots gave linear graphs with only small deviations (***Figure 55***).

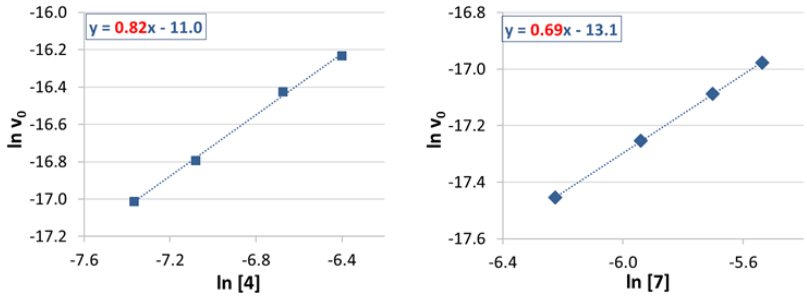

Figure 55: Double ln-plots to determine the substrate order of **4** and **7** using the initial rates method.

The substrate order can be derived from the slope of each graph. For the quinoline **4** the reaction order is 0.82 and for the Hantzsch ester **7** it is 0.69. For a more direct read-out of the reaction order from the processed conversion curve VTNA analysis was used. For this the data from the different excess experiments was reused.

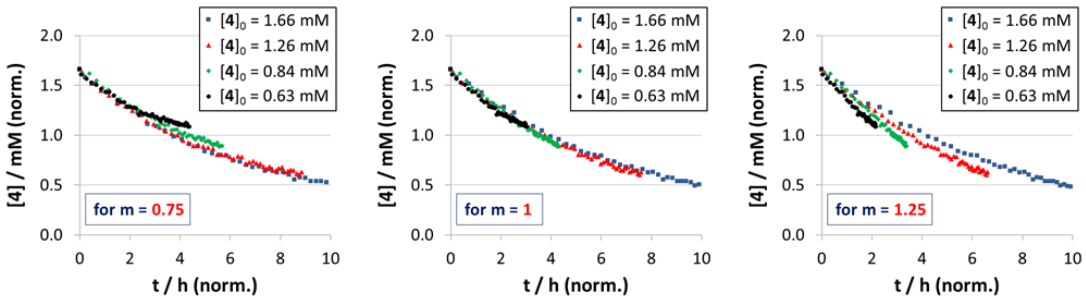

Figure 56: Determination of substrate order m for quinoline 4 using VTNA analysis.

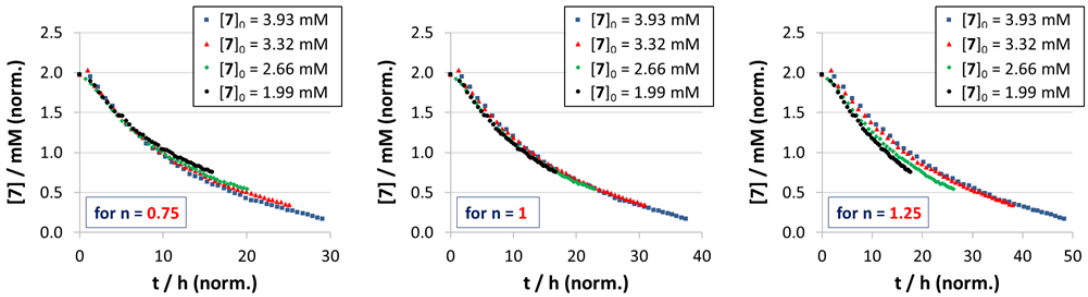

Figure 57: Determination of substrate order n for Hantzsch ester **7** using VTNA analysis.

Best overlaps were found for a reaction order of 1 for both, the quinoline as well as the Hantzsch ester. Since classical kinetic analysis and visual kinetic analysis were used the results of both methods can be compared among each other.

Even though there is a small difference of about 0.2 for quinoline **4** and 0.3 in the case of Hantzsch ester **7,** the results are in a very similar region. Thus the true substrate order in quinoline **4** is in the region between 0.8 and 1 while the true substrate order in Hantzsch ester **7** is between 0.7 and 1.

Considering that in VTNA the results were obtained from the conversion curves after a simple mathematical treatment of the time axis and a quick screening for the right order, it has to be noted that VTNA is the quicker method to determine reaction orders for this reaction. In addition to the graphically appealing presentation, the amount of different excess experiments can be further reduced if the orders are determined solely by VTNA.

Substrate orders using macrocycle 2c and acyclic acid 3 as catalyst

Since VTNA grants access to the substrate orders with fewer experiments and with less processing of the raw data, the substrate order of quinoline and Hantzsch ester were determined by VTNA only. Again, different excess experiments using two different concentrations were carried out, where one concentration was kept constant (3.98 mM **7** for determination of m; 1.26 mM **4** for determination of n) while the concentration of the other substrate was varied (1.66/1.26 mM for determination of m; 3.24/4.02 mM or 3.37/4.42 mM for determination of n).

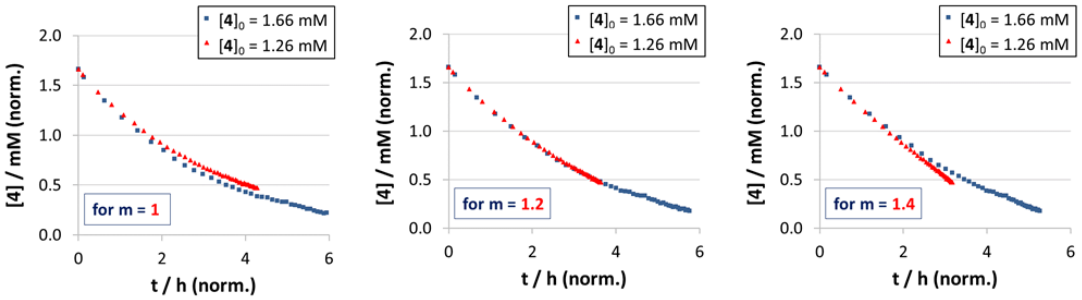

Figure 58: Determination of substrate order m of quinoline **4** by VTNA for reaction with macrocyclic catalyst **2c**.

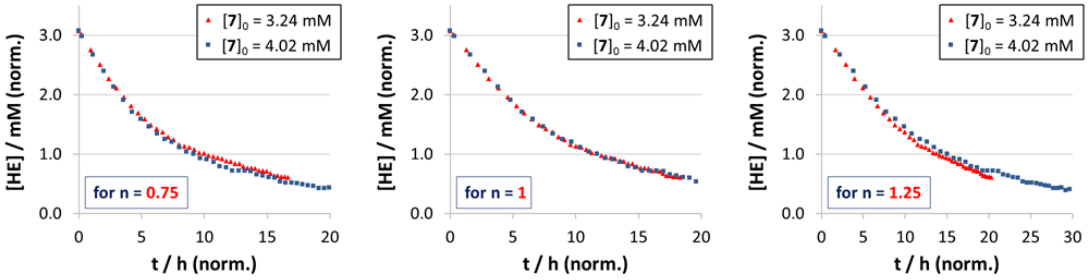

Figure 59: Determination of substrate order n of Hantzsch ester **7** by VTNA for reaction with macrocyclic catalyst **2c**.

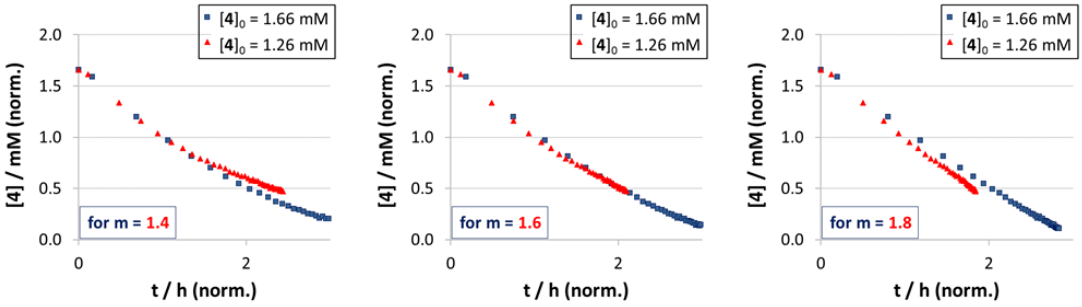

Figure 60: Determination of substrate order m of quinoline **4** by VTNA for reaction with acyclic catalyst **3**.

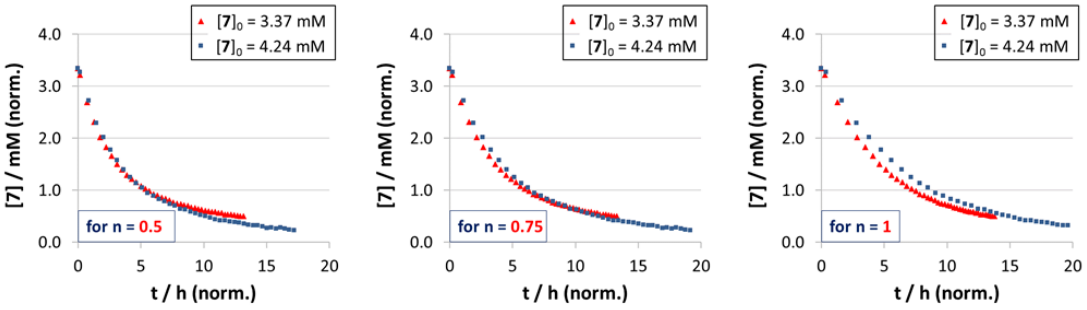

Figure 61: Determination of substrate order n of Hantzsch ester **7** by VTNA for reaction with acyclic catalyst **3**.

The substrate orders were again obtained by screening different values for the different reaction orders. Thus, this method shows that it can be of relative high accuracy. Even small differences in reaction order stand out, so that it can determined with up to 0.2 accuracy (***Figure 58***).

The substrate orders obtained for all catalysts are summarized in the following table.

Table 6: Substrate order for **4** and **7** for all three catalysts obtained by the initial rates method (for **1c**) and VTNA.

	Reaction order determined by initial rates method	**Reaction order determined by VTNA**		
	Substrate order using 1c		**Substrate order using 2c**	**Substrate order using 3**
Quinoline	0. 8	1	1.2	1.6
Hantzsch Ester	0.7	1	1.0	0.75

The reaction order of the quinoline is in the same region for the experiments with catenane **1c** and macrocycle **2c**, however when using the acyclic catalyst an order of 1.6 was obtained. Despite this big difference, this does not allow to draw conclusions about a possibly different mechanism. Rather, the difference could stem from small errors from during conducting on of the two experiments. Repeating the determination of this substrate order could further clarify this circumstance, but was not conducted during this work. In contrast to this, the orders for Hantzsch ester using the three different catalyst are closer together, being in the region between 0.7 and 1.

In summary the substrate orders do not give insight into the reaction mechanisms of the different catalysts, thus the orders of the catalysts are determined hereafter.

3.7.3 Catalyst orders and aggregation

Since the acyclic phosphoric acid **3** showed a change in stereoselectivity upon variation of the catalyst loading in the transfer hydrogenation of 2-phenylquinoline, which was attributed to a possible dimerization of this catalyst at higher catalyst concentrations, it is of high interest to examine the reaction with this catalyst kinetically.[35]

When examining the kinetics regarding the catalysts, there are two aspects to consider. Firstly, examining the development of the reaction rate at different catalyst loadings should give a linear correlation (e.g. double catalyst loading should have double the reaction rate for a catalyst order of 1) when the mechanism does not change upon changing the catalysts concentration. The second aspect is the reaction order of the catalyst. Similar to the reaction rate, the reaction order should not change, if the mechanism is independent of the catalyst loading.

To investigate this, reactions were carried out at different concentrations of each catalyst. To get information about the influence on the reaction rate, the initial reaction rate was plotted against the catalyst loading for each catalyst (***Figure 62***).

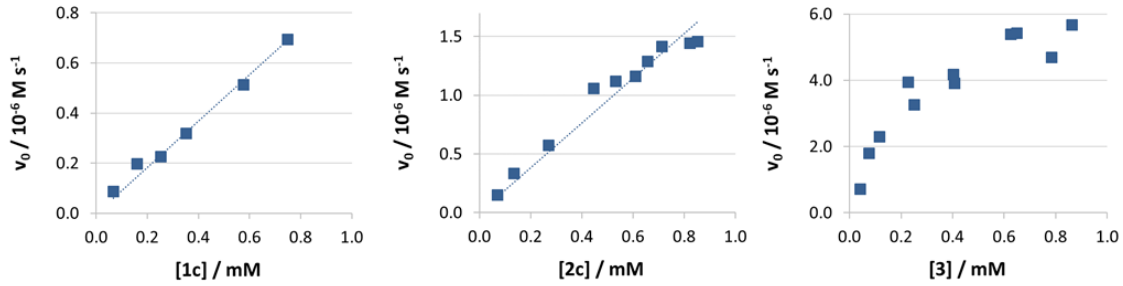

Figure 62: Initial rates vs. catalyst concentration plots for all three catalysts.

In the case of the catenated and macrocyclic catalysts a linear increase of reaction rate with increasing catalyst loading was observed, albeit a small deviation from linearity might be concluded for **2c**. This is most likely due to a consistent catalytic pathway of these catalysts. When comparing the reaction rates among the two catalysts the reaction containing the macrocycle proceeds considerably faster than the reaction with the catenane even though the catenane possess two phosphoric acid moieties per molecule. However, the reaction rates of the two catalyst cannot directly be compared, since the catenane is composed of more ethylene glycol units, which can diminish the reaction rate by sterical hindrance. In addition, the influence of the interlocked nature of the catenane on the reaction rates can also not be determined easily. One point, however, that could speak for a slower reaction with the catenane is its possibility to catalyse the reaction cooperatively (i.e. via a phosphoric acid dimer), which would be in line with a higher activation barrier for a dimeric pathway as suggested by DFT calculations.[35]

Ultimately, these circumstances do not allow a precise assignment of the two catalyst to a monomeric or a dimeric pathway.

In contrast to this, the acyclic phosphoric acid **3** shows a nonlinear behavior. While the increase in reaction rate in the low catalyst loading area (0.01 mM to 0.25 mM) is rather high, it levels off for higher catalyst loadings (0.6 mM to 0.83 mM). Reconsidering the different activation barriers for the monomeric and the dimeric catalytic pathway, this indicates that the acyclic phosphoric acid mainly reacts as a monomer at lower loadings and then starts to aggregate and react via the dimeric pathway at higher catalyst loadings.

These findings are supported by the catalyst orders. Similar to the determination of the substrate orders, the catalyst order where determined by plotting ln(v_0) against ln(catalyst) (initial rates method) as well as by VTNA analysis for the macrocycle and the catenane.

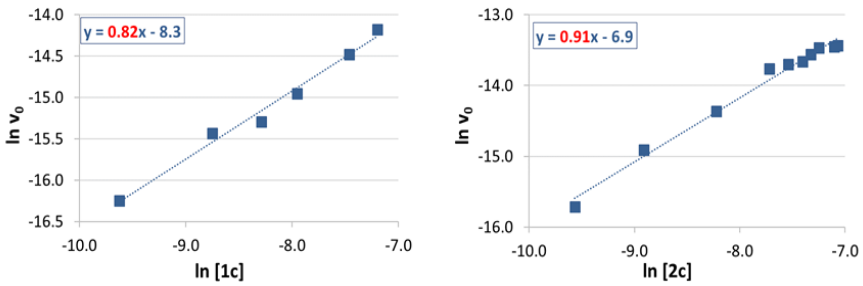

Figure 63: Double ln-plot to determine the order in catalysts **1c** and **2c** by the initial rates methods.

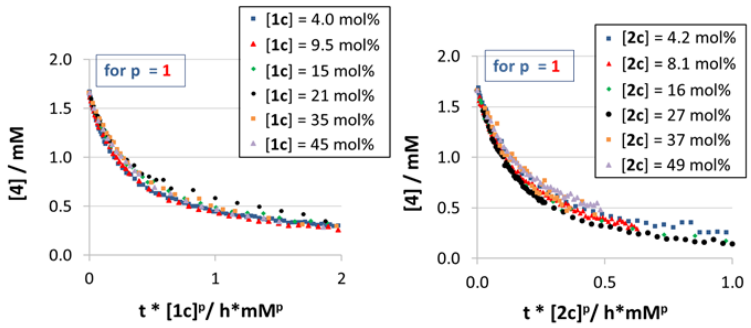

Figure 64: VTNA analysis for determination of catalyst orders for **1c** and **2c**. Only best overlaps for reaction with catenane (left) and macrocycle (right) as catalyst are shown.

Both methods result in catalyst orders of 1 for the catenated and the macrocyclic catalysts. For the macrocycle this means that the catalyst reacts mainly via the monomeric pathway, while for the catenane these results do not confirm, if the catenane reacts via monomeric or dimeric pathway, since one catenane molecule features two phosphoric acid units. Thus, interpretation of the catalyst order is more difficult and not unambiguous in this case.

When performing VTNA analysis for the acyclic phosphoric acid, the aforementioned nonlinear behavior has to be taken into account. Otherwise the different behavior at the extreme ends of catalyst loading are not considered in the determination of the catalyst order. Thus, the catalyst order was determined between a catalyst concentration of 4.5 mol% and 14 mol% as well as between 38 mol% and 52 mol%.

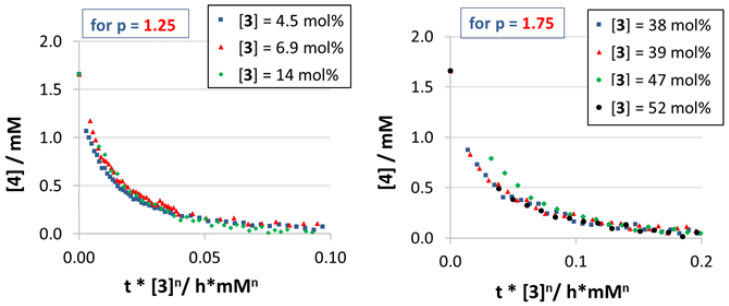

Figure 65: Catalyst order of **3** at low catalyst loadings (left) and high catalyst loadings (right). Determined by VTNA analysis.

The best overlap for low catalyst loadings was found for a reaction order of 1.25 while the best overlap for high catalyst loadings was achieved at 1.75. Whereas the first order is close to those of the other catalysts, the catalyst order at high concentrations is close to 2. As an order in catalyst greater than 1 is uncommon, this can be interpreted as more than one catalyst molecule being involved in the catalytic reaction.[132] Naturally, the concentration dependent change from a monomeric catalyst system towards a dimeric one, does not occur strictly when a certain concentration is surpassed, but rather is a fluent transition over a broad range. However, these results are sufficiently significant to conclude the aforementioned dimerization of the acyclic phosphoric acid at higher concentrations.

[132] D. G. Blackmond, *J. Am. Chem. Soc.* **2015**, *137*, 10852–10866.

3.7.4 Normalized initial rates of all three catalysts

Another way to interpret the experimental data of the three catalyst is to plot normalized initial rates (v_0/[cat]) against the catalyst loading. For a catalyst system that reacts via a single mechanism, independent of catalyst concentration, a horizontal line is expected. Moreover, the mean values express the catalyst-independent initial rates (i.e. normalized initial rate).

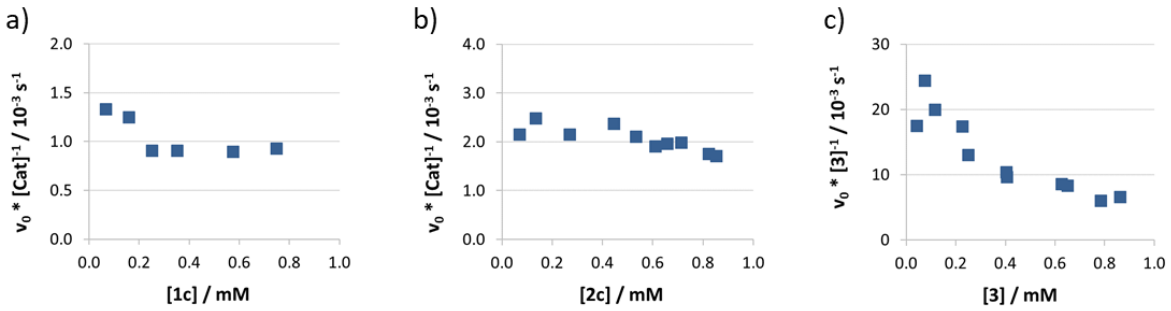

Figure 66: Normalized initial rates v_{Norm} at different catalyst concentration for a) catenane **1c** b) macrocycle **2c** c) Acyclic phosphoric acid **3**

The average normalized initial rate can be determined easily for the catenane and the macrocycle. The normalized initial rates stay almost constant in the case of catenane and macrocycle. This is different for the acyclic catalyst, for which we observe that the normalized initial rates decrease with increasing catalyst concentrations and until a plateau seems to be reached for catalyst concentrations above 0.6 mM. As found in the kinetic investigation earlier, this can be attributed to dimerization of the acyclic phosphoric acid at higher concentrations. Upon aggregation the catalytic pathway changes from the monomeric towards the dimeric pathway. This makes it impossible to determine an average normalized initial rate over the whole concentration range. Thus, a linear regression line was fitted for the first four normalized initial rates to obtain the y-intercept. This intercept represents the normalized initial rate for a fully monomeric catalyst system. To obtain the normalized initial rate for a fully dimeric catalyst system, the average of the last four points was taken, as the curve starts to reach a plateau in this region. It has to be noted, that the catalyst system is always an equilibrium between monomeric and dimeric species, so that these normalized initial rates are an approximation only. In the following table the normalized initial rates for each catalyst system are summarized (***Table 7***).

Table 7: Normalized initial rates for all three catalysts. Due to dimerization of **3,** two values (monomeric + dimeric) are necessary.

Catalyst	v_0/[Cat] (10^{-3} s^{-1})
1c	1.04
2c	2.06
3_{Di} (>0.6mM)	6.29
3_{mono}(<0.25 mM)	22.7

As already indicated by the initial rates the reaction with the catenane appears to be slower than the reaction with the macrocycle. Again, this could be explained by the higher activation energy in the dimeric pathway compared to the monomeric pathway if the catenane is able to react via the dimeric pathway. The fact that the macrocycle seems to solely react as a monomer over the whole concentration range can be explained with the ethylene glycol chain that inhibits dimerization. The normalized initial rates can also be used to estimate the influence of dimerization on the reaction rate. In the case of the acyclic phosphoric acid there is factor of about 3.6 in reaction rates between $\mathbf{3}_{\mathbf{Di}}$ and $\mathbf{3}_{\mathbf{mono}}$. This proves the higher activation energy for the dimeric pathway as it was calculated by DFT calculations.[35] Furthermore, the influence of the macrocycle can be estimated when comparing the normalized initial rates of **2c** and $\mathbf{3}_{\mathbf{mono}}$. Here we found a factor of about 11 which further confirms the big influence of the ethylene glycol chains on the reaction rates.

3.7.5 Detailed analysis for the acyclic phosphoric acid 3

To shed more light on the dimerization behavior of **3**, the v_0 vs [cat] plot is examined in more detail. For this the contribution of the two pathways of the acyclic catalyst **3** is further investigated. This can be done by using the approximation that the normalized initial rate at high concentrations reflects the dimeric pathway, while the normalized initial rate at low concentrations reflects the monomeric pathway (i.e. the y-intercept of the linear regression line). This normalized initial rate (v_{norm}) together with the catalyst concentration ([cat]) describes the reaction rate v_{max} at a given concentration as follows:

$$v_{max}(\mathbf{3}_{Mono}) = v_{Norm}(\mathbf{3}_{Mono}) * [\mathbf{3}_{Mono}]$$

$$v_{max}(\mathbf{3}_{Di}) = v_{Norm}(\mathbf{3}_{Di}) * [\mathbf{3}_{Di}]$$

The total initial rate v0 is the sum of the two single initial rates of both pathways:

$$v_0 = v_0(\mathbf{3}_{Mono}) + v_0(\mathbf{3}_{Di})$$

With the mole fractions of each species taken into account the equation reads as follows:

$$v_0(\mathbf{3}_{Mono}) = v_{max}(\mathbf{3}_{Mono}) * x_{Mono}$$

$$v_0(\mathbf{3}_{Di}) = v_{max}(\mathbf{3}_{Di}) * x_{Di}$$

$$v_0 = v_{max}(\mathbf{3}_{Mono}) * x_{Mono} + v_{max}(\mathbf{3}_{Di}) * x_{Di}$$

Solving for X_{mono} gives:

$$\frac{v_0}{v_{max}(\mathbf{3}_{Mono})} = x_{Mono} + \frac{v_{max}(\mathbf{3}_{Di})}{v_{max}(\mathbf{3}_{Mono})} * x_{Di}$$

The expression $\frac{v_{max}(\mathbf{3}_{Di})}{v_{max}(\mathbf{3}_{Mono})}$ is equal to to $\frac{v_{Norm}(\mathbf{3}_{Di})}{v_{Norm}(\mathbf{3}_{Mono})}$ which can be calculated from the experimentally obtained normalized initial rates (***Table 7***): $\frac{6.29}{22.7} = 0.277$. Additionally, x_{Di} can also be expressed as $1 - x_{Mono}$.

$$\frac{v_0}{v_{max}(\mathbf{3}_{Mono})} = x_{Mono} + 0.277 * (1 - x_{Mono})$$

$$\frac{v_0}{v_{max}(\mathbf{3}_{Mono})} = x_{Mono} + 0.277 - 0.277 * x_{Mono}$$

$$\frac{v_0}{v_{max}(\mathbf{3}_{Mono})} = 0.723 * x_{Mono} + 0.277$$

$$x_{Mono} = \frac{\frac{v_0}{v_{max}(\mathbf{3}_{Mono})} - 0.277}{0.723}$$

This equation allows the calculation of the mole fraction of catalyst that is present as a monomeric catalyst X_{Mono} as well as the mole fraction of catalyst that is bound in a catalyst aggregate of two molecules ($X_{Di} = 1 - X_{Mono}$) at a given concentration. The resulting speciation plot is depicted in ***Figure 67***.

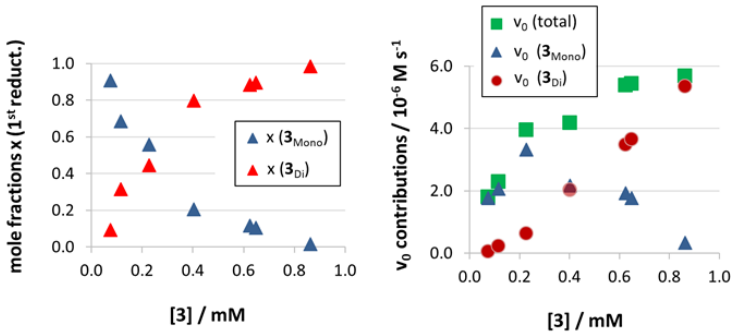

Figure 67: Speciation plot: Left: Contribution of monomeric and dimeric catalyst to the overall catalyst molecules. Right: Contribution of each of the two catalyst species towards the overall initial rate.

The speciation plot reveals that the two species are present equimolar at a catalyst concentration of about 0.2 mM. Naturally, this is only the case for the given reaction conditions (1.66 mM quinoline, 3.93 mM Hantzsch-ester, in toluene). Based on the speciation, the contribution of each species towards the overall reaction rate can be calculated (***Figure 67***, right). The contribution of the catalyst dimer is almost neglectable at concentrations between 0.07 mM and 0.11 mM, the crossing point for the contributions lies around 0.4 mM. In the further course the contribution of the dimeric pathway is increasing more and more until it dominates the catalysis at 0.9 mM.

3.8 Analysis of the second reduction step - Stereoselectivity

3.8.1 Concentration dependent enantiomeric excess

The kinetic analysis of the first catalytic cycle revealed the interesting dimerization behavior of the acyclic phosphoric acid and the consequences for the reaction rate. In contrast to this, the second catalytic cycle of 1,4-dihydro-2-phenylquinoline towards the tetrahydroquinoline is the enantiodetermining step. Considering the ability of the acyclic phosphoric acid catalyst **3** to catalyze via the monomeric pathway as well as the dimeric pathway through aggregation, the stereoselectivity should be affected by changing the amount of catalyst used for the reaction. To check on this, the transfer hydrogenation of 2-phenylquinoline was carried out applying the conditions used earlier (1.66 mM **4**, 3.98 Mm **7**) with varying catalyst concentrations (0.0017 mM to 0.83 mM) to determine the enantiomeric excess at different concentrations. (***Figure 68***)

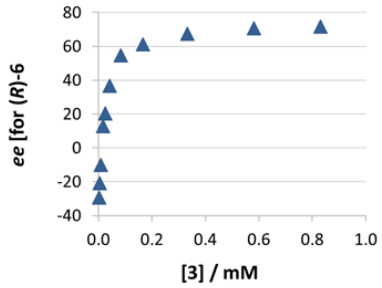

Figure 68: Enantiomeric excess for (*R*)-**6** at different concentrations of catalyst **3.**

Indeed, the stereoselectivity changes upon variation of the catalyst concentration. At the lowest concentrations the enantiomeric excess is 31 % in favor of the (*S*)-enantiomer. This fits to the observed enantiomeric excess for the reaction with the macrocyclic catalyst, which gave 17 % *ee*, also in favor of the (*S*)-enantiomer. On the other end using a high concentration like 0.83 mM of **3**, the enantiomeric excess is 73 % in favor of the (*R*)-enantiomer, which is similar to the stereoselectivity of the catenated catalysts (79% - 82% *ee*). This is in perfect agreement with the data obtained from the kinetic analysis before, in which **3** started to dimerize at higher concentrations.

This now also clarifies the picture of the catenated catalyst. While the reaction rates and catalyst order were not sufficient to attribute the dimeric catalytic pathway to the catenated catalyst unambiguously, the similarity in stereoselectivity of the dimeric acyclic phosphoric acid species **3** and the catenane **1c** confirms that the catenane indeed reacts as a dimer independent of the catalyst concentration employed. Regarding the stereoselectivity of the two pathways, the monomeric pathway seems to not only yield lower *ee*s, but even favor the formation of the opposite enantiomer compared to the dimeric pathway. The experimentally obtained enantiomeric excesses also support the DFT-calculations, in which the energetic difference in the transition states are higher for the dimeric pathway, equaling a higher stereoselectivity. It has to be noted, however, that the energies from the DFT calculations are not exact. On the one hand the calculations predict a slight enantiomeric excess for the (*R*)-product for the monomeric pathway, while the experimental data show that this pathway favours formation of the (*S*)-product. On the other hand, the calculated difference in energy for the transition states in the dimeric pathway (3.9 kcal/molm, equivalent to 99.7% *ee* at 298 K) would predict a much higher enantiomeric excess, also with a preference for the (*R*)-product. While we find the (*R*)-isomer as the main product, only 79 – 82% *ee* were found. This might be explained by a considerable

contribution of the monomeric pathway or by an overestimation of the selectivity by DFT. Nevertheless, the calculations serve as an adequate model to explain the rough trend of stereoselectivity.

Since the enantiomeric excesses differ from previous catalytic experiments[35] where a quinoline concentration of 5 mM was used, several experiments at this overall substrate concentration with varying catalyst concentrations were performed as well (***Figure 69***).

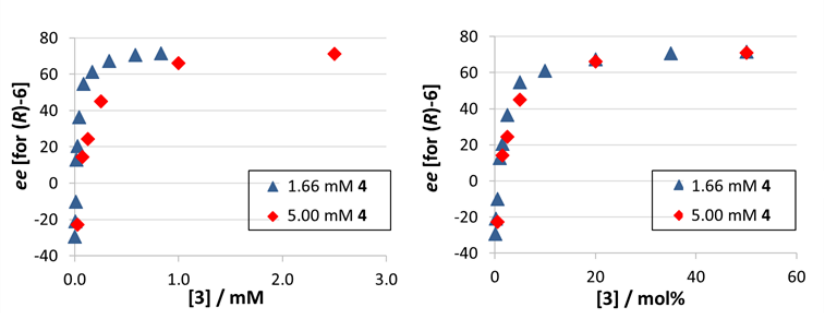

Figure 69: Enantiomeric excess for (*R*)-**6** at different concentrations of catalyst **3** for reactions carried out at [**4**]=1.66 mM (blue) and [**4**]=5.00 mM (red). Comparison of plot of *ee* against catalyst concentration (left) and *ee* against catalyst loading (right).

When examining the *ee* vs. catalyst concentration plot, the difference in observed enantiomeric excesses for the same catalyst concentration could be reproduced. When changing the x-axis to the catalyst loading, however, both curves overlap almost perfectly. This indicates that the aggregation of the APA does not only rely solely on concentration of the catalyst, but rather on the ratio of catalyst and substrates. This is conclusive since a higher concentration of substrates promotes the formation of a catalyst*substrate aggregate rather than a catalyst*catalyst aggregate at same catalyst concentration.

3.8.2 Evolution of enantiomeric excess over time

Another interesting point arises from the fact, that during the reaction one quinoline is converted to a secondary amine, while two Hantzsch ester are converted to two pyridines. Considering that the basicity and binding behaviors of secondary and aromatic amines are different and the stereoselectivity rather relies on catalyst loadings (i.e. the catalyst/substrate ratio) than on concentrations, it is conceivable that the enantiomeric excess changes over the course of the reaction.

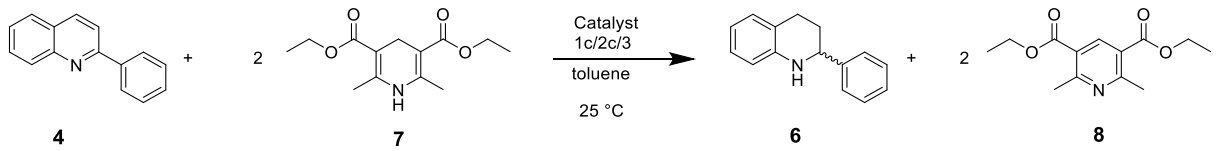

Figure 70: Transfer hydrogenation of 2-phenylquinoline with Hantzsch ester. Different basic groups are highlighted blue.

To check on this, the reaction was carried out under the previously used conditions (1.66 mM **4**, 3.98 mM **7** and 1% **3**) and samples were taken in regular intervals. Quenching of the sample was assured by directly applying it to silica gel column chromatography after withdrawal, separating the catalyst from the rest of the reaction mixture. The conversion was simultaneously observed during the chiral HPLC analysis of the

sample. For this, we used the approximation of identical extinction coefficients of 2-phenylquinoline and the product, which might give a systematic over- or underestimation of the conversion, but still enables to follow conversion over time.

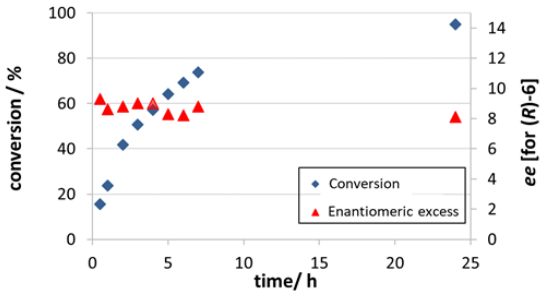

Figure 71: Evolution of enantiomeric excess over time using 1% of catalyst **3**.

Even though the stereoselectivity of **3** seems to be very sensitive towards the ratio of substrate and catalyst, the enantiomeric excess stays nearly identical over the course of the reaction.

3.8.3 Influence of the second reduction cycle on the overall reaction

When comparing the influence of the catalyst concentration on the initial rates and on the evolution of the enantiomeric excess, it appears that the *ee* curve has a significantly stronger curvature (***Figure 72***).

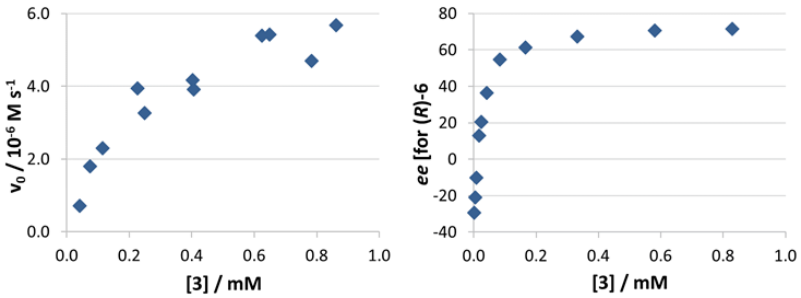

Figure 72: Comparison of the concentration dependency of the initial rates (left) and enantiomeric excess (right) for catalyst **3**.

To gain further insight, the contribution of each catalyst species of **3** ($ee_{contr.(3Mono)}$ and $ee_{contr.(3Di)}$) on the overall enantiomeric excess ee_{Tot} is investigated.

$$ee_{Tot} = \frac{ee_{contr.(\mathbf{3}Mono)} + ee_{contr.(\mathbf{3}Di)}}{X_{Mono} * k_{Mono} + X_{Di} * k_{Di}}$$

Each *ee* contribution can be written as the product of *ee*, its mole fraction and the relative rate in the second reduction cycle $k_{Mono/Di}$. Since the relative rates are not known, it is approximated based on the energetic differences in the DFT calculations (1.7 kcal/mol). The ratio f between the relative rates is 17.7.

Inserting the alternative expression yields:

$$ee_{Tot} = \frac{X_{Mono} * k_{Mono} * ee_{Mono} + X_{Di} * k_{Di} * ee_{Di}}{X_{Mono} * k_{Mono} + X_{Di} * k_{Di}}$$

Normalizing the enantiomeric excess allows expressing the *ee* of the monomeric and dimeric pathway as relative enantiomeric excesses.

$$1 = \frac{X_{Mono} * k_{Mono} * ee_{rel\_Mono} + X_{Di} * k_{Di} * ee_{rel\_Di}}{X_{Mono} * k_{Mono} + X_{Di} * k_{Di}}$$

The mole fraction of x_{Di} and the relative rate k_{Di} can be expressed using $(1\text{-}x_{Mono})$ and $f*k_{Mono}$ respectively.

$$1 = \frac{X_{Mono} * k_{Mono} * ee_{rel_{Mono}} + (1 - X_{Mono}) * f * k_{Mono} * ee_{rel\_Di}}{X_{Mono} * k_{Mono} + (1 - X_{Mono}) * f * k_{Mono}}$$

This allows elimination of k_{Mono} from the equation

$$1 = \frac{X_{Mono} * ee_{rel_{Mono}} + (1 - X_{Mono}) * f * ee_{rel\_Di}}{X_{Mono} + (1 - X_{Mono}) * f}$$

$$X_{Mono} + (1 - X_{Mono}) * f = X_{Mono} * ee_{rel_{Mono}} + (1 - X_{Mono}) * f * ee_{rel\_Di}$$

$$X_{Mono} * (1 - f) + f = (X_{Mono} * ee_{rel_{Mono}} - f * ee_{rel_{Di}}) + f * ee_{rel_{Di}}$$

$$X_{Mono} * (1 - f) - X_{Mono} * \left(ee_{rel_{Mono}} - f * ee_{rel_{Di}}\right) = f * ee_{rel_{Di}} - f$$

$$X_{Mono} * (1 - f - ee_{rel_{Mono}} + f * ee_{rel_{Di}}) = f * ee_{rel_{Di}} - f$$

$$X_{Mono} = \frac{f * ee_{rel_{Di}} - f}{1 - f - ee_{rel_{Mono}} + f * ee_{rel_{Di}}}$$

This equation allows to determine the ratio of the two catalytic pathways of **3** as well as its relative contributions towards the enantiomeric excess at different concentrations of **3**. The resulting speciation plots are depicted below (***Figure 73***).

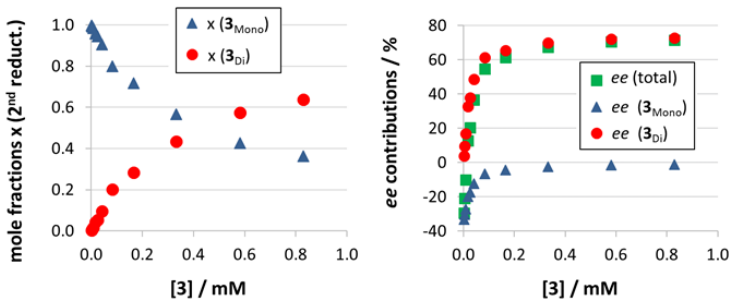

Figure 73: Mole fractions in the second catalytic cycle (left) and relative *ee* contribution (right) of the dimeric and monomeric pathway at different concentrations of **3**.

The speciation plot reveals that the two species (monomer and dimer) are distributed differently in the second catalytic cycle than they are in the first cycle. Here, both species are present equimolar at a concentration of **3** of about 0.4 mM (0.2 mM for the first cycle). Even though higher concentrations are necessary to populate the dimeric channel in the second cycle, the higher relative rate of dimeric pathway in the second cycle enormously increases the impact of the dimeric pathway on the overall stereoselectivity of the reduction. This is indicated by the *ee* contributions of the dimeric pathway (33% *ee*) and the monomeric pathway (-20% *ee*) towards the overall *ee* (13 %) for a small concentration of 0.017 mM or 1 mol% catalyst loading. At a higher concentration of 0.17 mM or 10 mol% the contribution to the overall *ee* (61%) of the dimeric pathway (65% *ee*) is already much more pronounced than the contribution of the monomeric pathway (-4% *ee*). These findings underline the great impact of the dimeric pathway on the stereoselectivity even at low catalyst concentrations.

3.9 DFT calculations and NMR-spectroscopic investigation of catalyst dimerization

The spectroscopic work in this chapter was carried out by Johannes Gramüller and Prof. Dr. Ruth Gschwind, whereas the DFT calculations were done by Dr. Hui Zhu and Prof Dr. Stefan Grimme as part of our collaborative work on this topic. Thus, the results are presented in a very condensed fashion. A more detailed presentation can be found in the published results of this collaborative work.[133]

This spectroscopic investigation aims to investigate the interactions between quinolines and the acyclic phosphoric acid as well as the dimerization of two catalyst molecules to act as a single catalyst aggregate as it was found in the studies concerning the kinetics and the stereoselectivity.

To observe interactions between the aforementioned species, it is necessary to cool down the sample to a point (180-200 K) where the line width of the signals for hydrogen bonds in ^{1}H-NMR spectroscopy are sharp enough to be analysed properly. Due to poor solubility of the acyclic phosphoric acid at these temperatures in toluene, deuterated dichloromethane was used instead. To prove that the effects that appear in toluene also are present in dichloromethane, DFT calculations were carried out, examining the two catalytic cycles in a dichloromethane environment. A difference in stereoselectivity for the monomeric pathway and dimeric pathway was predicted in dichloromethane as well. However, the differences in energy of the transition states are lower in dichloromethane than they are in toluene.

Table 8: Calculated energiy difference for the diastereomeric transisition states in toluene and dichloromethane.

	$\Delta\Delta G^{\ddagger}$ in toluene [kcal/mol]	**$\Delta\Delta G^{\ddagger}$ in DCM [kcal/mol**
Monomeric pathway	1.0	0.8
Dimeric pathway	3.9	3.3

Similar to the calculations for the reaction in toluene, the energetic difference of the transition states towards each enantiomer is higher for the dimeric pathway (3.3 kcal/mol for the dimeric pathway vs. 0.8 kcal/mol for the monomeric pathway). However, the calculations predict, that the overall stereoselectivity in dichloromethane is lower than in toluene (i.e. 3.9 kcal/mol in toluene vs. 3.3 kcal/mol in DCM).

To verify that the catalyst loading dependency also exists in dichloromethane experimentally, a row of experiments in dichloromethane with varying catalyst loadings was performed.

[133] D. Jansen, J. Gramüller, F. Niemeyer, T. Schaller, M. C. Letzel, S. Grimme, H. Zhu, R. M. Gschwind, J. Niemeyer, *Chem. Sci.* **2020**, *11*, 4381–4390.

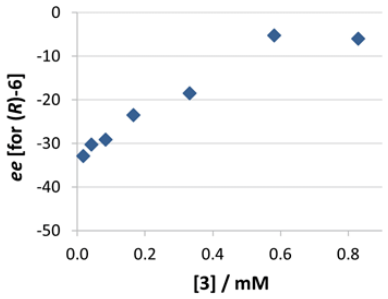

Figure 74: Enantiomeric excess for (*R*)-**6** for different catalyst concentrations of **3** in dichloromethane.

Just like in toluene, the preference for the (*S*)-enantiomer lowers with increasing catalyst loadings. At catalyst concentrations of 0.02 mM the enantiomeric excess is -33% for (*R*)-**6**. This value is similar to the one obtained in toluene at the same catalyst loading. At high catalyst concentrations such as 0.8 mM however, the enantiomeric excess is only about 5 % in favor of (*R*)-enantiomer, while for the reaction in toluene at this catalyst loading yields an enantiomeric excess of 78 % of the (*R*)-enantiomer. While this difference in *ee* at high catalyst loadings is substantial, the same trend of change in stereoselectivity in dichloromethane can be observed even though it is not as pronounced as in toluene. This can be explained with a generally lower stereoselectivity in dichloromethane as it was also found in the DFT calculations (*vide supra*). Additionally, there is always an equilibrium between monomeric and dimeric species so the enantiomeric excess at high catalyst concentrations does not necessarily represent the stereoselectivity of the pure dimeric species. The NMR studies conducted in this chapter were carried out at much higher concentration of **3** where a higher population of the dimeric species is to be expected. Thus, inferences about the dimerization behavior of **3** can be drawn from NMR experiments performed in DCM as well.

3.9.1 1:1 stoichiometries (3•Qu complexes)

To investigate hydrogen bonding between quinolines **4b**/**c**/**d** and the acyclic phosphoric acid **3**, first, a 1:1 mixture of quinolines and **3** were used.

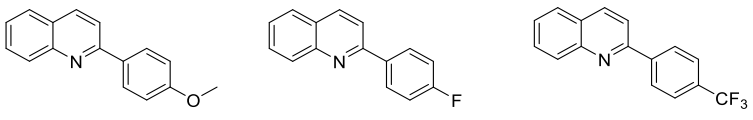

4b **4c** **4d**

Figure 75: Different 2-substituted quinolines used in this study.

Similar to previous investigations on CPA-imine complexes,[134] more basic quinolines (pK_b: **4b** > **4c** > **4d**) form stronger hydrogen bonds with the phosphoric acid. This is indicated by a more pronounced low field shift N*H*-signals of the respective quinolines in the ^{1}H-NMR spectrum.

[134] N. Sorgenfrei, J. Hioe, J. Greindl, K. Rothermel, F. Morana, N. Lokesh, R. M. Gschwind, *J. Am. Chem. Soc.* **2016**, *138*, 16345–16354.

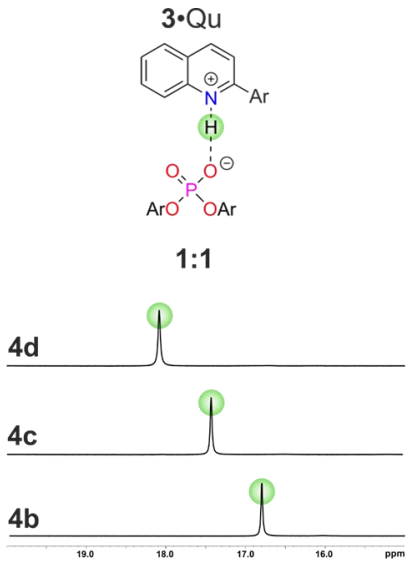

Figure 76: Excerpt of ^{1}H-NMR spectra for the 1:1 mixtures of quinolines **4b/c/d** with acyclic catalyst **3**.[135]

The signals for the hydrogen bonding protons appear at a shift between 16.5 and 18.5 ppm (**4b**: 16.83 ppm, **4c**: 17.42 ppm, **4d**: 18.08 ppm). This is in good agreement with typical shifts of signals of similar hydrogen bonds.[136] In addition to that, DOSY measurements revealed hydrodynamic radii, that fit to the size of an imine-CPA aggregate.[92] The distinct signals of the aggregate were assigned using standard 2D NMR analysis.[133]

3.9.2 2:1 stoichiometries (3•3•Qu complexes)

According to the results obtained during the kinetic and stereoselectivity studies, a ratio with a higher amount of catalyst leads to formation of the dimeric catalyst aggregate. Thus, after the 1:1 mixtures were used successfully to identify the monomeric quinoline catalyst complex, 1:2 mixtures of each of the quinolines with the acyclic phosphoric acid were investigated.

[135] Reproduced with permission from D. Jansen, J. Gramüller, F. Niemeyer, T. Schaller, M. C. Letzel, S. Grimme, H. Zhu, R. M. Gschwind, J. Niemeyer, Chem. Sci., 11, 2020, pp. 4381–4390 – Published by The Royal Society of Chemistry.
[136] a) N. Sorgenfrei, J. Hioe, J. Greindl, K. Rothermel, F. Morana, N. Lokesh, R. M. Gschwind, *J. Am. Chem. Soc.* **2016**, *138*, 16345–16354,T. Steiner, *Angew. Chem., Int. Ed.* **2002**, *41*, 48–76.

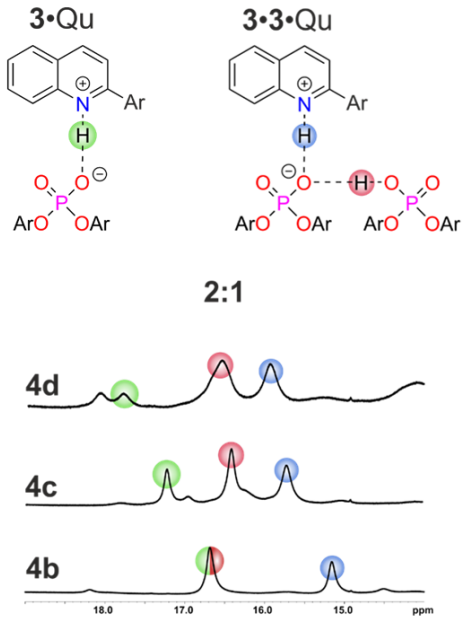

Figure 77: Excerpt of 1H-NMR spectra for the 1:2 mixtures of quinolines **4b/c/d** with acyclic catalyst **3**.[133]

Interestingly, three different protons could be assigned to the signals that appeared in this 1:2 mixtures. H_{green} belongs to the hydrogen bond of the monomeric species. H_{red} and H_{blue} presumably belong to a species which consists of two molecules of **3** and one quinoline molecule (i.e. quinoline bound by the dimeric catalyst). In more detail, H_{red} belongs to the hydrogen bonding proton between the two phosphoric acids, whereas H_{blue} is the hydrogen bonding proton between quinoline and the catalyst dimer (***Figure 77***). Similar to the 1:1 mixtures, the 1:2 mixtures were analysed by DOSY NMR as well. Here an increase in size of the hydrodynamic radii for the complexes with quinolines **4b** (~2.2 Å) and **4c** (3 Å) was found which lies in the range for similar imine-CPA complexes and their corresponding dimers.[92]

Thus, the combined results of the hydrogen bonds in ^{1}H-NMR and the DOSY-NMR together with the findings during kinetic and stereoselectivity investigations lead to the conclusion that acyclic phosphoric acid is able to form catalytically active dimers, which possess different behaviour regarding the reaction rate as well as the stereoselectivity, which is summarized in the revised mechanistic picture for the transfer-hydrogenation of 2-substituted quinolines (***Figure 78***). Such acid-acid interactions have not been widely acknowledged in Brønsted acid organocatalysis, even though aggregation behaviour is likely to be present for similar chiral phosphoric acid organocatalysts.

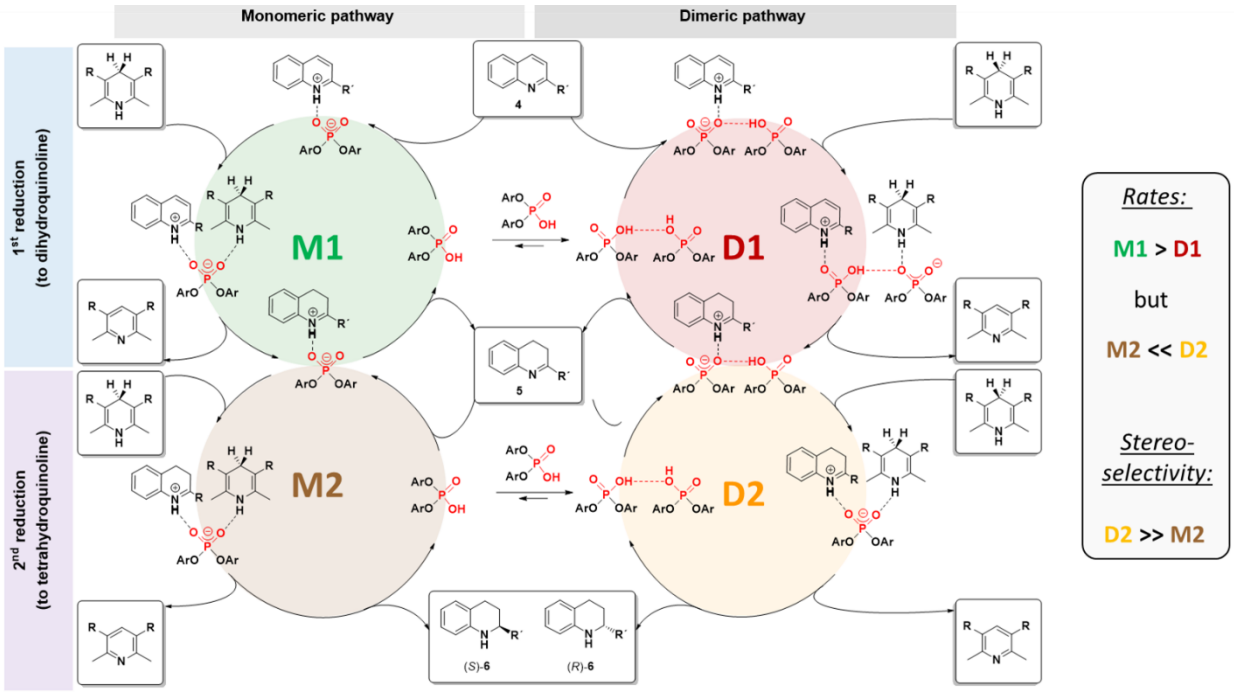

Figure 78: Revised mechanistic overview of the transfer hydrogenation of 2-substituted quinoline via monomeric and dimeric phosphoric acids.

4. Active metal template synthesis of a BINOL-based heterocatenane and its application in asymmetric catalysis

This chapter will deal with the synthesis and application of phosphoric acid based [2]- and [3]catenanes. We will first give an overview (chapter 4.1) over commonly employed strategies for the synthesis of catenanes and then describe our results with regard to the synthesis of our catenanes (chapter 4.2) and their application in catalysis (chapter 4.3).

4.1 Synthetic strategies for MIM synthesis

When it comes to synthesis of mechanically interlocked molecules the beginning era was dominated by statistical approaches or covalent-directed synthesis.[137] The first example of catenane synthesis was published by *Wasserman* in 1960 (***Figure 79***).[12]

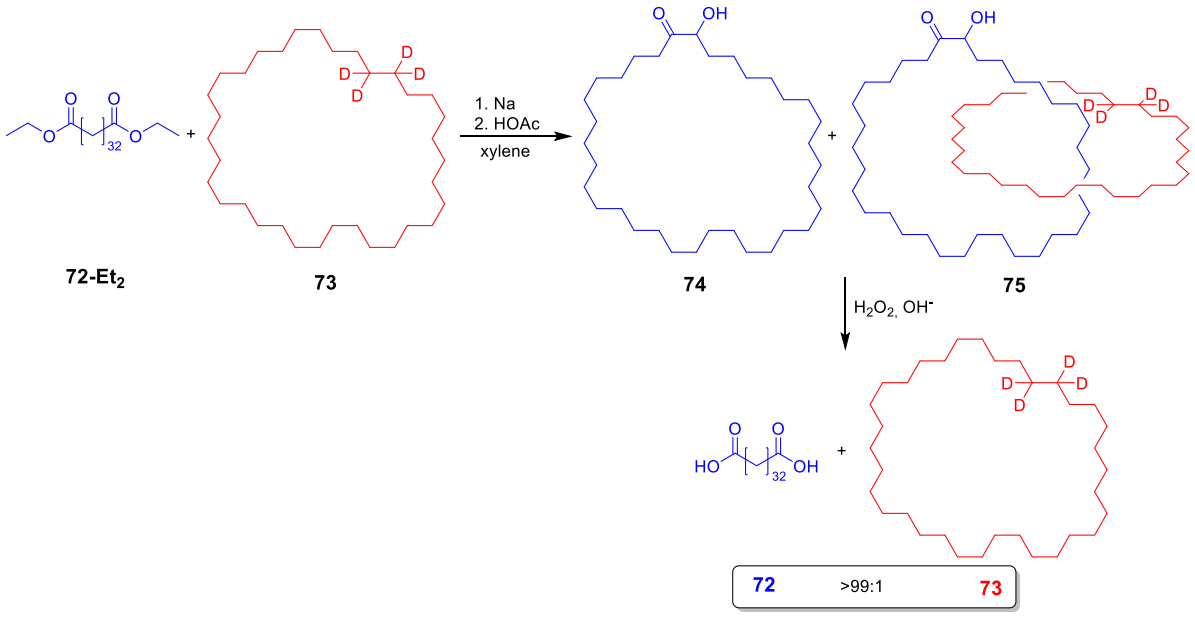

Figure 79: Synthesis of a hetero[2]catenane by *Wasserman* using a statistical formation approach.

Wasserman started the synthesis from a C34 chain with two terminal ester functionalities **72-Et$_2$**, which was cyclised through an acyloin condensation reaction in presence of the same amount of the deuterated macrocycle **73**. The resulting mixture was purified chromatographically to easily separate the macrocycle **73** from the reaction mixture. The fraction of acyloin also contained an unknown compound which contained a deuterated species. To check if this deuterated species is the desired catenane, the mixture was treated with alkaline hydrogen peroxide, which cleaved the acyloin and thus opened the ring (blue). An additional chromatographic treatment of this mixture revealed that the acyloin ring was indeed opened to yield dicarboxylic acid **72** as well as very small portion of deuterated macrocycle **73**. This confirmed that the deuterated species in the first reaction mixture was indeed the desired catenane **75**. While the yield in

[137] G. Schill, A. Lüttringhaus, *Angew. Chem. Int. Ed.* **1964**, *3*, 546–547.

catenane was stated as 1% in the original paper, the author later corrected the yield to be around 0.0001% based on deuterated macrocycle **73**.[138]

Because of the low probability of catenane formation in the statistical approach or the long synthesis route in the covalent-directed synthesis,[139] ultimately also leading to a low overall yield, such methods are rarely used in MIM synthesis today.

Even though *Wasserman* already mentioned the idea in 1962 to "synthesize a molecule in which both rings are attached to a central core in such a way that when the core is removed by chemical reactions, a pair of interlocked rings remains"[138], it took about two more decades to translate this idea into the template-directed synthesis of mechanically interlocked molecules.

4.1.1 Templated synthesis of MIMs

Templated synthesis of mechanically interlocked molecules (MIM) describes a technique in which the covalent capture takes place after the subcomponents of the MIM have been preorganized by a templating agent (***Figure 80***).

Figure 80: Schematic representation of a templated synthesis of a catenane.

The goal of the preorganization is the creation of the crossing points, that are also found in the desired MIM afterwards. The result is an increased yield of the desired interlocked molecules while decreasing the amount of by-products such as non-interlocked macrocycles or non-interlocked oligomeric structures. The first templated synthesis of a MIM was reported by *Sauvage* et al. in 1983[24] which was then followed by other examples in the next decades where chemists used various templates that exploit different types of non-covalent interactions for formation of the template complexes, such as π-π-interactions[140], π-donor/π-acceptor systems[141], hydrogen bonding templates[142] and ion pairing[143] which can even be found in templated synthesis of biomolecular MIMs.[144]

[138] E. Wasserman, *Sci. Am.* **1962**, 94–106.
[139] Schills first covalently-directed synthesis of a catenane was a 22-step synthesis
[140] W. Wang, L. Wang, B. J. Palmer, G. J. Exarhos, A. D. Q. Li, *J. Am. Chem. Soc.* **2006**, *128*, 11150–11159.
[141] P. R. Ashton, T. T. Goodnow, A. E. Kaifer, M. V. Reddington, A. M. Z. Slawin, N. Spencer, J. F. Stoddart, C. Vicent, D. J. Williams, *Angew. Chem. Int. Ed.* **1989**, *28*, 1396–1399.
[142] a) C. A. Hunter, *J. Am. Chem. Soc.* **1992**, *114*, 5303–5311,A. Tron, P. J. Thornton, M. Rocher, H.-P. Jacquot de Rouville, J.-P. Desvergne, B. Kauffmann, T. Buffeteau, D. Cavagnat, J. H. R. Tucker, N. D. McClenaghan, *Org. Lett.* **2014**, *16*, 1358–1361,F. Vögtle, S. Meier, R. Hoss, *Angew. Chem. Int. Ed.* **1992**, *31*, 1619–1622.
[143] R. Shukla, M. J. Deetz, B. D. Smith, *Chem. Commun.* **2000**, 2397–2398,R. C. Knighton, P. D. Beer, *Chem. Commun.* **2014**, *50*, 1540–1542.
[144] a) L. Z. Yan, P. E. Dawson, *Angew. Chem. Int. Ed.* **2001**, *40*, 3625–3627,Y. Liu, A. Kuzuya, R. Sha, J. Guillaume, R. Wang, J. W. Canary, N. C. Seeman, *J. Am. Chem. Soc.* **2008**, *130*, 10882–10883,K. Ryan, E. T. Kool, *Chem. Biol.* **1998**, *5*, 59–67.

The template effect is brought about either by direct intermolecular interaction of the subcomponents or by addition of external templating agents that interact with the subcomponents.[145] Most prominently, cations (mostly metal cations) and anions have been used as external templating agents.[146]

4.1.2 Passive metal templates

The aforementioned first example of a templated synthesis of a catenane from *Sauvage* relied on a copper template. Because the copper ion is just serving to arrange the precursors and does not interact in the ring closing step, it is called a passive metal template.

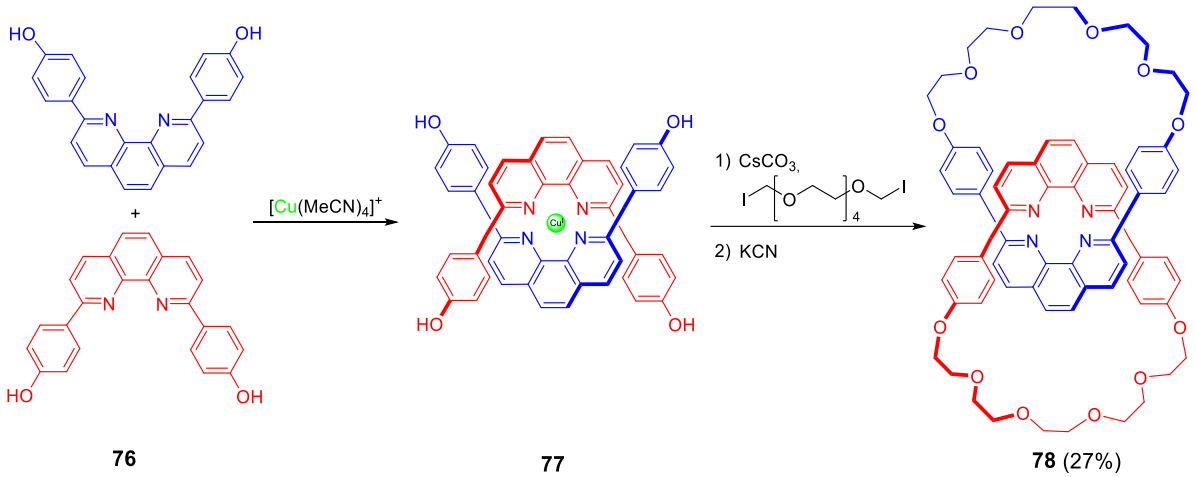

76 **77** **78** (27%)

Figure 81*:* Templated synthesis of a homo[2]catenane by preorganization of the phenanthroline units by Cu(I).

Two precursors containing a phenanthroline unit were coordinated by Cu(I). Since Cu(I) strictly coordinates its ligands in a tetrahedral orientation two crossing points were created with this template. Catenation was achieved by two twofold *Williamson* ether syntheses (i.e. double cyclisation method) to yield the homo[2]catenane with 27% yield. Compared to earlier techniques of MIM synthesis this first example of templated MIM synthesis constitutes a big step in this research field.

Next to Cu(I), other metals such as Fe(II), Co(III) and Pd(II)[147] which also allow other geometries to be applied for the passive metal template.[148] In addition to the coordination geometry of the passive metal, another important aspect of the template are ligand-ligand interactions. Those include interactions between the subcomponents of the MIM precursors. The interactions can be of different nature and usually increase the template strength.

An example of the use of such ligand-ligand interactions was shown by *Leigh* et al. in 2001 (***Figure 82***).[149]

[145] W.-X. Gao, H.-J. Feng, B.-B. Guo, Y. Lu, G.-X. Jin, *Chem. Rev.* **2020**, *120*, 6288–6325.
[146] a) M. J. Langton, P. D. Beer, *Acc. Chem. Res.* **2014**, *47*, 1935–1949,G. T. Spence, P. D. Beer, *Acc. Chem. Res.* **2013**, *46*, 571–586,A. Caballero, F. Zapata, P. D. Beer, *Coord. Chem. Rev.* **2013**, *257*, 2434–2455,N. H. Evans, P. D. Beer, *Chem. Soc. Rev.* **2014**, *43*, 4658–4683.
[147] B. A. Blight, J. A. Wisner, M. C. Jennings, *Angew. Chem. Int. Ed.* **2007**, *46*, 2835–2838.
[148] J. E. Beves, B. A. Blight, C. J. Campbell, D. A. Leigh, R. T. McBurney, *Angew. Chem. Int. Ed.* **2011**, *50*, 9260–9327.
[149] D. A. Leigh, P. J. Lusby, S. J. Teat, A. J. Wilson, J. K. Y. Wong, *Angew. Chem. Int. Ed.* **2001**, *40*, 1538–1543.

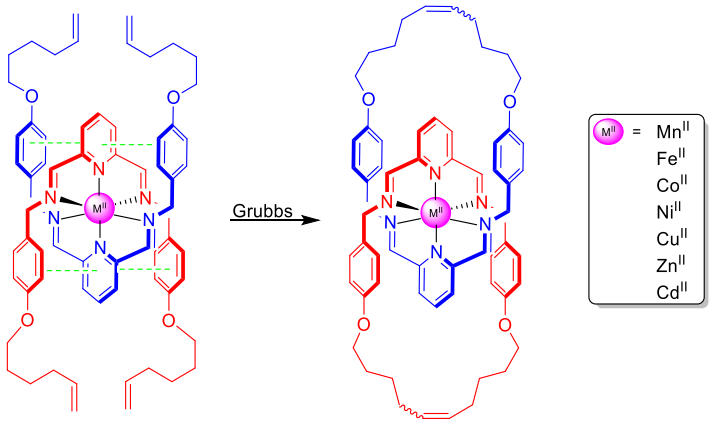

Figure 82: π-Stacking as secondary interactions (light green) in the passive metal template synthesis of a homo[2]catenane.

The precursors for the catenane consist of 2,6-diimines substituted pyridines containing terminal alkenes for a ring closing metathesis. These molecules can act as strong tridentate ligand for a metal ion. Naturally, this setup is prone bind to an octahedral coordinated metal by two of the catenane precursors. In this publication up to seven different metals were used to create this octahedral passive metal template. In addition to the interaction of the nitrogens-donors with the metals, ligand-ligand interactions played a crucial role in this template as well. Through π-π interactions between the phenyl groups of the one subcomponent with the pyridine of the other subcomponent the effect of the template was even more pronounced. Ring closing was achieved by ring closing metathesis using Grubbs II and yield between 32% and 82%.

4.1.3 Active metal templates

In contrast to passive metal templates, there is also the possibility to make use of the catalytic potential of a metal. If a metal is used to not only prearrange the MIM precursors, but also promotes the covalent capture reaction, it is called active metal template (AMT). This was firstly explored by *Leigh* et al. who used Cu(I) which was ligated by a 2,6-substituted pyridine based macrocycle to form a [2]rotaxane by AMT with up to 94 % yield (***Figure 83***).[150]

[150] V. Aucagne, K. D. Hänni, D. A. Leigh, P. J. Lusby, D. B. Walker, *J. Am. Chem. Soc.* **2006**, *128*, 2186–2187.

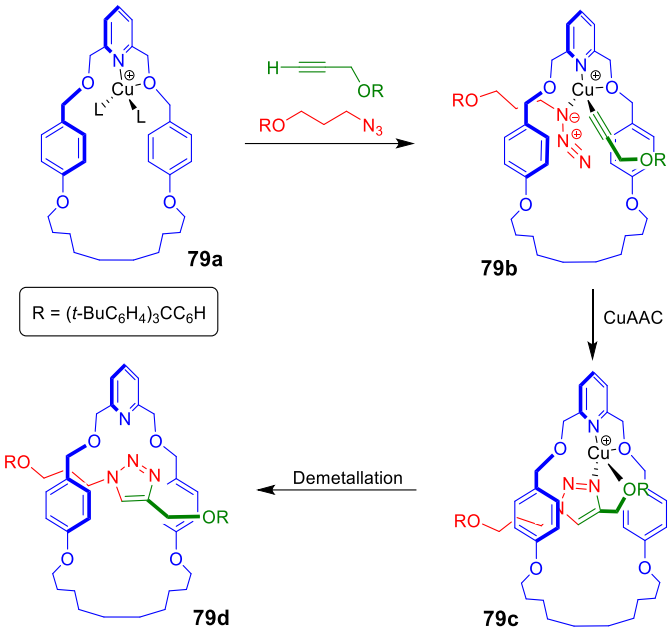

Figure 83: First active metal template synthesis of a [2]rotaxane.

The key to this approach is the formation of the bidentate Cu(I) complex **79b** within the macrocycle. Since Cu(I) prefers to be coordinated by four ligands, the other two positions can be filled by the alkyne and the azide. Copper(I) has a tetrahedral coordination geometry, thus, the azide and the alkyne are coordinated from opposing sides of the macrocycle bearing the catalytic copper. Therefore, after Cu(I) catalyses the covalent capture by CuAAC reaction, the resulting bond must be formed through the macrocycle, promoting the formation of the desired [2]rotaxane, since reactions outside the macrocycle are only possible if Cu(I) exists outside the macrocycle. Due to the bidentate binding of the Cu(I) by O- and N-donors of the macrocycle, the macrocycle is a good ligand and copper is present almost exclusively in the complexed form. A high yield of 94% in rotaxane was achieved with this method. That Cu(I) can still be exchanged was also shown in the same publication. By only using a catalytic amount (20 mol%) of copper(I), a yield of 82 % was reached, which is explained by “hopping” of Cu(I) from one macrocycle to another after successfully promoting the rotaxane formation.

Besides copper, other metals have also been applied in the means of active metal templated MIM synthesis and even metal free active templates have been reported.[151][152] Naturally, the other metals have the same requirements as Cu(I) in the previous example. They need to have a coordination geometry that is suitable to catalyse are reaction in such way that crossing points between the MIM subcomponent precursors are created. Examples for such metals include Pd(II), which was used in an active metal template heck coupling,[153] Ni(II) in a sp^3-sp^3 homocoupling[154] and Zn(II).[155]

[151] C. Tian, S. D. P. Fielden, G. F. S. Whitehead, I. J. Vitorica-Yrezabal, D. A. Leigh, *Nat. Commun.* **2020**, *11*, p. 744.
[152] G. de Bo, G. Dolphijn, C. T. McTernan, D. A. Leigh, *J. Am. Chem. Soc.* **2017**, *139*, 8455–8457.
[153] J. Berná, J. D. Crowley, S. M. Goldup, K. D. Hänni, A.-L. Lee, D. A. Leigh, *Angew. Chem. Int. Ed.* **2007**, *46*, 5709–5713.
[154] S. M. Goldup, D. A. Leigh, R. T. McBurney, P. R. McGonigal, A. Plant, *Chem. Sci.* **2010**, *1*, 383–386.
[155] a) J. D. Crowley, K. D. Hänni, D. A. Leigh, A. M. Z. Slawin, *J. Am. Chem. Soc.* **2010**, *132*, 5309–5314,M. Denis, S. M. Goldup, *Nat Rev Chem* **2017**, *1*.

All the active metal templates have several advantages compared to a passive metal template (PMT) approach. For example, with PMT sterically hindered MIMs are usually not accessible because the driving force of the template is countered by the repulsion of the subcomponents.[156] AMT provides a method with which such sterically hindered MIMs are formed with high yield. In addition, AMT does not rely on permanent functionalities that are necessary for the PMT approach to implement a strong interaction with the metal.[157] The active metal approach is also very versatile. In addition to formation of rotaxanes by AMT, integrating the two functionalities that perform the reaction at the metal centre into one molecule, a catenane instead of a rotaxane is obtained.[158] This was demonstrated recently by *Goldup* (***Figure 84***).[156]

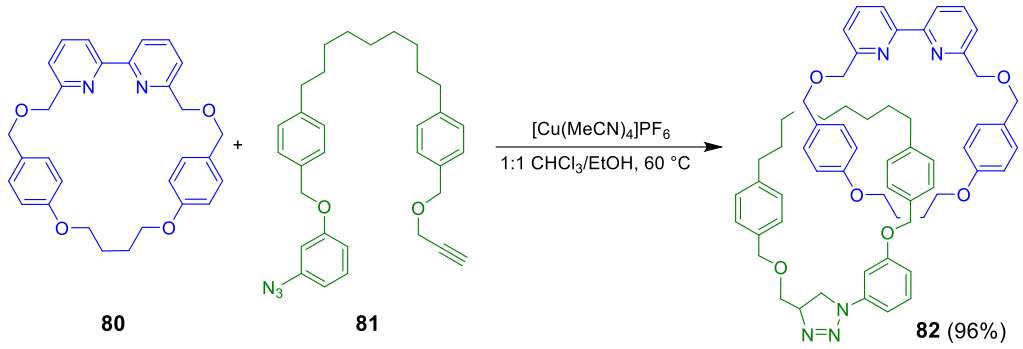

Figure 84: AMT Synthesis of a catenane using a bipyridine macrocycle and a molecule featuring an azide and an alkyne (A-B system).

In this example macrocycles which consist of a 2,2'-bipyridine were chosen. If the bipyridine is present as the *cis*-conformer, it can bind metals such as Cu(I) through both nitrogens and thus only allow bond formation via CuAAC through the macrocycle. Similar to the active metal template approach with the rotaxane, high yields are also obtained in this example as well (96%). In addition to this, AA-BB systems (i.e. bisazide and bisalkyne) were applied to the same active metal templates in multicomponent reactions (***Figure 85***).

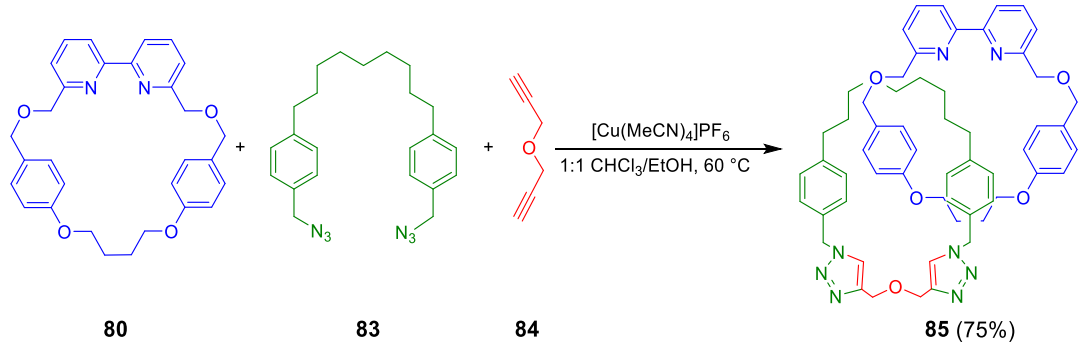

Figure 85*:* Multicomponent active metal template synthesis of hetero[2]catenane **85**.

Despite the possibility to form oligomers in this case, high yields (32% - 84%) were also achieved in these systems. Even very small catenanes with macrocycle sizes of 26 and 32 atoms were easily accessible with the multicomponent approach.

[156] J. E. M. Lewis, F. Modicom, S. M. Goldup, *J. Am. Chem. Soc.* **2018**, *140*, 4787–4791.
[157] M. Denis, S. M. Goldup, *Nat Rev Chem* **2017**, *1*.
[158] S. M. Goldup, D. A. Leigh, T. Long, P. R. McGonigal, M. D. Symes, J. Wu, *J. Am. Chem. Soc.* **2009**, *131*, 15924–15929.

4.2 Synthesis

To use catenanes in asymmetric catalysis, two aspects have to be taken into account. Firstly, a stereogenic element is needed in order for the catenated catalyst to induce stereoselectivity in a catalytic reaction. Since the axial chirality on the basis of 3,3'-substituted BINOLS proved to be excellent chiral backbones for stereoselective catalysis, this motif was chosen to be the stereogenic unit in the desired catenane. Secondly, a suitable template for the synthesis of the catenane has to be chosen. Given the advantages of active metal templates (AMT) in the synthesis of MIMs compared to other templates (e.g. passive metal templates) and the good results published recently in the multicomponent synthesis of catenanes,[156] AMT via CuAAC click reaction was chosen. For this a macrocycle which strongly binds Cu(I) plus a bisazide and a bisalkyne are needed.[156]

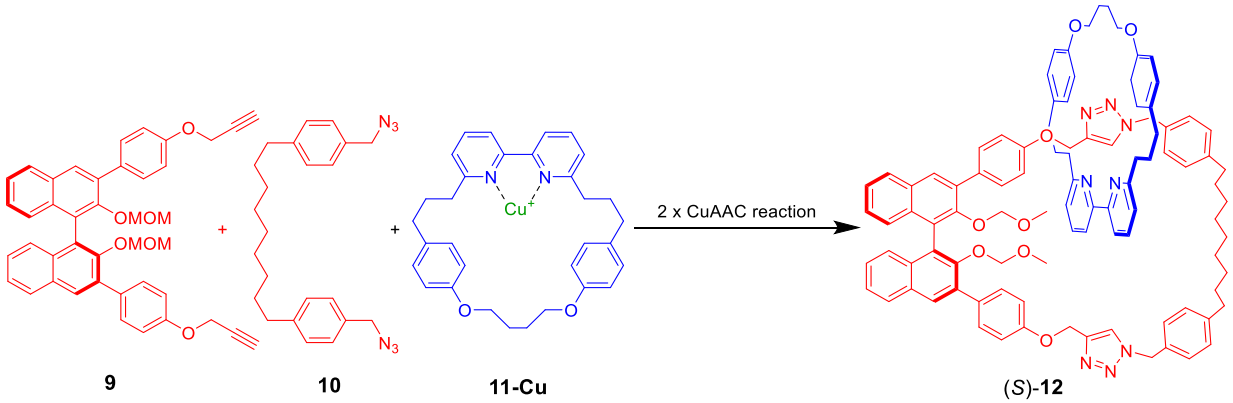

Figure 86: Overview of the synthetic approach used in this chapter: BINOL based bisalkyne, bisazide (both red) and a macrocycle bearing copper. Covalent capture is achieved by a twofold copper-azide-alkyne cycloaddition (CuAAC).

This setup does not only allow an easy synthesis of the catenane, but also enables the catenane to be used in asymmetric catalysis in which the mechanical bond can be exploited in two different ways (see chapter 4.3 catalysis).

4.2.1 Synthesis of precursors for catenation

4.2.1.1 Bisalkyne

Considering the good stereoinduction of chiral catalysts based on 3,3'-substituted BINOLs[77] as well as the synthetic experience of our group on such systems,[159] the alkyne was prepared using bisphenol (*S*)-**66**, which also served as a precursor for the catenane in chapter 3. Starting from bisphenol (*S*)-**66**, the desired bisalkyne was obtained in a single-step reaction.

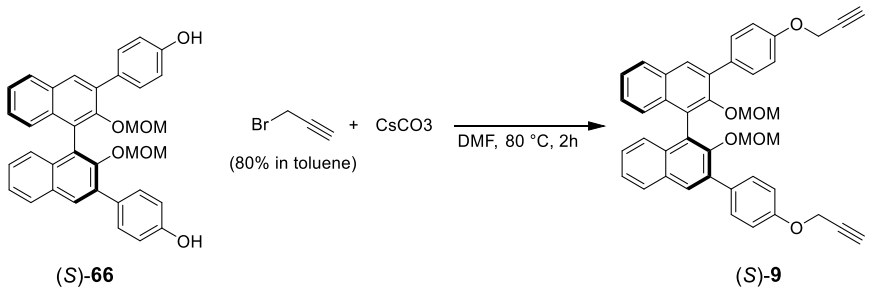

Figure 87: Synthesis of BINOL based bisalkyne (*S*)-**9** starting from bisphenol (*S*)-**9**.

The reaction proceeded via a double *Williamson ether synthesis* of the bisphenol with propargyl bromide (80 % solution in toluene). Caesium carbonate was chosen as a base to obtain the corresponding phenolates from bisphenol (*S*)-**66** as it proved to be a good base for this kind of reactions.[160] The reaction finished within two hours at 80 °C ([Bisphenol] = 0.2 M) and the product was easily obtained after an aqueous workup with a yield of 93%. Notably, it is not fruitful to carry out the reaction at elongated reaction times (e.g. overnight) as dark precipitate starts to form, which lowers the yield after workup. In addition, the MOM-protecting group can be partly cleaved off in long reactions at elevated temperature. Successful synthesis was verified by ^{1}H-NMR after purification of the crude mixture.

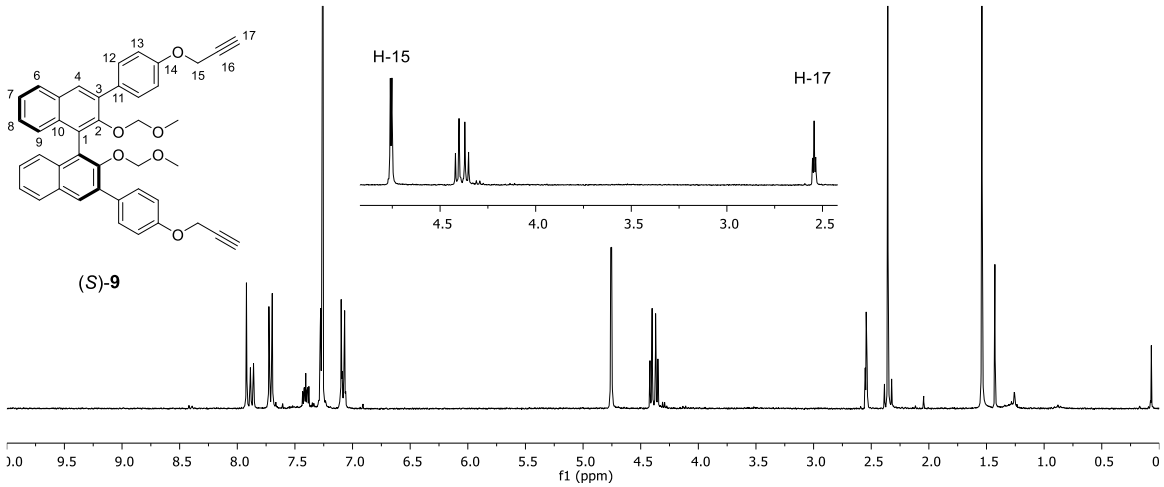

Figure 88: ^{1}H-NMR spectrum of bisalkyne (*S*)-**9** with highlighted signals for the distinctive alkyne signals ([D_1]-chloroform, 300 MHz, 298 K).

[159] R. Mitra, H. Zhu, S. Grimme, J. Niemeyer, *Angew. Chem. Int. Ed.* **2017**, *56*, 11456–11459,S. Thölke, H. Zhu, D. Jansen, F. Octa-Smolin, M. Thiele, K. Kaupmees, I. Leito, S. Grimme, J. Niemeyer, *Eur. J. Org. Chem.* **2019**, *2019*, 5190–5195,R. Mitra, M. Thiele, F. Octa-Smolin, M. C. Letzel, J. Niemeyer, *Chem. Commun.* **2016**, *52*, 5977–5980,D. Jansen, J. Gramüller, F. Niemeyer, T. Schaller, M. C. Letzel, S. Grimme, H. Zhu, R. M. Gschwind, J. Niemeyer, *Chem. Sci.* **2020**, *11*, 4381–4390.

[160] R. Rabie, M. M. Hammouda, K. M. Elattar, *Res. Chem. Intermed.* **2017**, *43*, 1979–2015.

The product was identified by the distinctive signals for the propargylic groups (doublet at 4.76 ppm and triplet at 2.54 ppm) in the right ratio of integrals compared to the BINOL signals (***Figure 88***).

4.2.1.2 Bisazide 10

Another building block that is needed for the multicomponent catenane synthesis is a bisazide. For this the bisazide recently published by *Goldup* et al. was used.[156] Therefore the synthesis is described only briefly.

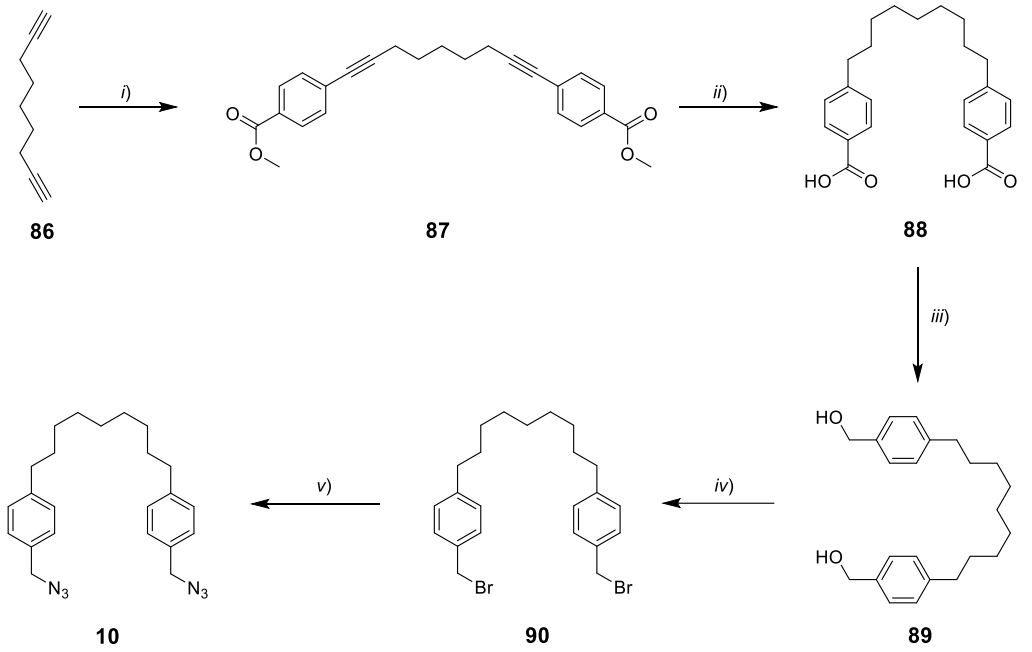

Figure 89: Synthesis of bisazide 1**0**. *i*) Methyl-4-bromobenzoate, Cu(I), $Pd(PPh_3)_2Cl_2$, $^iPr_2NH$, 60 °C, 23 h, 75%. *ii*) Pd/C (10 wt%), H_2, methanol, RT, 19 h, 91%. *iii*) $LiAlH_4$ (2.4 M in tetrahydrofuran), tetrahydrofuran, 0 °C during addition, then 60 °C, 4 h, 86%. *iv*) PPh_3, CBr_4, dichloromethane, 0 °C during addition, then RT, 16 h, 86%. *v*) NaN_3, dimethylformamide, 80 °C, 20 h, 62%.

The five step synthesis starts from commercially available bisalkyne **86** and methyl-4-bromobenzoate which react in a palladium catalysed *Sonogashira* coupling to obtain diester **87**. This is firstly hydrogenated by hydrogen gas using a palladium on carbon catalyst before it is reduced to the corresponding diol **89** by lithium aluminium hydride. Formation of bisbromide **90** is achieved by a twofold *Appel* reaction, which is then followed by a S_N2 reaction using N_3^- as a nucleophile to yield the desired bisazide **10**. Thus the bisazide was obtained in a total yield of 31% over five steps.

4.2.1.3 Macrocycle 11

To enable the bisazide and the bisalkyne to react in an active metal template fashion, a macrocycle which binds Cu(I) is needed. For this, the group around *Goldup* established a synthesis protocol for the high yield synthesis of 2,2'-bipyridine based macrocycles.[161] Symmetric macrocycle **11** was chosen for the active template synthesis.

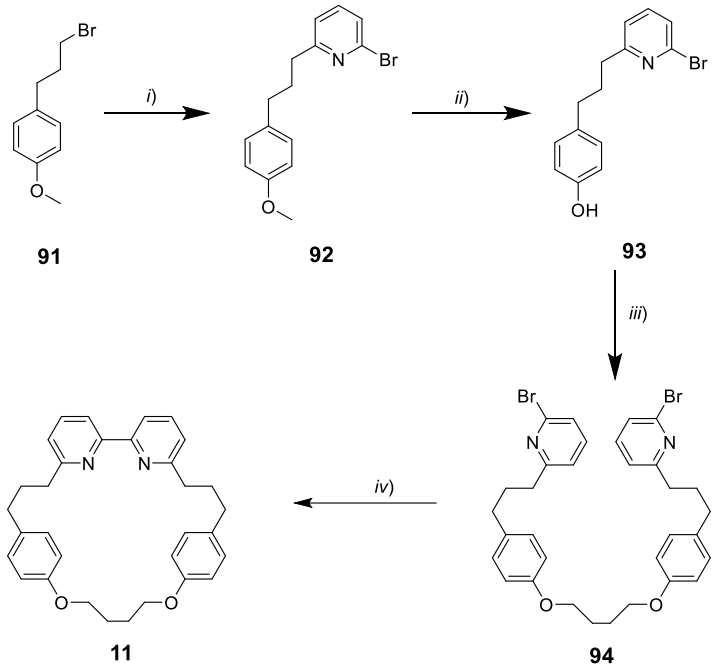

Figure 90: Synthesis overview for macrocycle **11**. *i*) 2,6-dibromopyridine, Zn, I_2, $Pd(PPh_3)_2Cl_2$, dimethylformamide, 90 °C, 2 h, 45%. ii) $HBr_{aq.}$ (48%), 100 °C, 16 h, 88%. iii) 1,4-dibromobutane, K_2CO_3, acetonitrile, 80 °C, 16 h, 65%. iv) $Ni[PPh_3]_2Br_2$, PPh_3, Mn, NEt_4I, dimethylformamide, 50 °C, 5 h, 51%.

For the synthesis of macrocycle **11**, bromide **91** is reacted with 2,6-dibromopyridine in a *Negishi* coupling reaction. Phenolic desymmetrized pyridine **93** is obtained after cleavage of the methyl ether under acid conditions. The ring precursor **94** is then obtained in a twofold S_N2 reaction of 1,4-dibromobutane, which is then cyclised in a nickel catalysed homocoupling reaction. In summary, macrocycle **11** was obtained in 13% yield over four steps

[161] J. E. M. Lewis, R. J. Bordoli, M. Denis, C. J. Fletcher, M. Galli, E. A. Neal, E. M. Rochette, S. M. Goldup, *Chem. Sci.* **2016**, *7*, 3154–3161.

4.2.2. Active metal template synthesis and investigations on its selectivity

4.2.2.1 Reaction setup and first results

After obtaining all components to synthesize the desired catenane by the means of active metal template synthesis in a three component reaction (bisalkyne, bisazide, macrocycle) the catenation reaction was carried out. Due to the similarity of the components to the catenane synthesis of *Goldup* the optimised setup was also applied to this approach.[156] This setup bears some important points which are vital for the success of the reaction. Firstly, the reaction has to be carried out under an oxygen-free atmosphere, because otherwise Cu(I) might oxidise to Cu(II) which is not catalytically active in the CuAAC reaction anymore. Secondly, the reaction has to be carried out under high dilution conditions to favour catenane formation over oligomerization that occurs at higher concentrations due to minimum amounts of free Cu(I) outside the macrocycle. To avoid the use of copious amounts of solvent, the reaction was carried out under pseudo-high dilution conditions. This is achieved by preformation of the copper-bipyridine complex at a concentration of 10 mM in 1:1 chloroform/ethanol and addition of a 25 mM 1:1 mixture of the azide and alkyne in the same solvent mixture to the first solution by a syringe pump. In the original report of *Goldup* an addition time of four hours seemed to be a good trade-off between relatively small initial concentrations and reaction time,[156] so the same addition time was applied here. Cu(I) was used slightly substoichiometric compared to the macrocycle to avoid catalysis outside the macrocycle.

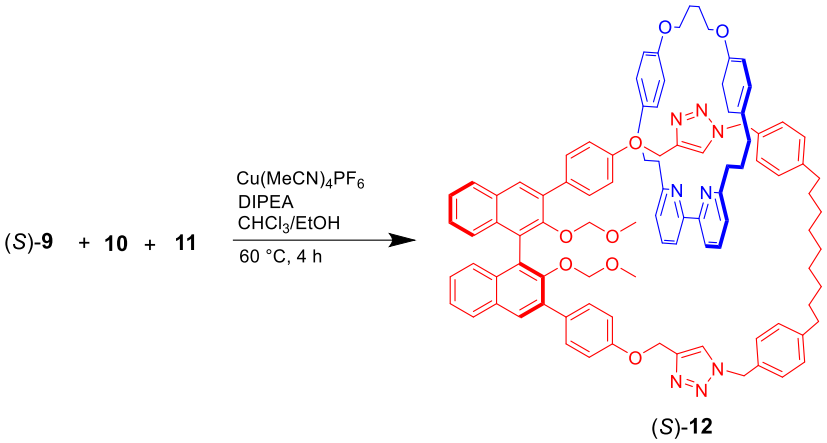

Figure 91: Envisioned reaction overview of catenation reaction.

After complete addition of the azide/alkyne mixture, the reaction mixture was allowed to stir for another hour to ensure full completion of the reaction. To analyse the outcome of the reaction, copper has to be removed from the mixture first. For this two different methods were used. The first method relies on the competitive binding of copper to cyanide. By using an excess of potassium cyanide copper can be removed by aqueous extraction. The second method uses the strong binding of copper to ethylenediaminetetraacetate (EDTA) ions by chelation of the metal. An ammonium-EDTA solution was used to wash a dichloromethane solution of the crude mixture. In both cases fading of the strong orange colour coming from the copper(I)-bipyridine complex was a good indicator for the successful demetallation of catenane. It has to be noted that both methods gave very similar results as confirmed by ^{1}H-NMR, but only the potassium cyanide method was used in the further course to ensure full reproducibility.

When performing reversed phase UHPLC/MS of the first crude mixture, two major signals were visible, indicating the reaction did not proceed as selective as expected to yield the desired [2]catenane (***Figure 92***).

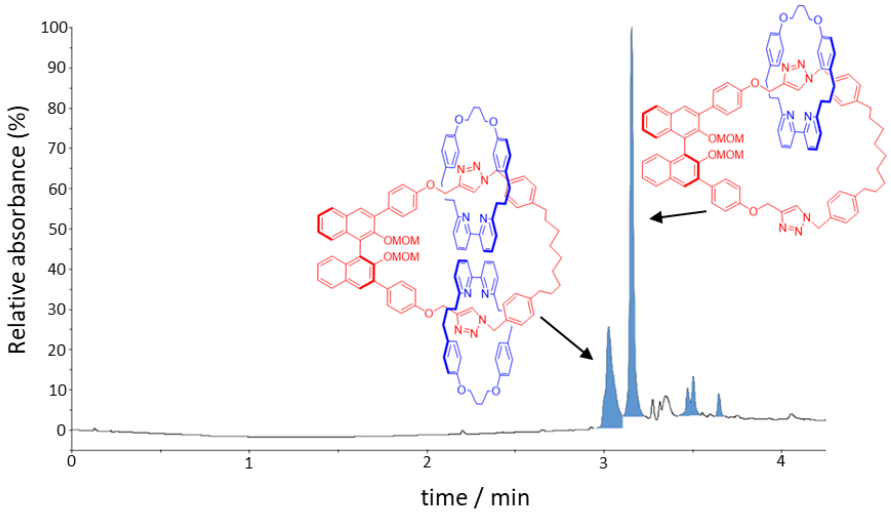

Figure 92: Chromatogram of the UHPLC/MS analysis of the first crude mixture obtained from catenation reaction. Formation of [2]catenane as well as [3]catenane was observed.

Instead, the two most intense signals were identified as the [2]catenane as well as to a [3]catenane that consists of two bipyridine macrocycles and one BINOL-based macrocycle. Even though formation of [3]catenane was not intended, this catenane offers great possibilities to study the effect of the mechanical bond in asymmetric catalysis in more detail than it would be possible with only the [2]catenane.

The formation of the two different catenanes can be explained as follows. After the first active metal template assisted click reaction an intermediate is formed which consists of a copper-triazolyl species. To finalise the reaction, this species has to be protonated to release the triazole and the copper-bipyridine macrocycle, enabling it to either catalyse the click reaction on the other side of the molecule or to completely dissociate from the molecule. This would lead to formation of [2]catenane. To form the [3]catenane, protonation and dissociation after the first click reaction has to be slow enough for another copper-bipyridine macrocycle to approach and catalyse the second triazole formation. Thus, two bipyridine macrocycles are trapped, resulting in the [3]catenane.

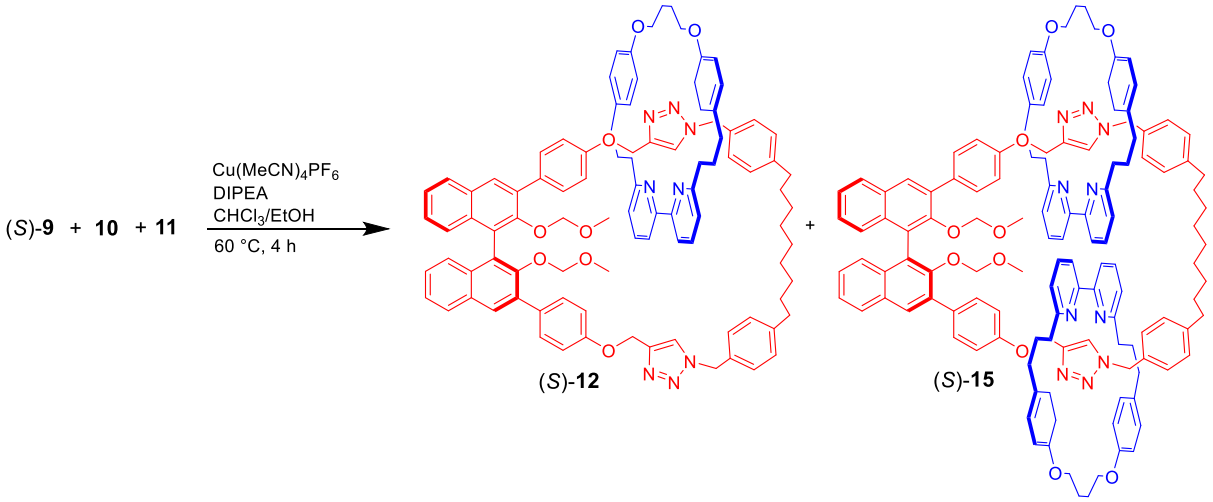

Figure 93: Revised reaction overview for catenation reaction.

When it comes to isolation of the two catenanes from the reaction mixture it turns out that it is crucial to deactivate the silica that is used for column chromatography by treating it with triethylamine before usage. Otherwise no difference in retention time between the catenanes can be seen and the chromatographic purification is not fruitful. This is most likely to be attributed to the bipyridine macrocycle which can be protonated easily or at least strongly interacts with SiOH groups of the silica. This is indicated by streaking of the catenanes during thin layer chromatography allowing no separation of the two catenanes, if the silica is not deactivated.

After successfully isolating the catenanes (yields: [2]catenane: 24%, [3]catenane: 5%) using the optimised conditions in silica gel column chromatography (cyclohexane/ethyl acetate 70/30 + 2 vol% triethylamine), the spectrum of the crude mixture can be compared to the spectra of the pure [2]catenane, [3]catenane and the bipyridine macrocycle **11** (***Figure 94***). In the spectrum of the [2]catenane (***Figure 94*** a) some distinctive signals are discernible which allow identification of the [2]catenane. Most evidently the signal for the C-*H* of the triazole moiety (8.04 ppm) indicates the successful click reaction. In addition to that signals for the phenyl protons *H*-j (6.63 ppm) and *H*-k (6.55 ppm) of the bipyridine are present with the correct integral, indicating a ratio of 1:1 of the signals of the BINOL based and bipyridine macrocycle. In contrast to this, the spectrum of the [3]catenane (***Figure 94*** b) slightly differs from the spectrum of the [2]catenane. Most prominently the C-*H* of the triazole moiety is shifted to high field (8.83 ppm) and the ratio of the signals for the bipyridine macrocycle and the BINOL based macrocycle is 2:1 in favour of the bipyridine macrocycle. The different shifts in the [2]- and [3]catenane could be explained by different environments. In the case for the [2]catenane only one bipyridine macrocycle exists, which most likely performs movement between the two triazoles along the other ring on the NMR time scale. Therefore, the residence time at the triazoles and thus the influence on the protons nearby is reduced on average. This is substantiated by the absence of two sets of signals which would appear through desymmetrization if the bipyridine rested on one side of the other ring. For the [3]catenane the influence on the aforementioned protons appears to be higher. This is conclusive since the two bipyridines cannot travel from one triazole to the other, because they block each other. The result is a higher average residence time for each bipyridine at the respective triazole compared to the [2]catenane. Another interesting difference is, that there are two sets of signals for the protons of the bipyridine macrocycle for the [3]catenane. This is surprising as the macrocycles in this catenane are C_{2v} symmetric and thus formation of diastereomers should not be possible. One explanation

could be that the two bipyridine macrocycles become unequal (e.g. in a tilted conformation) due to the crowdedness (i.e. restricted movement) inside of the [3]catenane structure. In addition to the identification by ^{1}H-NMR spectroscopy, high resolution mass spectrometry further confirmed the successful formation of the [2]catenane (m/z: 1503.8098 for $[M+H]^{+}$) and [3]catenane (m/z: 992.0208 for $[M+2H]^{2+}$).

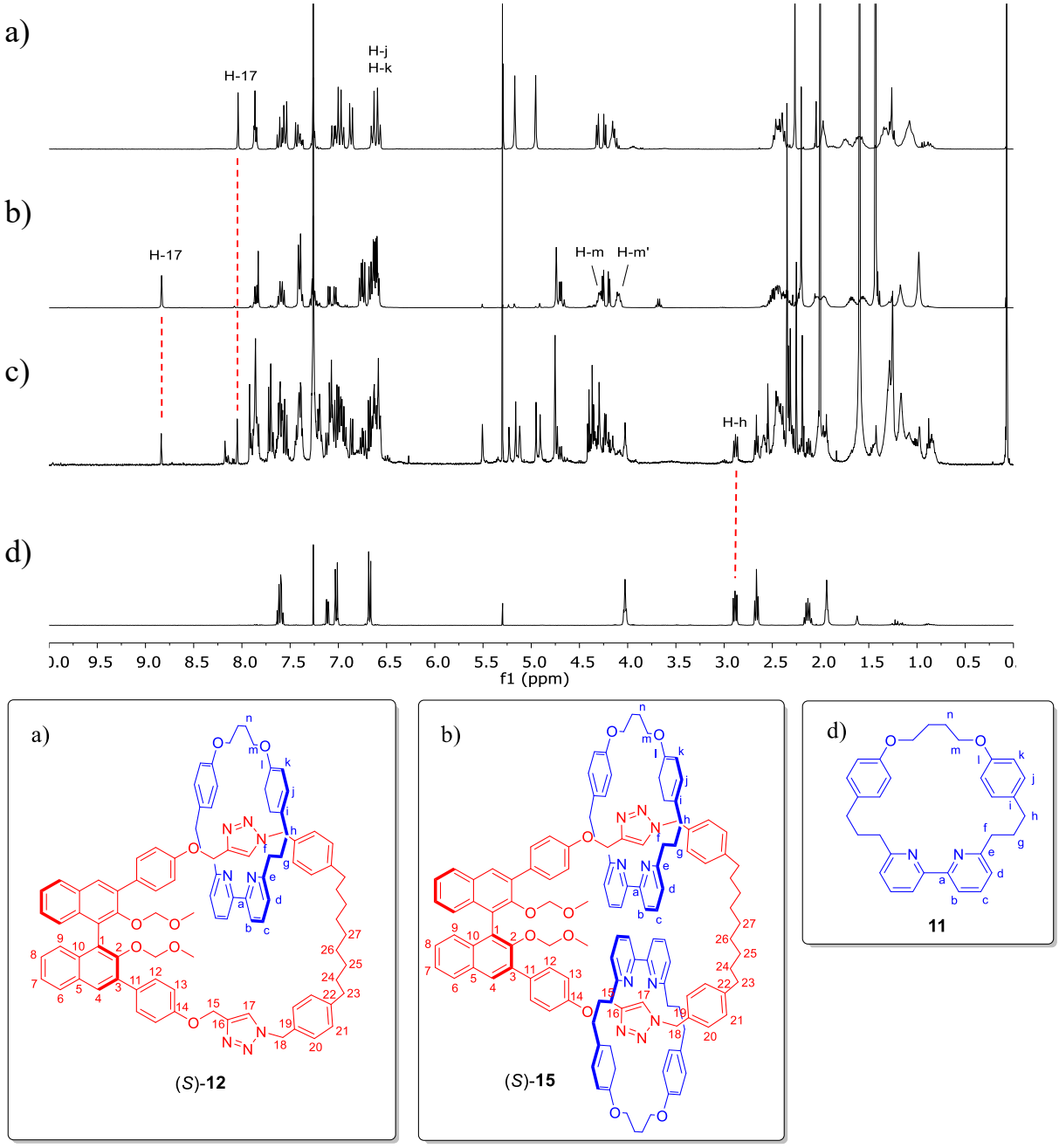

Figure 94: Comparison of ^{1}H-NMR spectra of: a) [2]catenane (*S*)-**12** b) [3]catenane (*S*)-**15**, c) reaction mixture after demetallation and d) bipyridine macrocycle **11**. Distinctive signals of the pure compounds that are also visible as separate signals in the reaction mixture are indicated by red dotted lines ([D_1]-chloroform, 400 MHz, 298 K).

As mentioned before, separate signals for H-17 for the [2]catenane, [3]catenane as well as H-h of the bipyridine macrocycle are discernible in the ^{1}H-NMR spectrum of the crude mixture (***Figure 94***, red dotted lines). This allows the determination of the ratio of [2]catenane and [3]catenane as well as the conversion of the macrocycle starting material.

4.2.2.2 Selectivity of catenation reaction

The ratio of the two catenanes depends on how fast the second click reaction occurs relative to the stability of the copper-triazole complex after the first click reaction. Since the rate depends on the concentration of the copper-bipyridine complex (assuming a reaction order greater than 0 for the copper-bipyridine complex), lowering the initial concentration should favour the formation of [2]catenane while a higher initial concentration should shift the ratio towards more [3]catenane. To test this, different reaction conditions were tested, including a screening of concentrations of the copper-bipyridine complex.

The following setups were used (***Table 9***), with a range of concentration of macrocyclic copper-complex from 2.5 mM to 25 mM, as well as different reaction temperatures and solvents.

Table 9: Reagent concentrations and the resulting fraction of [3]catenane (*S*)-**15** as well as the conversion of bipyridine macrocycle **11**.

Entry	[11] mM	[alkyne/azide] mM	Fraction of (*S*)-15 [%]	Fraction of (*S*)-12 [%]	Conversion of 11 [%]
1	2.5	25	0	100	15
2[a)]	5	25	15	85	58
3[b)]	5	25	23	77	92
4[c)]	5	25	43	57	55
5[d)]	5	25	20	80	69
6[e)]	10	50	35	65	93
7	7.5	25	29	71	87
8[f)]	10	25	34	66	90
9	20	25	36	64	90
10	25	25	37	63	91

Reactions carried out in 1:1 chloroform/ethanol (degassed) at 60 °C in a pressure vial. 4 eq. DIPEA added. Addition of alkyne/azide over 4 hours. One hour of stirring after complete addition. Fraction of (*S*)-**15** and conversions determined by ^{1}H-NMR. a) Mean value from four experiments. b) Reaction in degassed THF. c) Addition at RT over 20 hours. d) Reaction at 70 °C. e) 2 equivalents of azide/alkyne relative to macrocycle **11**. f) Mean value from two experiments.

Different parameters were changed to check for its influence on the reaction outcome (fraction of (*S*)-**15** and conversion of **11**) (***Table 9***). Increasing the temperature by 10 °C (entry 2 vs. entry 5) did not result in any difference. However, performing the addition at room temperature over 20 hours (entry 4) results in more formation of [3]catenane as well as much lower conversions. Interestingly, changing the solvent to tetrahydrofuran increased the conversion to over 90%, while the ratio of [2]catenane and [3]catenane stays similar.

When looking at the experiments concerning the different macrocycle concentrations an interesting trend can be observed (***Figure 95*** and ***Table 9*** entry 1-2 and entry 7-10).

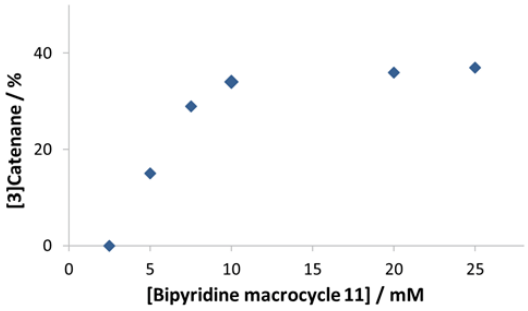

Figure 95: Dependency of [3]catenane formation on the initial concentration of macrocycle **11**.

Indeed, the initial concentration of the copper-bipyridine complex alters the outcome of the reaction. Starting at 2.5 mM formation of the [3]catenane was completely suppressed. Increasing the concentration to 10 mM, the fraction of [3]catenane rises almost linearly before the curve flattens out. At concentrations above 10 mM the curve reaches a plateau at around 36 %. The flattening of the curve is most likely due to insolubility of the copper-bipyridine complex which solubility in chloroform/ethanol (1:1) is around 10 mM. At higher concentrations insolubility is indicated by an inhomogeneous mixture. Changing the solvent could increase the solubility and therefore allow higher proportions of [3]catenane. The conversion also depends on the concentration of the macrocycle **11**. Lowering the concentration to 2.5 mM resulted in only 15% conversion. Therefore, even though sole formation of [2]catenane might be desirable, yields drastically fall at lower concentrations due to incomplete reaction.

Another approach to check for the concentration dependency was done by carrying out the catenation reaction in a time resolved fashion. For this, samples of 1 ml were withdrawn at different times. After workup, the ratio of the two catenanes was determined by integration of the signals for the catenanes in the chromatogram of the UHPLC/MS run.

Table 10: Fraction of [3]catenane formed over the course of the reaction.

Reaction time (hours)	Fraction of [3]catenane (%)
1	> 95
2	31
3	24
4	15

In the beginning (1 hour) of the reaction [3]catenane is formed almost exclusively. In the further course of the reaction the ratios proceed to change in favour of [2]catenane. Already after 2 hours into the reaction, the product is a mixture of 31 % [3]catenane and 69 % [2]catenane. After complete reaction the fraction changed to 15% [3]catenane and 85% [2]catenane. This final result is in good agreement with the previous obtained results obtained at this concentration of macrocycle **11** (12 – 15% [3]catenane; ***Table 9***). The

changing ratios can again be explained with the dependency on the concentration of the macrocycle as it quickly decreases during the course of the reaction.

These findings allow to steer the selectivity of this reaction easily by this one parameter. Since the solubility of the Cu(I)-macrocycle complex is only around 10 mM in chloroform/ethanol (1:1), other solvents might be used to increase the formation of [3]catenane to a point where it is formed exclusively. This is especially of high interest since this kind of reaction can be performed from a toolbox of reagents. Therefore, it is important to know how different products can be formed selectively. However, further optimisations are not part of this thesis and remain interesting aspects to investigate in the future.

When it comes to preparative synthesis of the catenanes a high conversion as well as a similar yield of the two catenanes is desirable. However, during column chromatography, the [2]catenane elutes shortly after the [3]catenane and therefore produces fractions which are contaminated by small amounts of [3]catenane thus reducing the effective yield of [2]catenane after purification. To take this into account, conditions where more [2]catenane is formed were chosen for the preparative synthesis of the catenanes (First solution – 28 ml chloroform/ethanol: Bipyridine macrocycle **11**: 0.139 mmol + $Cu(MeCN)_4PF_6$: 0.133 mmol + DIPEA: 0.278 mmol; Second solution – 6 ml chloroform/ethanol: Bisalkyne (*S*)-**9**: 0.139 mmol + bisazide **10**: 0.139 mmol; i.e. ***Table 9***, entry 2) to obtain the yields mentioned before.

4.2.3 Further modification of the catenanes and macrocycle synthesis

4.2.3.1 Synthesis of BINOL-based macrocycle

The aim of this chapter is the investigation of the influence of the mechanical bond of a catenane in catalysis. To verify the results, each subcomponent of the catenane has to be used solely in a control experiment. For this, the cyclisation reaction was carried out using nearly the same protocol as for the catenane, but without the bipyridine macrocycle. In contrast to the catenation reaction the MOM-protected bisalkyne (*S*)-**9** was deprotected prior to the cyclisation in order to reduce the amount of post modification steps. Due to the high polarity and expected difficulties during column chromatography for the phosphoric acid macrocycle, the phosphorylation was carried out after obtaining the pure diol-macrocycle.

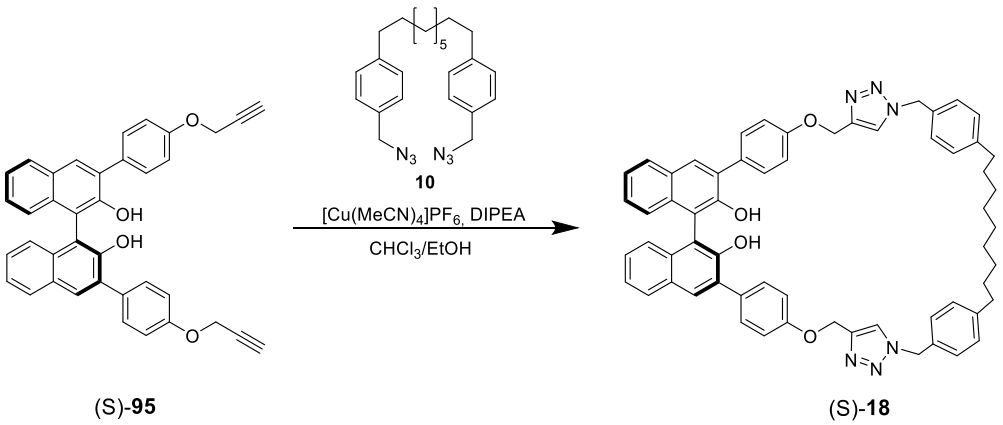

Figure 96: Cyclisation of bisalkyne (*S*)-**95** through copper-azide-alkyne cycloaddition.

The reaction proceeds via a twofold CuAAC click reaction of bisalkyne (*S*)-**9** with bisazide **10** catalysed by $[Cu(MeCN)_4]PF_6$. In a first attempt using a concentration of 10 mM of the solution containing the copper species, formation of precipitate was observed during addition of the solution containing the alkyne/azide mixture. This indicates that oligomers formed during this reaction, which are not soluble anymore in the given solvent mixture. The low yield (< 5%) which was obtained after purification by silica gel column chromatography substantiates this assumption.

In a second attempt, the concentration of the solution containing the copper was reduced to 6 mM by increasing the amount of solvent while keeping the amount of copper constant, since higher dilution should increase the formation of macrocyclic product over oligomers. During the addition of the solution containing the alkyne/azide mixture, precipitation was observed again, albeit to visually lesser extent. The yield of the desired macrocycle **11** after column chromatography was 10%. Even though the yield remained unsatisfying after lowering the concentration of the Cu(I) source, the reaction was not further optimised.

Identification of the successful formation of the cyclic product was done by ^{1}H-NMR spectroscopy.

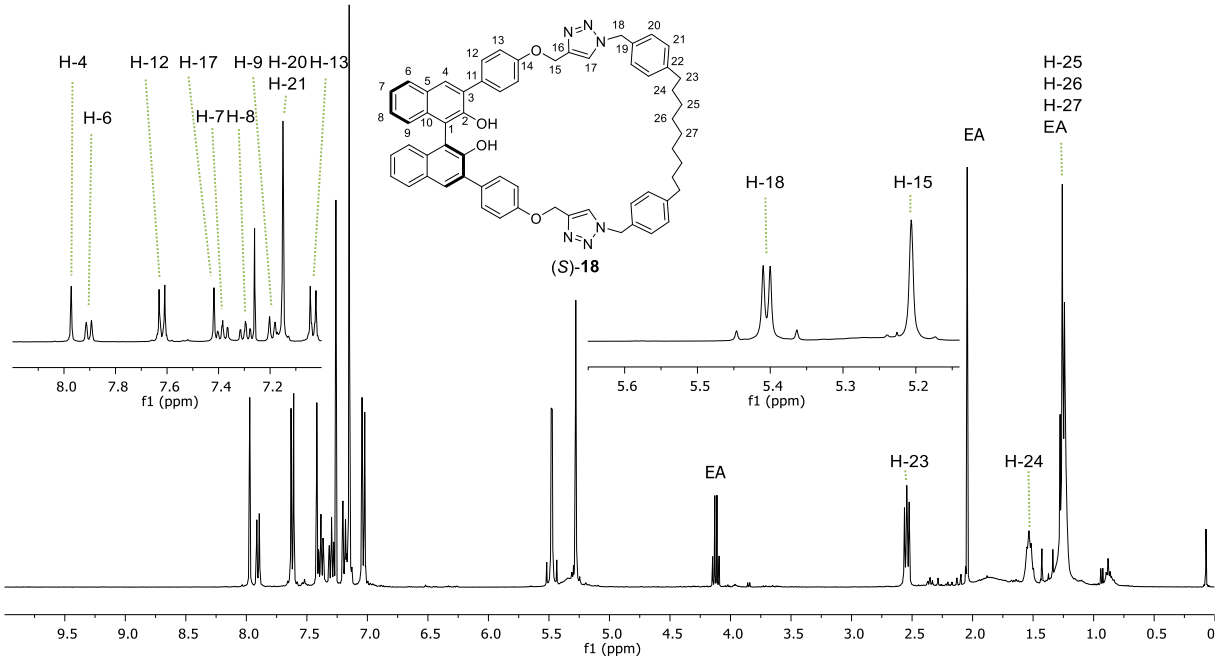

Figure 97 ^{1}H-NMR of macrocycle (*S*)-**18** and excerpts showing the aromatic region as well as the region between 5.2 ppm and 5.8 ppm. EA = Ethyl acetate. ([D_1]-chloroform, 400 MHz, 298 K).

The product exhibits distinctive signals for the CH_2 groups at position 18 and 15. While a singlet is discernible for the protons at position 15, the two protons at position 18 are diasterotopic and thus show coupling with each other. Interestingly, protons H-20 and H-21 show a singlet at 7.15 ppm, which is unusual for such phenyl protons. Mass spectrometry as well as the ratio of integration of the aforementioned signals with e.g. the signal for H-6 confirmed the successful synthesis of diol-macrocycle (*S*)-**18**.

In the last step the macrocyclic diol was phosphorylated by phosphorus oxychloride using the same protocol as established earlier (see chapter 3.4)

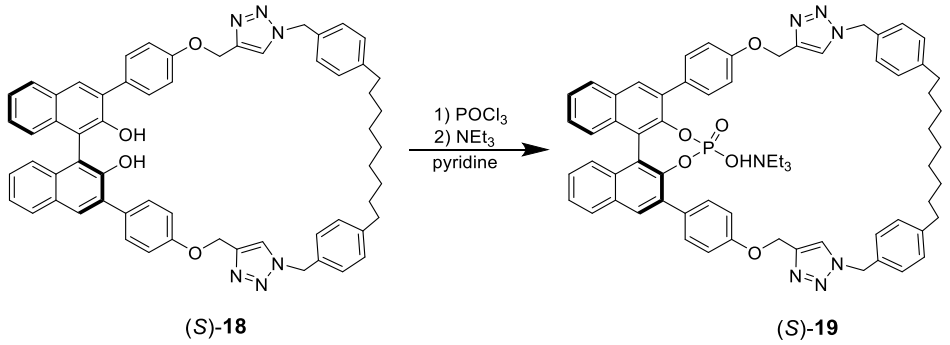

Figure 98: Synthesis of triethylammonium phosphate macrocycle (*S*)-**19**.

The triethylammonium phosphate macrocycle (*S*)-**19** was obtained in 63% yield after column chromatography with deactivated silica.

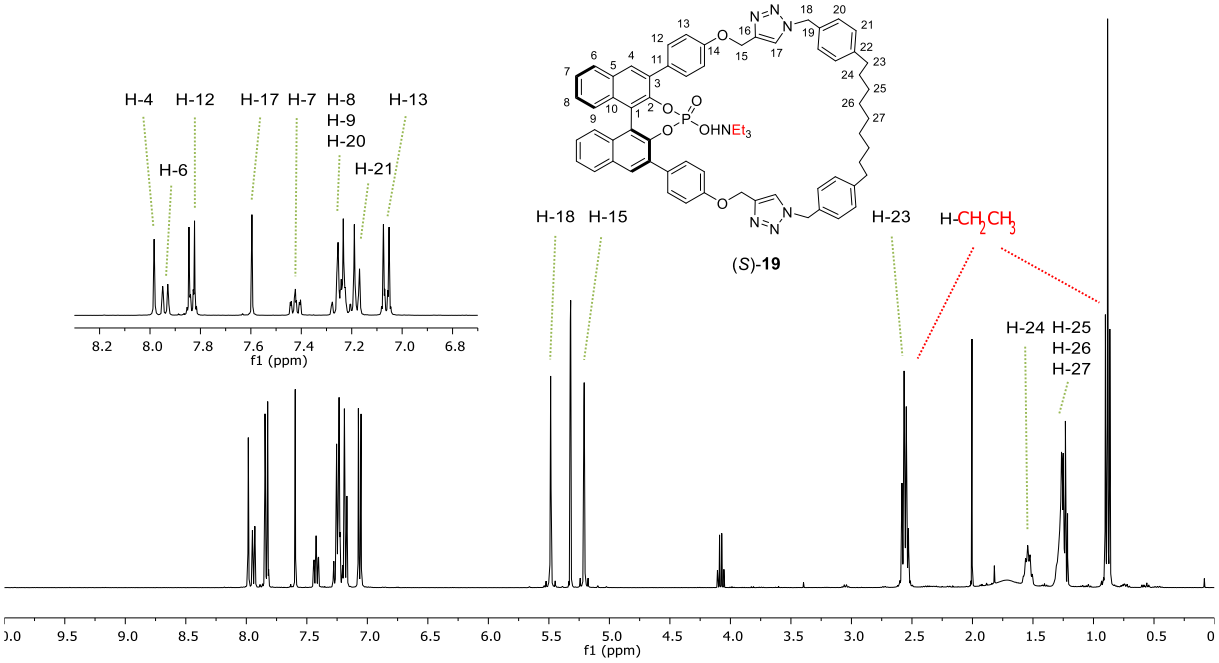

Figure 99*:* Overview of the ^{1}H-NMR spectrum and the excerpt of the ^{31}P-NMR spectrum. Distinctive signals are highlighted ([D_2]-dichloromethane, ^{1}H-NMR: 400 MHz, ^{31}P-NMR: 162 MHz, 298 K).

In the ^{1}H-NMR spectrum formation of the product is indicated by shifts of signals. Additionally, the signals for the triethylammonium are discernible in the right ratio to e.g. protons H-18 and H-15. The product is further identified by a single signal at 3.28 ppm in the ^{31}P-NMR spectrum.

4.2.3.2 Further modification of the catenanes

To obtain catenanes that are suitable to be applied in catalysis, some further modifications of the catenanes had to be done. One position that proved suitable for such modifications are the 2,2'positions of the BINOL. For this the MOM-protecting group had to be removed first.

The following reactions were carried out under the same conditions for both, the [2]catenane and [3]catenane, and yielded very similar results. Accordingly, the further modifications shown for the [2]catenane are representative for both catenanes.

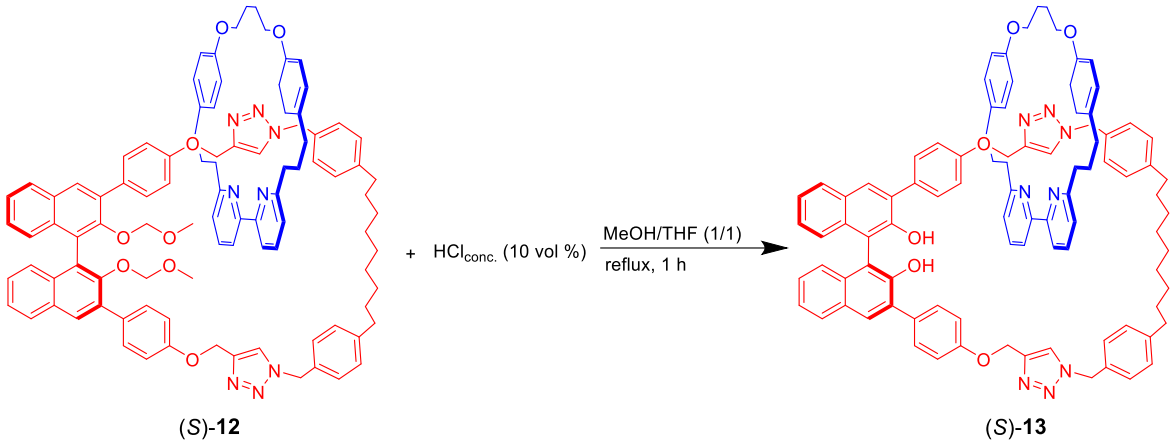

(*S*)-**12** (*S*)-**13**

Figure 100: MOM-deprotection representatively shown for the [2]catenane (*S*)-**13**.

The removal of the acid labile MOM-protecting group is achieved by dissolving the catenane in a 1:1 mixture of methanol and tetrahydrofuran and successive addition of 10 vol% concentrated hydrochloric acid, followed by 1 hour of stirring at reflux. Completion and success of the reaction was verified by ^{1}H-NMR spectroscopy. Chromatographic purification of the [3]catenane was not conducted despite the small impurities visible in the ^{1}H-NMR spectrum (***Figure 101*** bottom). These impurities were removed in the following step. The yield for the [2]catenane was 90% while the yield for the [3]catenane was 96%.

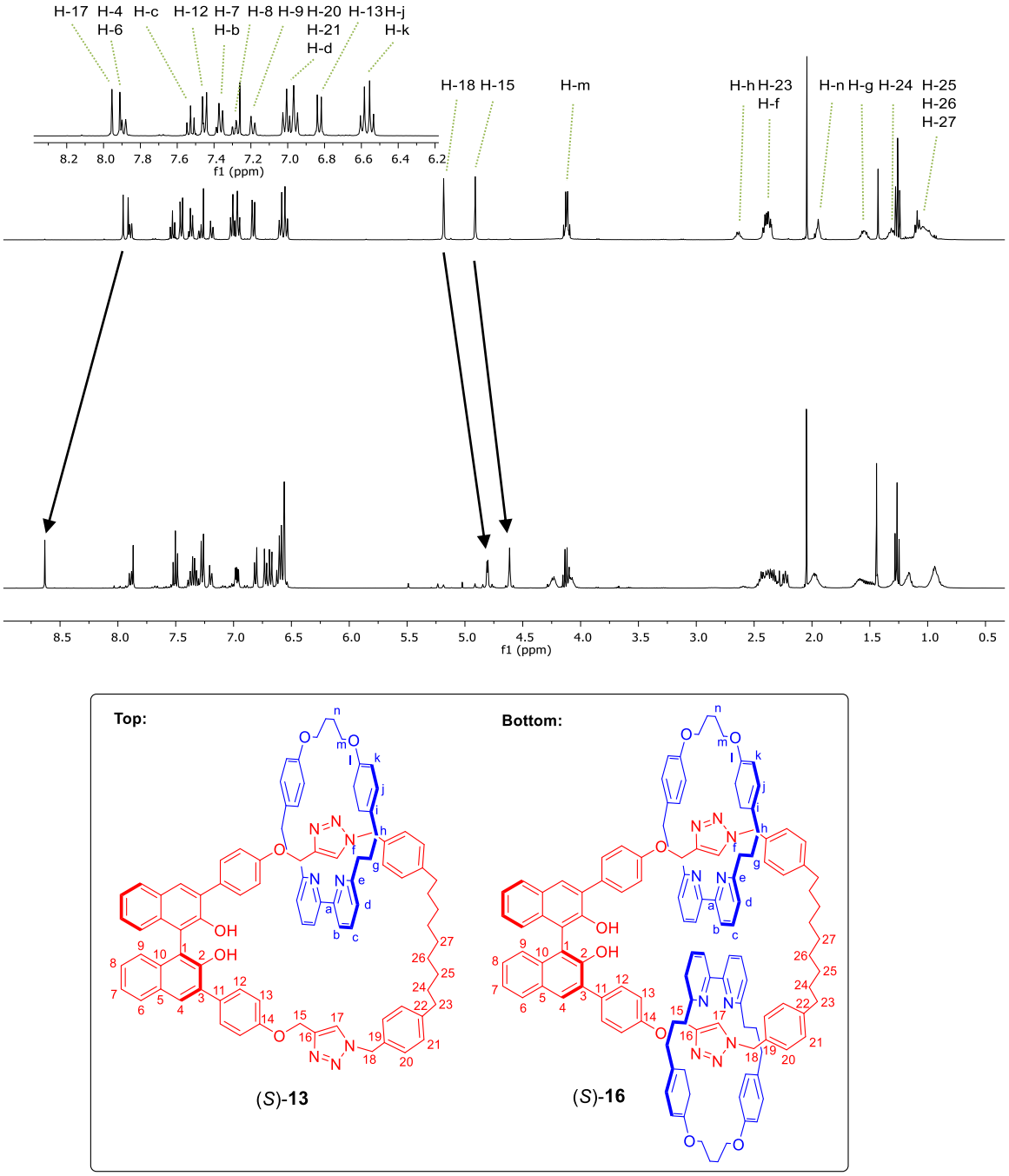

Figure 101: ^{1}H-NMR spectra of diol [2]catenane (*S*)-**13** and diol [3]catenane (*S*)-**16** ([D$_1$]-chloroform, 400 MHz, 298 K).

Identification of the product was achieved by checking for the absence of the specific signals of the MOM-protecting group (MOM-C*H*$_3$ at 2.26 ppm for (*S*)-**12** and 2.21 ppm for (*S*)-**15**). In Addition, mass spectrometry confirmed that the catenanes stayed intact during reaction. When comparing the ^{1}H-NMR spectra of the [2]catenane and the [3]catenane, the spectra are very similar, however, some signals show different chemical shifts (***Figure 101***). This is most pronounced for the C-*H* of the triazoles (H-17) as well as the signals for H-18 and H-15. Interestingly, two sets of signals again appear for the signals of the bipyridine macrocycle in the ^{1}H-NMR spectrum for the [3]catenane (e.g. H-m and H-m'). As discussed earlier these two sets of signals could arise from the bipyridines being unequal in the crowded [3]catenane.

The diol [2]catenane and [3]catenane then were further treated in a phosphorylation reaction to obtain the desired functionality in the BINOL based macrocycle. Because of the similarity of this BINOL-based subunit of the catenane and the previous BINOL-based catenanes (see chapter 3) as well as the macrocycle **2c**, the same protocol for phosphorylation was applied again.

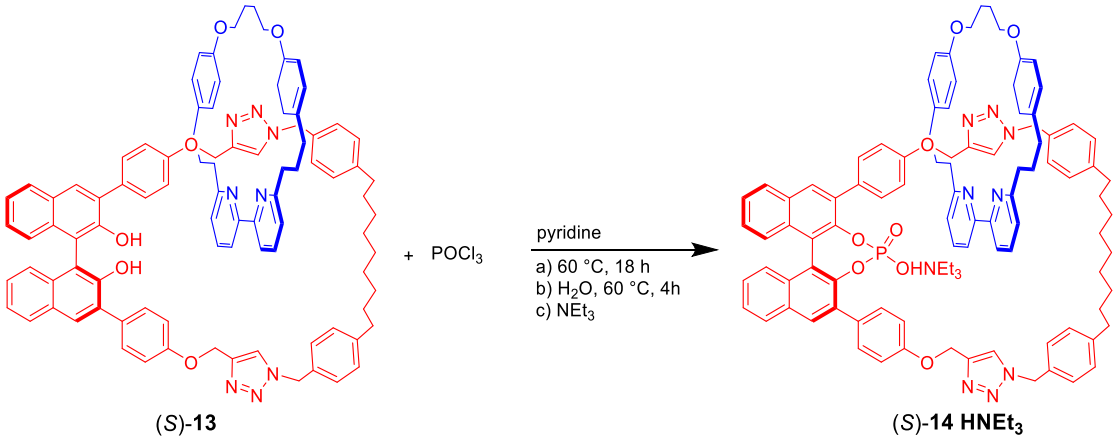

Figure 102: Phosphorylation of [2]catenane. Triethylammonium salt is obtained after column chromatography with silica deactivated by triethylammonium.

Again the success of the phosphorylation was confirmed by shifts of several signals as well as the presence of signals in the ^{1}H-NMR of the triethylammonium in the expected ratio to the integrals of the rings. Mass spectrometry also confirmed that the products were formed and the rings stood intact during the reaction.

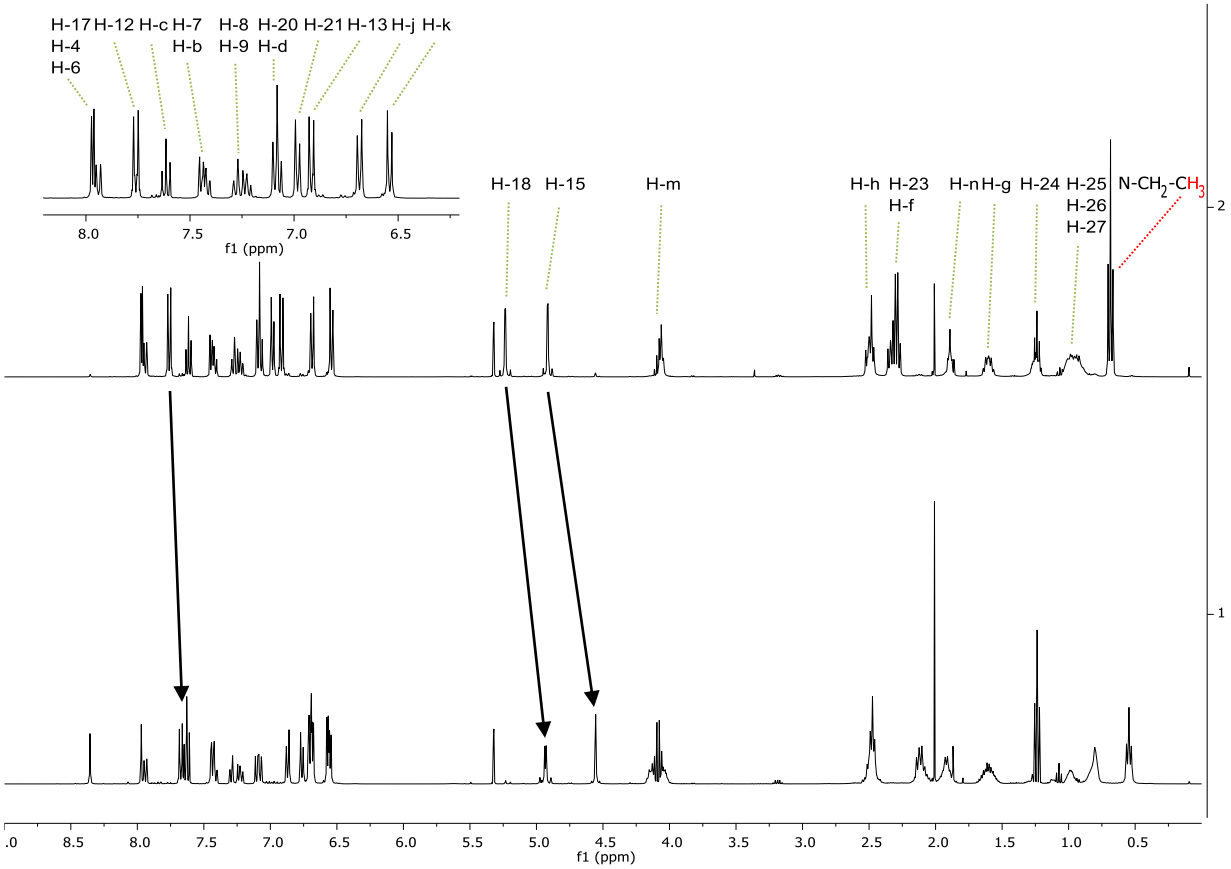

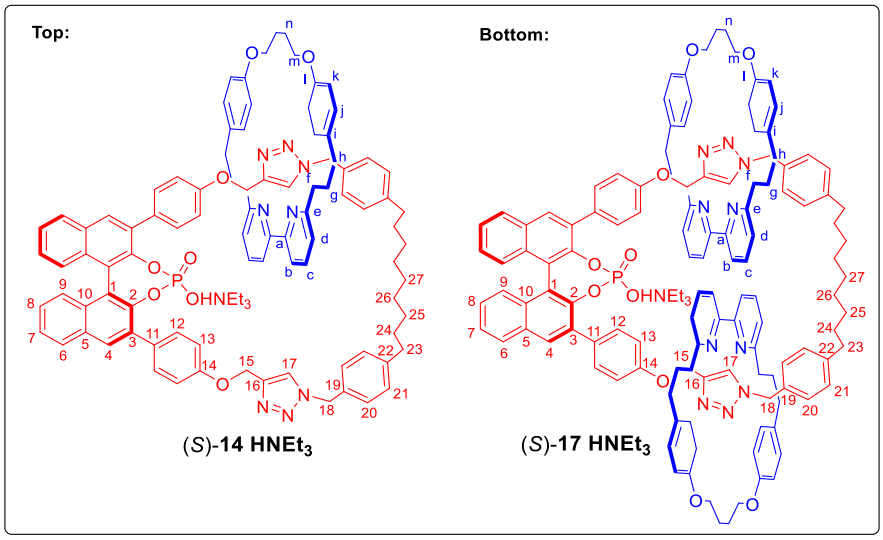

Figure 103: ^{1}H-NMR spectra of [2]catenane phosphate (top) and [3]catenane phosphate (bottom) ([D_2]-dichloromethane, 400 MHz, 298 K).

Just like before, the ^{1}H-NMR spectra of the [2]catenane and the [3]catenane look very similar. Again, when comparing the spectra of the two catenanes, shifts of signals of protons which are close to the triazole moiety can be observed. In more detail, this is the case for protons H-18 and H-15 as well as for proton H-13. Especially the difference for H-13 is interesting when it comes to application of the catenanes in asymmetric catalysis. Since these protons are located at the phenyl substituent of the BINOL in 3,3'-positions, which are known to be crucial for the stereoinduction of BINOL based chiral phosphoric acids, interaction of the bipyridine macrocycles with these substituents could induce interesting differences in stereoselectivity.

4.3 Catalysis

While in the beginning catenanes have been synthesized to just prove the feasibility of the synthesis, nowadays a lot of applications for catenanes have emerged (see chapter 1.2). One sophisticated application is the use of catenanes in asymmetric catalysis, which was only shown once by *Niemeyer* recently.[35]

To further contribute to this intriguing topic of research, the two catenanes presented in this chapter were applied in asymmetric catalysis. For this, two different promising ways to exploit the mechanical bond in the catenanes were tested. In the first method the catenanes were applied in asymmetric metal catalysis (***Figure 104***).

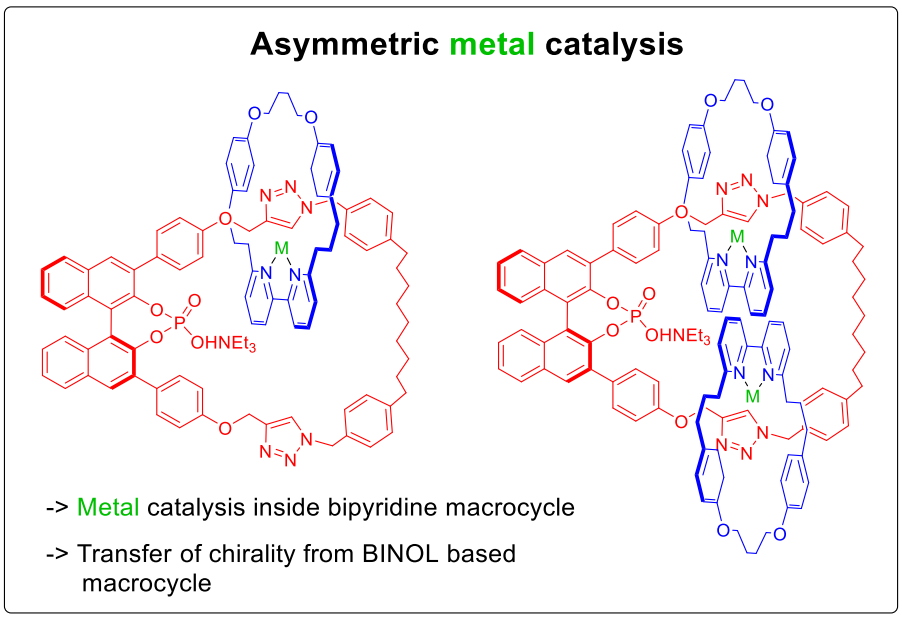

Figure 104: Envisioned application of the two catenanes in asymmetric catalysis.

Metal based, Lewis acid catalysis can be conducted, where the bipyridine strongly binds the metal cation endohedrally to perform Lewis acidic activation. In this scenario, the BINOL-based macrocycle creates a chiral environment by its axially chiral phosphate by the means of asymmetric counteranion-directed catalysis (ACDC) (see chapter 1.3). In contrast to ordinary ACDC, the mechanical bond prevents dissociation of the BINOL-based macrocycle from the catalytically active bipyridine macrocycle. This high local molarity of the two components has the great advantage that only relatively weak interactions between the chiral phosphate and the intermediate substrate are necessary to induce stereoselectivity. In a similar approach using the same subcomponents without the mechanical bond, much higher concentrations or much stronger interactions would be necessary.

4.3.1 Trials with Lewis acids inside the bipyridine macrocycle

The first part of this catalysis chapter is about the use of the catenanes as Lewis acid catalysts according to scenario 1 (***Figure 104*** a). To determine suitable reactions for catenane-based catalysis, different reaction types were screened which are described hereafter. To save material of the precious catenanes, all reactions were carried out using the bipyridine macrocycle **11** first.

A3-reaction

The first reaction that was tried was the A3-reaction between imine **96** and phenylacetylene. The macrocyclic Cu(I)bipyridine complex was formed prior to addition of the substrates to activate the alkyne for the nucleophilic attack on the imine.[162]

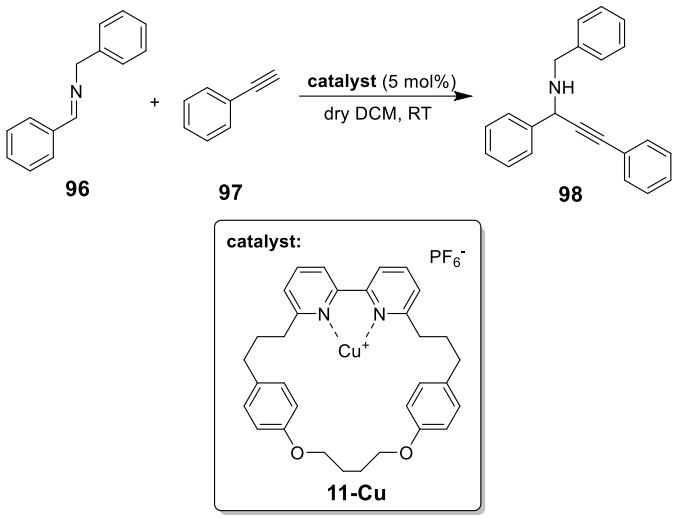

Figure 105: A3-reaction of preformed imine **96** and alkyne **97**.

No conversion was observed. Increasing the temperature (T= 35 °C or 80 °C in 1,1,2,2-tetrachloroethane) as well as addition of five equivalents of *N*,*N*-diisopropylethylamine to help activating the alkyne gave no product either.

[162] C. Wei, C.-J. Li, *J. Am. Chem. Soc.* **2002**, *124*, 5638–5639.

Ring-opening of epoxide 99

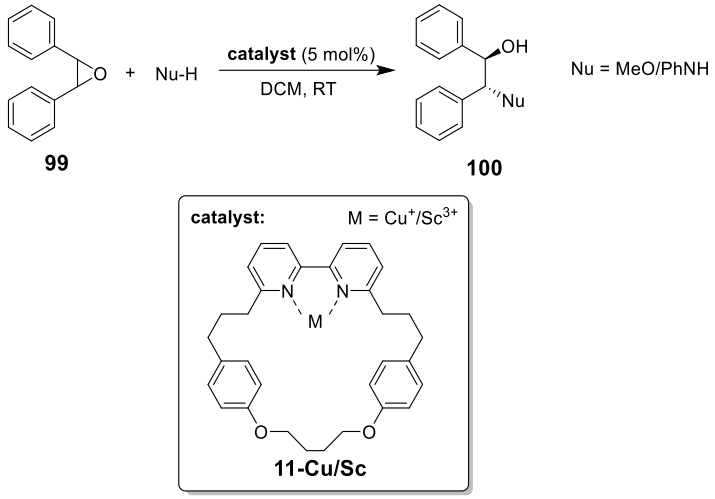

Figure 106: Epoxide ring opening reaction catalysed by macrocyclic catalysts **11-Cu/Sc**.

Cu(I) or Sc(III) were complexed by the bipyridine macrocycle to act as Lewis acids, activating the epoxide for a nucleophilic attack.[163] Methanol or aniline were used as nucleophiles. In all cases no conversion was observed.

Henry reaction

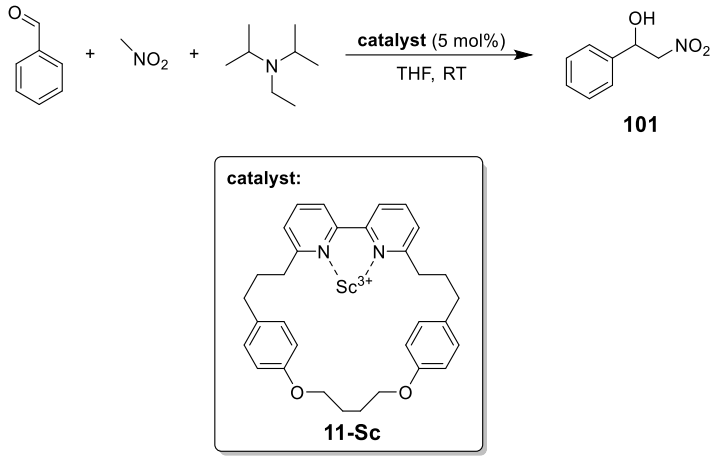

Figure 107: Henry reaction of benzaldehyde and nitromethane catalysed by macrocycle **11-Sc**.

Henry reactions proceed through deprotonation of nitromethane and the following nucleophilic attack on a carbonyl group.[164] The carbonyl group can be activated by a Lewis acid. In this case scandium(III) was complexed by the bipyridine macrocycle to fill the role of the catalyst but no reaction was observed after 20 hours at room temperature.

[163] C. Schneider, A. R. Sreekanth, E. Mai, *Angew. Chem. Int. Ed.* **2004**, *43*, 5691–5694.
[164] H. Mei, X. Xiao, X. Zhao, B. Fang, X. Liu, L. Lin, X. Feng, *J. Org. Chem.* **2015**, *80*, 2272–2280.

Michael addition

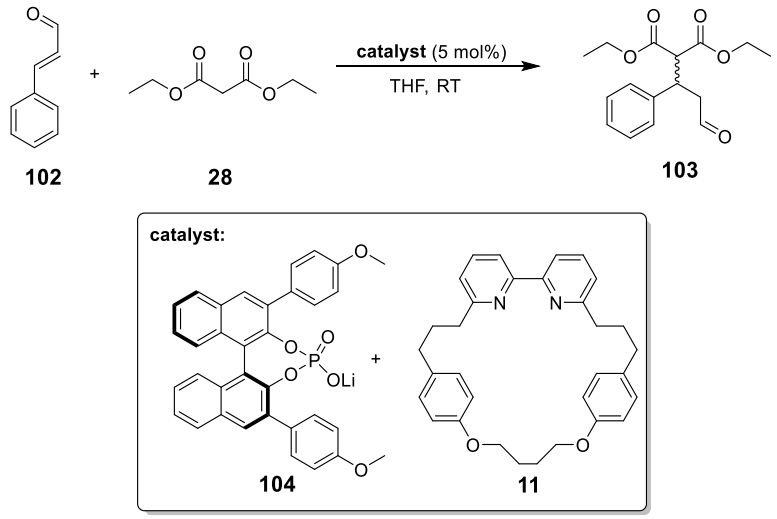

Figure 108: Michael addition of malonate to trans-cinnamaldehyde.

Michael additions rely on the nucleophilic attack of a carbanion to α-β-unsaturated carbonyl compounds. The idea behind the reaction shown above, is the deprotonation of the malonate by the bipyridine macrocycle **11** while the lithium phosphate (*S*)-**104** activates either the malonate for the deprotonation or the carbonyl for the nucleophilic attack. The reaction is inspired by a recent publication by *Niemeyer* et al. where a rotaxane, composed of a metal-phosphate macrocycle and a thread bearing a secondary amine, catalysed the reaction with superior stereoselectivity compared to the non-interlocked subcomponents only.[165] No conversion was observed in this reaction.

Hydrocyanation of imines

Hydrocyanation describes the addition of hydrogen cyanide to an electrophile such as an imine (i.e. Strecker reaction). This reaction can be catalysed by Lewis acids which bind to the imine and thus activate it for the nucleophilic attack of the cyanide ion. This cyanide ion can either come from HCN gas directly (or an aqueous solution of it) or derivatives that can release HCN in situ such as trimethylsilyl cyanide, which forms HCN upon reaction with protic substances e.g. methanol.

The catalysts were prepared prior to the reaction by stirring a mixture of $Sc(OTf)_3$ and [2]catenane and [3]catenane respectively in dichloromethane overnight to incorporate the metal. Acetylation of the product by trifluoroacetic anhydride is used to prevent the elimination reaction, which would yield again the starting material.

[165] N. Pairault, H. Zhu, D. Jansen, A. Huber, C. G. Daniliuc, S. Grimme, J. Niemeyer, *Angew. Chem. Int. Ed.* **2020**, *59*, 5102–5107.

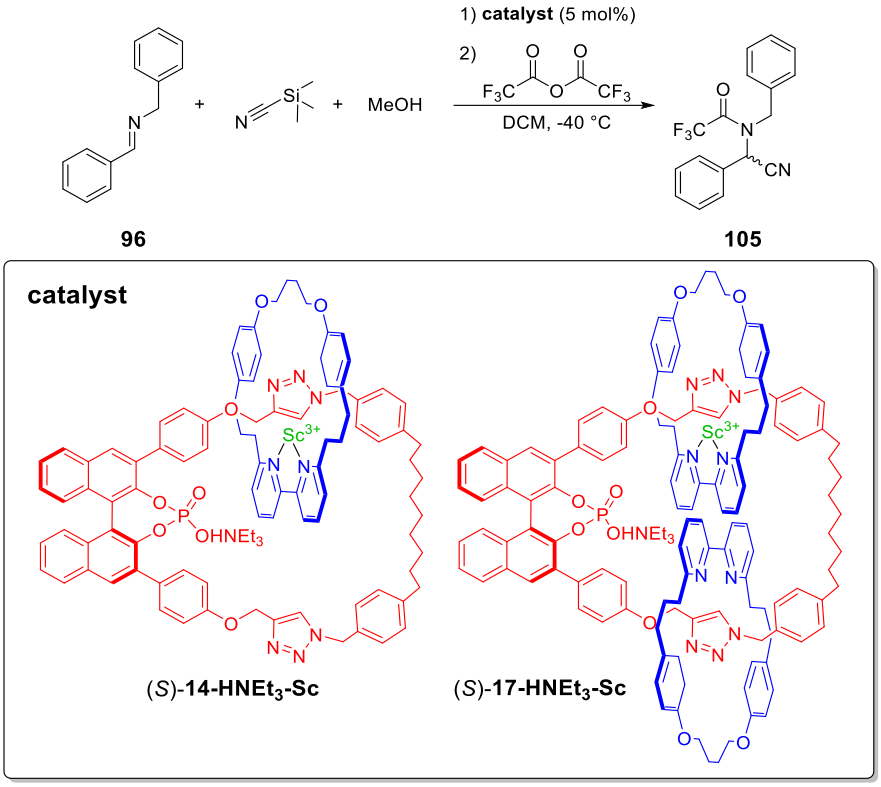

Figure 109: Hydrocyanation of imine **96** by TMSCN catalysed by the catenated Sc-catalysts (*S*)-**14-HNEt$_3$-Sc** or (*S*)-**17-HNEt$_3$-Sc**.

The reaction was completed after 24 hours in both cases, however, chiral HPLC analysis revealed that the reaction yielded no enantiomeric excess. Thus, asymmetric hydrocyanation catalysed by the catenated catalysts was not successful and was discarded.

Tsuji-Trost reaction using Iridium catalysts

Another reaction that was examined was the Tsuji-Trost reaction of *trans*-cinnamyl phosphate with *N*,*N*'-di-Boc-guanidine which is catalysed by transition metals such as palladium or iridium.[166] In contrast to the reaction using a palladium based catalyst, using an iridium based catalyst yielded two products, a linear and a branched one. This is the results of the intermediate allyl-cation which can be attacked by a nucleophile at two positions in iridium catalysed reactions (***Figure 110***).

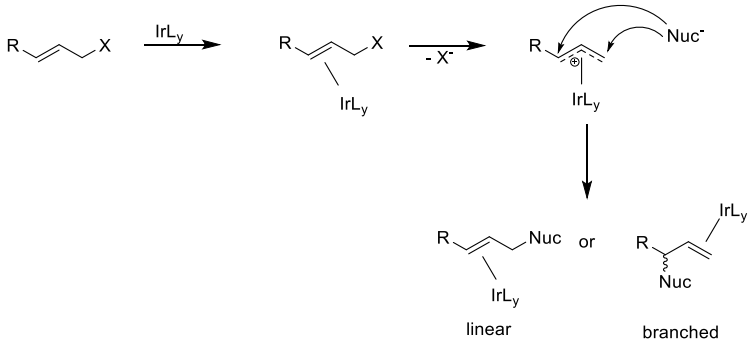

Figure 110: Mechanistic view on the formation of the linear and branched product in the Tsuji-Trost reaction.

The linear product is achiral so the branched product will be the focus for the investigations regarding the stereoselectivity. Additionally, the selectivity regarding the ration of the linear and branched products was investigated, thus four different catalysts were applied in the reaction (**Figure 111**). The iridium based catalysts were prepared beforehand by mixing each ligand with 1,5-cyclooctadien-iridium(I)-chloride-dimer in dichloromethane. The reaction proceeded successfully within two days in all cases.

[166] H. Miyabe, K. Yoshida, V. K. Reddy, Y. Takemoto, *J. Org. Chem.* **2009**, *74*, 305–311.

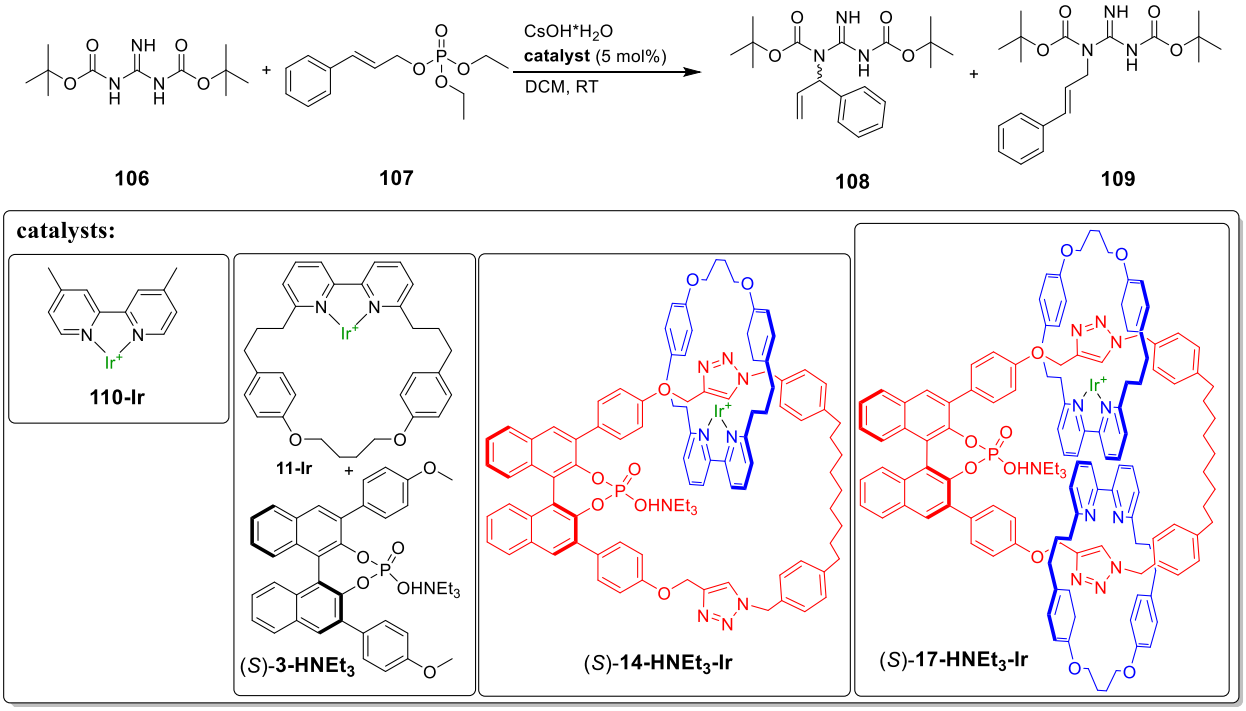

Catalyst	Ratio 108/109 (branched/linear)	Enantiomeric excess for (*R*)-108 [%]
110-Ir	23/77	0
11-Ir	49/51	<5
(S)-14-HNEt$_3$-Ir	63/37	0
(S)-17-HNEt$_3$-Ir	58/42	0

Figure 111: Tsuji-Trost reaction catalysed by the different iridium based catalysts (top) and the resulting ratio of products and enantiomeric excesses (bottom).

Interestingly, different ratios for the linear and branched product were obtained for all catalysts. However, differences for the catenanes are rather small and cannot be attributed to an influence of the mechanical bond. Additionally, the reaction proceeded non-stereoselectively for both catenated catalysts. Another try in toluene with the iridium-[2]catenane catalyst was not fruitful due to poor solubility of the complex in the solvent. No conversion was observed. Therefore, this reaction is not suitable to test the influence of the mechanical bond on the stereoselective outcome in asymmetric catalysis and was discarded.

4.3.2 Brønsted acid catalysed transfer hydrogenation

The first approach to utilize the catenanes (S)-**14-HNEt$_3$** and (S)-**17-HNEt$_3$** with endohedrally bound Lewis acids in the bipyridine macrocycle was not successful when applied to the asymmetric reactions described before. It was not possible to induce stereoselectivity by the chiral BINOL based macrocycle through transfer of chirality onto the other macrocycle. In the second scenario catalysis is performed directly at the BINOL based macrocycle, namely by the phosphoric acid (**Figure 112**). The second macrocycle is used to alter the environment of the catalytic centre by steric interactions and therefore modulate the stereoselectivity. This is especially interesting since in the [2]catenane the bipyridine macrocycle can freely travel between the two triazole units while the existence of the second bipyridine macrocycle in the [3]catenane prevents such movement. Thus, it is conceivable that higher steric interactions with the catalytically active site prevail in the [3]catenane.

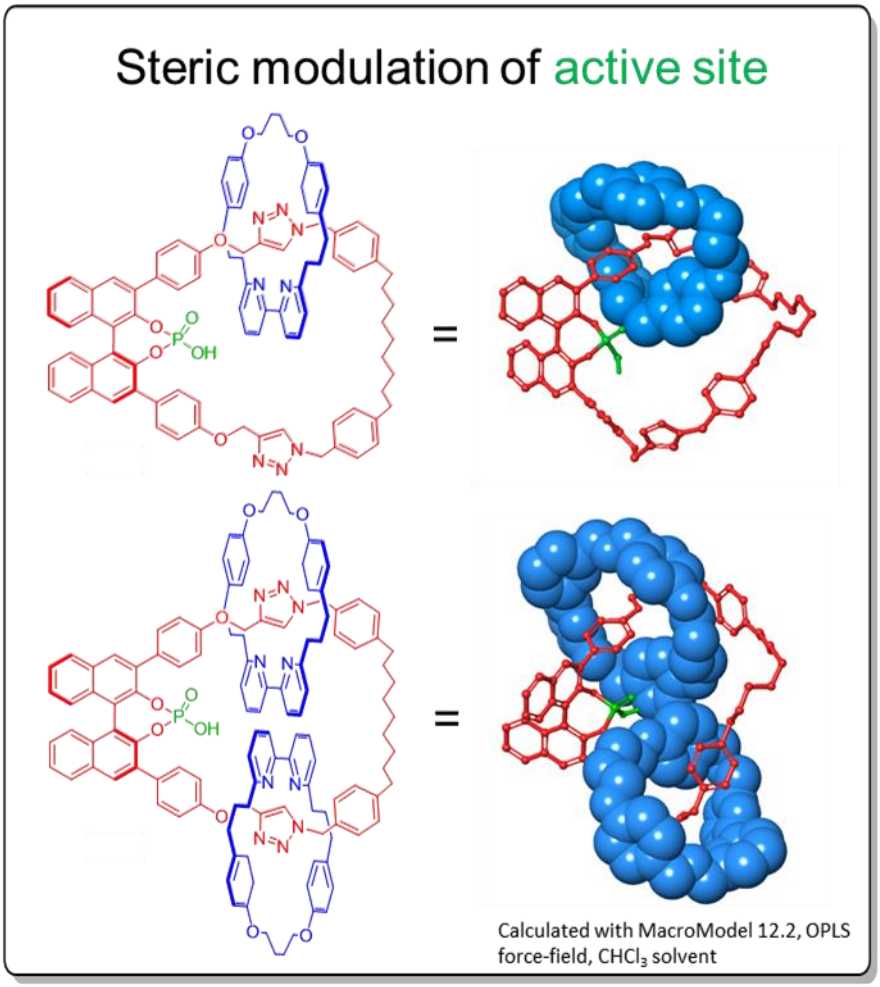

Figure 112: Protonated [2]catenane and [3]catenane and their 3D-models showing a possible steric influence of the bipyridine macrocycle (blue) on the catalytic centre (green) of the BINOL based phosphoric acid macrocycle (red).

The active site of this macrocycle is composed of a phosphate which can be protonated and consequently act as a chiral phosphoric acid (CPA; see chapter 1.3) in Brønsted acid organocatalysis.

To investigate the influence of the mechanical bond, transfer hydrogenation of 2-substituted quinolines by Hantzsch ester was chosen. The mechanism of this reaction is well understood and analysis of the outcome can therefore easily be interpreted. In order for the catenane to function as Brønsted acid it has to be

protonated first. Next to the phosphate the catenanes bear two more functional groups, namely the bipyridines and the triazoles, that could be protonated (***Figure 113***).

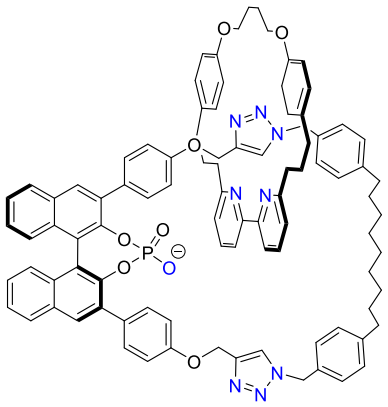

Figure 113: Basic functional groups (highlighted blue) in the [2]catenane.

Therefore, two methods of protonating the catenane were compared experimentally. The first method is the same that was also used to protonate phosphoric acid catalysts in chapter 3. This was done by dissolving the compound in dichloromethane (50 mM) and washing it with hydrochloric acid (2M; 3 times with half the volume of dichloromethane). The organic phase was separated from the aqueous phase and dichloromethane was removed under reduced pressure without further treatment of the organic phase.

The second method is similar in handling, but protonation is achieved by washing the organic phase with an aqueous citric acid solution (50 mM; 3 times with the same volume as dichloromethane). Since citric acid is a weak acid, this method is considered a mild protonation procedure, which might show difference regarding protonation of the basic sites.

In the following the ^{1}H-NMR spectra of the triethylammonium phosphate [2]catenane and the two protonated [2]catenane spectra are compared among each other (***Figure 114***).

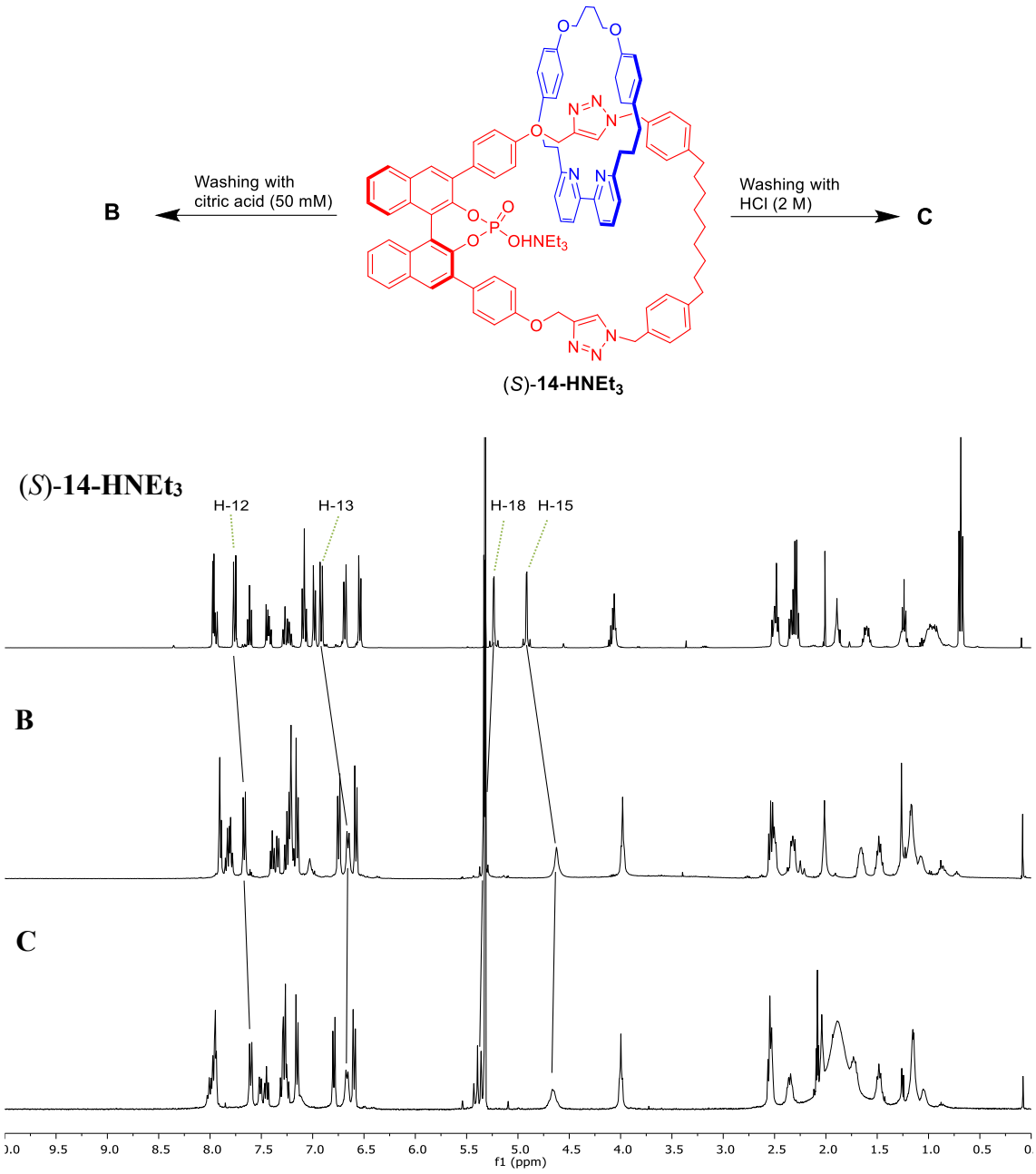

Figure 114: Comparison of spectra of [2]catenane **Top**: As triethylammonium phosphate, **B**: Protonated by washing with citric acid solution (50 mM) and **C**: Protonated by washing with HCl (2M) ([D_2]-dichloromethane, 400 MHz, 298 K).

When comparing the phosphate spectrum some shifts can be discerned (H-13, H-15, H-18) which indicates successful conversion to the desired product. Another point that speaks for the successful protonation is the missing triethylammonium signal at 0.70 ppm (***Figure 114***). The ^{1}H-NMR spectra for the differently protonated species (**B** and **C**) exhibit high similarity. Especially the similar shifts for H-12 and H-13 suggest that the environment close to the catalytically active site is similar for both protonated species. Protonation was achieved in the same way for the [3]catenane.

The protonated [2]catenanes and [3]catenanes were then applied in the transfer hydrogenation of 2-substituted quinolines (***Figure 115***). The catalysts are depicted with only the phosphoric acid being protonated, however, the exact protonation states of the catalysts are unknown. For this, –**HCl** refers to the

triethylammonium phosphate pre-catalyst being protonated by hydrochloric acid (2M) while –**HC** refers to the triethylammonium phosphate pre-catalyst being protonated by citric acid (50 mM).

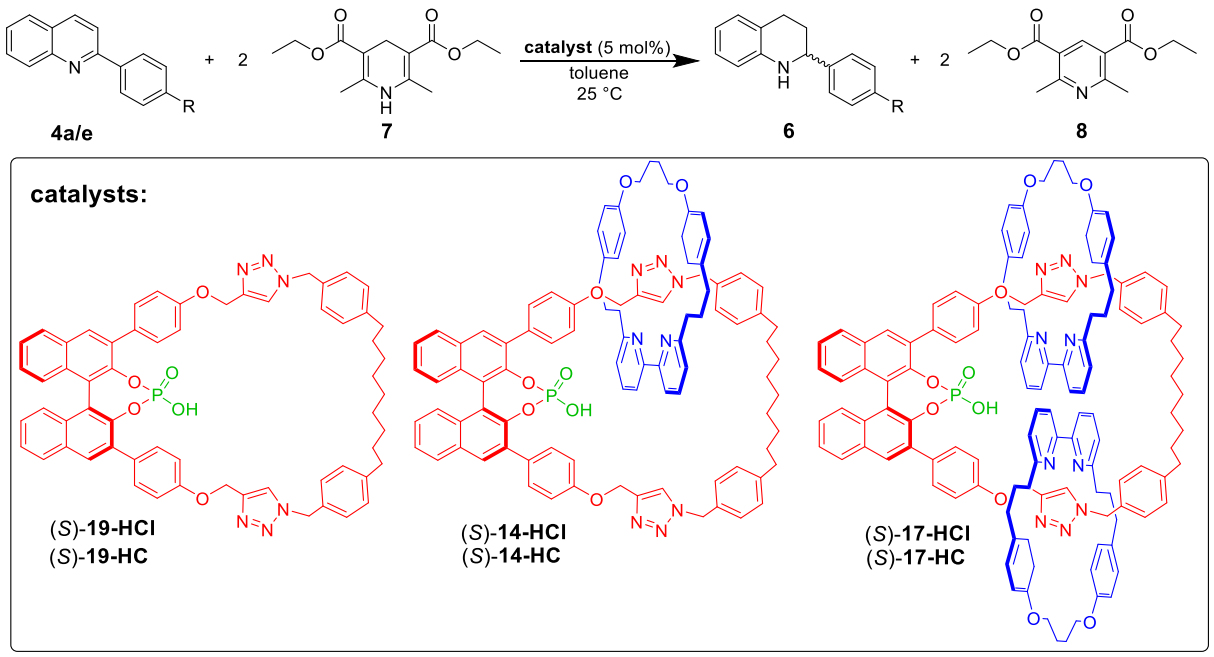

Entry	R =	Catalyst[a]	Enantiomeric excess (%)[b]
1	H	(*S*)-**14-HCl**	18
2	H	(*S*)-**14-HC**	18
3	H	(*S*)-**17-HCl**	0
4	H	(*S*)-**17-HC**	0
5	*tert*-butyl	(*S*)-**19-HCl**	75
6	*tert*-butyl	(*S*)-**19-HC**	78
7[c]	*tert*-butyl	(*S*)-**19-HCl**	78
8	*tert*-butyl	(*S*)-**14-HCl**	33
9	*tert*-butyl	(*S*)-**14-HC**	33
10	*tert*-butyl	(*S*)-**17-HCl**	13

Figure 115: Top: Transfer hydrogenation of 2-(4-tert-butylphenyl)quinoline using differently protonated [2]catenanes ((*S*)-**14-HCl** and (*S*)-**14-HC**)) and [3]catenanes ((*S*)-**17-HCl** and (*S*)-**17-HC**)). Bottom: (a) 5 mol% catalyst loading relative to quinoline. (b) Determined by chiral HPLC (Chiralcel OD-H column). (c) Additional 5 mol% of **11**.

No major difference between the differently protonated species of [2]catenane as well as for the [3]catenane was observed. Enantiomeric excesses using 2-phenylquinoline as a substrate (Entry 1-4) were low (18% *ee* for [2]catenanes) or non-existent (for [3]catenanes). Using the *tert*-butyl derivative increased the enantiomeric excesses for the [2]catenanes (33% *ee*) and [3]catenane (13% *ee*) (Entry 8-10). In addition, reaction with the sole BINOL based macrocycle afforded much higher enantiomeric excesses (78% *ee*). The results obtained from this set of experiments clearly show that the stereoselectivity decreases with increasing number of bipyridine macrocycles in a molecule. A comparative reaction where 5 mol% of the

bipyridine macrocycle **11** were added to the reaction with the BINOL based catalyst (Entry 7) the same enantiomeric excesses were obtained. This suggests that the observed differences in stereoselectivity can be directly attributed to the mechanically bound bipyridine macrocycle.

4.3.3 Investigation of the protonation states

Since the exact protonation states of the catenanes and the macrocycle are not known, the observed differences in stereoselectivity may stem from a steric modulation of the catalytically active site, but also from other effects such as non-stereoselective catalysis by basic moieties that have been protonated during the treatment with HCl or citric acid. A look at the pK_a values of the different functional groups (acids or corresponding acids) allows a first estimation of the likelihood of protonation of different groups (***Figure 116***).

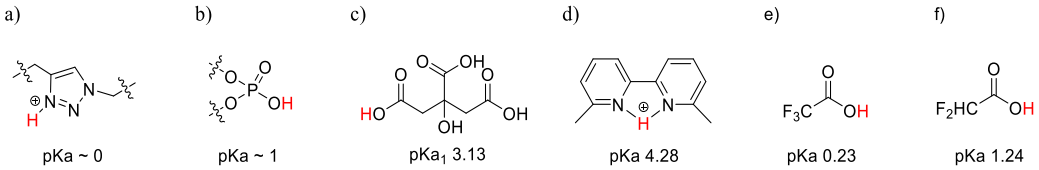

Figure 116: pK_a values for a) 1,4-disubstituted 1,2,3-triazoles,[167] b) BINOL based phosphoric acids,[168] c) citric acid[169] and d) 6,6'-dimethyl-2,2'-bipyridine,[170] e) trifluoroacetic acid and f) difluoroacetic acid.[171]

Due to the low basicity (i.e. high acidity of the corresponding acid) of the triazole moiety, it is the functional group that is least likely to be protonated by treatment of the catenane via the mild protonation method (i.e. washing with citric acid solution). Even though the phosphoric acid is roughly 100 times more acidic than citric acid, the successful application of the BINOL based macrocycle (*S*)-**19-H** in Brønsted acid catalysis proved that it is still possible to protonate it under such mild conditions. In contrast to this, 6,6'-dimethyl-2,2'-bipyridine is the most basic molecule among the four, with a pK_a difference of the corresponding acid of 1.15 compared to citric acid. It has to be noted, however, that this pK_a (4.28) was measured using an acyclic version of a bipyridine. Considering the possible influence which incorporation of such bipyridines into a macrocycle might have on the energetic difference of the *cis* and *trans*-conformers (and therefore on the basicity) of the bipyridine, the given pK_a value only serves as an approximation.

In any case, the differences in pK_a values are not pronounced enough to predict the behaviour of the catenanes upon treatment with citric acid or hydrochloric acid, also considering the fact that the different groups might influence each other with regard to their acidity/basicity. Therefore, it is of high interest to shed light on the protonation state of the [2]catenane, [3]catenane and the macrocycle that were applied in the transfer hydrogenation of 2-(4-*tert*-butylphenyl)quinoline.

[167] J.-L. M. Abboud, C. Foces-Foces, R. Notario, R. E. Trifonov, A. P. Volovodenko, V. A. Ostrovskii, I. Alkorta, J. Elguero, *Liebigs Ann. Chem.* **2001**, *2001*, 3013–3024.
[168] K. Kaupmees, N. Tolstoluzhsky, S. Raja, M. Rueping, I. Leito, *Angew. Chem. Int. Ed.* **2013**, *52*, 11569–11572.
[169] A. M. N. Silva, X. Kong, R. C. Hider, *Biometals* **2009**, *22*, 771–778.
[170] M. Sánchez-Castellanos, M. M. Flores-Leonar, Z. Mata-Pinzón, H. G. Laguna, K. M. García-Ruiz, S. S. Rozenel, V. M. Ugalde-Saldívar, R. Moreno-Esparza, J. J. H. Pijpers, C. Amador-Bedolla, *Phys. Chem. Chem. Phys.* **2019**, *21*, 15823–15832.
[171] R. S. Forgan, *Chem. Sci.* **2020**, *11*, 4546–4562.

Unfortunately, the protonation states cannot be determined directly in the spectra of the protonated [2]catenane (***Figure 114***) since the signal for a possible citrate counteranion cannot be clearly assigned. Therefore, two methods that allow the quantification of counteranions and consequently the determination of protonation states were tested and compared among each other. Both methods rely on protonation of the sodium phosphate [2]catenane (***Figure 117***) which was obtained by washing a solution of the [2]catenane in dichloromethane (50 mM) with an aqueous sodium hydroxide solution (2M). The sodium phosphate was chosen over the triethylammonium phosphate to avoid partial evaporation of the triethylammonium salt (i.e. the adduct of NEt_3 and TFA/DFA) which is formed upon protonation of the phosphoric acid. Thus, in each case one equivalent sodium trifluoroacetate/difluoroacetate remains in the mixture, since no washing steps but only solvent evaporation was carried out. This has to be take into account for the quantification of the protonation state, as detailed below. However, we assume that the salts do not have any influence on the catalytic behaviour of the protonated macrocycle or catenanes.

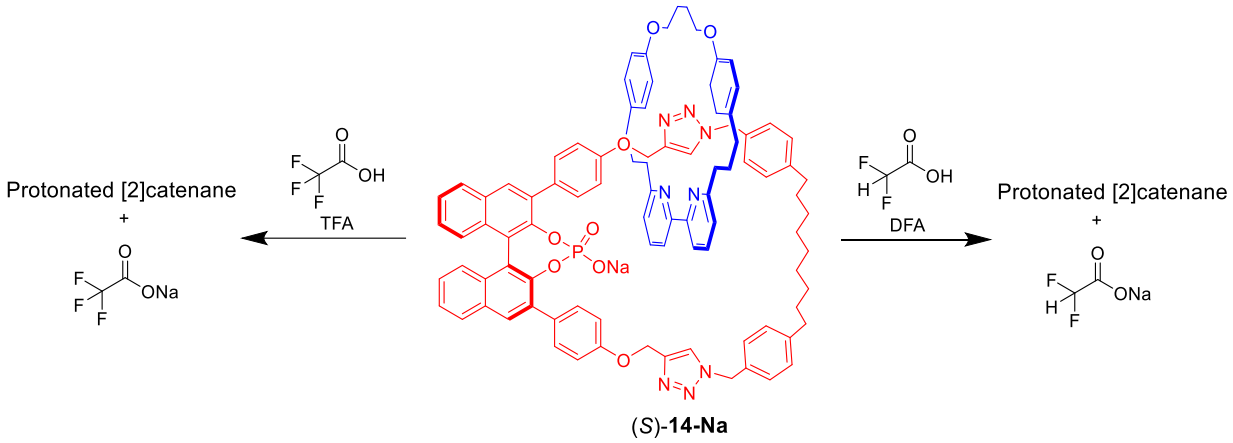

Figure 117: Overview of the two methods of determination of the protonation state of the [2]catenane. One equivalent of TFA/DFA salt is formed upon protonation of the phosphate.

In the first method the sodium phosphate [2]catenane was dissolved in dichloromethane and then protonated by trifluoroacetic acid (TFA; 100 eq.) by stirring the reagents for 30 minutes at room temperature. Volatiles were first removed in the rotary evaporator and the mixture was then dried under high vacuum for three days to ensure complete removal of the TFA excess. The TFA anion does not possess any protons, so in order to quantify the amount of anions in ^{1}H-NMR an internal standard has to be used. This internal standard needs to show a signal in the ^{1}H-NMR spectrum which can be integrated as well as a signal in ^{19}F-NMR spectrum which allows determination of the ratio of internal standard and the TFA anion. For this, trifluoroethanol was chosen.

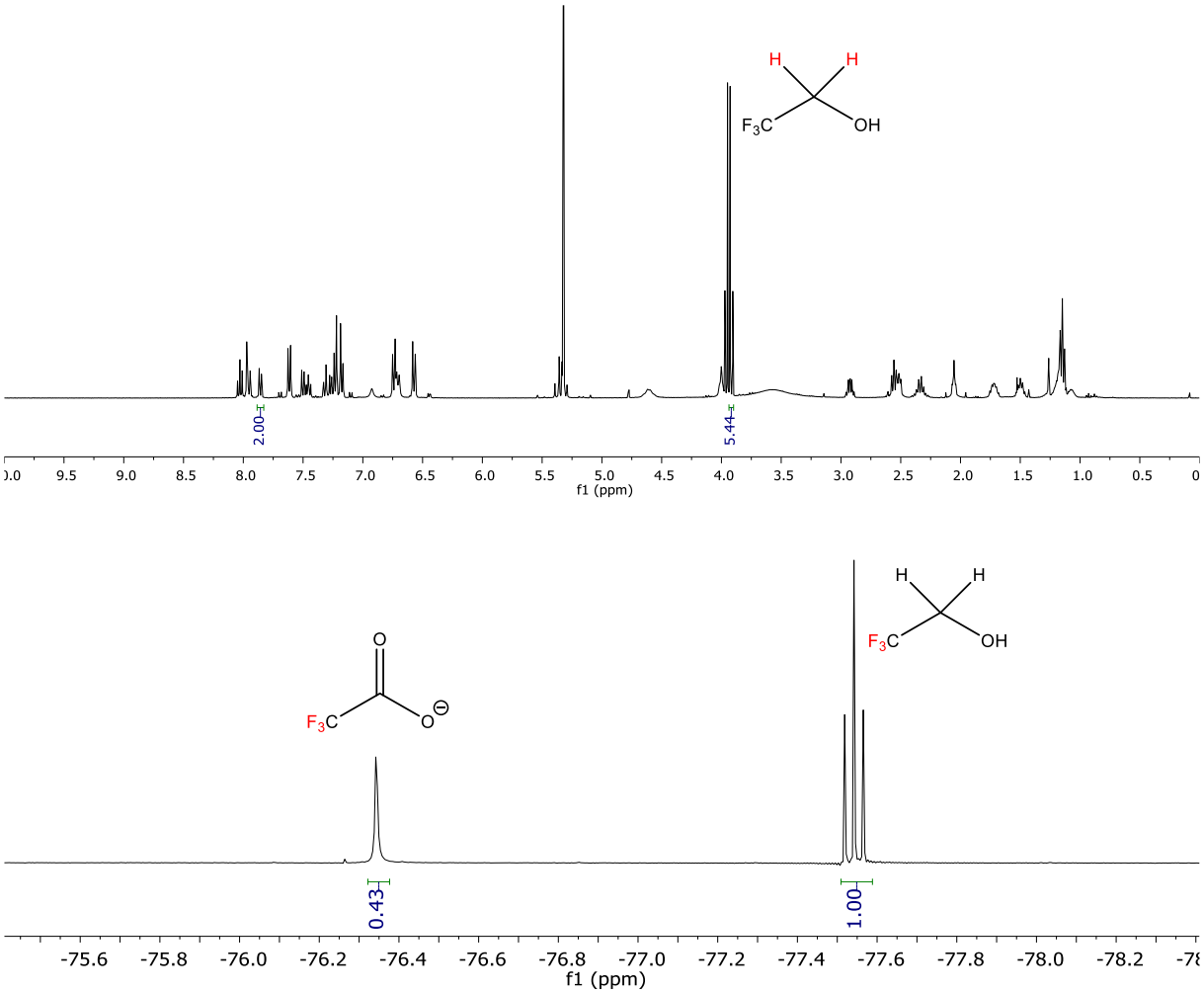

Figure 118: ^{1}H-NMR (top) and ^{19}F-NMR (bottom) spectra for the determination of the protonation state of [2]catenane ([D$_2$]-dichloromethane, 400 MHz (^{1}H-NMR) / 377 MHz (^{19}F-NMR), 298 K).

To obtain the amount of TFA counteranions the ratio of trifluoroethanol and [2]catenane signals was determined in the ^{1}H-NMR first (***Figure 118*** top). This is done by setting the signals of the [2]catenane to their correct integral and integrating half of the signal of trifluoroethanol. Since half of the signal of trifluoroethanol corresponds to one proton this integral gives the ratio in trifluoroethanol and [2]catenane. In the case of [2]catenane this leads to:

$$\frac{trifluoroethanol}{[2]catenane} = \frac{5.44}{1} = 5.44$$

To calculate the amount of TFA counteranions the ratio above (5.44) has to be multiplied by the ratio of TFA anions and trifluoroethanol which is obtained from the ^{19}F-NMR (***Figure 118*** bottom):

$$TFA\ counteranions = 5.44 * \frac{0.43}{1} = 2.34$$

This means that 2.34 equivalents of TFA anions relative to the [2]catenane are present. Considering that one sodium-TFA salt forms upon protonation of the phosphoric acid, this means that one addition group has been protonated which likely to be the bipyridine macrocycle since it is the most basic group in the catenane.

In the second method protonation of the sodium phosphate [2]catenane was achieved similarly to the first method, however, this time difluoroacetic acid (DFA) was used a proton source. The corresponding base of DFA contains a proton which is visible in the ^{1}H-NMR as a triplet at 5.59 ppm (in CD_2Cl_2). Thus, no internal standard is needed to calculate the amount of counteranions after protonation. A disadvantage could be the high boiling point of DFA, which possibly makes it more difficult to evaporate the excess. Incomplete evaporation of excess DFA would result in ratios of integrals that do not represent the correct number of counteranions and therefore indicate a false protonation state. Thus, after drying on high vacuum, the mixture was coevaporated with perfluorohexane three times and subsequently dried on high vacuum for a second time.

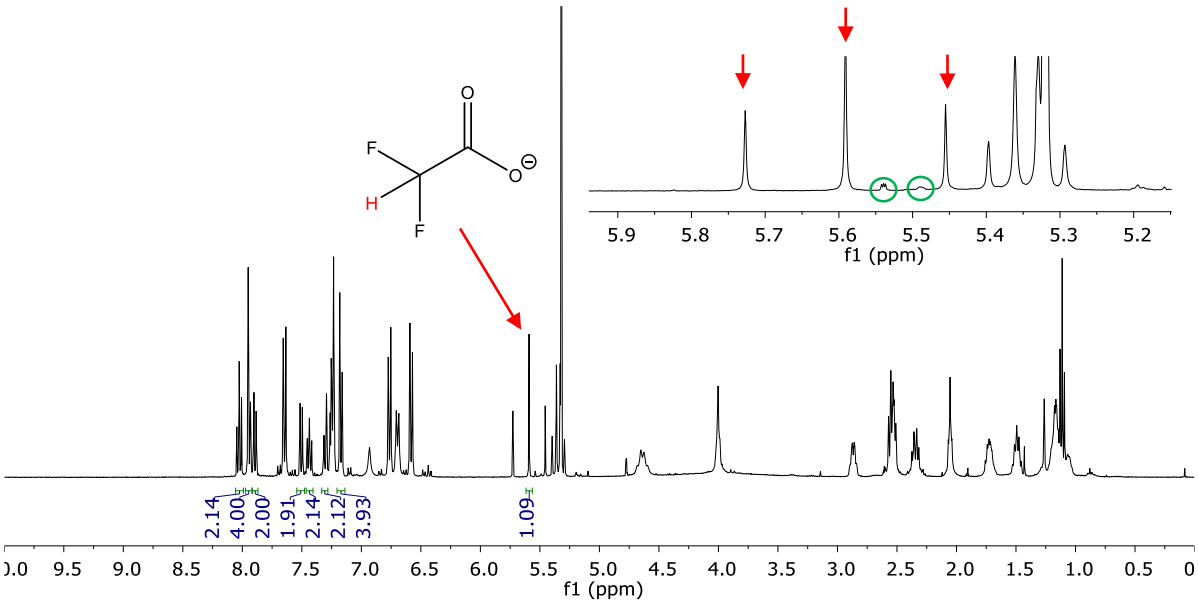

Figure 119: ^{1}H-NMR spectrum of the [2]catenane protonated by DFA. The signal for DFA is marked with red arrows. Green circles highlight impurities ([D_2]-dichloromethane, 400 MHz, 298 K).

Quantification in this method was achieved by setting the correct integrals of the [2]catenane and integrating the signal of DFA. For this only the central peak of the triplet was integrated, because small impurities (green circles) that would cause a too high integral were visible in between the peaks (red arrows; **Figure 119**). This middle peak of the triplet corresponds to half a proton of DFA. Thus, the protonation state is calculated by multiplying this value by 2. In the [2]catenane case (**Figure 119**) this results in 2.18 equivalents of DFA counteranions.

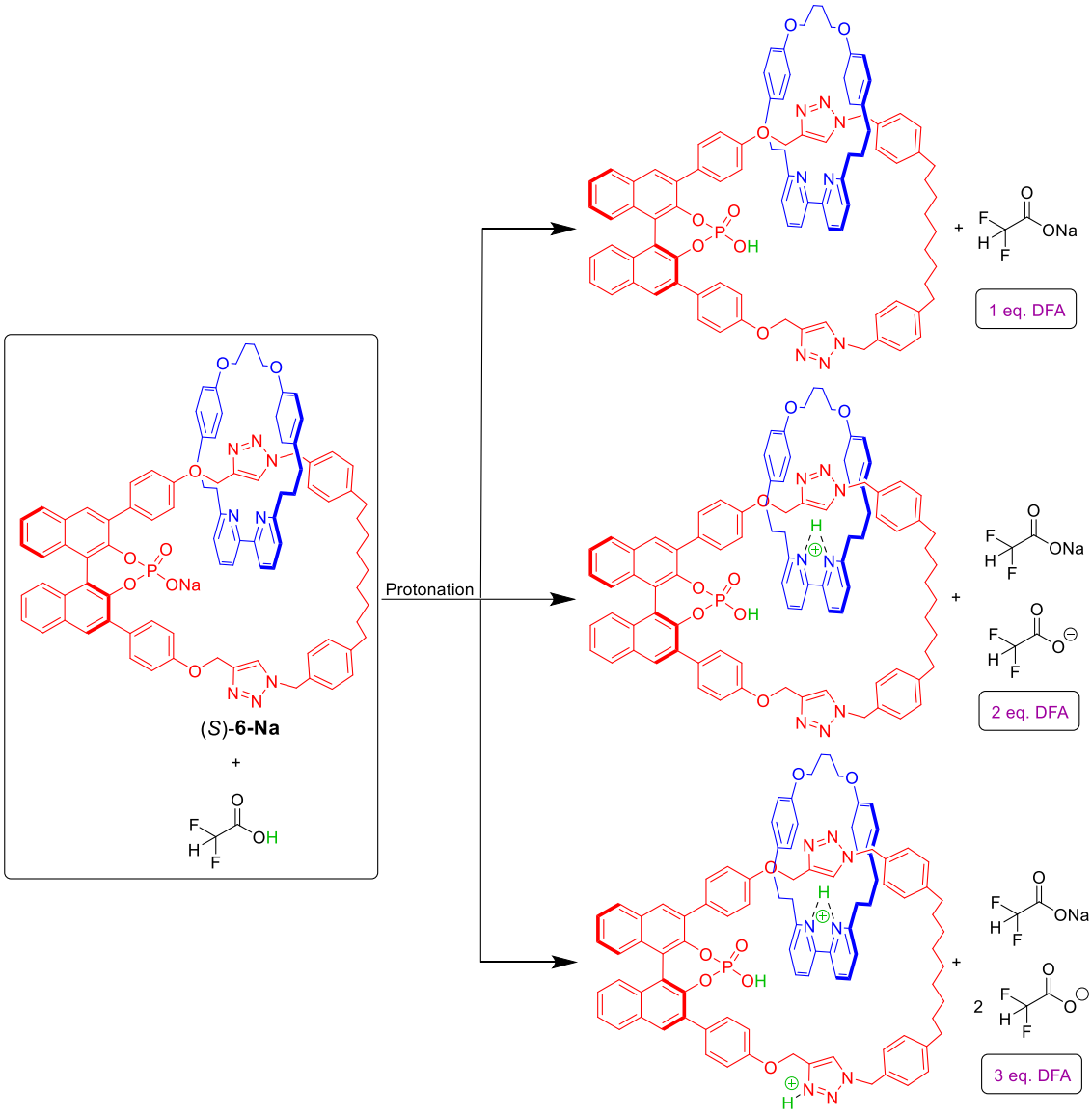

Figure 120: Possible protonation states and the resulting equivalents of DFA counterions.

One equivalent is composed of sodium-DFA which forms upon protonation of the phosphoric acid while the other equivalent is the result of the bipyridine macrocycle being protonated (***Figure 120***).

Both methods gave similar results (TFA: 2.34 equivalents. DFA: 2.18 equivalents). Since the method using DFA does not require an internal standard, it was used in the further course to determine the protonation states of macrocycle and [3]catenane. All three catalysts which were protonated by DFA were then applied in the transfer hydrogenation of 2-(4-*tert*-butylphenyl)quinoline as it was conducted before (chapter 4.3.2). The results are summarized in the following table (**Table 11**).

Table 11: Equivalents of difluoroacetic acid (i.e. protonation state) and the enantiomeric excess that was achieved with each catalyst.

Catalysts	Equivalents of DFA	Enantiomeric excess for (*R*)-4e (%)[(a)]
Macrocycle (*S*)-19-DFA	0.94	77
[2]Catenane (*S*)-14-DFA	2.18	37
[3]Catenane (*S*)-17-DFA	3.04	8

Transfer hydrogenation of 2-(4-*tert*-butylphenyl)quinoline using [2]catenane and [3]catenane and macrocycle protonated by DFA with each 5 mol% catalyst loading relative to quinoline. (a) Determined by chiral HPLC (Chiralcel OD-H column).

All three catalysts show the same stereoselectivity like their counterparts which were protonated by hydrochloric acid or citric acid. Studies regarding the protonation states revealed that in the case for macrocycle only one group has been protonated (***Table 11***). Considering the higher basicity of a phosphate than a triazole, this means that it can be assumed triazoles are not protonated by the method that was applied here. Consequently, the roughly two equivalents in the [2]catenane and the three equivalents in the [3]catenane case mean that in addition to the phosphate, the bipyridines are protonated. Thus, we assume the protonation states of these molecules as follows:

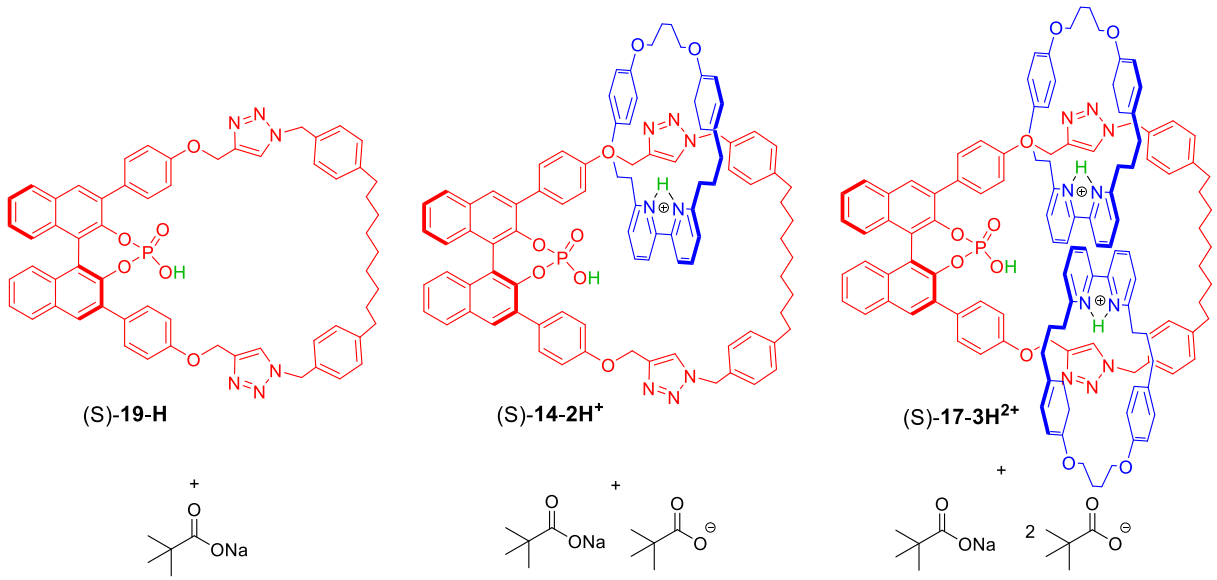

Figure 121: Assumed protonation state in the macrocycle, [2]catenane and [3]catenane after protonation with DFA.

Ultimately, the circumstance that the bipyridines are protonated in the catenanes, means that the origin for the different stereoselectivity cannot be concluded unambiguously. Lower stereoselectivities could either stem from steric modulation of the phosphoric acid moiety by the bipyridßine macrocycles or by catalytic activity of the protonated bipyridines with proceeds in a non-stereoselective fashion. To shed more light on the origin of the stereoselectivity, the protonation studies could be repeated with substoichiometric amounts of protonation agents to form catenanes which are only partially protonated. Thus, a protonation state-dependent stereoselectivity of the catenanes could be investigated. Alternatively, the protonated bipyridinium macrocycle could be tested for its catalytic activity in order to see if the unit can really act as a non-stereoselective catalytic centre.

5. Summary

5.1 Investigations on the transfer hydrogenation of 2-phenylquinoline

In the first part of the thesis the mechanism of the transfer hydrogenation of 2-phenylquinoline catalyzed by acyclic phosphoric acid **3**, macrocyclic phosphoric **2c** acid and bisphosphoric acid catenane **1c** was examined. Using classical and visual kinetic analysis, kinetically relevant data (orders in reaction, initial rates, reaction rate constants) was extracted and revealed that the three catalyst react via different mechanisms. Macrocyclic phosphoric acid **2c** reacts via a monomeric pathway, while the catenane reacts via a dimeric pathway, because the mechanical bond ensures that always two phosphoric acids are in close proximity and thus act as dimers. Normalized initial rates show, that the dimeric pathway reacts slower than the monomeric pathway.

Both catalysts do not change the pathway upon variation of the catalyst loading, which is indicated by constant normalized initial rates over a broad range of catalyst loadings. This is different for the acyclic phosphoric acid, which reacts mainly via the monomeric pathway at low catalyst loadings and mainly via the dimeric pathway at high catalyst loadings. A catalyst order of about 2 at high catalyst loadings as well as NMR spectroscopic studies revealed that the acyclic phosphoric acid forms catalyst-catalyst-substrate complexes at high catalyst loadings which then react via the dimeric pathway similar to the catenane. The similar enantiomeric excess at these high catalyst loadings (72% with 50 mol% **3**, 82% with 2.5 mol% (*S*,*S*)-**1c**) confirm this.

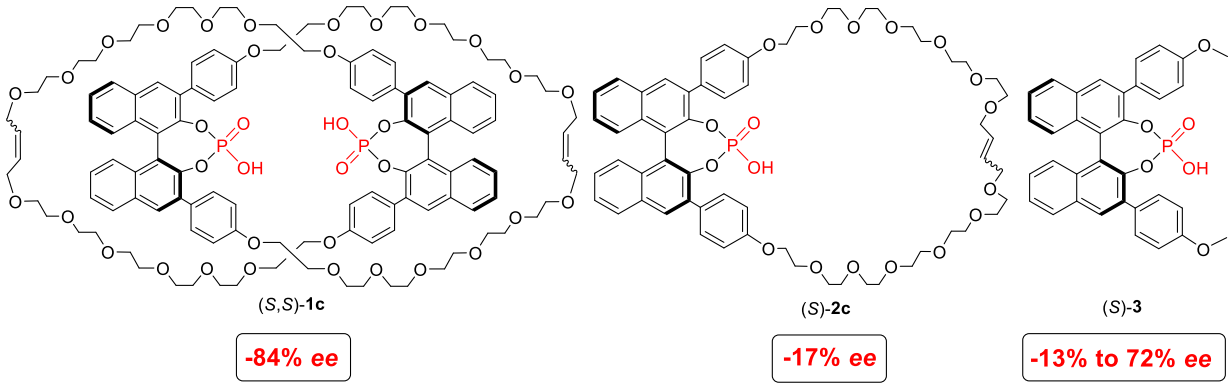

Figure 122: Differences in stereoselectivity of the three catalyst investigated in the transfer hydrogenation of 2-phenylquinoline.

These findings suggest that acid-acid interaction as they were found for acyclic phosphoric acid **3** could play a crucial role in chiral Brønsted acid catalysis in general. It has to be noted, however, that such acid-acid interactions strongly depend on the structure of the chiral phosphoric acid as it is indicated by macrocyclic phosphoric acid **3** which does not show any dimerization behaviour.

5.2 Active metal template synthesis of a BINOL-based heterocatenane and its application in asymmetric catalysis

In the second part multicomponent active metal template synthesis of hetero[2]catenane and hetero[3]catenane was accomplished. The approach relied on a literature known bisazide and bipyridine macrocycle and a new, axially chiral bisalkyne. Different parameters were varied to alter the ratio of [2]catenane and [3]catenane that were formed during the reaction. The highest impact was achieved by variation of the initial concentration of copper-bipyridine macrocycle which led to complete supression of [3]catenane formation at 2.5 mM or formation of up to a ratio of 37/63 ([3]catenane/[2]catenane) at 25 mM.

Further modification of the catenanes was achieved by removal of the MOM-protecting group and successive phosphorylation of the BINOL based macrocycle. Both reactions proceeded without any complication with moderate to high yields (91% and 84% for [2]catenane , 97% and 46% for [3]catenane).

Application of the catenanes in asymmetric Lewis acid catalysis with a metal in the bipyridine macrocycle and the BINOL based macrocycle as a chiral phosphate counteranion was not successful. Either no conversion was observed or no stereoinduction was achieved (hydrocyanation and Tsuji-Trost reaction).

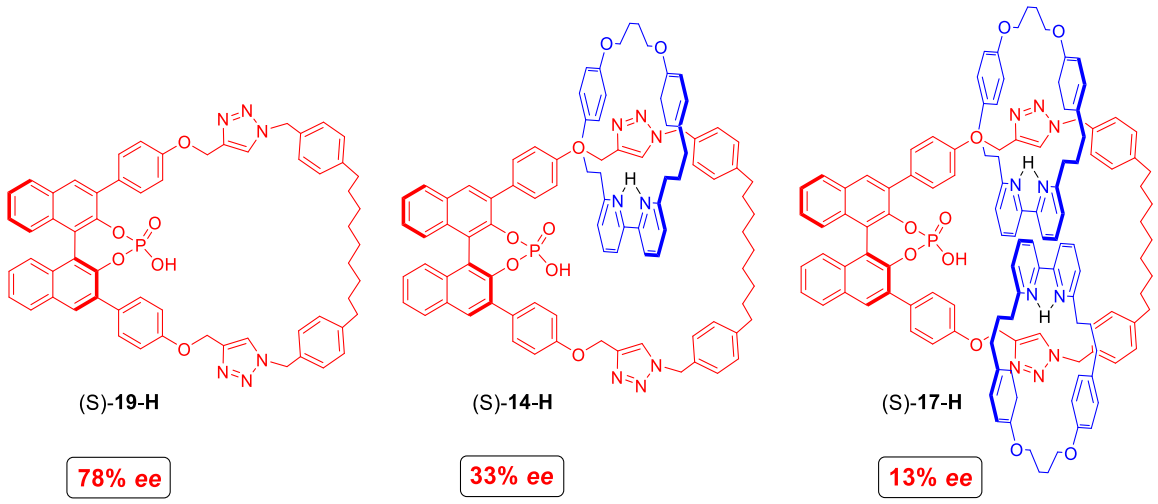

Figure 123: Different stereoselectivities for the examined macrocyclic and catenated catalysts in the transfer hydrogenation of 2-(4-*tert*-butylphenyl)quinoline.

However, the two catenanes as well as the corresponding BINOL based macrocycle were successfully applied in Brønsted acid catalysis. In a first try transfer hydrogenation of 2-phenylquinoline was catalysed by the catenated and macrocyclic catalyst. Modest or no enantiomeric excesses were observed for the [2]catenane and the [3]catenane respectively. Thus, 2-(4-*tert*-butylphenyl)quinoline as a sterically more demanding substrate was used, resulting in higher *ee*s in all cases (33% for [2]catenane (*S*)-**14-H**, 13% for [3]catenane (*S*)-**17-H** and 78% for macrocycle (*S*)-**19-H**). Most notably, the stereoselectivity decreases with increasing numbers of bipyridine macrocycles. Protonation studies revealed that these bipyridine macrocycles are protonated in the catenanes. Therefore, it cannot be concluded from the obtained results, if the lower stereoselectivities stem from steric modulation of the active centre by the mechanically bound bipyridine macrocycles or if the protonated bipyridine macrocycles catalyse the investigated reaction non-stereoselectively. An interesting approach for further studies regarding these catenanes would be the determination of the protonation states after using a sub-stoichiometric amount of protonation agent and the subsequent application of these catenanes in catalysis to investigate the influence of the protonated bipyridine macrocycles.

6. Zusammenfassung

6.1 Untersuchungen zur Transferhydrierung von 2-Phenylchinolin

Im ersten Teil dieser Arbeit wird der Mechanismus der Transferhydrierung von 2-Phenylchinolin, welche durch die azyklische Phosphorsäure **3**, die makrozyklische Phosphorsäure (*S*)-**2c** und dem Bisphosphorsäurecatenan (*S*,*S*)-**1c** katalysiert wird, untersucht. Es wurde klassische und visuelle kinetische Analyse (*visual kinetic analysis*) benutzt, um kinetisch relevante Daten (Reaktionsordnungen, Anfangsgeschwindigkeiten, Reaktionsgeschwindigkeitskonstanten) zu erhalten und es wurde herausgefunden, dass die drei Katalysatoren mittels verschiedener Mechanismen reagieren. Die makrozyklische Phosphorsäure (*S*)-**2c** reagiert mittels eines monomeren Weges, während das Catenan mittels eines dimeren Weges reagiert, da die mechanische Bindung dafür sorgt, dass sich immer zwei Phosphorsäuren in räumlicher Nähe befinden und daher als Dimer agieren. Normalisierte Anfangsgeschwindigkeiten zeigten, dass die Reaktion über den dimeren Weg langsam abläuft als über den monomeren Weg.

Beide Katalysatoren ändern bei Veränderung der Katalysatorbeladungen nicht ihren Katalyse-Weg, was durch gleichbleibende normalisierte Anfangsgeschwindigkeiten über einen großen Katalysatorbeladungsbereich gekennzeichnet ist. Dieses konstante Verhalten liegt nicht bei der azyklischen Phosphorsäure vor, welche bei niedrigen Katalysatorbeladungen hauptsächlich über den monomeren und bei hohen Katalysatorbeladungen hauptsächlich über den dimeren Weg reagiert. Eine Katalysatorordnung nahe 2 bei hohen Katalysatorbeladungen sowie NMR-Studien deckten auf, dass die azyklische Phosphorsäure bei hohen Katalysatorbeladungen Katalysator*Katalysator*Substrat-Komplexe bildet, welche dann analog zum Catenan über den dimeren Weg reagieren. Das wird weiterhin durch die dem Catenan ähnlichen Enantiomerenüberschüsse (72% mit 50 mol% **3**, 82% mit (*S*,*S*)-**1c)** bei diesen hohen Katalysatorbeladungen bestätigt.

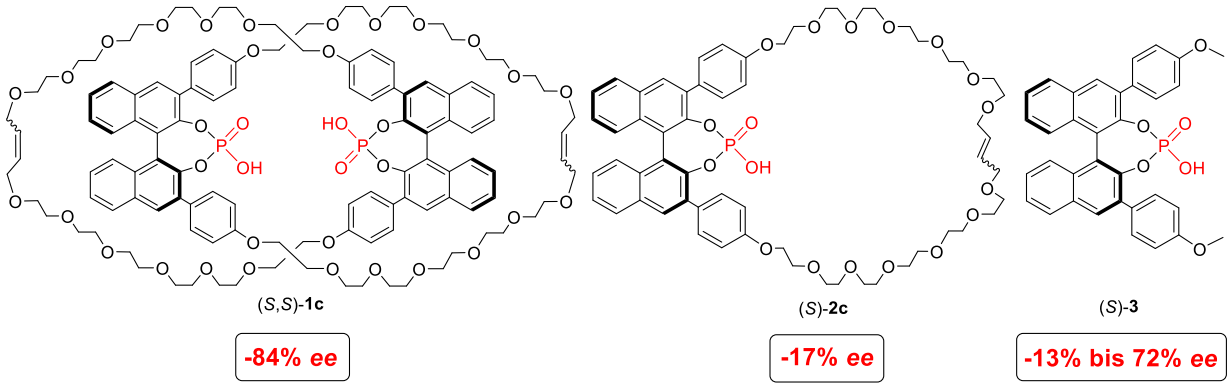

Abbildung 1: Unterschiede der Stereoselektivitäten der der Katalysatoren in der Transferhydrierung von 2-Phenylchinolin.

Diese Ergebnisse deuten an, dass solche Säure-Säure Wechselwirkungen, wie sie bei der azyklischen Phosphorsäure **3** gefunden wurden, generell eine große Rolle in der Brønsted-Säure-Katalyse spielen könnten. Es muss jedoch erwähnt werden, dass diese Säure-Säure Wechselwirkungen stark von der Struktur der chiralen Phosphorsäure abhängen, was unter anderem durch die makrozyklische Phosphorsäure **2c**, welche keine Dimerisierung zeigt, hervorgehoben wird.

6.2 Aktiv-Metall-Templat-Synthese BINOL-basierter Heterocatenane und deren Anwendung in der asymmetrischen Katalyse

Im zweiten Teil wurde die Multikomponentensynthese eines Hetero[2]catenans und eines Hetero[3]catenans mittels aktivem Metall-Templat erfolgreich durchgeführt. Dieser Syntheseansatz fußte auf dem literaturbekannten Bisazid und Bipyridin-Makrozyklus und einem neuen, axial-chiralen Bisalkin. Es wurden verschiedene Parameter variiert, um das Verhältnis zwischen erhaltenem [2]- und [3]-Catenan zu verändern. Variation der Anfangskonzentration des Kupfer-Bipyridin-Makrozyklus zeigte hierbei den größten Einfluss. Bei einer Anfangskonzentration von 2.5 mM konnte die Bildung des [3]Catenans vollständig unterdrück werden, während bei einer Anfangskonzentration von 25 mM ein Verhältnis von 37/63 ([3]Catenan/[2]Catenan) erhalten wurde.

Die weiteren Modifikationen der Catenane beinhalteten die Entfernung der MOM-Schutzgruppe sowieso die Phosphorylierung des BINOL-basierten Makrozyklus. Beide Reaktionen verliefen für beide Catenane ohne Komplikationen und gute bis sehr gute Ausbeuten konnten erhalten werden (91% und 84% für das [2]Catenan, 97% und 46% für das [3]Catenan).

Die Anwendung der Catenane in der asymmetrischen Lewis-Säure-Katalyse mit einem Metall in dem Bipyridin-Makrozyklus und einem BINOL basierten Makrozyklus als chirales Gegenanion war nicht erfolgreich. Entweder konnte kein Umsatz erreicht werden oder es erfolgte keine Stereoinduktion (Hydrocyanierung und Tsuji-Trost Reaktion).

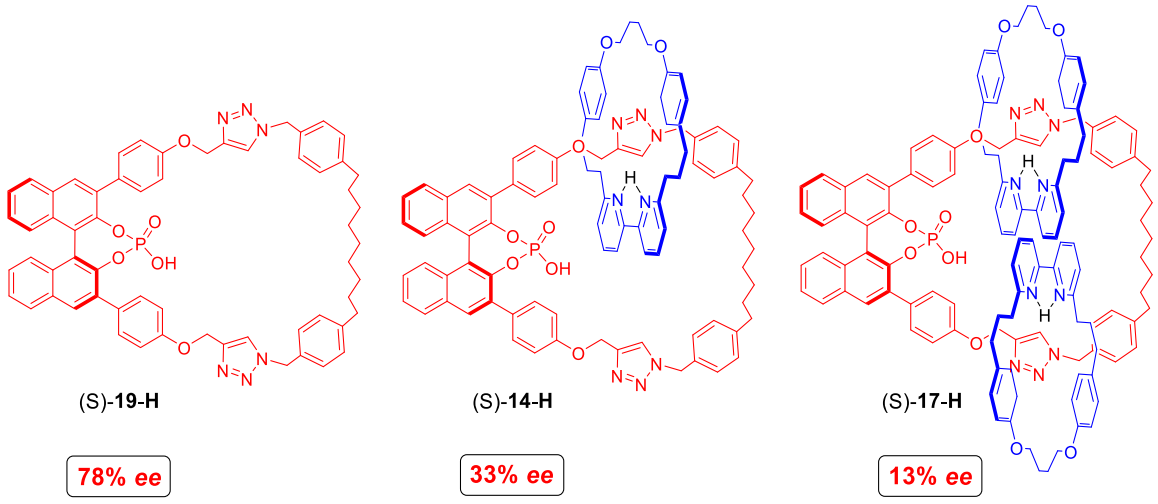

Figure 124: Unterschiedliche Stereoselektivitäten des makrozyklischen und der Catenan-basierten Katalysatoren in der Transferhydrierung von 2-(4-*tert*-butylphenyl)chinolin.

Die beiden Catenane sowie der entsprechende BINOL basierte Makrozyklus konnten jedoch erfolgreich in der Brønsted-Säure-Katalyse eingesetzt werden. In einem ersten Versuch wurde die Transferhydrierung von 2-Phenylchinolin durch die Catenane und den Makrozyklus katalysiert. Es wurden nur mäßige (für das [2]Catenan) oder keine (für das [3]Catenan) Enantiomerenüberschüsse beobachtet, weshalb 2-(4-*tert*-butylphenyl)chinolin als sterisch anspruchsvolleres Substrat eingesetzt wurde. Dies führte für alle Katalysatoren zu höheren Enantiomerenüberschüssen (33% für das [2]Catenan, 13% für das [3]Catenan und 78% für den Makrozyklus). Auffallend ist der Trend, dass mit steigender Anzahl an Bipyridin-Makrozyklen die Stereoselektivität sinkt. Protonierungsstudien haben gezeigt, dass die

Bipyridin-Makrozyklen in den Catenanen protoniert vorliegen. Dadurch bleibt die Frage offen, ob die geringeren Stereoselektivitäten durch eine sterische Modulation des aktiven Zentrums durch die mechanisch gebundenen Bipyridin-Makrozyklen entstehen oder ob die protonierten Bipyridin-Makrozyklen die untersuchte Reaktion zusätzlich nicht-stereoselektiv katalysieren. Eine interessante Herangehensweise für zukünftige Studien zu diesen Catenanen wäre die Bestimmung des Protonierungszustands nach Anwendung eines unterschüssigen Protonierungsagens und die anschließende Anwendung der Catenane in der Katalyse, um den Einfluss der protonierten Bipyridin-Makrozyklen zu untersuchen.

7. Experimental Part

7.1 Material and Methods

Materials

Polygram® SOL G/UV254 TLC plates (silica gel, 0.2 mm x 40 mm x 80 mm) were used for thin layer chromatography (TLC). A UV lamp was used to visualize spots at either 254 nm or 365 nm wavelength. The products were purified by flash column chromatography on silica gel 60M (particle size: 40-63 µm) which was purchased from MACHERY-NAGEL GmbH & Co. KG.

Solvents

Dichloromethane and toluene were distilled over calcium hydride and stored over molecular sieves under argon. Deuterated dichloromethane was freshly distilled over calcium hydride and deuterated toluene over sodium prior to use. Dry tetrahydrofuran was distilled freshly from Na/benzophenone prior to use. Phosphoryl chloride ($POCl_3$) was distilled under vacuum and stored under argon. Pyridine was distilled over potassium hydroxide under vacuum and stored over molecular sieves under argon. Dimethoxyethane (DME) and aqueous sodium carbonate solution (2 M) were degassed with argon for 15 minutes and were then stored under argon.

Chemicals

p-Toluenesulfonyl chloride, 2-phenylquinoline, 2-bromoquinoline, 4-fluorophenyl boronic acid, 4-methoxyphenyl boronic acid and diethyl 2,6-dimethylpyridine-3,5-dicarboxylate were purchased from Tokyo Chemical Industry (TCI). Pentaethylene glycol, heptaethylene glycol, and diethyl 1,4-dihydro-2,6-dimethyl-pyridine-3,5-dicarboxylate (Hantzsch ester) were purchased from Fluorochem. [D_8]-toluene was purchased from Deutero. Amberlyst® 15 hydrogen form and Grubb's 2nd generation catalyst were purchased from Sigma-Aldrich. Allyl bromide and potassium *tert*-butoxide were purchased from Acros Organics. All commercially available compounds were used without any further purification.

2-(4-Methoxyphenyl)quinoline was synthesized according to literature procedure.[172]

The same conditions were used for the preparation of 2-(4-fluorophenyl)quinoline. Analytical data can be found in the literature.[173]

Cinnamyl phosphate **107** was synthesized according to literature procedure.[166]

EDTA-NH_3solution refers to an aqueous solution of NH_3(17% w/w) saturated with sodium-ethylenediaminetetraacetate.

[172] M. Tobisu, I. Hyodo, N. Chatani, *J. Am. Chem. Soc.* **2009**, *131*, 12070–12071.
[173] A. V. Iosub, S. S. Stahl, *Org. Lett.* **2015**, *17*, 4404–4407.

7.2 Analytical Methods

NMR spectra were recorded with a Bruker DMX 300 spectrometer [^{1}H: 300 MHz, ^{13}C: 75.5 MHz, ^{31}P: 121.5 MHz], with a Bruker Neo 400 or Bruker AV400 [^{1}H: 400 MHz, ^{13}C: 101 MHz, ^{31}P: 162 MHz] or with a Bruker DMX 600 spectrometer [^{1}H: 600 MHz, ^{13}C: 151 MHz, ^{31}P: 243 MHz]. All measurements were performed at room temperature, using [D_1]-chloroform, [D_6]-dimethylsulfoxide, [D_6]-benzene, [D_4]-methanol, [D_2]-methylene chloride, [D_6]-acetone or [D_8]-toluene as solvents. The chemical shifts are referenced relative to the residual proton signals of the solvents in the ^{1}H-NMR ([D_1]-chloroform: δ = 7.26 ppm, [D_6]-benzene: δ = 7.16 ppm, [D_4]-methanol: δ = 3.31 ppm, [D_6]-dimethylsulfoxide: δ = 2.50 ppm, [D_6]-acetone: δ = 2.05 ppm, [D_2]-methylene chloride: δ = 3.20 ppm, [D_8]-toluene: δ = 2.08, 6.87, 7.01, 7.09 ppm) or relative to the solvent signal in the ^{13}C-NMR ([D_1-chloroform: δ = 77.16 ppm, [D_6]-benzene: δ = 128.06 ppm, [D_4]-methanol: δ = 49.15 ppm, [D_6]-dimethylsulfoxide: δ = 39.51 ppm, [D_6]-acetone: δ = 28.84, 206.26 ppm, [D_2]-methylene chloride: δ = 53.84 ppm, [D_8]-toluene: δ = 137.48, 128.87, 127.96, 125.13, 20.43 ppm). The apparent coupling constants are given in Hertz. The description of the fine structure means: s = singlet, bs = broad singlet, d = doublet, ps d = pseudo dublet, dd = doublet of doublets, dt = doublet of triplets, t = triplet, m = multiplet.

NMR structural investigations on binary and ternary **3•4b-d** systems were performed on a Bruker Avance DRX 600 MHz spectrometer with TBI (Triple resonance broadband inverse) 5 mm CPPBBO ^{1}H/^{19}F-BB probe head with Z-gradient and BVT unit. Temperature was controlled in the VT-experiments by a BVT 3000 and BVT 3900 unit and liquid nitrogen. Additional NMR experiments were performed on Bruker Avance III HD 400 MHz spectrometer equipped with 5 mm BBO BB-1H/D probe head with Z-Gradients. Spectrometer control and spectra processing was performed with Bruker Software TopSpin (Version 3.2 PL 1). Data procession, data preparation and data presentation was performed with Microsoft Excel (Version 16.0.9126.2259 32 Bit), Corel Draw X7 and ChemBioDraw Ultra 14.0. ^{1}H and ^{13}C chemical shifts were referenced to TMS. The heteronuclei ^{15}N,^{19}F and ^{31}P were referenced, employing $\nu(X) = \nu(TMS) \cdot \Xi_{reference} / 100$ % according to Harris et al.[174] The following frequency ratios and reference compounds were used: $\Xi(^{15}N)$ = 10.132912 (lq. NH_3), $\Xi(^{19}F)$ = 94.094011 (CCl_3F) and $\Xi(^{31}P)$ = 40.480742 (H_3PO_4).

IR spectra were measured on a Jasco FT/IR-430 spectrometer.

Low resolution ESI mass spectra were recorded on a Bruker Amazon SL spectrometer. High resolution ESI mass spectra were recorded on a Bruker Maxis 4G spectrometer. MS/MS spectra were recorded on Thermo Fisher Scientific Orbitrap LTQ-XL mass spectrometer. UHPLC/MS (low resolution) was carried out by the mass spectrometry services at University of Southampton (Waters TQD mass spectrometer equipped with a triple quadrupole analyser with UHPLC injection (BEH C18 column; MeCN-H2O gradient (0.2% formic acid)).

Reversed phase medium performance liquid chromatography (MPLC) was performed with the following setup: Armen Instrument Spot Liquid Chromatography Flash system (detection wavelength: 263 nm), YMC GEL ODS-AQ 12 nm, S-50 µm in Kronlab glass columns with 10 mm diameter and 500 mm length. Water for MPLC was purified with a TKA MicroPure ultrapure water system. Chiral normal phase analytical high performance liquid chromatography (HPLC) was performed was performed with the following setup: Erma Degasser ERC-3512, Merck Hitachi Intelligent Pump L-6200A, Chiralcel OD-H column (0.46 x 25 cm),

[174] R. K. Harris, E. D. Becker, S. M. Cabral De Menezes, R. Goodfellow, P. Granger, *Concepts Magn. Reson.* **2002**, *14*, 326–346.

Knauer Smartline UV-Detector 2600 (detection wavelength 225 nm). Reversed phase analytical high performance liquid chromatography (RP-HPLC) was performed with the following setup: Dionex HPLC system: P680 pump, ASI-100 automated sample injector, UVD-340U UV detector (detection wavelength: 263 nm), UltiMate 3000 Column Compartment; YMC-Pack ODS-Acolumn (3.0 x 150 mm, 5 μm, 12 nm; type: AA12S05-1503QT).

Elemental analyses were performed on Euro EA – CHNSO Elemental Analyser from HEKAtech GmbH.

7.3 Synthetic Procedures and Analytical Data

7.3.1 Synthesis of precursors

7.3.1.1 Synthesis of MOM-BINOL (*S*)-64[175]

Described experiment: DEJ141

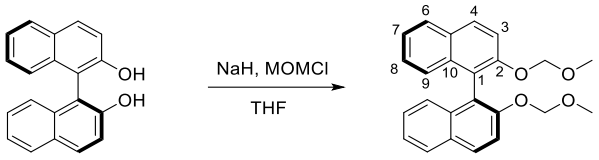

(*S*)-**63** (*S*)-**64**

Sodium hydride (60% dispersion in mineral oil, 3.08 g, 77.0 mmol, 2.2 eq.) was weighed into a flask and dry tetrahydrofuran (200 ml) was added. A solution of 1,1'-Bi-2-naphthol (10.0 g, 34.9 mmol, 1 eq.) in tetrahydrofuran (100 ml) was added dropwise at 0° C. The resulting mixture was allowed to stir at 0° C for one hour and 30 more minutes at room temperature. After cooling the mixture to 0°C chloromethyl methyl ether (5.85 ml, 6.20 g, 0.0770 mmol, 2.2 eq.) was added and the mixture was stirred for 20 hours at room temperature. Dichloromethane (100 ml) and a saturated aqueous ammonium chloride solution (150 ml) were added and the resulting two phases were separated. The organic phase was washed with a saturated sodium chloride solution (2 x 100 ml), dried over anhydrous sodium sulfate and filtered. The organic solvent was evaporated in the rotary evaporator and *n*-hexane (50 ml) was added. After decanting *n*-hexane and drying of the residual in the rotary evaporator (*S*)-**64** (13.1 g, 34.9 mmol, 96 %) was obtained as a white solid.

$C_{20}H_{22}O_4$ 374.44 g/mol

^{1}H-NMR (300 MHz, [D_1]- Chloroform, 300 K) δ [in ppm] = 7.93 (d, ^3J= 8.9 Hz, 2 H, CH_{aryl}), 7.87 (d, ^3J= 8.2 Hz, 2 H, CH_{aryl}), 7.58 (d, ^3J= 9.0 Hz, 2 H, CH_{aryl}), 7.34 (ddd, ^3J= 8.1 Hz, ^3J= 6.6 Hz, ^2J= 1.4 Hz, 2 H, CH_{aryl}), 7.22 (ddd, ^3J= 8.0 Hz, ^3J= 6.6 Hz, ^4J= 1.4 Hz, 2 H, CH_{aryl}), 7.18 – 7.13(m, 2 H, CH_{aryl}), 5.08 (d, ^2J= 6.7 Hz, 2 H, OCH_2), 4.98 (d, ^2J= 6.7 Hz, 2 H, OCH_2'), 3.14 (s, 6 H, OCH_3).

[DEJ141-2]

[175] T. R. Wu, L. Shen, J. M. Chong, *Org. Lett.* **2004**, *6*, 2701–2704.

7.3.1.2 Synthesis of Diiodo (*S*)-65 [175]

Described experiment: DEJ213 Repeated: DEJ129, DEJ143, DEJ223

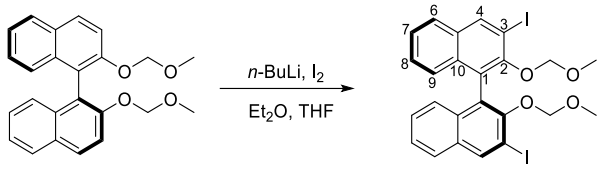

(*S*)-**64** (*S*)-**65**

(*S*)-**64** (10.0 g, 26.8 mmol, 1 eq.) was dissolved in dry diethyl ether (350 ml). While stirring at 0° C, *n*-butyllithium (29.8 ml, 80.2 mmol, 3 eq.) was added and the mixture was stirred for two hours. Dry tetrahydrofuran (150 ml) was added and the mixture was stirred for another hour before iodine (20.4 g, 80.2 mmol, 3 eq.) was added at 0° C. The reaction mixture was stirred at room temperature for 20 hours. To quench unreacted iodine a solution of sodium bisulfite (250 ml, 3.23 mol, 243 eq.) was added and stirred for 30 minutes. After phase separation the organic layer was washed with a saturated sodium chloride solution (200 ml), dried over anhydrous sodium sulfate and filtered. The organic solvent was evaporated in the rotary evaporator. After silica gel flash column chromatography (22 x 4 cm, cyclohexane/ethyl acetate: 20/1) (*S*)-**65** was obtained as a light brown solid (11.8 g, 18.8 mmol, 70.5%).

$C_{24}H_{20}I_2O_4$ 626.23 g/mol

^{1}H-NMR (300 MHz, [D$_1$]- Chloroform, 300 K) δ [in ppm] = 8.52 (s, 2 H, H-4), 7.76 (d, ^3J(H-6,7) = 8.2 Hz, 2 H, H-6), 7.40 (ddd, ^3J(H-8,9) = 8.1 Hz, ^3J(H-8,7) = 6.8 Hz, ^4J(H-8,6) = 1.2 Hz, 2 H, H-8), 7.28 (ddd, ^3J(H-7,6) = 8.2 Hz, ^3J(H-7,8) = 6.8 Hz, ^2J(H-7,9) = 1.3 Hz, 2 H, H-7), 7.15 (d, ^3J(H-9,8) = 8.1 Hz, 2 H, H-9), 4.79 (d, ^2J= 5.7 Hz, 2 H, OCH_2), 4.67 (d, ^2J= 5.7 Hz, 2 H, OCH_2‘), 3.14 (s, 6 H, OCH_3).

[DEJ213-02]

7.3.1.3 Synthesis of Bisphenol (*S*)-66[175]

Described experiment: DEJ144 Repeated: DEJ98, DEJ217, DEJ224, DEJ279, DEJ296

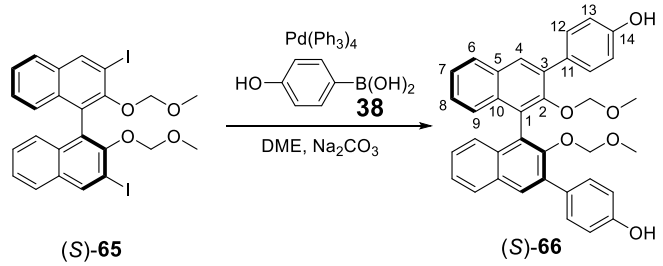

(*S*)-**65** (3.00 g, 4.79 mmol, 1 eq.), tetrakis(triphenylphosphine)palladium(0) (0.554 g, 0.479 mmol, 0.1 eq.) and 4-hydroxyphenylboronic acid (2.64 g, 19.1 mmol, 4 eq.) were charged in a Schlenk flask and dissolved in dry dimethoxyethane (20 ml) under argon atmosphere. To that mixture a degassed solution of sodium carbonate (2 M, 8.00 ml, 16.00 mmol, 3.3 eq.) was added and it was stirred for 6 hours at 80° C. After addition of tetrahydrofuran (50 ml) and saturated sodium chloride solution (30 ml) the resulting two phases were separated. The aqueous phase was washed with tetrahydrofuran (2 x 50 ml) and the organic phases were combined, dried over anhydrous sodium sulfate, filtered and concentrated in the rotary evaporator. After silica gel flash column chromatography (15 x 5 cm, cyclohexane/ethyl acetate: 4/1) (*S*)-**66** was obtained (1.99 g, 3.56 mmol, 74.3%) as a yellow solid.

$C_{36}H_{30}O_6$ 558.63 g/mol

^{1}H-NMR (300 MHz, [D_1]- Chloroform, 300 K) δ [in ppm] = 7.92 (s, 2 H, H-4), 7.88 (d, ^3J(H-6,7) = 8.3 Hz, 2 H, H-6), 7.64 (ps d, ^3J(H-12,13) = 8.7 Hz, 4 H, H-12), 7.41 (ddd, ^3J(H-7,9) = 8.1 Hz, ^3J(H-7,8) = 4.1 Hz, ^4J(H-7,6) = 1.3 Hz, 2 H, H-7), 7.29 - 7.23 (m, 4 H, H-8, H-9 merged with $CDCl_3$ signal), 6.9 (ps d, ^3J(H-13,12) = 8.7 Hz, 4 H, H-13), 5.33 (s, 2 H, OH), 4.44 (d, ^2J= 5.6 Hz, 2 H, OCH_2),), 4.37 (d, ^2J= 5.6 Hz, 2 H, OCH_2'), 2.37 (s, 6 H, OCH_3).

[DEJ144-2]

7.3.2 Synthesis of macrocycles (*S*)-1a/c, catenanes (*S*,*S*)-1a/c and acyclic phosphoric acid (*S*)-3[176]

7.3.2.1 Synthesis of MOM-protected bismethoxyphenyl-BINOL (S)-111

Described experiment: DEJ85 Repeated: DEJ216

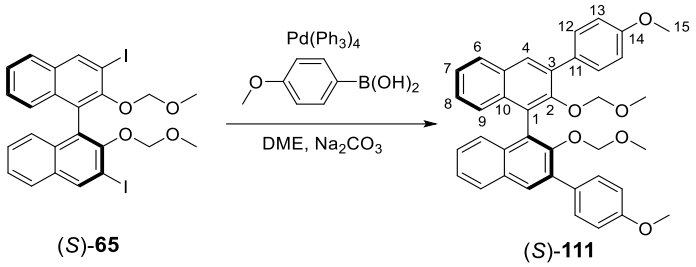

(*S*)-**65** (300 mg, 0.479 mmol, 1 eq.), tetrakis(triphenylphosphine)palladium(0) (55.4 mg, 0.050 mmol, 0.1 eq.) and 4-methoxyphenylboronic acid (292 mg, 1.92 mmol, 4 eq.) were charged in a Schlenk flask and dissolved in dry dimethoxyethane (5 ml) under argon atmosphere. To that mixture a degassed solution of sodium carbonate (2 M, 1.00 ml, 2.00 mmol, 4.2 eq.) was added and it was stirred for 2 hours at 85° C. After addition of tetrahydrofuran (20 ml) and saturated sodium chloride solution (10 ml) the resulting two phases were separated. The aqueous phase was washed with tetrahydrofuran (2 x 30 ml) and the organic phases were combined, dried over anhydrous sodium sulfate, filtered and concentrated in the rotary evaporator. After silica gel flash column chromatography (20 x 3 cm, cyclohexane : ethyl acetate: 80 : 20) (*S*)-**111** (221 mg, 0.377 mmol, 78.7%) was obtained as a white solid.

$C_{38}H_{34}O_6$ 586.68 g/mol

^{1}H-NMR (300 MHz, [D$_1$]- Chloroform, 300 K) δ [in ppm] = δ 7.92 (s, 2H, H-4), 7.87 (d, ^3J = 8.2 Hz, 2H, H-6), 7.70 (psd, ^3J = 8.8 Hz, 4H, H-12), 7.40 (ddd, ^3J = 8.2 Hz, ^3J = 5.4 Hz, ^4J = 2.6 Hz, 2H, H-7), 7.31 – 7.22 (m, 6H, H-8, H-9, merged with $CDCl_3$ signal), 7.01 (psd, J = 8.8 Hz, 4H, H-13), 4.42 (d, ^2J = 5.7 Hz, 2 H, OCH_2), 4.37 (d, ^3J = 5.7 Hz, 2 H, OCH_2'), 3.87 (s, 6H, H-15), 2.36 (s, 6H, OCH_3).

[DEJ85-3]

[176] R. Mitra, H. Zhu, S. Grimme, J. Niemeyer, *Angew. Chem. Int. Ed.* **2017**, *56*, 11456–11459,R. Mitra, M. Thiele, F. Octa-Smolin, M. C. Letzel, J. Niemeyer, *Chem. Commun.* **2016**, *52*, 5977–5980.

7.3.2.2 Synthesis of diol (S)-112

Described experiment: DEJ312 Repeated: DEJ86, DEJ219

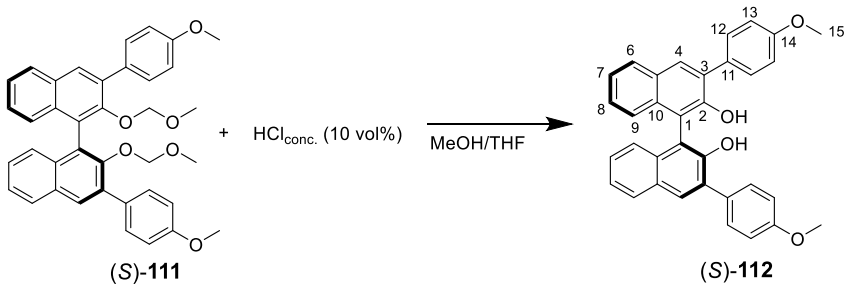

(*S*)-**111** (*S*)-**112**

(*S*)-**111** (647 mg, 1.10 mmol, 1 eq.) was dissolved in a 1:1 mixture of tetrahydrofuran/methanol (15 ml) and concentrated hydrochloric acid (1.5 ml) was added. The solution was stirred at 80 °C for 30 minutes. After cooling to room temperature, volatiles were removed and the crude mixture was purified by column chromatography (2 x 10 cm, cyclohexane : ethyl acetate = 89 : 11) to yield the product (*S*)-**112** (405 mg, 0.813 mmol, 73 %) as a white solid.

$C_{34}H_{26}O_4$ 498.58 g/mol

^{1}H-NMR (400 MHz, [D$_1$]- Chloroform, 300 K) δ [in ppm] = 7.99 (s, 2H, H-4), 7.92 (dd, ^3J = 8.1 Hz, ^4J = 1.3 Hz, 2H, H-6), 7.68 (psd, ^3J = 8.8 Hz, 4H, H-12), 7.38 (ddd, ^3J = 8.1 Hz, ^3J = 6.7 Hz, ^4J = 1.3 Hz, 2H, H-7), 7.30 (ddd, ^3J = 8.3 Hz, ^3J = 6.8 Hz, ^4J = 1.3 Hz, 2H, H-8), 7.21 (dd, ^3J = 8.3 Hz, ^3J = 1.3 Hz 2H, H-9), 7.03 (psd, ^3J = 8.8 Hz, 4H, H-13), 5.35 (s, 2H, O*H*), 3.87 (s, 6H, OC*H*$_3$).

[DEJ312-2]

7.3.2.3 Synthesis of acyclic phosphoric acid (S)-3

Described experiment: DEJ313 Repeated: DEJ88, DEJ220

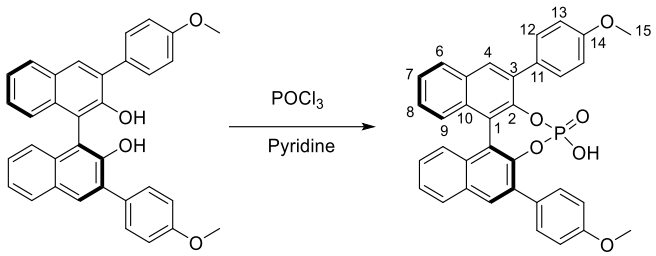

(*S*)-**112** (*S*)-**3**

(*S*)-**112** (375 mg, 0.752 mmol, 1 eq.) was charged in a Schlenk flask and dried at high vacuum for three hours. Dry pyridine (10 ml) and phosphoryl chloride (3.46 g, 2.06 ml, 22.6 mmol, 30 eq.) were added under argon and the resulting mixture was stirred for 16 hours at 60° C. After addition of water (3 ml) the mixture was stirred for another 3 hours at 60° C before dichloromethane (20 ml) was added and the resulting two phases were separated. The organic phase was washed with hydrochloric acid (2M, 3 x 20 ml), dried with anhydrous sodium sulfate, filtered and concentrated in the rotary evaporator. After silica gel flash column chromatography (15 x 4 cm, dichloromethane : methanol: 90 : 10), redissolving in dichloromethane (20 ml) and washing with hydrochloric acid (2 M, 10 ml) (*S*)-**3** (320 mg, 0.571 mmol, 75.9 %) was obtained as a white solid.

$C_{34}H_{25}O_6P$ 560.54 g/mol

^{1}H-NMR (400 MHz, [D$_1$]- Chloroform, 300 K) δ [in ppm] = 7.99 (s, 1H, H-4), 7.94 (dd, ^3J = 8.2 Hz, ^4J = 1.2 Hz, 2H, H-6), 7.57 (psd, ^3J = 8.8 Hz, 4H, H-12), 7.49 (ddd, ^3J = 8.2 Hz, ^3J = 6.5 Hz, ^4J = 1.5 Hz, 2H, H-7), 7.34 (dd, ^3J = 8.7 Hz, ^4J = 1.5 Hz, 2H, H-9), 7.29 (ddd, ^3J = 8.7 Hz, ^3J = 6.5 Hz, ^4J = 1.2 Hz, 2H, H-8), 6.85 (psd, ^3J = 8.8 Hz, 4H, H-13), 3.56 (s, 6H, H-15).

[DEJ313-1]

7.3.2.4 Synthesis of the precatenane (S,S)-70[133]

Described experiment: DEJ70

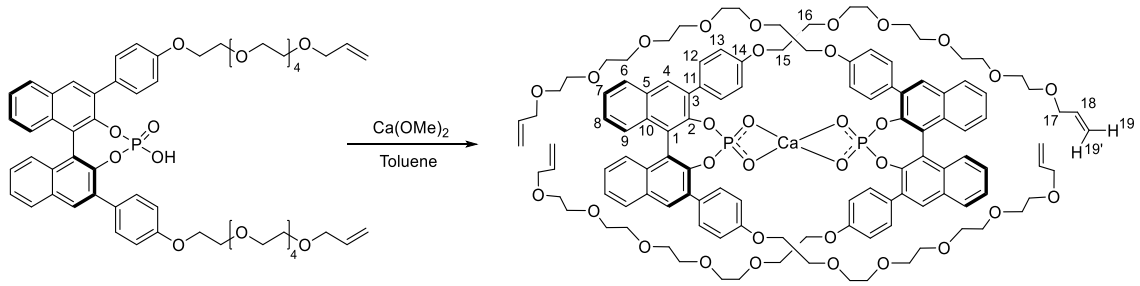

(*S*)-**69a** (*S*,*S*)-**70a**

Phosphoric acid (*S*)-**69a** (318 mg, 0.302 mmol, 1 eq.) was charged in a Schlenk flask and dried at high vacuum for three hours. Dry toluene (15 ml) and calcium methoxide (15.4 mg, 0.151 mmol, 0.5 eq.) were added and the mixture was stirred at room temperature for 16 hours. The mixture was filtered and the solvent was removed in the rotary evaporator to give the product (*S*,*S*)-**70a** (283 mg, 0.265 mmol, 88%) as a brown oil.

$C_{116}H_{138}O_{32}P_2Ca$ 2144.36 g/mol

^{1}H-NMR (600 MHz, [D_6]-Benzene, 298 K) δ [in ppm] = 7.94 (br s, 12H, H-4, H-12), 7.78-7.93 (m, 4H, H-6), 7.41 (d, ^3J= 8.7, 4H, H-9), 7.22 (t, ^3J = 7.4 Hz, 4H, H-7), 7.10 – 6.93 (m, 12H, H-8, H-13), 5.77 (m, 4H, H-18), 5.17 (d, ^3J = 17.5 Hz, 4H, H-19'), 4.99 (ddt, ^3J = 10.5 Hz, 4H, H-19), 4.04 – 3.84 (m, 8H, H-15), 3.78 (br s, 8H, H-17), 3.59-3.11 (m, 72H, H-16, core glycol OCH_2)

[DEJ70-1]

7.3.2.5 Synthesis of macrocycle (S)-1a and catenane (S,S)-1a[133]

Described experiment: DEJ72, DEJ63

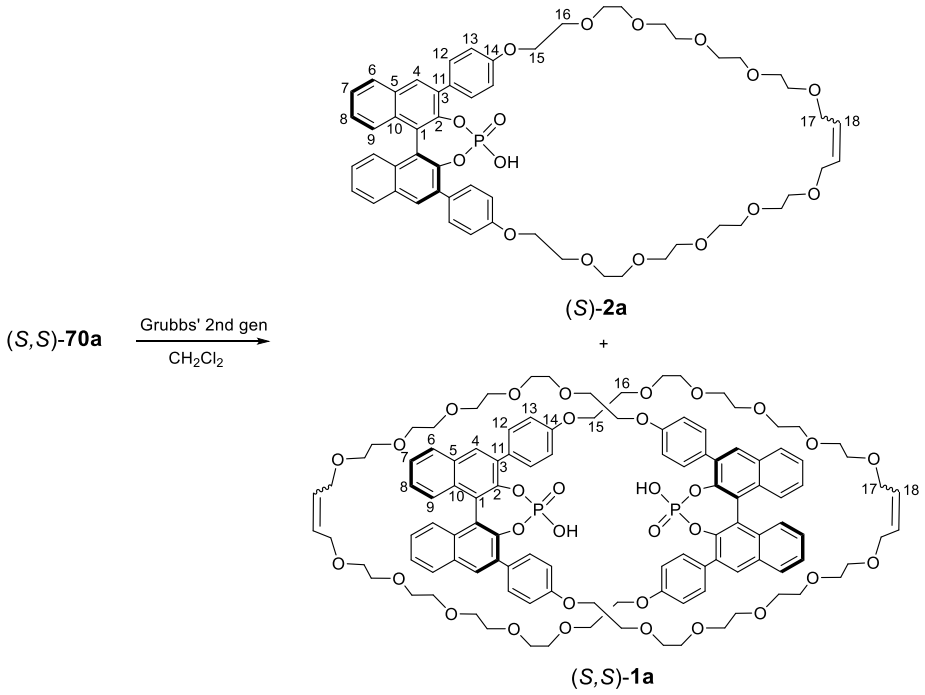

(*S*,*S*)-**70a** (283 mg, 0.132 mmol, 1 eq.) was dried in a Schlenk flask for four hours. Dry dichloromethane (110 ml) and 2nd generation catalyst (10.8 mg, 0.0132 mmol, 0.1 eq.) were added under argon and the reaction mixture was stirred at room temperature with the flask wrapped in aluminium foil to protect the catalyst from light. After five and 17 hours, 1 ml was withdrawn from the mixture to control the progress of the reaction by RP-18 HPLC. After 17 hours the reaction was completed and 250 mg QuadraSil was added and the mixture was stirred for 16 hours. After filtration, the solvent was removedin the rotary evaporator. The crude product was purified by preparative MPLC (RP-18 17g Kronlab column, MeOH with 0.05% TFA : water with 0.05% TFA = 65 : 35 gradient flow firstly up to 85:15 within 48 min, secondly up to 90:10 within 22 minutes, thirdly up to 100:0 within 10 minutes, 15 ml/min). The solvent was evaporated and each of the two compounds was redissolved in dichloromethane (50 ml) and washed with hydrochloric acid (2M, 10 x 2 ml). After removing the solvent in the rotary evaporator, the 5-EG macrocycle (*S*,*S*)-**2a** (9.30 mg, 7%) and the 5-EG catenane (*S*,*S*)-**1a** (6.10 mg, 3%) were obtained.

Macrocycle (*S*)-2a:

$C_{56}H_{65}O_{16}P$ 1025.09 g/mol

^{1}H-NMR (600 MHz, [D$_1$]-Chloroform, 298 K) δ [in ppm] = 7.99 (s, 2H, H-4), 7.94 (d, ^3J = 8.2 Hz, 2H, H-6), 7.71 (ps d, ^3J = 8.3 Hz, 4H, H-12), 7.45 (dd, ^3J = 7.4 Hz, ^3J = 7.4 Hz, 2H, H-7), 7.33 (d, ^3J = 8.6 Hz, 2H, H-9), 7.29 – 7.23 (m, 2H, H-8), 7.00 (ps d, ^3J = 8.4 Hz, 4H, H-13), 5.70 (s, 1.85H, H-18 (*E*-isomer)),

5.63 (s, 0.15H, H-18 (*Z*-isomer)), 4.25 – 4.15 (m, 4H, H-15), 3.97 – 3.82 (m, 8H, H-16, H-17), 3.72 - 3.44 (m, 32H, core glycol OC*H*$_2$).

[DEJ72-6]

Catenane (*S*,*S*)-1a:

$C_{112}H_{130}O_{32}P_2$ 2050.18 g/mol

^{1}H-NMR (600 MHz, [D$_1$]-Chloroform, 298 K) δ [in ppm] = 7.97 (s, 4H, H-4), 7.93 (d, ^3J = 8.3 Hz, 4H, H-6), 7.61 (ps d, ^3J = 8.2 Hz, 8H, H-12), 7.46 (dd, ^3J = 7.5 Hz, ^3J = 7.5 Hz, 4H, H-7), 7.31 (d, ^3J = 8.5 Hz, 4H, H-9), 7.28 – 7.24 (m, 4H, H-8), 6.89 (ps d, ^3J = 8.3 Hz, 8H, H-13), 5.69 (s, 3.7H, H-18 (*E*-isomer)), 5.62 (s, 0.3H, H-18 (*Z*-isomer)), 4.27 (br s, 2H, O*H*), 4.00 (t, ^3J = 4.7 Hz, 8H, H-15), 3.96 – 3.92 (m, 16H, H-16, H-17), 3.74 - 3.44 (m, 64H, core glycol OC*H*$_2$).

7.3.2.6 Synthesis of O-(allyl)heptaethylene glycol 113c

Described experiment: DEJ64 Repeated: DEJ65, DEJ92, DEJ95

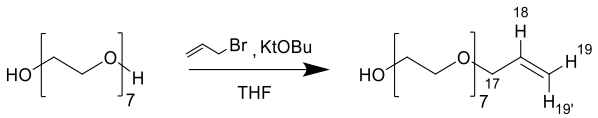

113c

Potassium *tert*-butoxide (182 mg, 1.62 mmol, 0.53 eq.) was dried at high vacuum in a Schlenk flask for three hours. After addition of dry tetrahydrofuran (40 ml), a solution of heptaethylene glycol (1.00 g, 3.06 mmol, 1 eq.) in dry tetrahydrofuran (10 ml) was added to the suspension. The mixture was stirred for 40 minutes before a solution of allylbromide (140 µL, 196 mg, 1.62 mmol, 0.53 eq.) in dry tetrahydrofuran (10 ml) was added dropwise. The reaction mixture was allowed to stir for 20 hours. The resulting suspension was filtered and the solvent was evaporated to give a light yellow oil. After silica gel chromatography (20 x 3 cm, ethyl acetate/methanol = 10:1) the product **113c** was obtained as a light yellow oil (512 mg, 1.18 mmol, 72 %).

$C_{17}H_{34}O_8$ 366.45 g/mol

^{1}H-NMR (600 MHz, [D_1]-Chloroform, 298 K) δ [in ppm] = 5.89 (ddt, ^3J = 17.3 Hz, ^3J = 10.5 Hz, ^3J = 5.7 Hz, 1H, H-18),), 5.25 (ddt, ^3J = 17.3 Hz, ^2J = 1.6 Hz, ^4J = 1.4 Hz, 1H, H-19'), 5.15 (ddt, ^3J = 10.5 Hz, ^2J = 1.6 Hz, ^4J = 1.4 Hz, 1H, H-19), 4.00 (dt, ^3J = 5.7 Hz, ^4J = 1.4 Hz, 2H, H-17), 3.75-3.55 (m, 28H, core glycol-OCH_2).

7.3.2.7 Synthesis of O-(allyl)heptaethylene glycol tosylate 114c

Described experiment: DEJ96 Repeated: DEJ66

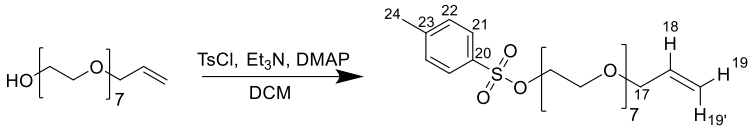

113c **114c**

113c (1.24 g, 3.33 mmol, 1 eq.), tosyl chloride (794 mg, 4.16 mmol, 1.25 eq.), triethylamine (739 µl, 5.33 mmol, 1.6 eq.) and 4-dimethylaminopyridine (81.7 mg, 0.668 mmol, 0.2 eq.) were dissolved in dichloromethane (30 ml). The reaction mixture was stirred at room temperature for 20 hours. Diethyl ether (100 ml) was added and the organic phase was washed with each hydrochloric acid (2M, 100 ml), sat. sodium bicarbonate (100 ml) and saturated sodium chloride solution (100 ml), respectively. The organic phase was dried over anhydrous sodium sulfate, filtered and concentrated in the rotary evaporator. The product **114c** was obtained as a light brown oil (1,70 g, 3.23 mmol, 96.9%).

$C_{24}H_{40}O_{10}S$ 520.63 g/mol

^{1}H-NMR (600 MHz, [D_1]-Chloroform, 298 K) δ [in ppm] = 7.79 (ps d, ^3J = 8.3 Hz, 2H, H-21), 7.35 (ps d, ^3J= 7.9 Hz, 2 H, H-22), 5.90 (ddt, ^3J = 17.2 Hz, ^3J = 10.4 Hz, ^3J = 5.7 Hz, 1H, H-18), 5.26 (ddt, ^3J = 17.2 Hz, ^2J = 1.6 Hz, ^4J = 1.4 Hz, 1H, H-19'), 5.17 (ddt, ^3J = 10.4 Hz, ^2J = 1.6 Hz, ^4J = 1.4 Hz, 1H, H-19), 4.01 (dt, ^3J = 5.7 Hz, ^4J = 1.4 Hz, 2H, H-17), 3.69-3.56 (m, 28H, core glycol-OCH_2), 2.44 (s, 3H, H-24).

7.3.2.8 Synthesis of MOM-protected precursor (S)-67c

Described experiment: DEJ67 Repeated: DEJ100

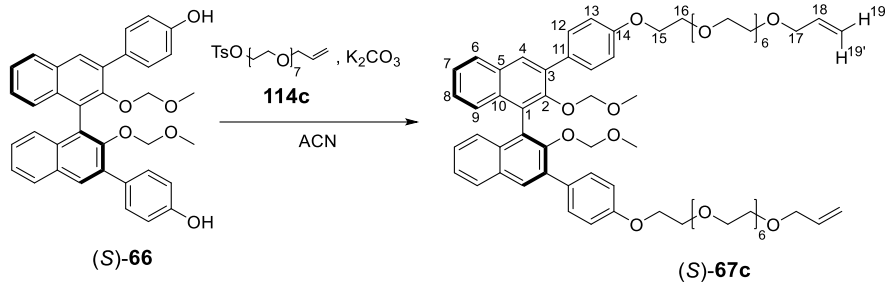

(*S*)-**66** (396 mg, 0.710 mmol, 1 eq.), **114c** (890 mg, 1.71 mmol, 2.4 eq) and potassium carbonate (469 mg, 3.41 mmol, 4.8 eq.) were charged in a flask (100 ml) and acetonitrile (50 ml) was added. The resulting suspension was refluxed for 24 hours. After cooling down to room temperature the reaction mixture was filtered and the organic solvent was evaporated in the rotary evaporator. After silica gel flash column chromatography (15 x 3 cm, ethyl acetate/methanol = 40/1) the product (*S*)-**67c** was obtained as a brown oil (607 mg, 0.478 mmol, 67%).

$C_{70}H_{94}O_{20}$ 1255.50 g/mol

^{1}H-NMR (600 MHz, [D$_1$]-Chloroform, 298 K) δ [in ppm] = 7.88 (s, 2H, H-4), 7.84 (d, ^3J = 8.4 Hz, 2H, H-6), 7.66 (ps d, ^3J = 8.7 Hz, 4H, H-12), 7.37 (ddd ^3J = 8.1 Hz, ^3J = 5.8 Hz, ^4J = 2.1 Hz, 2H, H-7), 7.28–7.23 (m, 4H, H-8, H-9), 6.99 (ps d, ^3J = 8.8 Hz, 4H, H-13), 5.88 (ddt ^3J = 17.2 Hz, ^3J = 10.3 Hz, ^3J = 5.7 Hz, 2H, H-18), 5.24 (ddt, ^3J = 17.2 Hz, ^2J = 1.6 Hz, ^4J = 1.7 Hz, 2H, H-19'), 5.15 (ddt, ^3J = 10.4 Hz, ^2J = 1.4 Hz, ^4J = 1.4 Hz, 1H, H-19), 4.38 (d, ^2J *b*= 5.8 Hz, 2H, MOM-OCH_2), 4.33 (d, ^2J = .8 Hz, 2H, MOM-OCH_2'), 4.16 (t, ^3J = 4.9 Hz, 4H, H-15), 3.99 (dt, ^3J = 5.7 Hz, ^4J = 1.4 Hz, 4H, H-17), 3.87 (t, ^3J = 4.9 Hz, 4H, H-16), 3.77-3.56 (m, 48H, core glycol-OCH_2), 2.32(s, 6H, MOM-OCH_3).

[DEJ100-2]

7.3.2.9 Synthesis of diol (S)-68c

Described experiment: DEJ106 Repeated: DEJ68, DEJ245

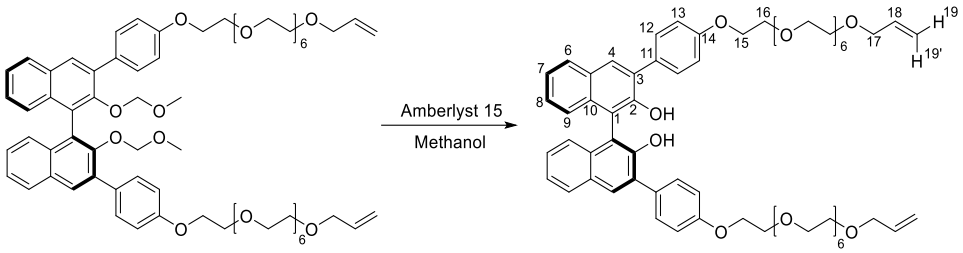

(*S*)-**67c** (*S*)-**68c**

(*S*)-**67c** (656 mg, 0.521 mmol, 1 eq.) and Amberlyst 15 (261 mg, 1.00 g/2 mmol) were charged in a flask and methanol (20 ml) was added. The resulting mixture was refluxed for three days. After cooling down to room temperature, the mixture was filtered and the solvent was evaporated in the rotary evaporator to give the product (*S*)-**68c** (481 g, 0.480 mmol, 92%) as a light brown oil.

$C_{66}H_{86}O_{18}$ 1167.40 g/mol

^{1}H-NMR (600 MHz, [D_1]-Chloroform, 298 K) δ [in ppm] = 7.95 (s, 2H, H-4), 7.88 (d, ^3J = 8.1 Hz, 2H, H-6), 7.64 (ps d, ^3J = 8.8 Hz, 4H, H-12), 7.35 (ddd ^3J = 8.2 Hz, ^3J = 6.8 Hz, ^4J = 1.2 Hz, 2H, H-7), 7.27 (ddd ^3J = 8.5 Hz, ^3J = 6.7 Hz, ^4J = 1.3 Hz, 2H, H-8), 7.18 (dd, ^3J = 8.6 Hz, ^4J = 1.1 Hz 2H, H-9), 7.01 (ps d, ^3J = 8.7 Hz, 4H, H-13), 5.87 (ddt ^3J = 17.3 Hz, ^3J = 10.4 Hz, ^3J = 5.7 Hz, 2H, H-18), 5.41 (br s, 2H, O*H*), 5.24 (ddt, ^3J = 17.2 Hz, ^2J = 1.7 Hz, ^4J = 1.7 Hz, 2H, H-19'), 5.14 (ddt, ^3J = 10.3 Hz, ^2J = 1.4 Hz, ^4J = 1.4 Hz, 1H, H-19), 4.17 (t, ^3J = 5.0 Hz, 4H, H-15), 3.98 (dt, ^3J = 5.7 Hz, ^4J = 1.4 Hz, 4H, H-17), 3.86 (t, ^3J = 5.0 Hz, 4H, H-16), 3.74-3.53 (m, 48H, core glycol OCH_2).

[DEJ106-1]

7.3.2.10 Synthesis of the phosphoric acid (S)-69c

Described experiment: DEJ113 Repeated: DEJ60, DEJ71, DEJ223, DEJ250

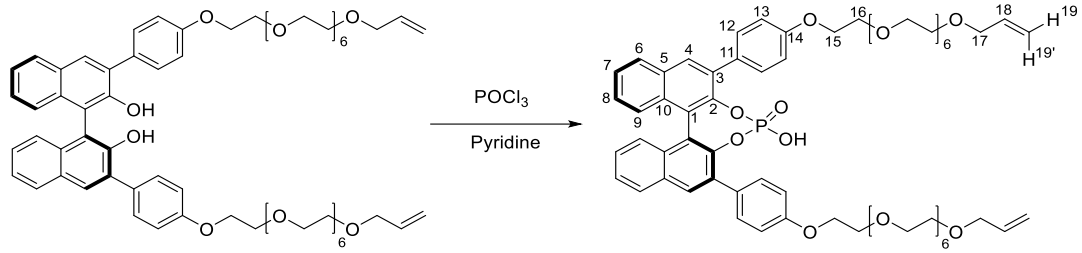

(*S*)-**68c** (*S*)-**69c**

(*S*)-**68c** (561 mg, 0.480 mmol, 1 eq.) was charged in a Schlenk flask and dried at high vacuum for three hours. Pyridine (4 ml) and phosphoryl chloride (1.47 g, 875 µl, 9.6 mmol, 20 eq.) were added under argon and the resulting mixture was stirred for 16 hours at 60° C. After addition of water (2 ml) the mixture was stirred for another 3 hours at 60° C before dichloromethane (20 ml) was added and the resulting two phases were separated. The organic phase was washed with hydrochloric acid (2M, 3 x 15 ml), dried over anhydrous sodium sulfate and filtered. After removing the solvent in the rotary evaporator (*S*)-**69c** was obtained as a brown oil (553 mg, 0.446 mmol, 93%).

$C_{66}H_{85}O_{20}P$ 1229.36 g/mol

^{1}H-NMR (600 MHz, [D$_1$]-Chloroform, 298 K) δ [in ppm] = 7.95 (s, 2 H, H-4), 7.91 (d, ^3J(H-6,7) = 8.3 Hz, 2 H, H-6), 7.60 (ps d, ^3J(H-12,13) = 8.7 Hz, 4 H, H-12), 7.44 (ddd ^3J(H-7,6) = 8.1 Hz, ^3J(H-7,8) = 6.7 Hz, ^4J(H-7,9) = 1.3 Hz, 2 H, H-7), 7.30 (d, ^3J(H-9,8) = 8.6 Hz, 2 H, H-9), 7.27 – 7.23 (m, 2 H, H-8 merged with $CDCl_3$ peak), 6.88 (ps d, ^3J(H-13,12) = 8.7 Hz, 4 H, H-13), 5.85 (ddt ^3J(H-18,19') = 17.3 Hz, ^3J(H-18,19) = 10.3 Hz, ^3J(H-18,17) = 5.7 Hz, 2 H, H-18), 5.21 (ddt, ^3J(H-19',18) = 17.3 Hz, ^2J(H-19',19) = 1.7 Hz, ^4J(H-19',17) = 1.7 Hz, 2 H, H-19'), 5.12 (ddt, ^3J(H-19,18) = 10.4 Hz, ^2J(H-19,19') = 1.4 Hz, ^4J(H-19,17) = 1.4 Hz, 1 H, H-19), 4.01 (t, ^3J(H-15,16) = 4.8 Hz, 4 H, H-15), 3.94 (dt, ^3J(H-17,18) = 5.7 Hz, ^4J(H-17,19/19') = 1.4 Hz, 4 H, H-17), 3.70 (t, ^3J(H-16,15) = 4.8 Hz, 4 H, H-16), 3.61-3.50 (m, 48 H, core glycol OCH_2).

[DEJ71-1]

7.3.2.11 Synthesis of the precatenane (S,S)-70c

Described experiment: DEJ61 Repeated: DEJ73, DEJ77, DEJ91, DEJ117, DEJ234, DEJ251

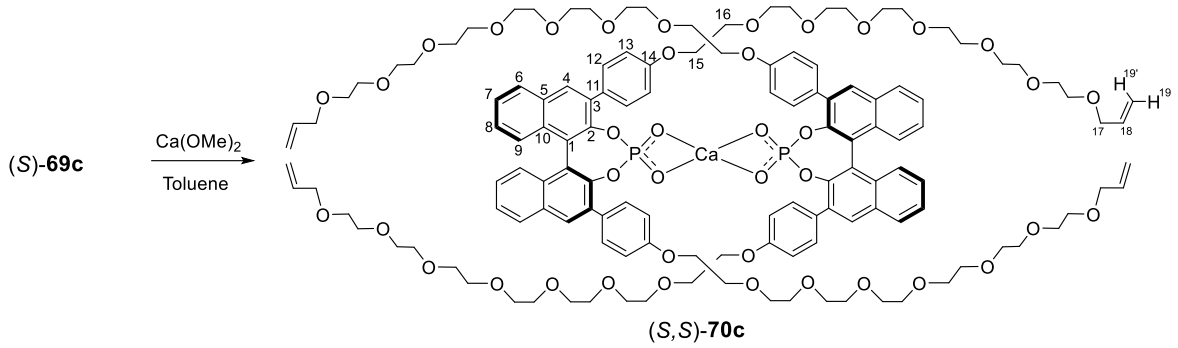

The phosphoric acid (*S*)-**69c** (100 mg, 0.0810 mmol, 1 eq.) was charged in a Schlenk flask and dried at high vacuum for three hours. Dry toluene (3 ml) and calcium methoxide (4.17 mg, 0.0410 mmol, 0.5 eq.) were added and the mixture was stirred at room temperature for 16 hours. The mixture was filtered and the solvent was removed in the rotary evaporator to give the product (*S*,*S*)-**70c** (100 mg, 0.0800 mmol, 98.8%) as a brown oil.

$C_{132}H_{168}O_{40}P_2Ca$ 2496.78 g/mol

^{1}H-NMR (600 MHz, [D_6]-Benzene, 298 K) δ [in ppm] = 8.05 (m, 8 H, H-12), 7.93 (br s, 4 H, H-4), 7.76 (d, ^3J(H-6,7) = 8.1, 4 H, H-6), 7.40 (d, ^3J(H-9,8) = 8.6 Hz, 4 H, H-9), 7.21 (t, ^3J(H-7,6/8) = 7.5 Hz, 4 H, H-7), 7.08 - 6.87 (m, 12 H, H-8, H-12), 5.78 (m, 4 H, H-18), 5.17 (d, ^3J(H-19',18) = 17.5 Hz, 4 H, H-19'), 5.01 (d, ^3J(H-19,18) = 10.5 Hz, 4 H, H-19), 3.93 (m, 8 H, H-15), 3.79 (br s, 8 H, H-17), 3.68-3.13 (m, 104 H, H-16, core glycol O*C*H_2).

[DEJ117]

7.3.2.12 Synthesis of macrocycle (S)-2c and catenane (S,S)-1c

Described experiment: DEJ82 Repeated: DEJ84, DEJ118, DEJ206, DEJ235, DEJ252

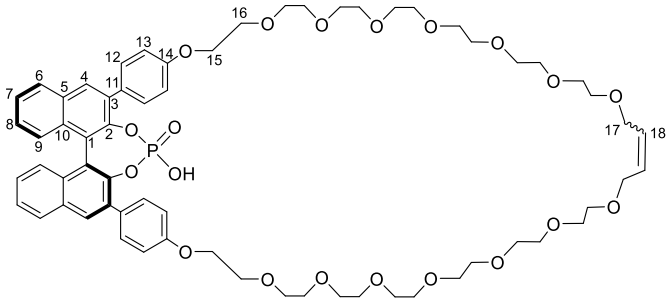

(*S*)-**2c**

(*S,S*)-**70c** —Grubbs' 2nd gen, $CHCl_2$→ +

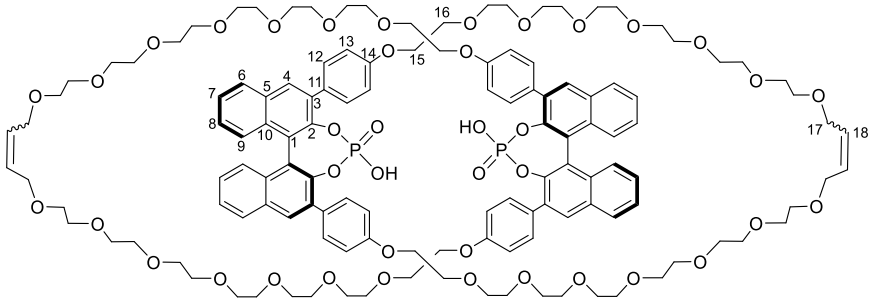

(*S,S*)-**1c**

(*S*,*S*)-**70c** (166 mg, 0.066 mmol, 1 eq.) was dried in a Schlenk flask for four hours. Dry dichloromethane (60 ml) and second generation Grubb's catalyst (5.6 mg, 0.00700 mmol, 0.1 eq.) were added under argon and the reaction mixture was stirred at room temperature with the flask wrapped in aluminium foil to protect the catalyst from light. After five and 17 hours, 1 ml was withdrawn from the mixture to control the progress of the reaction by RP-18 HPLC. After 20 hours further second generation Grubb's catalyst (6 mg, 0.00700 mmol, 0.1 eq.) was added. Additional 30 hours of reaction lead to full conversion and ethyl vinyl ether (4ml) and QuadraSil (400 mg) were added. The mixture was stirred for 16 hours. After filtration volatiles were removed in the rotary evaporator to give 110 mg of a brown solid. The crude product was purified by preparative MPLC (RP-18 17g Kronlab column, MeOH with 0.05% TFA : water with 0.05% TFA = 65 : 35 gradient flow firstly up to 85:15 within 48 min, secondly up to 90:10 within 22 minutes, thirdly up to 100:0 within 10 minutes, 15 ml/min). The solvent was evaporated and each of the two compounds was redissolved in dichloromethane (10 ml) and washed with hydrochloric acid (2M, 10 x 2 ml). After removing the solvent in the rotary evaporator, the 7-EG macrocycle (*S*)-**2c** (8.00 mg, 10%) and the 7-EG catenane (*S*)-**1c** (27.0 mg, 16%) were obtained.

Macrocycle (*S*)-**2c:**

$C_{64}H_{81}O_{20}P$ 1201.31 g/mol

^{1}H-NMR (600 MHz, [D$_1$]-Chloroform, 298 K) δ [in ppm] = 7.99 (s, 2 H, H-4), 7.93 (d, ^3J(H-6,7) = 8.2 Hz, 2 H, H-6), 7.71 (ps d, ^3J(H-12,13) = 8.3 Hz, 4 H, H-12), 7.45 (dd, ^3J(H-7,6) = 7.4 Hz, ^3J(H-7,8) = 7.4 Hz, 2 H, H-7), 7.33 (d, ^3J(H-9,8) = 8.6 Hz, 2 H, H-9), 7.29 – 7.23 (m, 2 H, H-8 merged with $CDCl_3$ peak), 7.02 (ps d, ^3J(H-13,12) = 8.4 Hz, 4 H, H-13), 5.70 (s, 1.85 H, H-18 (*E*-isomer)), 5.63 (s, 0.15 H, H-18 (*Z*-isomer)), 4.25 – 4.15 (m, 4 H, H-15), 3.97 – 3.82 (m, 8 H, H-16, H-17), 3.76-3.44 (m, 48 H, core glycol OC*H*$_2$).

[DEJ206-M]

Catenane (*S*,*S*)-**1c:**

$C_{128}H_{162}O_{40}P_2$ 2402.62 g/mol

^{1}H-NMR (600 MHz, [D$_1$]-Chloroform, 298 K) δ [in ppm] = 7.97 (s, 4 H, H-4), 7.93 (d, ^3J(H-6,7) = 8.3 Hz, 4 H, H-6), 7.61 (ps d, ^3J(H-12,13) = 8.2 Hz, 8 H, H-12), 7.46 (dd, ^3J(H-7,6) = 7.5 Hz, ^3J(H-7,8) = 7.5 Hz, 4 H, H-7), 7.31 (d, ^3J(H-9,8) = 8.5 Hz, 4 H, H-9), 7.28 – 7.24 (m, 4 H, H-8 merged with $CDCl_3$ peak), 6.89 (ps d, ^3J(H-13,12) = 8.3 Hz, 8 H, H-13), 5.73 (s, 3.7 H, H-18 (*E*-isomer)), 5.65 (s, 0.3 H, H-18 (*Z*-isomer), 4.00 (t, ^3J(H-15,16) = 4.7 Hz, 8 H, H-15), 3.96 – 3.92 (m, 16 H, H-16, H-17), 3.74 - 3.44 (m, 96 H, core glycol OC*H*$_2$).

[DEJ206-2]

7.3.3 Synthesis of precursors of bipyridine catenane (S)-12 and (S)-15 and macrocycle (S)-18

7.3.3.1 Synthesis of bisalkyne (S)-9

Described experiment: DEJ154 Repeated: DEJ153, DEJ225, DEJ254, DEJ281, DEJ298, DEJ368

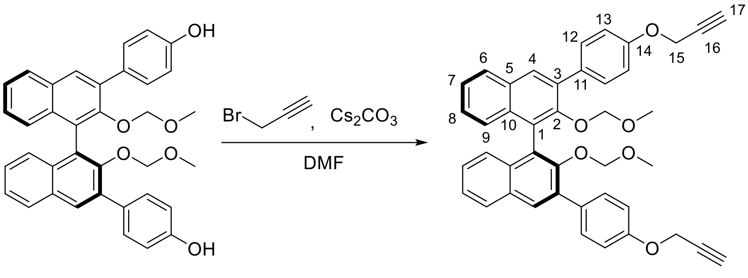

(*S*)-**66** (*S*)-**9**

(*S*)-**66** (0.903 g, 1.62 mmol, 1 eq.) and caesium carbonate (2.54 g, 7.78 mmol, 4.8 eq.) were charged in a Schlenk-flask (100 ml) and dried under high vacuum for three hours. Dry dimethylformamide (30 ml) was added under argon followed by addition of propargyl bromide (80 wt% in toluene, 420 µl, 3.89 mmol, 2.4 eq.). The resulting suspension was stirred at 80 °C for 20 hours. After cooling down to room temperature the reaction mixture was diluted with water (200 ml) and extracted with ethyl acetate (3 x 150 ml). The combined organic phases were washed with saturated aqueous sodium chloride solution (50 ml) and dried over magnesium sulfate. After filtration and removal of the solvent, the desired compound (*S*)-**9** was obtained as a pale yellow solid (0.960 g, 1.51 mmol, 93%).

$C_{42}H_{34}O_6$ 634.73 g/mol

^{1}H-NMR (400 MHz, [D$_1$]-Chloroform, 298 K) δ [in ppm] = 7.94 (s, 2H, H-4), 7.88 (d, ^3J = 8.2 Hz, 4H, H-6), 7.73 (ps d, ^3J = 8.7 Hz, 4H, H-12), 7.42 (ddd, ^3J = 8.1 Hz, ^3J = 5.6 Hz, ^4J = 2.4 Hz, 2H, H-7), 7.32 – 7.24 (m, 4H, H-8,H-9), 7.10 (psd, ^3J = 8.8 Hz, 4H, H-13), 4.77 (d, ^4J = 2.4 Hz, 4H, H-15), 4.43 (d, ^2J = 5.7 Hz, 2H, OC*H*$_2$), 4.38 (d, *J* = 5.8 Hz, 2H, OC*H*$_2$'), 2.56 (t, ^4J = 2.4 Hz, 2H, H-17), 2.37 (s, 6H, OC*H*$_3$).

^{13}C-NMR (101 MHz, [D$_1$]-Chloroform, 298 K) δ [in ppm] = 157.1 (C-14), 151.4 (C-2), 135.0 (C-11), 133.6 (C-5), 132.5 (C-1), 131.0 (C-10), 130.9 (C-12), 130.4 (C-4), 127.9 (C-6), 126.7 (C-9), 126.6 (C-8), 126.3 (C-3), 125.3 (C-7), 114.9 (C-13), 98.6 (O*C*H$_2$), 78.6 (C-16), 75.7 (C-17) 56.0 (O*C*H$_3$), 56.0 (C-15).

COSY (400 MHz/400 MHz, [D$_1$]-Chloroform, 298 K) δ [in ppm] = 7.88/7.42 (H-6/H-7), 7.73/7.10 (H-12/H-13), 7.42/7.88, 7.28 (H-7/H-6, H-8, H-9), 7.10/7.88 (H-13/H-12), 4.77/2.56 (H-15/H-17), 4.43/4.38 (OC*H*$_2$/OC*H*$_2$‘), 4.38/4.43(OC*H*$_2$‘/OC*H*$_2$), 2.56/4.77 (H-17/H-15).

HSQC (400 MHz/101 MHz, [D$_1$]-Chloroform, 298 K) δ [in ppm] = 7.94/130.4 (H-4/C-4), 7.88/127.9 (H-6/C-6), 7.73/130.9 (H-12/C-12), 7.42/125.3 (H-7/C-7), 7.28/126.7 (H-9/C-9), 7.28/126.6 (H-8/C-8), 7.10/114.9 (H-13/C-13), 4.77/56.0 (H-15/C-15), 4.43/98.6 (OC*H*$_2$/ O*C*H$_2$), 2.53/75.7 (H-17/C-17), 2.36/56.0 (OC*H*$_3$/ OC*H*$_3$).

HMBC (400 MHz/101 MHz, [D$_1$]-Chloroform, 298 K) δ [in ppm] = 7.94/151.4, 133.6, 127.9 (H-4/C-2, C-5, C-6), 7.88/133.6, 130.4, 126.3 (H-6/C-5, C-4, C-3), 7.73/157.1, 135 (H-12/C-14, C-11), 7.42/126.6,

131.0 (H-7/C-8, C-10), 7.28/133.6, 131.0, 127.9, 125.3 (H-8,H-9/ C-5, C-10, C-6, C-7), 7.10/157.1 (H-13/C-14), 4.77/157.1, 78.6, 75.7 (H-15/C-14, C-16, C-17), 4.43/151.4, 56.0 (OCH_2/C-2, OCH_3), 2.53/56.0 (H-17/C-15), 2.36/98.6 (OCH_3/ OCH_2).

[XHX74-1-2 MOM bisalkin]

HR-MS [ESI-pos, methanol/water]: m/z = 657.2173 $[M+Na]^+$, calculated 657.2248 for $[C_{42}H_{34}O_6Na]^+$.

Elemental analysis: calculated for $C_{42}H_{34}O_6$: C, 79.48; H, 5.40; O, 15.12; found C, 78.1; H, 5.43; O, 13.7.

IR (ATR): ν = 3274, 2952, 1606, 1508, 1427, 1216, 1180, 1153, 1025, 970, 912, 829, 752, 669 cm^{-1}.

7.3.3.2 Synthesis of diol (S)-95

Described experiment: DEJ231 Repeated: DEJ158, DEJ197

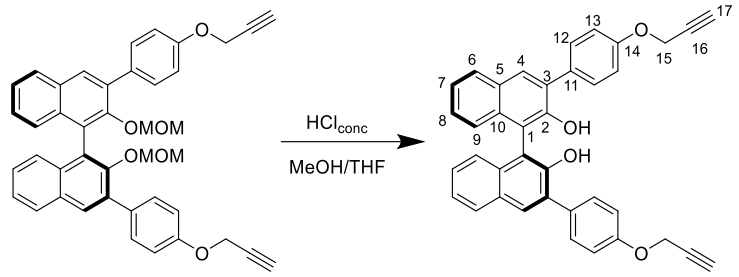

(*S*)-**9** (*S*)-**95**

MOM-protected bisalkyne (*S*)-**9** (600 mg, 1.06 mmol, 1 eq.) was dissolved in a 1:1 mixture of tetrahydrofuran/methanol (10 ml) and concentrated hydrochloric acid (1 ml) was added. The solution was stirred at 80 °C for three hours. After cooling to room temperature, volatiles were removed in the rotary evaporator and the crude mixture was purified by silica gel column chromatography (2 x 20 cm, cyclohexane : ethyl acetate = 87 : 13) to yield the product (*S*)-**95** as a white solid (447 mg, 0.816 mmol, 76.9%).

$C_{38}H_{26}O_4$ 546.62 g/mol

^{1}H-NMR (400 MHz, [D$_1$]-Chloroform, 298 K) δ [in ppm] = 8.00 (s, 2H, H-4), 7.91 (d, ^3J = 8.1 Hz, 2H, H-6), 7.69 (d, ^3J = 8.8 Hz, 4H, H-12), 7.39 (ddd, ^3J = 8.1 Hz, ^3J = 6.8 Hz, ^4J = 1.3 Hz, 2H, H-7), 7.31 (ddd, ^3J = 8.2 Hz, ^3J = 6.8 Hz, ^3J = 1.3 Hz, 2H, H-8), 7.21 (d, ^3J = 8.5 Hz, 2H, H-9), 7.10 (d, ^3J = 8.8 Hz, 4H, H-13), 5.34 (s, 2H, O*H*), 4.76 (d, ^4J = 2.4 Hz, 4H, H-15), 2.55 (t, ^4J = 2.4 Hz, 2H, H-17).

^{13}C-NMR (101 MHz, [D$_1$]-Chloroform, 298 K) δ [in ppm] = 157.5 (C-14), 150.4 (C-11), 132.9 (C-10), 131.2 (C-4), 130.9 (C-12), 130.8 (C-2), 130.3 (C-3), 129.6 (C-5), 128.5 (C-6), 127.4 (C-8), 124.5 (C-7), 124.4 (C-9), 115.0 (C-13), 112.4 (C-1), 78.6 (C-16), 75.8 (C-17), 56.0 (C-15).

COSY (400 MHz/400 MHz, [D$_1$]-Chloroform, 298 K) δ [in ppm] = 7.91/7.39 (H-6/H-7), 7.69/7.10 (H-12/H-13), 7.39/7.91 (H-7/H-6), 7.31/7.21 (H-8/H-9), 7.21/7.31 (H-9/H-8), 7.10/7.69 (H-13/H-12), 4.76/2.55 (H-15/H-17), 2.55/4.76 (H-17/H-15).

HSQC (400 MHz/101 MHz, [D$_1$]-Chloroform, 298 K) δ [in ppm] = 8.00/131.2 (H-4/C-4), 7.91/128.5 (H-6/C-6), 7.69/130.9 (H-12/C-12), 7.39/124.5 (H-7/C-7), 7.31/127.4 (H-8/C-8), 7.21/124.4 (H-9/C-9), 7.10/115.0 (H-13/C-13), 4.67/56.0 (H-15/C-15), 2.55/75.8 (H-17/C-17).

HMBC (400 MHz/101 MHz, [D$_1$]-Chloroform, 298 K) δ [in ppm] = 8.00/150.4, 132.9, 130.8, 128.5 (H-4/C-11, C-10, C-2, C-6), 7.91/132.9, 131.2, 127.4 (H-6/C-10, C-4, C-8), 7.69/157.5, 115.0 (H-12/C-14, C-13), 7.39/129.6, 124.4 (H-7/C-5, C-9), 7.31/132.9, 128.5 (H-8/C-10, C-6), 7.21/129.6, 124.5, 112.4 (H-9/C-5, C-7, C-1), 7.10/157.5, 130.9 (H-13/C-14, C-12), 5.34/150.4, 130.3, 112.4 (O*H*/C-11, C-3, C-1), 4.76/157.5, 78.6, 75.8 (H-15/C-14, C-16, C-17), 2.55/56.0 (H-17/C-15).

[XHX82-5]

HR-MS [ESI-pos, methanol/water]: m/z = 547.1908 $[M+H]^+$, calculated 547.1904 for $[C_{38}H_{27}O_4]^+$.

Elemental analysis: calculated for $C_{38}H_{26}O_4$: C, 83.50; H, 4.79; O, 11.71; found C, 83.0; H, 4.87; O, 11.5.

IR (ATR): ν = 3502, 3284, 3054, 1606, 1508, 1436, 1359, 1216, 1178, 1024, 829, 750, 636 cm^{-1}.

7.3.3.3 Synthesis of diester 87[156]

Described experiment: DEJ260

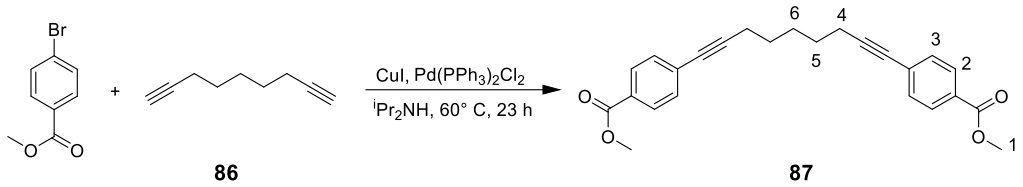

86 **87**

Methyl-4-bromobenzoate (787 mg, 3.66 mmol, 2.2 eq.), CuI (15.9 mg, 0.0800 mmol, 0.05 eq.) and Pd(PPh3)2Cl2 (35.0 mg, 0.05 mmol, 0.03 eq.) were placed in a Schlenk flask which was then evacuated and backfilled with argon three times. Degassed diisopropylamin (6 ml) was added followed by addition of 1,8-nonadiyne **86** (200 mg, 1.66 mmol, 1 eq.). The mixture was stirred under argon for 16 hours. After cooling to room temperature, the mixture was filtered over a pad of celite and volatiles were removed in the rotary evaporator. The crude mixture was purified by silica gel column chromatography (2.5 x 20 cm, cyclohexane : diethyl ether = 85 : 15) to yield the product **87** (488 mg, 1.25 mmol, 75.3%) as an off white solid.

$C_{25}H_{24}O_4$ 388,46 g/mol

^{1}H-NMR (400 MHz, [D_1]-Chloroform, 298 K) δ [in ppm] = 7.92 (psd, ^3J = 8.4 Hz, 4H, H-2), 7.42 (psd, ^3J = 8.4 Hz, 4H, H-3), 3.91 (s, 6H, H-1), 2.51 – 2.43 (m, 4H, H-4), 1.66 (m, 6H, H-5,H-6).

[DEJ260-1]

7.3.3.4 Synthesis of diester 88[156]

Described experiment: DEJ261

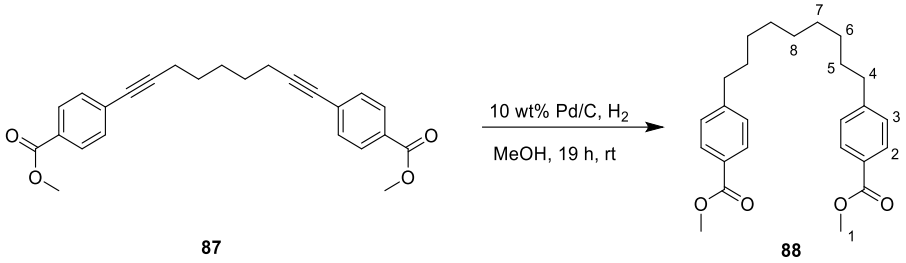

87 (450 mg, 1.16 mmol, 1 eq.) and Pd/C (10 wt%, 30.0 mg, 0.02 eq.) were placed in a round bottom flask with a septum. Methanol was added and the suspension was flushed with H_2. The mixture was stirred for 16 hours under H_2-atmosphere. After filtration over a pad of celite and evaporation of the solvent in the rotary evaporator the product **88** (420 mg, 1.06, 91.4 %) was obtained as a white solid.

$C_{25}H_{32}O_4$ 396,53 g/mol

^{1}H-NMR (400 MHz, [D$_1$]-Chloroform, 298 K) δ [in ppm] = δ 7.94 (psd, ^3J = 8.3 Hz, 4H, H-2), 7.23 (psd, ^3J = 8.3 Hz, 4H), 3.90 (s, 6H, H-1), 2.68 – 2.60 (t , ^3J = 7.9 Hz, 4H, H-4), 1.63 – 1.56 (m, 4H, H-5), 1.29 (m, 10H, H-6, H-7, H-8).

[DEJ261-1]

7.3.3.5 Synthesis of diol 89[156]

Described experiment: DEJ268

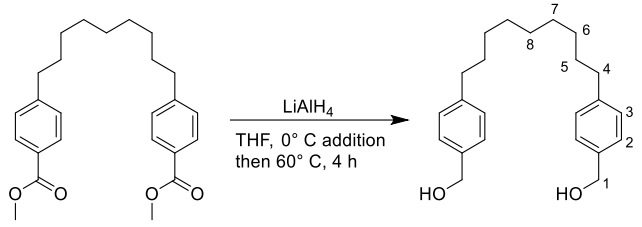

88 89

$LiAlH_4$ (2.4 M in THF, 2.70 ml, 6.5 eq) was added to a dry Schlenk flask and cooled to 0 °C. To this a solution of **88** (420 mg, 1.06 mmol, 1 eq.) in dry tetrahydrofuran (5 ml) was added dropwise under argon. After addition the mixture was stirred at 60 °C for four hours. The reaction was carefully quenched by addition of water (5ml) at 0 °C followed by addition of HCl_{aq} (2M, 5 ml). Tetrahydrofuran was removed in the rotary evaporator before dichloromethane (30 ml) was added. After phase separation, the organic phase was washed with saturated sodium chloride solution (30 ml), dried over $MgSO_4$, filtrated and evaporated in the rotary evaporator. The product **89** (308 mg, 0.91 mmol, 85.8 %) was obtained as a white solid.

$C_{23}H_{32}O_2$ 340,51 g/mol

^{1}H-NMR (400 MHz, [D_1]-Chloroform, 298 K) δ [in ppm] = δ 7.27 (psd, ^3J = 8.5 Hz, 4H, H-2), 7.17 (psd, ^3J = 8.5 Hz, 4H, H-3), 4.65 (s, 4H, H-1), 2.59 (t, ^3J = 7.9 Hz, 4H, H-4), 1.63 – 1.56 (m, 4H, H-5), 1.29 (m, 10H, H-6, H-7, H-8).

[DEJ268-1]

7.3.3.6 Synthesis of bisbromide 90[156]

Described experiment: DEJ274

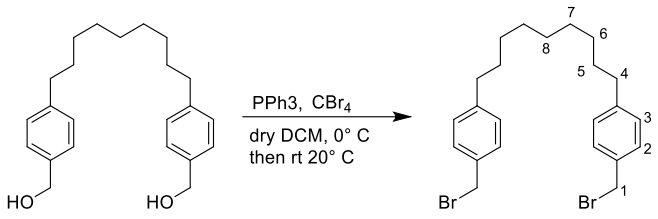

89 **90**

90 (308 mg, 0.910 mmol, 1 eq.) and triphenylphosphine (711 mg, 2.83 mmol, 3 eq.) were dissolved in dichloromethane (10 ml) in a round bottom flask. At 0 °C carbon tetrabromide (898 mg, 2.83 mmol, 3 eq.) was added portion-wise and the mixture was stirred at room temperature for 16 hours. The solvent was removed in the rotary evaporator and the crude mixture was purified by silica gel column chromatography (2.5 x 20 cm, cyclohexane : dichloromethane = 100 : 0 to 0 : 100) to yield the product **90** (363 mg, 0,779 mmol, 85.6 %) as a white solid.

$C_{23}H_{30}Br_2$ 466,30 g/mol

^{1}H-NMR (400 MHz, [D$_1$]-Chloroform, 298 K) δ [in ppm] = δ 7.30 (psd, ^3J = 8.1 Hz, 4H, H-2), 7.14 (psd, ^3J = 8.1 Hz, 4H, H-3), 4.49 (s, 4H, H-1), 2.58 (t, ^3J = 7.9 Hz, 4H, H-4), 1.63 – 1.56 (m, 4H, H-5), 1.35 – 1.24 (m, 10H, H-6, H-7, H-8).

[DEJ274-3]

7.3.3.7 Synthesis of bisazide 10[156]

Described experiment: DEJ277 Repeated: DEJ280, DEJ359, DEJ361

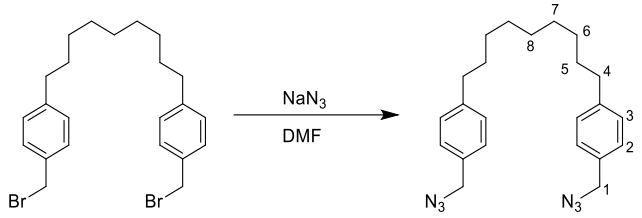

90 **10**

90 (758 mg, 1.63 mmol, 1 eq.) and sodium azide (265 mg, 4.08 mmol, 2.5 eq.) were placed in a round bottom flask and dissolved in dimethylformamide (15 ml). The mixture was stirred at 80 °C for 20 hours. After cooling to room temperature water (200 ml) was added and the aqueous phase was extracted with ethyl acetate (4 x 25 ml). The combined organic phases were dried over $MgSO_4$, filtered and volatiles were removed in the rotary evaporator to yield the product **10** (400 mg, 1.02 mmol, 61.8%) as a white solid.

$C_{23}H_{30}N_6$ 390,54 g/mol

^{1}H-NMR (400 MHz, [D$_1$]-Chloroform, 298 K) δ [in ppm] = δ 7.27 (psd, ^3J = 8.2 Hz, 4H, H-2), 7.23 (psd, J = 8.2 Hz, 4H, H-3), 4.34 (s, 4H, H-1), 2.65 (t, ^3J = 7.9 Hz, 4H, H-4), 1.65 (m, 4H, H-5), 1.42 – 1.21 (m, 10H, H-6, H-7, H-8).

[DEJ277-2]

7.3.3.8 Synthesis of methoxy derivative 92[161]

Described experiment: DJS02

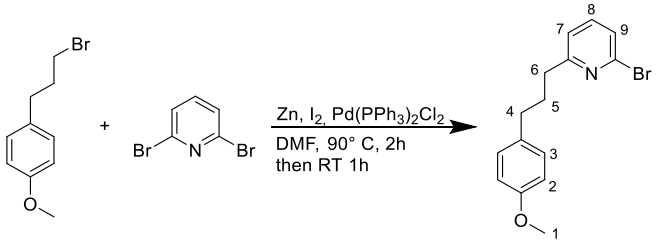

91 **92**

Zinc (0.856 g, 13.09 mmol, 1.5 eq.) and iodine (0.062 g, 0.350 mmol, 0.04 eq.) were added to a dry round bottom flask and were flushed with nitrogen. To this a solution of 1-(3-bromopropyl)-4-methoxybenzene (2.00 g, 8.73 mmol, 1 eq.) in dry dimethylformamide (4 ml) was added and the mixture was stirred rigorously at 90 °C for two hours. In a second dry round bottom flask bis(triphenylphosphin)-palladium(II)-chlorid (0.112 g, 0.44 mmol, 0.05 eq.) and 2,6-dibromopyridine (1.653 g, 6.98 mmol, 0.8 eq.) were added and flushed with nitrogen. After cooling to room temperature the mixture in flask 1 was transferred to flask 2 and the resulting mixture was stirred at room temperature for one hour. Saturated NH_4Cl_{aq} (10 ml) was added and the aqueous phase was extracted with diethyl ether (3 x 10 ml). The combined organic phases were washed with saturated lithium chloride solution, dried with anhydrous magnesium sulfate, filtered and evaporated in the rotary evaporator. The crude mixture was purified by column chromatography (petrol ether : diethyl ether = 95 : 5) to yield the product **92** (0.968, 3.60 mmol, 45 %) as a light brown oil.

$C_{15}H_{16}BrNO$ 306,20 g/mol

^{1}H-NMR (400 MHz, [D$_1$]-Chloroform, 298 K) δ [in ppm] = δ 7.46 (dd, ^3J = 7.7 Hz, ^4J = 0.9 Hz, 1H. H-8), 7.32 (d, ^3J = 7.9 Hz, 1H, H-9), 7.13 (psd, ^3J = 8.8 Hz, 2H, H-3), 7.10 (dd, ^3J = 7.7, ^4J = 0.9 Hz, 1H, H-7), 6.85 (psd, ^3J = 8.7 Hz, 2H, H-2), 3.81 (s, 3H, H-1), 2.81 (t, J = 15.6 Hz, 1H, H-6), 2.64 (t, J = 15.3 Hz, 1H, H-4), 2.10 – 1.98 (m, 2H, H-5).

[DJS02]

7.3.3.9 Synthesis of pyridine 93[161]

Described experiment: DJS04

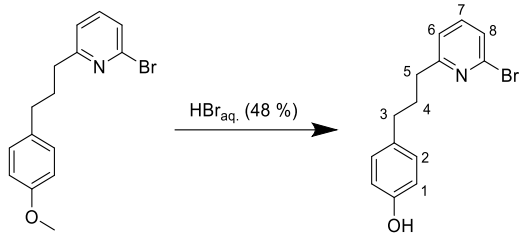

92 **93**

92 (0.968 g, 3.16 mmol, 1 eq.) and HBr_{aq} (48 %, 8 ml) were added to a round bottom flask. The mixture was stirred at 100 °C for 16 hours. After addition of water (10 ml) and neutralization with sodium hydroxide solution (10M) the aqueous phase was extracted with dichloromethane (2 x 20 ml). The combined organic phases were dried over anhydrous magnesium sulfate, filtered and evaporated in the rotary evaporator. The crude mixture was purified by passing it through a pad of silica (2 x 5 cm, 2 CV dichloromethane, then 3 CV diethyl ether) to yield the product **93** (0.816 g, 0.278, 88 %) as an off white solid.

$C_{14}H_{14}BrNO$ 292,18 g/mol

^{1}H-NMR (400 MHz, [D$_1$]-Chloroform, 298 K) δ [in ppm] = δ 7.43 (dd, ^3J = 7.7 Hz, 1H, H-7), 7.30 (dd, ^3J = 7.8, ^4J = 0.9 Hz, 1H, H-8), 7.07 (dd, ^3J = 7.8, ^4J = 0.9 Hz, 1H, H-6), 7.04 (psd, ^3J = 8.6 Hz, 2H, H-2), 6.75 (psd, ^3J = 8.5 Hz, 2H, H-1), 4.72 (s, 1H, O*H*), 2.78 (t, *J* = 15.7 Hz, 2H, H-5), 2.60 (t, *J* = 15.3 Hz, 2H, H-3), 2.08 – 1.91 (m, 2H, H-4).

[DJS04]

7.3.3.10 Synthesis of macrocycle precursor 94[161]

Described experiment: DJS07

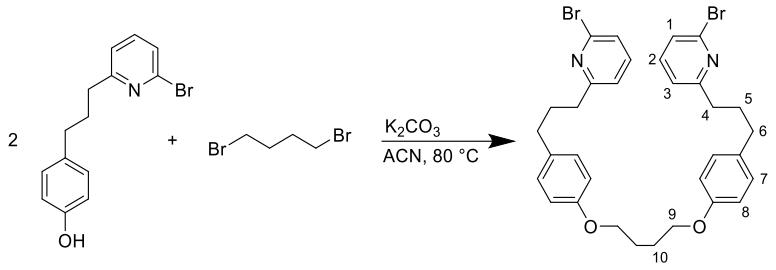

93 **94**

93 (5.05 g, 17.3 mmol, 2 eq.), 1-4-dibromobutane (1.87 g, 8.64 mmol, 1 eq.) and potassium carbonate (9.55 g, 69.1 mmol, 8 eq.) were added to a round bottom flask and dissolved in acetonitrile (60 ml). The mixture was stirred at 80 °C for 16 hours. After cooling down to room temperature dichloromethane (500 ml) was added and the organic phase was washed with water (2 x 500 ml) and saturated sodium chloride solution (400 ml). After drying over anhydrous magnesium sulfate and filtrating the solvent was removed *in vacuo.* The crude mixture was purified by column chromatography (petrol ether : dichloromethane = 50 : 50 to petrol ether : dichloromethane : ethyl acetate = 45 : 45 : 5) to yield the product **94** (3.57 g, 5.61 mmol, 64.9 %) as an off white solid.

$C_{32}H_{34}Br_2N_2O_2$ 638,44 g/mol

^{1}H-NMR (400 MHz, [D$_1$]-Chloroform, 298 K) δ [in ppm] = δ 7.43 (dd, ^3J = 7.7 Hz, 2H, H-2), 7.29 (dd, ^3J = 7.7, ^4J = 0.9 Hz, 2H, H-1), 7.08 (psd, ^3J = 8.6 Hz, 4H, H-7), 7.07 (d, J = 7.9 Hz, 2H, H-3), 6.82 (psd, ^3J = 8.6 Hz, 4H, H-8), 4.00 (t, ^3J = 5.5 Hz, 4H, H-9), 2.82 – 2.75 (dd, ^3J = 7.6 Hz, 4H, H-4), 2.61 (dd, ^3J = 7.6 Hz, 1H, H-6), 2.08 – 1.93 (m, 8H, H-5, H-10).

[DJS07]

7.3.3.11 Synthesis of macrocycle 11[161]

Described experiment: DJS18 Repeated: DJS28, DEJ293, DEJ299, DEJ301, DJS06, DJS10, DJS12

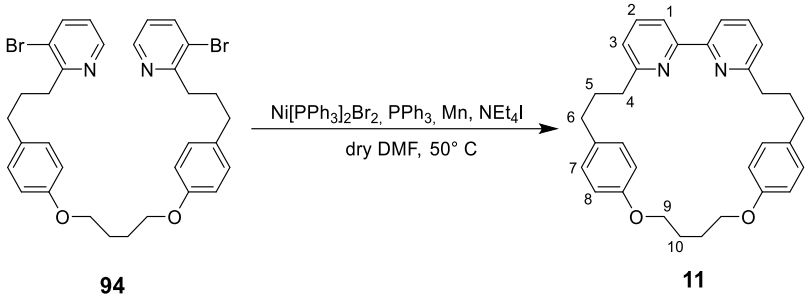

94 **11**

Dibromo-bis-(triphenylphosphin)-nickel(II) (0.910 g, 1.22 mmol, 1 eq.), triphenylphosphine (0.640 g, 2.44 mmol, 2 eq.) manganese (0.670 g, 12.2 mmol, 10 eq.) and tetraethylammonium iodide (0.310 g, 1.22 mmol, 1 eq.) were placed in a dry round bottom flask, flushed with nitrogen and dissolved in dimethylformamide (12 ml). The suspension was sonicated for ten minutes at room temperature before it was stirred at 50 °C for one hour. To this a solution of **94** (0.78 g, 1.22 mmol, 1 eq.) in dimethylformamide (10 ml) was added over four hours at 50 °C. After cooling down to room temperature dichloromethane (20 ml) and EDTA-NH_3 (20ml) were added. After filtration over a pad of celite and phase separation the aqueous phase was extracted with dichloromethane (2 x 20 ml) and the combined organic phases were washed with water (2 x 20 ml) and saturated sodium chloride solution (20 ml). After drying over anhydrous magnesium sulfate and filtration the solvent was removed in the rotary evaporator. The crude mixture was filtered over a pad of silica (petrol ether : dichloromethane = 1 : 1 then petrol ether : dichloromethane : acetonitrile = 40 : 40 : 20) to remove PPh_3. After column chromatography (petrol ether : dichloromethane : ethyl acetate = 45 : 45 : 10) the product **11** (295 mg, 0.620 mmol, 50.8 %) was obtained as an off white solid.

$C_{32}H_{34}N_2O_2$ 478,64 g/mol

^{1}H-NMR (400 MHz, [D_1]-Chloroform, 298 K) δ [in ppm] = δ 7.64 – 7.56 (m, 4H, H-1, H-2), 7.12 (dd, ^3J = 7.0 Hz, ^4J =1.7 Hz, 2H, H-3), 7.03 (psd, J = 8.6 Hz, 4H, H-7), 6.69 (psd, J = 8.6 Hz, 4H, H-8), 4.02 (t, J = 5.8 Hz, 4H, H-9), 2.89 (t, ^3J = 7.9 Hz, 4H, H-4), 2.67 (t, ^3J = 7.1 Hz, 1H, H-6), 2.14 (tt, ^3J = 7.2 Hz, ^3J = 7.8 Hz 4H, H-5), 1.94 (t, ^3J = 5.8 Hz, 4H, H-10).

[DJS18]

7.3.3.12 Synthesis of diol macrocycle (S)-18

Described experiment: DEJ354 Repeated: DEJ352

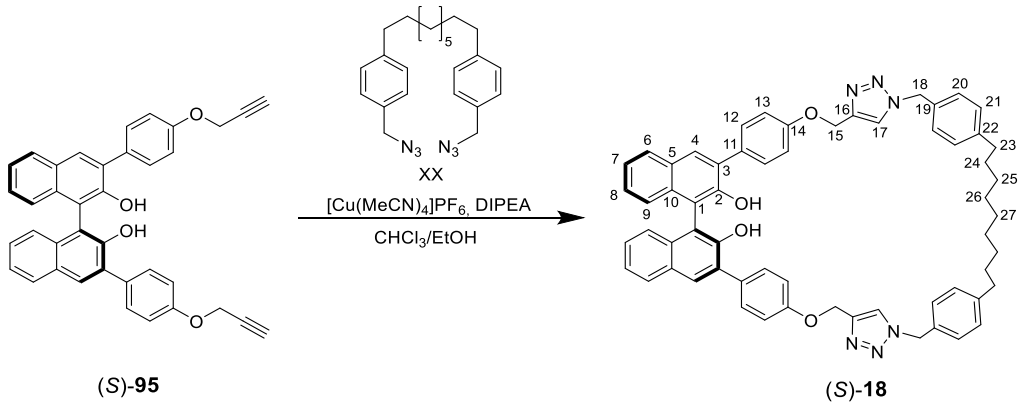

Tetrakis(acetonitrile)copper(I) hexafluorophosphate (29.5 mg, 0.790 mmol, 0.96 eq.) was weighed into a round bottom flash with septum. After purging with nitrogen for five minutes, a degassed 1:1 mixture of chloroform/ethanol (12 ml) and *N*,*N*-diisopropylethylamine (0.028 ml, 0.165 mmol, 2 eq.) were added. To this, a solution of alkyne (*S*)-**95** (45.0 mg, 0.0820 mmol, 1 eq.) and azide (32.2 mg, 0.0820 mmol, 1 eq.) in a degassed 1:1 mixture of chloroform/ethanol (10 ml) was added over four hours at 60 °C. After cooling to room temperature the solvent was removed. The residue was dissolved in dichloromethane (20 ml), washed with EDTA-NH_3 solution (3 x 20 ml) and saturated aqueous sodium chloride solution (20 ml) and dried over magnesium sulfate. After filtration and removal of the solvent, the crude mixture was obtained as a light orange solid. The crude mixture was purified by column chromatography on silica gel (2.5 x 20 cm, cyclohexane : ethyl acetate = 1 : 1) to give (*S*)-**18** (8.00 mg, 8.62 µmol, 11.0 %) as a white solid.

$C_{60}H_{58}N_6O_4$ 927.16 g/mol

^{1}H-NMR (400 MHz, [D$_1$]-Chloroform, 298 K) δ [in ppm] = 7.97 (s, 2H, H-4), 7.90 (dd, ^3J = 8.5 Hz, ^4J = 1.4 Hz, 2H, H-6), 7.62 (psd, ^3J = 8.8 Hz, 4H, H-12), 7.42 (s, 2H, H-17), 7.38 (ddd, ^3J = 8.1 Hz, ^3J = 6.8 Hz, ^4J = 1.2 Hz, 2H, H-7), 7.30 (ddd, ^3J = 8.2, ^3J = 6.8, ^4J = 1.4 Hz, 2H, H-8), 7.19 (dd, ^3J = 8.2 Hz, ^4J = 1.2 Hz, 2H, H-9), 7.17 – 7.13 (m, 8H, H-20, H-21), 7.03 (psd, J = 8.8 Hz, 4H, H-13), 5.50 (d, ^2J = 14.7 Hz, 1H, H-18), 5.45 (d, ^2J = 14.7 Hz, 1H, H-18'), 5.28 (s, 4H, H-15), 2.53 (t, ^3J = 7.8 Hz, 4H, H-23), 1.53 (m, 4H, H-24), 1.35 – 1.13 (m, 10H, H-25, H-26, H-27).

^{13}C-NMR (101 MHz, [D$_1$]-Chloroform, 298 K) δ [in ppm] = 158.0 (C-14), 150.1 (C-2), 144.7 (C-16), 144.1 (C-22), 133.1 (C-5), 131.4 (C-19), 131.0 (C-4), 130.5 (C-11), 130.2 (C-3), 129.6 (C-10), 129.4 (C-21), 128.5 (C-20), 127.3 (C-8), 124.6 (C-9), 124.5 (C-7), 122.5 (C-17), 115.0 (C-13), 112.5 (C-1), 62.5 (C-15), 54.4 (C-18), 35.8 (C-23), 31.7 (C-24), 29.8 (C-25), 29.5 (C-26, C-27).

COSY (400 MHz/400 MHz, [D$_1$]-Chloroform, 298 K) δ [in ppm] = 7.90/7.38 (H-6/H-7), 7.62/7.03 (H-12/H-13), 7.38/7.90 (H-7/H-6), 7.03/7.62 (H-13/H-12), 2.53/1.53 (H-23/H-24), 1.53/2.53, 1.23 (H-24/H-23, H-25, H-26, H-27), 1.23/1.53 (H-23, H-25, H-26, H-27/H-24).

HSQC (400 MHz/101 MHz, [D_1]-Chloroform, 298 K) δ [in ppm] = 7.97/131 (H-4/C-4), 7.90 (H-6/C-6), 7.62 (H-12/C-12), 7.42/122.5 (H-17/C-17), 7.38/124.5 (H-7/C-7), 7.30/127.3 (H-8/C-8), 7.19/124.6 (H-9/C-9), 7.15/128.5 (H-20, H-21/C-20, C-21), 7.03/115.0 (H-13/C-13), 5.50/54.4 (H-18/C-18), 5.45/54.4 (H-18‘/C-18), 5.28/62.5 (H-15/C-15), 2.53/35.8 (H-23/C-23), 1.53/31.7 (H-24/C-24), 1.24/29.8, 29.5 (H-25, H-26, H-27/C-25, C-26, C-27).

HMBC (400 MHz/101 MHz, [D_1]-Chloroform, 298 K) δ [in ppm] = 7.97/150.1, 133.1, 130.5, 128.4 (H-4/C-2, C-5, C-11, C-6), 7.90/133.1, 131.0, 127.3 (H-6/C-5, C-4, C-8), 7.62/158.0 (H-12/C-14), 7.42/144.7 (H-17/C-16), 7.38/129.6 (H-7/C-10), 7.30/133.1, 128.4 (H-8/C-5, C-6), 7.19/129.6, 124.5, 112.5 (H-9/C-10, C-7, C-1), 7.15/144.1, 131.4, 129.4, 128.5, 35.8 (H-20,H-21/C-22, C-19, C-21, C-20, C-23), 7.03/158.0, 130.5 (H-13/C-14, C-11), 5.50, 5.45/131.4, 128.5 (H-18/C-19, C-20), 5.28/158.0, 144.7, 122.5 (H-15/C-14, C-16, C-17), 2.53/144.1, 129.4, 31.7, 29.8 (H-23/C-22, C-21, C-24, C-25), 1.24/29.4 (H-25, H-26, H-27/C-25, C-26, C-27).

[DEJ354-4]

7.3.3.13 Synthesis of phosphoric acid macrocycle (S)-19

Described experiment: DEJ357 Repeated: DEJ367

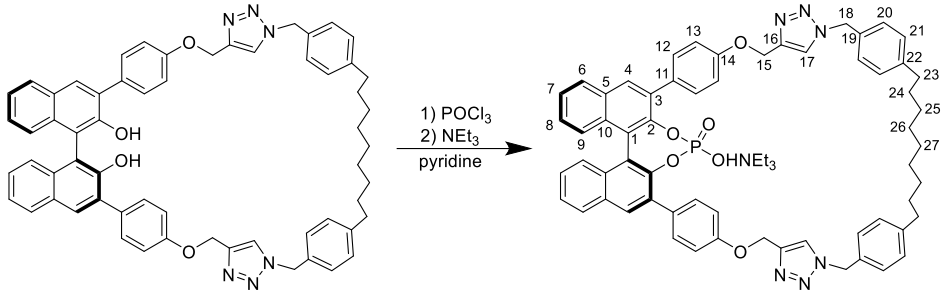

(*S*)-**18** (*S*)-**19**

Diol (*S*)-**18** (3.00 mg, 3.23 µmol, 1 eq.) was weighed into a Schlenk-tube and dried under high vacuum for three hours. Dry pyridine (2 ml) and phosphoryl chloride (9.00 µl, 0.0960 mmol, 30 eq.) were added under argon. The mixture was stirred at 60 °C for 20 hours. After cooling to room temperature, water (2 ml) was added dropwise, followed by 3 hours of stirring at 60 °C. After cooling to room temperature the solution was diluted with dichloromethane (10 ml) and washed with hydrochloric acid (2M, 3 x 10 ml). The organic solvent was removed and the residue was purified by column chromatography (0.5 x 5 cm, ethyl acetate : methanol : triethylamine = 78 : 21 : 1) to give the product (2.00 mg, 2.00 µmol, 61.9%) as a white solid.

$C_{61}H_{55}N_6O_6P$ 999.12 g/mol

^{1}H-NMR (400 MHz, [D$_2$]-Methylene chloride, 298 K) δ [in ppm] = 7.98 (s, 2H, H-4), 7.94 (d, ^3J = 8.1 Hz, 2H, H-6), 7.83 (psd, ^3J = 8.8 Hz, 4H, H-12), 7.60 (s, 2H, H-17), 7.42 (ddd, ^3J = 8.1 Hz, ^3J = 6.4 Hz, ^4J = 1.6 Hz, 2H, H-7), 7.29 – 7.22 (m, 8H, H-8, H-9, H-20), 7.18 (psd, ^3J = 8.2 Hz, 4H, H-21), 7.06 (psd, ^3J = 8.8 Hz, 4H, H-13), 5.49 (s, 2H, H-18), 5.21 (s, 1H, H-15), 2.62 – 2.50 (m, 10H, H-23, HN^+-CH_2CH$_3$), 1.63 – 1.47 (m, 4H, H-24), 1.38 – 1.19 (m, 10H, H-25, H-26, H-27), 0.88 (t, ^3J = 7.3 Hz, 9H, HN^+-CH$_2$CH_3).

^{31}P-NMR (162 MHz, [D$_2$]-Methylene chloride, 298 K) δ [in ppm] = 3.28 (s).

^{13}C-NMR (101 MHz, [D$_2$]-Methylene chloride, 298 K) δ [in ppm] = 158.4 (C-14), 147.7 (C-2), 144.9 (C-16), 144.5 (C-22), 134.5 (C-3), 132.6 (C-5), 132.0 (C-12), 131.5 (C-10), 130.6 (C-4), 129.6 (C-21), 129.0 (C-20), 128.7 (C-6), 127.3 (C-9), 126.3 (C-8), 125.5 (C-7), 123.9 (C-1), 123.3 (C-17), 114.7 (C-13), 62.6 (C-15), 54.4 (C-18), 36.1 (C-23), 32.2 (C-24), 30.1 (C-25), 30.0 (C-26), 29.8 (C-27).

COSY (400 MHz/400 MHz, [D$_2$]-Methylene chloride, 298 K) δ [in ppm] = 7.94/7.42 (H-6/H-7), 7.83/7.06 (H-12/H-13), 7.42/7.94 (H-7/H-6), 7.06/7.83 (H-13/H-12), 2.53/1.54, 0.88 (H-23, HN^+-CH_2CH$_3$/H-24, HN^+-CH_2CH$_3$), 1.54/2.53, 0.88 (H-24/H-23, HN^+-CH_2CH$_3$).

HSQC (400 MHz/101 MHz, [D$_2$]-Methylene chloride, 298 K) δ [in ppm] = 7.98/130.6 (H-4/C-4), 7.94/128.7 (C-6/H-6), 7.83/132.0 (H-12/C-12), 7.60/123.3 (H-17/C-17), 7.42/125.5 (H-7/C-7), 7.24/126.3 (H-8/C-8), 7.24/127.3 (H-9/C-9), 7.24/129.0 (H-20/C-20), 7.18/129.6 (H-21/C-21), 7.06/114.7 (H-13/C-13), 5.49/54.5 (H-18/C-18), 5.21/62.6 (H-15/C-15), 2.56/36.1 (H-23/C-23), 1.55/32.2 (H-24/C-24), 1.28/30.1, 29.9, 29.8 (H-25, H-26, H-27/C-25, C-26, C-27).

HMBC (400 MHz/101 MHz, [D_2]-Methylene chloride, 298 K) δ [in ppm] = 7.98/147.7, 132.6, 128.7 (H-4, C-2, C-5, C-6), 7.94/132.6, 130.6, 126.3 (H-6/C-5, C-4, C-8), 7.83/158.3, 134.6 (H-12/C-14, C-11), 7.60/144.9 (H-17/C-16), 7.42/131.5, 127.3 (H-7, C-10, C-9), 7.24/132.6, 131.5, 125.5, (H-8, H-9/C-5, C-10, C-7), 7.24/144.5, 132.7, 129.6, 54.4 (H-20/C-22, C-19, C-21, C-18), 7.18/132.7, 129.0, 36.1 (H-21/C-19, C-20, C-23), 7.06/158.4, 132.0 (H-13/C-14, C-12), 5.49/132.7, 129.0 (H-18/C-19, C-20), 5.21/158.4, 144.9, 123.3 (H-15/C-14, C-16, C-17), 2.56/144.5, 129.6, 32.3, 30.1 (H-23/C-22, C-21, C-24, C-25).

[DEJ367-NET3]

HR-MS [ESI-pos, methanol/water]: m/z = 999.4005 $[M+H]^+$, calculated 999.3993 for $[C_{61}H_{56}N_6O_6P]^+$.

7.3.3.14 Synthesis of catenane (*S*)-12 and (*S*)-15

Described experiment: DJS52

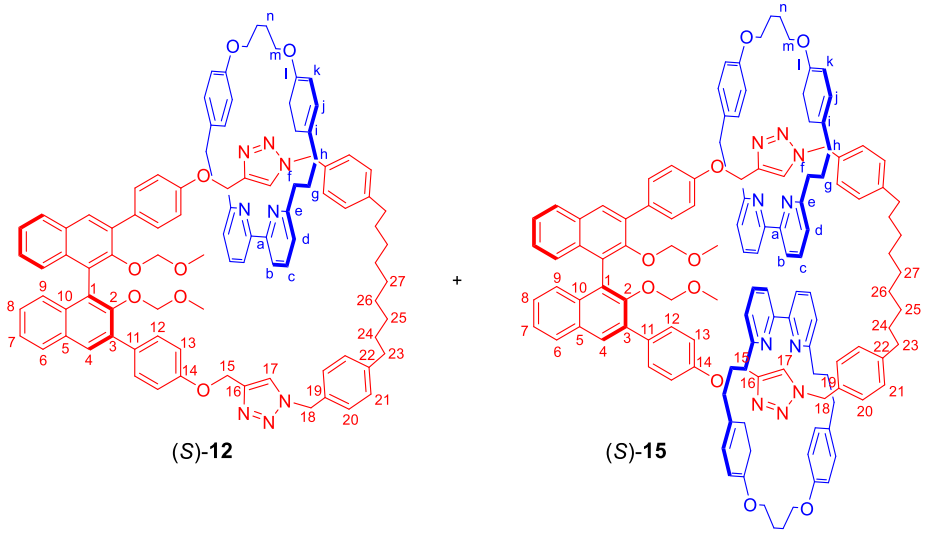

Macrocycle **11** (66.0 mg, 0.139 mmol, 1 eq.) and tetrakis(acetonitrile)copper(I) hexafluorophosphate (49.0 mg, 0.133 mmol, 0.96 eq.) were weighed into a round bottom flash with septum. After purging with nitrogen for five minutes, a degassed 1:1 mixture of chloroform/ethanol (28 ml) and *N*,*N*-diisopropylethylamine (0.047 ml, 0.278 mmol, 2 eq.) were added. The solution was stirred at 60 °C for 30 minutes. To this, a solution of alkyne (*S*)-**9** (86.0 mg, 0.139 mmol, 1 eq.) and azide (54.0 mg, 0.139 mmol, 1 eq.) in a degassed 1:1 mixture of chloroform/ethanol (6 ml) was added over four hours at 60 °C. After cooling to room temperature the solvent was removed. The residue was dissolved in dichloromethane (30 ml), washed with EDTA-NH_3 solution (2 x 30 ml) and saturated aqueous sodium chloride solution (30 ml) and dried over anhydrous magnesium sulfate. After filtration and removal of the solvent, the crude mixture was obtained as a light orange solid. The crude mixture was purified by column chromatography on silica gel (2.5 x 20 cm, cyclohexane : ethyl acetate : triethylamine = 69 : 29 : 2) to give [2]catenane (*S*)-(*S*)-**12** as a white solid (50.0 mg, 0.0330 mmol, 24%) and [3]catenane (*S*)-**15** as a white solid (14.0 mg, 0.00700 mmol, 5%)

[2]catenane: $C_{97}H_{98}N_8O_8$ 1502.75 g/mol

^{1}H-NMR (400 MHz, [D$_1$]-Chloroform, 298 K) δ [in ppm] = 8.04 (s, 2H, H-17), 7.88 – 7.83 (m, 4H, H-4, H-6), 7.61 (t, ^3J = 7.7 Hz, 2H, H-c), 7.55 (psd, ^3J = 8.7 Hz, 4H, H-12), 7.43 (d, ^3J = 7.8, 2H, H-b), 7.40 (ddd, ^3J = 8.1, ^3J = 5.9, ^4J = 2.0 Hz, 2H, H-7), 7.29 – 7.23 (m, 2H, H-8), 7.18 (d, ^3J = 6.9 Hz, 2H, H-9), 7.05 (d, ^3J = 7.8 Hz, 2H, H-d), 7.01 (d, ^3J = 8.0 Hz, 4H, H-20), 6.96 (d, ^3J = 8.0 Hz, 4H, H-21), 6.87 (d, ^3J = 8.7 Hz, 4H, H-13), 6.64 (d, ^3J = 8.6 Hz, 4H, H-j), 6.58 (d, ^3J = 8.6 Hz, 4H, H-k), 5.17 (s, 2H, H-18), 4.95 (s, 2H, H-15), 4.31 (d, ^2J = 5.8 Hz, 2H, MOM-OCH_2), 4.24 (d, ^2J = 5.8 Hz, 2H, MOM-OCH_2), 4.15 (t, ^3J = 6.5 Hz , 4H, H-m), 2.46 (t, ^3J = 6.8 Hz, 4H, H-f), 2.45 – 2.37 (m, 8H, H-23, H-h), 2.26 (s, 6H, MOM-OCH_3), 1.98 (t, ^3J = 6.5 Hz , 4H, H-n), 1.62 – 1.55 (m, 4H, H-g), 1.37 – 1.31 (m, 4H, H-24), 1.13 – 1.04 (m, 10H, H-25, H-26, H-27).

^{13}C-NMR (101 MHz, [D$_1$]-Chloroform, 298 K) δ [in ppm] =162.7 (C-e), 158.0 (C-14), 157.9 (C-a), 157.3 (C-i), 144.3 (C-16), 143.6 (C-22), 136.7 (C-c), 133.7 (C-l), 133.5 (C-5), 131.7 (C-19), 131.0 (C-10), 130.6 (C-12), 130.5 (C-11), 130.1 (C-4) 129.3 (C-j), 129.2 (C-9), 129.0 (C-21), 128.7 (C-20), 128.0 (C-6), 126.6 (C-8), 125.2 (C-7), 123.8 (C-17), 121.4 (C-d), 120.1 (C-b), 115.3 (C-k), 114.9 (C-13), 98.6 (MOM-CH2), 67.1 (C-m), 62.1 (C-15), 56.0 (C-MOM-CH3), 53.8 (C-18), 37.0 (C-23), 35.8 (C-h), 35.0 (C-f), 32.3 (C-g), 31.8 (C-24), 29.9 (C-25), 29.6 (C-26), 29.5 (C-27), 25.1 (C-n).

COSY (400 MHz/400 MHz, [D$_1$]-Chloroform, 298 K) δ [in ppm] = 8.04/4.95 (H-17/H-15), 7.85/7.40, 7.26 (H-4, H-6/H-7, H-8), 7.61/7.43, 7.05 (H-c/H-b, H-d), 7.55/6.87 (H-12/H-13), 7.43/7.61, 7.05 (H-b/H-c, H-d), 7.40/7-85, 7.26 (H-7/H-6, H-8), 7.26/7.85, 7.40 (H-8/H-6, H-7), 7.05/7.61, 7.43 (H-d/H-c, H-b), 6.87/7.55 (H-13/H-12), 6.64/6.58 (H-j/H-k), 6.58/6.64 (H-k/H-j), 4.95/8.04 (H-15/H-17), 4.31/4.24 (MOM-OCH$_2$/MOM-OCH$_2$'), 4.24/4.31 (MOM-OCH$_2$'/MOM-OCH$_2$), 4.15/1.98 (H-m/H-n), 2.46/1.60 (H-f/H-g), 1.98/4.14 (H-n/H-m), 1.60/2.46 (H-g/H-f).

HSQC (400 MHz/101 MHz, [D$_1$]-Chloroform, 298 K) δ [in ppm] = 8.04/123.8 (H-17/C-17), 7.86/130.1 (H-4/C-4), 7.86/128.0 (H-6/C-6), 7.61/136.7 (H-c/C-c), 7.55/130.6 (H-12/C-12), 7.43/120.1 (H-b/C-b), 7.40/125.2 (H-7/C-7), 7.26/126.6 (H-8/C-8), 7.18/129.2 (H-9/C-9), 7.05/121.4 (H-d/C-d), 7.01/128.7 (H-20/C-20), 6.96/129.0 (H-21/C-21), 6.87/114.9 (H-13/C-13), 6.64/129.3 (H-j/C-j), 6.58/115.3 (H-k/C-k), 5.17/53.8 (H-18/C-18), 4.95/62.1 (H-15/C-15), 4.15/67.1 (H-m/C-m), 2.46/35.0 (H-f/C-f), 2.41/37.0 (H-23/C-23), 2.41/35.8 (H-h/C-h), 1.98/25.1 (H-n/C-n), 1.60/32.3 (H-g/C-g), 1.34/31.8 (H-24/C-24), 1.08/29.9, 29.6, 29.5 (H-25, H-26, H-27/ C-25, C-26, C-27).

HMBC (400 MHz/101 MHz, [D$_1$]-Chloroform, 298 K) δ [in ppm] = 8.04/144.3 (H-17/C-16), 7.86/151.6, 126.6, 128.0 (H-4/C-2, C-1, C-6), 7.86/130.1, 133.5, 131.5 (H-6/C-4, C-5, C-3), 7.55/158.0, 130.5 (H-12/C-14, C-11), 7.43/121.4, 157.9 (H-b/C-d, C-a), 7.26/125.2 (H-8/C-7), 7.05/120.1, 162.7 (H-d/C-b, C-e), 7.01/143.6, 128.7, 53.8 (H-20/C-22, C-20, C-18), 6.96/131.7, 129.0 (H-21/C-19, C-21), 6.64/157.3, 129.3, 35.8 (H-j/C-i, C-j, C-h), 6.58/157.3, 133.7, 115.3 (H-k/C-i, C-l, C-k), 5.17/131.7, 128.7, 123.8 (H-18/C-19, C-20, C-17), 4.95/158.0, 144.3, 123.8 (H-15/C-14, C-16, C-17), 4.15/25.1 (H-m/C-n), 2.46/162.7, 129.3 (H-f/C-e, C-j), 2.41/129.0, 31.8 (H-23/C-21, C-24) .

[DJS52-3]

HR-MS [ESI-pos, methanol/water]: m/z = 1503.8098 $[M+H]^+$, calculated 1503.7580 for $[C_{97}H_{99}N_8O_8]^+$.

Elemental analysis: calculated for $C_{97}H_{98}N_8O_8$: C, 77.27; H, 6.82; N, 7.43; found C, 76.3; H, 6.69; N, 6.63.

[3]catenane: $C_{129}H_{132}N_{10}O_{10}$ 1982.49 g/mol

^{1}H-NMR (400 MHz, [D$_2$]-Methylene chloride, 298 K) δ [in ppm] = 8.52 (s, 2H, H-17), 7.89 (d, ^3J = 8.3 Hz, 2H, H-6), 7.86 (s, 2H, H-4), 7.67 – 7.54 (m, 4H, H-c), 7.45 – 7.35 (m, 10H, H-b, H-7, H-12), 7.26 – 7.20 (m, 4H, H-8, H-9), 7.12 – 7.02 (m, 4H, H-d), 6.88 (d, ^3J = 8.1 Hz, 4H, H-20), 6.77 (d, ^3J = 8.1 Hz, 4H, H-21), 6.69 (d, ^3J = 8.8 Hz, 4H, H-13), 6.69 – 6.62 (m, 8H. H-j), 6.58 – 6.50 (m, 8H, H-k), 4.93 (s, 4H, H-18), 4.59 (s, 4H, H-15), 4.23 (d, ^2J = 5.7 Hz, 2H, MOMCH_2), 4.17 (d, ^2J = 5.7 Hz, 2H, MOM-CH_2'), 4.16

– 3.98 (m, 8H, H-m), 2.59 – 2.37 (m, 16H, H-f, H-h), 2.21 (m, 10H, MOMC*H*$_3$, H-23), 1.97 – 1.89 (m, 8H, H-n), 1.73 – 1.47 (m, 8H, H-g), 1.16 – 1.06 (m, 8H, H-24, H-28), 0.92 (m, 6H, H-26, H-27).

^{13}C-NMR (101 MHz, [D$_2$]-Methylene chloride, 298 K) δ [in ppm] = 163.2 (C-e), 158.3 (C-14), 158.3 (C-a), 157.8 (C-l), 152.1 (C-3), 144.1 (C-16), 143.8 (C-22), 137.2 (C-c), 134.1 (C-i), 133.8 (C-1), 133.8 (C-5), 132.5 (C-19), 131.5 (C-10), 131.3 (C-2), 131.3 (C-11), 130.6 (C-12), 130.4 (C-4), 129.7 (C-j), 129.1 (C-20), 129.1 (C-21), 128.4 (C-6), 126.9 (C-9), 126.8 (C-8), 125.5 (C-7), 125.3 (C-17), 121.8 (C-d), 120.4 (C-b), 115.6 (C-k), 115.1 (C-13), 100.0 (MOMCH2), 67.5 (C-m), 62.2 (C-15), 56.2 (MOM*C*H3), 53.9 (C-18), 37.4 (C-f), 36.0 (C-23), 35.3 (C-h), 32.7 (C-g), 32.2 (C-24), 30.1 (C-26), 30.1 (C-27), 25.6 (C-n).

COSY (400 MHz/400 MHz, [D$_2$]-Methylene chloride, 298 K) δ [in ppm] = 7.89/7.40 (H-6/H-7), 7.60/7.40, 7.07 (H-c/H-b, H-d), 7.40/7.60 (H-b/H-c), 7.40/7.89 (H-7/H-6), 7.40/6.69 (H-12/H-13), 7.23/7.40 (H-8/H-7), 7.07/7.60 (H-d/H-c), 6.88/6.77 (H-20/H-21), 6.77/6.88 (H-21/H-20), 6.69/7.40 (H-13/H-12), 6.65/6.54 (H-j/H-k), 6.54/6.65 (H-k/H-j), 4.07/1.93 (H-m/H-n), 2.49/1.60 (H-h/H-g), 2.21/1.11 (H-23/H-24), 1.93/4.07 (H-n/H-m), 1.60/2.49 (H-g/H-h), 1.11/2.21 (H-24/H-23).

HSQC (400 MHz/101 MHz, [D$_2$]-Methylene chloride, 298 K) δ [in ppm] = 8.52/125.3 (H-17(C-17), 7.89/128.4 (H-6/C-6), 7.86/130.4 (H-4/C-4), 7.60/137.2 (H-c/C-c), 7.40/125.5 (H-7/C-7), 7.40/130.6 (H-12/C-12), 7.40/120.4 (H-b/C-b), 7.23/126.9 (H-9/C-9), 7.23/126.8 (H-8/C-8), 7.07/121.8 (H-d/C-d), 6.88/129.1 (H-20/C-20), 6.77/129.1 (H-21/C-21), 6.69/115.1 (H-13/C-13), 6.65/129.7 (H-j/C-j), 6.54/115.6 (H-k/C-k), 4.93/53.9 (H-18/C-18), 4.59/62.2 (H-15/C-15), 4.23, 4.17/100.0 (MOMC*H*$_2$/MOM*C*H$_2$), 4.07/67.5 (H-m/C-m), 2.49/37.4 (H-f/C-f), 2.49/35.3 (H-h/C-h), 2.21/36.0 (H-23/C-23), 2.21/56.2 (MOMC*H*$_3$/MOM*C*H$_3$), 1.93/25.6 (H-n/C-n), 1.60/32.7 (H-g/C-g), 1.11/32.2 (H-24/C-24), 1.11 (H-25/C-25), 0.92/30.1 (H-26, H-27/C-26, C-27).

HMBC (400 MHz/101 MHz, [D$_2$]-Methylene chloride, 298 K) δ [in ppm] = 8.52/144.1 (H-17/C-16), 7.89/130.4, 126.8 (H-6/C-4, C-8), 7.86/152.1, 133.8, 131.3, 128.4 (H-4/C-3, C-1, C-2, C-6), 7.60/163.2, 158.3 (H-c/C-e, C-a), 7.40/126.8 (H-7/C-8), 7.40/158.3 (H-12/C-14), 7.40/121.8 (H-b/C-d), 7.23/128.4, 125.5 (H-8/C-6, C-7), 7.23/133.8, 131.5 (H-9/C-1, C-10), 7.07/163.2, 120.4, 37.4 (H-d/C-e, C-b, C-f), 6.88/143.8, 129.1, 53.9 (H-20/C-22, C-21, C-18), 6.77/132.5, 129.1, 53.9 (H-21/C-19, C-20, C-18), 6.69/158.3, 131.3 (H-13/C-14, C-11), 6.65/157.8, 35.3 (H-j/C-l, C-h), 6.54/157.8, 134.1 (H-k/C-l, C-i), 4.93/132.5, 129.1, 125.3 (H-18/C-19, C-20, C-17), 4.59/158.3, 144.1, 125.3 (H-15/C-14, C-16, C-17), 4.23/56.2 (MOMC*H*$_2$/MOM*C*H$_3$), 4.07/25.6 (H-m/C-n), 2.49/32.7 (H-f/C-g), 2.49/134.1, 129.7, 37.4 (H-h/C-i, C-j, C-f), 2.21/144.1, 129.1, 32.3 (H-23/C-16, C-21, C-24), 2.21/100.0 (MOMC*H*$_3$/MOM*C*H$_2$), 1.93/67.5 (H-n/C-m), 1.60/134.1 (H-g/C-i).

[DEJ-3catenane]

HR-MS [ESI-pos, methanol/water]: m/z = 992.0208 $[M+2H]^{2+}$, calculated 992.0153 for $[C_{129}H_{134}N_{10}O_{10}]^{2+}$.

7.3.3.15 Synthesis of catenane (*S*)-13

Described experiment: DEJ310

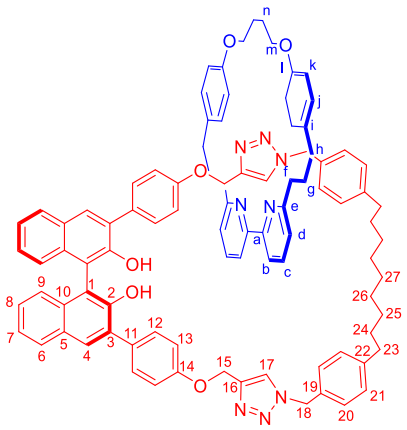

(*S*)-**13**

MOM-protected [2]catenane (*S*)-**12** (47.0 mg, 0.0310 mmol, 1 eq.) was dissolved in a 1:1 mixture of tetrahydrofuran/methanol (10 ml) and concentrated hydrochloric acid (1 ml) was added. The solution was stirred at 80 °C for one hour. After cooling to room temperature, volatiles were removed to yield the product as an off white solid (40.0 mg, 0.0280 mmol, 90.3%).

$C_{93}H_{90}N_8O_6$ 1415.76 g/mol

^{1}H-NMR (400 MHz, [D$_1$]-Chloroform, 298 K) δ [in ppm] = 7.93 – 7.87 (m, 6H, H-4, H-6, H17), 7.53 (t, ^3J = 7.7 Hz, 2H, H-c), 7.45 (d, ^3J = 8.6 Hz, 4H, H-12), 7.41 – 7.35 (m, 4H, H-b, H-7), 7.29 (ddd, ^3J = 8.0 Hz, ^3J = 6.0, ^4J = 1.9 Hz, 2H, H-8), 7.19 (d, ^3J = 8.4 Hz, 2H, H-9), 7.04 – 6.93 (m, 10H, H-20, H-21, H-d), 6.83 (d, ^3J = 8.8 Hz, 4H, H-13), 6.60 (d, ^3J = 8.7 Hz, 4H, H-j), 6.55 (d, ^3J = 8.7 Hz, 4H, H-k), 5.36 (s, 2H, OH), 5.19 (s, 4H, H-18), 4.91 (s, 4H, H-15), 4.11 (t, ^3J = 6.5 Hz, 4H, H-m), 2.45 – 2.33 (m, 12H. H-f, H-h, H-23), 1.95 (t, ^3J = 6.5 Hz, 4H, H-n), 1.61 – 1.51 (m, 4H, H-g), 1.35 – 1.29 (m, 4H, H-24), 1.14 – 0.94 (m, 10H, H-25, H-26, H-27).

^{13}C-NMR (101 MHz, [D$_1$]-Chloroform, 298 K) δ [in ppm] = 162.6 (C-e), 158.1 (C-14), 158.0 (C-a), 157.4 (C-l), 150.1 (C-3), 144.3 (C-16), 143.6 (C-22), 136.6 (C-c), 133.7 (C-i), 133.1 (C-5), 131.6 (C-19), 130.7 (C-4), 130.6 (C-12), 130.3 (C-2), 130.0 (C-10), 129.7 (C-11), 129.2 (C-j), 129.0 (C-21), 128.6 (C-20), 128.4 (C-6), 127.0 (C-8), 124.7 (C-9), 124.3 (C-7), 123.6 (C-17), 121.1 (C-d), 120.0 (C-b), 115.2 (C-k), 115.0 (C-13), 112.8 (C-1), 67.1 (C-m), 62.1 (C-15), 53.8 (C-18), 37.0 (C-23), 35.7 (C-h), 34.8 (C-f), 32.3 (C-g), 31.6 (C-24), 29.7 (C-25), 29.5 (C-26), 29.4 (C-27), 25.1 (C-n).

COSY (400 MHz/400 MHz, [D$_1$]-Chloroform, 298 K) δ [in ppm] = 7.89/7.38 (H-6/H-7), 7.53/7.38, 6.98 (H-c/H-a/H-d), 7.45/6.83 (H-12/H-13), 6.98/7.53 (H-d/H-c), 6.83/7.45 (H-13/H-12), 4.11/1.95 (H-m/H-n), 2.38/1.56 (H-f,H-h/H-g), 1.95/4.11 (H-n/H-m), 1.56/2.38 (H-g/H-f, H-h), 1.33/2.38,1.05 (H-24/H-23, C-25), 1.05/1.33 (C-25/C-24).

HSQC (400 MHz/101 MHz, [D$_1$]-Chloroform, 298 K) δ [in ppm] = 7.89/130.7 (H-4/C-4), 7.89/128.4 (H-6/C-6), 7.89/123.6 (H-17/C-17), 7.53/136.6 (H-c/C-c), 7.45/130.6 (H-12/C-12), 7.38/124.3 (H-7/C-7),

7.38/120.0 (H-b/C-b), 7.29/127 (H-8/C-8), 7.19/124.7 (H-9/C-9), 6.98/128.6 (H-20/C-20), 6.98/129.0 (H-21/C-21), 6.98/121.1 (H-d/C-d), 6.83/115 (H-13/C-13), 6.60/129.2 (H-j/C-j), 6.55/115.2 (H-k/C-k), 5.19/53.8 (H-18/C-18), 4.91/62.1 (H-15/C-15), 4.11/67.1 (H-m/C-m), 2.39/37.0 (H-23/C-23), 2.39/34.8 (H-f/C-f), 2.39/35.7 (H-h/C-h), 1.95/25.1 (H-n/C-n), 1.56/32.3 (H-g/C-g), 1.32/31.6 (H-24/C-24), 1.04/29.7 (H-25/C-25), 1.04/29.5 (H-26/C-26), 1.04/29.4 (H-27/C-27).

HMBC (400 MHz/101 MHz, [D_1]-Chloroform, 298 K) δ [in ppm] = 7.89/150.0, 133.1, 129.7, 128.4 (H-4/C-3, C-5, C-11, C-6), 7.98/130.7, 127.0 (H-6/C-4, C-8), 7.89/144.3 (H-17/C-16), 7.53/162.6, 158.0 (H-c/C-e, C-a), 7.45/158.1 (H-12/C-14), 7.38/124.7 (H-7/C-9), 7.38/121.1 (H-b/C-d), 7.29/133.1, 128.4 (H-8/C-5, C-6), 7.19/130.0, 124.3, 112.8 (H-9/C-10, C-7, C-1), 6.98/131.6, 129.0, 53.8 (H-20/C-19, C-21, C-18), 6.98/120.0, 35.7 (H-d/C-b, C-h), 6.60/157.4, 129.2, 115.2, 34.8 (H-j/C-l, C-j, C-k, C-f), 5.19/131.6, 128.6, 123.6 (H-18/C-19, C-20, C-17), 4.91/158.1, 144.3, 123.6 (H-15/C-14, C-16, C-17), 4.11/25.1 (H-m/C-n), 2.39/143.6, 129.0, 31.6 (H-23/C-22, C-21, C-24), 1.95/67.1 (H-n/C-m).

[DEJ310-1b]

HR-MS [ESI-pos, methanol/water]: m/z = 1416.7073 $[M+H]^+$, calculated 1416.7088 for $[C_{93}H_{91}N_8O_6]^+$.

Elemental analysis: calculated for $C_{93}H_{90}N_8O_6$: C, 78.67; H, 6.67; N, 7.89; found C, 77.9; H, 7.16; N, 6.50.

7.3.2.16 Synthesis of catenane (*S*)-14-HNEt$_3$

Described experiment: DEJ365 Repeated: DEJ258

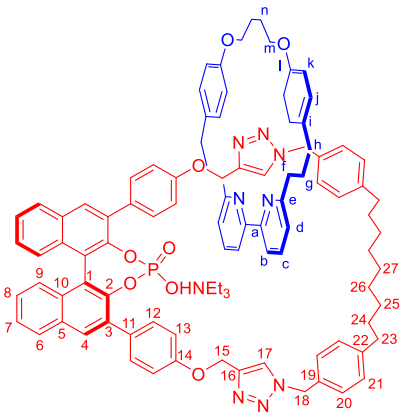

(*S*)-**14-HNEt$_3$**

Diol [2]catenane (*S*)-**13** (32.0 mg, 0.0230 mmol, 1 eq.) was weighed into a Schlenk-tube and dried under high vacuum for three hours. Dry pyridine (2 ml) and phosphoryl chloride (0.041 ml, 0.452 mmol, 20 eq.) were added under argon. The mixture was stirred at 60 °C for 20 hours. After cooling to room temperature, water (2 ml) was added dropwise, followed by 3 hours of stirring at 60 °C. After cooling to room temperature the solution was diluted with dichloromethane (15 ml) and washed with hydrochloric acid (2M, 3 x 10 ml). The organic solvent was removed and the residue was purified by column chromatography (0.5 x 5 cm, ethyl acetate : methanol : triethylamine = 79 : 19 : 2) to give the product (*S*)-**14-HNEt$_3$** as an off white foam (28.0 mg, 0.0190 mmol, 82.6%).

$C_{93}H_{89}N_8O_8P$ 1477.73 g/mol

^{1}H-NMR (400 MHz, [D$_6$]-Acetone, 298 K) δ [in ppm] = 8.16 (s, 1H, H-17), 8.01 (m, 4H, H-4, H-6), 7.86 (d, ^3J = 8.7 Hz, 4H, H-12), 7.64 (t , ^3J = 7.7 Hz, 2H, H-c), 7.51 (d, ^3J = 7.5 Hz, 2H, H-b), 7.43 (ddd, ^3J = 8.0 Hz, ^3J = 6.0, ^4J = 1.9 Hz, 2H, H-7), 7.26 (d, ^3J = 8.1 Hz, 4H, H-20), 7.25 – 7.18 (m, 4H. H-8, H-9), 7.12 (d, ^3J = 7.5 Hz, 2H, H-d), 7.04 (d, ^3J = 8.5 Hz, 4H, H-21), 6.98 (d, ^3J = 8.7 Hz, 4H, H-13), 6.74 (d, ^3J = 8.5 Hz, 4H, H-j), 6.55 (d, ^3J = 8.5 Hz, 4H, H-k), 5.46 (s, 4H, H-18), 5.01 (s, 4H, H-15), 3.99 (t, ^3J = 6.5 Hz, 4H, H-m), 2.65 – 2.56 (m, 4H, H-h), 2.52 – 2.40 (m, 8H, H-f, H-24), 2.31 – 2.23 (m, 4H, H-23), 1.81 (t, ^3J = 6.5 Hz, 4H, H-n), 1.72 – 1.61 (m, 4H, H-g), 0.91 – 0.71 (m, 10H, H-25, H-26, H-27).

^{13}C-NMR (400 MHz, [D$_6$]-Acetone, 298 K) δ [in ppm] = 162.6 (C-e), 158.0 (C-14), 158.0 (C-a), 157.3 (C-l), 147.7 (C-3), 143.8 (C-16), 143.4 (C-22), 136.8 (C-c), 134.0 (C-i), 133.0 (C-19), 132.2 (C-5), 131.3 (C-12), 131.0 (C-10), 130.9 (C-11), 130.3 (C-2), 129.7 (C-4), 129.2 (C-21), 129.2 (C-j), 128.5 (C-20), 128.3 (C-6), 125.7(C-8), 125.7 (C-9), 124.7 (C-7), 123.9 (C-17), 121.3 (C-d), 119.7 (C-b), 116.4 (C-1), 115.1 (C-k), 114.2 (C-13), 67.0 (C-m), 61.4 (C-15), 53.1 (C-18), 45.3 (C-24), 37.0 (C-h), 35.2 (C-23), 34.2 (C-f), 32.9 (C-g), 24.9 (C-n).

COSY (400 MHz/400 MHz, [D$_6$]-Acetone, 298 K) δ [in ppm] = 8.01/7.43 (H-6/H-7), 7.86/6.98 (H-12/H-13), 7.64/7.51 (H-c/H-b), 7.51/7.64 (H-b/H-c), 7.43/8.01 (H-7/H-8), 7.26/7.04 (H-20/H-21), 7.04/7.26

(H-21/H-20), 6.98/7.86 (H-13/H-12), 6.74/6.55 (H-j/H-k), 6.55/6.74 (H-k/H-j), 3.99/1.81 (H-m/H-n), 2.59/1.67 (H-h/H-g), 2.49/1.67 (H-f/H-g), 1.81/3.99 (H-n/H-m), 1.67/2.59, 2.49 (H-g/H-h, H-f).

HSQC (400 MHz, [D_6]-Acetone, 298 K) δ [in ppm] = 8.16/123.9 (H-17/C-17), 8.01/129.7 (H-4/C-4), 8.01/128.3 (H-6/C-6), 7.86/131.3 (H-12/C-12), 7.64/136.8 (H-c/C-c), 7.51/119.7 (H-b/C-b), 7.43/124.7 (H-7/C-7), 7.26/128.5 (H-20/C-20), 7.21/125.7 (H-8,H-9/C-8, C-9), 7.12/121.3 (H-d/C-d), 7.04/129.2 (H-21,C-21), 6.98/114.2 (H-13/C-13), 6.74/129.2 (H-j/C-j), 6.55/115.1 (H-k/C-k), 5.46/53.1 (H-18/C-18), 5.01/61.4 (H-15/C-15), 3.99/67.0 (H-m/C-m), 2.59/37.0 (H-h/C-h), 2.49/34.2 (H-f/C-f), 2.26/35.2 (H-23/C-23), 1.81/24.9 (H-n/C-n), 1.66/32.9 (H-g/C-g).

HMBC (400 MHz, [D_6]-Acetone, 298 K) δ [in ppm] = 8.16/143.7 (H-17/C-16), 8.01/147.7, 132.2, 128.3 (H-4/C-3, C-5, C-6), 8.01/125.7, 124.7 (H-6/C-9, C-7), 7.86/158.0, 114.2 (H-12/C-14, C-13), 7.64/162.2, 158 (H-c/C-e, C-a), 7.51/121.3 (H-b/C-d), 7.26/143.4, 53.1 (H-20/C-22, C-18), 7.21/119.7 (H-d/C-b), 7.04/133.0, 128.5, 35.2 (H-21/C-19, C-20, C-23), 6.98/158.0, 130.9 (H-13/C-14, C-11), 6.74/157.3, 115.1, 34.2 (H-j/C-l, C-k, C-f), 6.55/157.3, 134.0 (H-k/C-l, C-i), 5.46/133.0, 128.5, 123.9 (H-18/C-19, C-20, C-17), 5.01/158.0, 143.8, 123.9 (H-15/C-14, C-16, C-17), 3.99/67.0 (H-m/C-n), 2.59/162.2, 32.9 (H-h/C-e, C-g), 2.49/134.0, 129.2, 37.0 (H-f/C-i, C-j, C-h), 2.26/143.4 (H-23/C-22), 1.81/67.0 (H-n/C-m).

[DEJ258-Aceton]

HR-MS [ESI-pos, methanol/water]: m/z = 1478.6631 $[M+H]^+$, calculated 1478.6646 for $[C_{93}H_{90}N_8O_8P]^+$.

7.3.2.17 Synthesis of Diol [3]catenane (*S*)-16

Describe experiment: DEJ295 Repeated: DEJ311

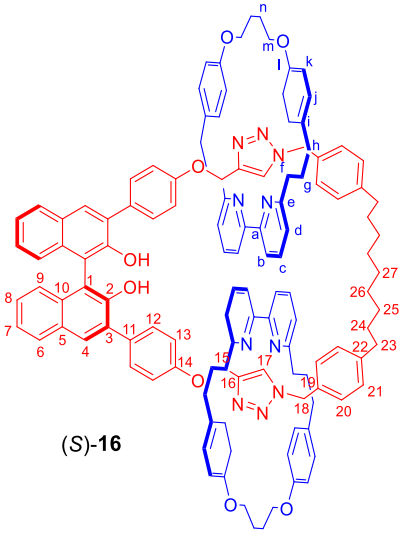

(*S*)-**16**

MOM-protected [3]catenane (*S*)-**15** (47.0 mg, 0.0240 mmol, 1 eq.) was dissolved in a 1:1 mixture of tetrahydrofuran/methanol (10 ml) and concentrated hydrochloric acid (1 ml) was added. The solution was stirred at 80 °C for one hour. After cooling to room temperature, volatiles were removed to yield the product (*S*)-**16** as a white solid (44.0 mg, 0.0230 mmol, 95.8%).

$C_{125}H_{124}N_{10}O_8$ 1892.39 g/mol

^{1}H-NMR (400 MHz, [D$_2$]-Methylene chloride, 298 K) δ [in ppm] = 8.63 (s, 2H, H-17), 7.92 – 7.81 (m, 4H, H-6, H-4), 7.54 – 7.47 (m, 4H, H-c), 7.41 – 7.11 (m, 16H, H-b, H-7, H-8, H-9, H-12), 7.04 – 6.93 (m, 4H, H-d), 6.84 – 6.74 (m, 4H, H-20), 6.76 – 6.50 (m, 24H, H-21, H-13, H-j, H-k), 4.80 (s, 4H, H-18), 4.61 (s, 4H, H-15), 4.28 – 3.95 (m, 8H, H-m), 2.60 – 2.11 (m, 20H, H-f, H-f, H-23), 2.07 – 1.82 (m, 8H, H-n), 1.65 – 1.50 (m, 8H, H-g), 1.21 – 1.04 (m, 4H, H-24), 1.05 – 0.83 (m, 10H, H-25, H-26, H-27).

^{13}C-NMR (101 MHz, [D$_2$]-Methylene chloride, 298 K) δ [in ppm] = 162.6 (C-e), 158.0 (C-a), 157.8 (C-14), 157.3 (C-l), 150.0 (C-3), 143.6 (C-16), 143.0 (C-22), 136.6 (C-c), 133.2 (C-5), 131.0 (C-19), 130.4 (C-6), 130.2 (C-12), 129.5 (C-10), 129.4 (C-i), 129.2 (C-j), 129.1 (C-11), 128.9 (C-2), 128.9 (C-20), 128.5 (C-21), 128.3 (C-4), 126.9 (C-8), 125.1 (C-17), 124.8 (C-9), 124.2 (C-7), 121.3 (C-d), 120.0 (C-b), 115.2 (C-k), 115.0 (C-13), 113.1 (C-1), 67.0 (C-m), 61.6 (C-15), 53.2 (C-18), 36.9 (C-h), 35.6 (C-23), 34.9 (C-f), 32.1 (C-g), 31.5 (C-24), 29.7 (C-25, C-26, C-27), 25.1 (C-n).

COSY (400 MHz/400 MHz, [D$_2$]-Methylene chloride, 298 K) δ [in ppm] = 7.87/7.37 (H-6/H-7), 7.50/7.33, 6.97 (H-c/H-b, H-d), 7.37/7.87 (H-7/H-6), 7.26/6.67 (H-12/H-13), 6.97/7.50 (H-d/H-c), 6.67/7.26 (H-13/H-12), 4.15/1.98 (H-m/H-n), 2.33/1.58 (H-h/H-g), 2.23/1.17 (H-23/H-24), 1.98/4.15 (H-n/H-m), 1.58/2.33 (H-g/H-h), 1.17/2.23, 0.95 (H-24/H-23, H-25), 0.95/1.17 (H-25/H-24).

HSQC (400 MHz/101 MHz, [D$_2$]-Methylene chloride, 298 K) δ [in ppm] = 8.63/125.1 (H-17/C-17), 7.90/128.3 (H-4/C-4), 7.87/130.4 (H-6/C-6), 7.50/136.6 (H-c/C-c), 7.37/124.2 (H-7/C-7), 7.33/120.0 (H-

b/C-b), 7.29/126.9 (H-8/C-8), 7.26/130.2 (H-12/C-12), 7.19/124.8 (H-9/C-9), 6.97/121.3 (H-d/C-d), 6.80/128.9 (H-20/C-20), 6.72/128.5 (H-21/C-21), 6.67/115.0 (H-13/C-13), 6.58/129.2 (H-j/C-j), 6.56/115.2 (H-k/C-k), 4.80/53.2 (H-18/C-18), 4.61/61.6 (H-15/C-15), 4.15/67.0 (H-m/C-m), 2.42/34.9 (H-f/C-f), 2.33/36.9 (H-h/C-h), 2.23/35.6 (H-23/C-23), 1.98/25.1 (H-n/C-n), 1.58/32.1 (H-g/C-g), 1.17/31.5 (H-24/C-24), 0.94/29.7 (H-25, H-26, H-27/C-25, C-26, C-27).

HMBC (400 MHz/101 MHz, [D_2]-Methylene chloride, 298 K) δ [in ppm] = 7.90/150, 133.2, 130.4, 128.9 (H-4/C-3, C-5, C-6, C.2), 7.87/126.9 (H-6/C-8), 7.50/162.6, 158.0 (H-c/C-e, C-a), 7.37/124.8 (H-7/C-9), 7.19/129.5, 124.2, 113.1 (H-9/C-10, C-7, C-1), 6.67/129.1 (H-13/C-11), 6.58/157.3 (H-j/C-l), 6.56/157.3, 34.9 (H-k/C-l, C-f).

[DEJ311-1b]

LR-MS [ESI-pos, methanol/water]: m/z = 948.1 $[M+2H]^{2+}$, calculated 948.0 for $[C_{125}H_{124}N_{10}O_8]^{2+}$.

Elemental analysis: calculated for $C_{125}H_{126}N_{10}O_8$: C, 79.00; H, 6.90; N, 7.37; found C, 78.30; H, 7.19; N, 6.67.

7.3.3.18 Synthesis of catenane (S)-17-HNEt$_3$

Described experiment: DEJ366

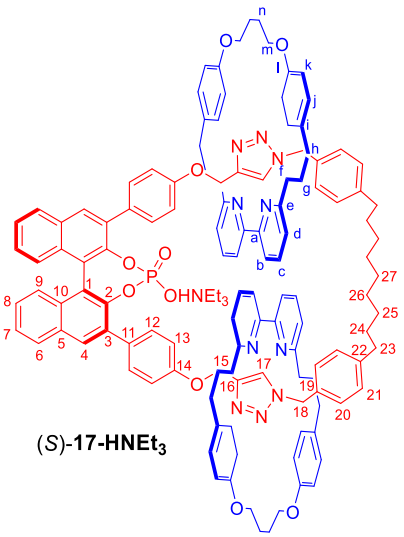

Diol [2]catenane (*S*)-**16** (44.0 mg, 0.0230 mmol, 1 eq.) was weighed into a Schlenk-tube and dried under high vacuum for three hours. Dry pyridine (2 ml) and phosphoryl chloride (0.0420 ml, 0.462 mmol, 20 eq.) were added under argon. The mixture was stirred at 60 °C for 20 hours. After cooling to room temperature, water (2 ml) was added dropwise, followed by 3 hours of stirring at 60 °C. After cooling to room temperature the solution was diluted with dichloromethane (15 ml) and washed with hydrochloric acid (2M, 3 x 10 ml). The organic solvent was removed and the residue was purified by column chromatography (0.5 x 5 cm, ethyl acetate : methanol : triethylamine = 79 : 19 : 2) to give the product as a pale brown solid (22.0 mg, 0.0110 mmol, 47.8%).

$C_{125}H_{123}N_{10}O_{10}P$ 1954.35 g/mol

^{1}H-NMR (600 MHz, [D$_6$]-Acetone, 298 K) δ [in ppm] = 8.29 (s, 2H, H-17), 8.02 (m, 4H, H-6, H-4), 7.81 (d, ^3J = 8.7 Hz, 4H, H-12), 7.74 – 7.66 (m, 4H, H-c), 7.56 – 7-50 (m, 4H, H-b), 7.43 (ddd, ^3J = 8.2, ^3J = 6.4, ^4J =1.5 Hz, 2H, H-7), 7.26 – 7.14 (m, 8H, H-8, H-9, H-d), 7.06 (d, ^3J = 7.8 Hz, 4H, H-20), 6.87 (d, ^3J = 7.7 Hz, 4H, H-21), 6.79 – 6.70 (m, 12H, H-13, H-j), 6.60 – 6.55 (m, 8H, H-k), 5.23 (d, ^2J = 14.4 Hz, 2H, H-18), 5.20 (d, ^2J = 14.4 Hz, 2H, H-18'), 4.68 (s, 4H, H-15), 4.10 – 4.00 (m, 8H, H-m), 2.65 – 2.35 (m, 16H, H-f, H-h), 2.08 – 2.04 (m, 4H, H-23), 1.91 – 1.86 (m, 8H, H-n), 1.73 – 1.63 (m, 8H, H-g), 0.91 – 0.80 (m, 4H, H-24), 0.65 – 0.49 (m, 10H, H-25, H-26, H-27).

^{31}P-NMR (162 MHz, [D$_6$]-Acetone, 298 K) δ [in ppm] = 2.80 (s).

^{13}C-NMR (400 MHz, [D$_6$]-Acetone, 298 K) δ [in ppm] = 163.3 (C-e), 159.0 (C-14), 158.8 (C-a), 158.2 (C-l), 148.8 (C-3), 144.7 (C-16), 144.4 (C-22), 137.7 (C-c), 134.8 (C-i), 133.2 (C-19), 133.1 (C-2), 132.0 (C-12), 131.8 (C-5), 131.4 (C-11), 130.4 (C-6), 130.2 (C-j), 129.5 (C-21), 129.2 (C-20), 127.3 (C-8), 126.6 (C-10), 125.6 (C-7), 125.0 (C-17), 122.4 (C-d), 122.3 (C-9), 120.7 (C-b), 120.7 (C-1), 116.0 (C-k), 115.0 (C-13), 67.8 (C-m), 62.3 (C-15), 54.0 (C-18), 37.9 (C-h), 36.0 (C-23), 35.3 (C-f), 33.4 (C-g), 32.4 (C-24), 30.3 (C-25, C-26, C-27), 25.8 (C-n).

COSY (400 MHz/400 MHz, [D$_6$]-Acetone, 298 K) δ [in ppm] = 8.02/7.43 (H-6/H-7), 7.81/6.75 (H-12/H-13), 7.70/7.53, 7.20 (H-c/H-b, H-d), 7.53/7.70 (H-b/H-c), 7.43/8.02 (H-7/H-6), 7.06/6.87 (H-20/H-21), 6.87/7.06 (H-21/H-20), 6.75/7.81 (H-13/H-12), 6.75/6.58 (H-j/H-k), 6.58/6.75 (H-k/H-j), 4.05/1.88 (H-m/H-n), 2.50/1.68 (H-h, H-f/H-g), 2.06/0.86 (H-23/H-24), 1.88/4.05 (H-n/H-m), 1.68/2.50 (H-g/H-h, H-f), 0.86/2.06, 0.57 (H-24/-H-23, H-25), 0.57/0.86 (H-25/H-24).

HSQC (400 MHz, [D$_6$]-Acetone, 298 K) δ [in ppm] = 8.29/125.0 (H-17/C-17), 8.02/129.2 (H-4/C-4), 8.02/130.4 (H-6/C-6), 7.81/132.0 (H-12/C-12), 7.70/137.7 (H-c/C-c), 7.53/120.7 (H-b/C-b), 7.43/125.6 (H-7/C-7), 7.20/127.3 (H-8/C-8), 7.20/122.3 (H-9/C-9), 7.20/122.4 (H-d/C-d), 7.06/129.2 (H-20/C-20), 6.87/ 129.5 (H-21/C-21), 6.75/115.0 (H-13/C-13), 6.75/130.2 (H-j/C-j), 6.58/116.0 (H-k/C-k), 5.23, 5.20/54.0 (H-18, H-18'/C-18), 4.68/62.3 (H-15/C-15), 4.05/67.8 (H-m/C-m), 2.50/35.3 (H-f/C-f), 2.50/37.9 (H-h/C-h), 2.06/36.0 (H-23/C-23), 1.88/25.8 (H-n/C-n), 1.68/33.4 (H-g/C-g), 0.86/32.4 (H-24/C-24), 0.57/30.3 (H-25, H-26, H-27/C-25, C-26, C-27).

HMBC (400 MHz, [D$_6$]-Acetone, 298 K) δ [in ppm] = 8.29/144.7 (H-17/C-16), 8.02/148.8, 133.1, 131.4 (H-4/C-3, C-2, C-11), 8.02/131.8, 129.2 (H-6/C-5, C-4), 7.81/159.0 (H-12/14), 7.70/163.3, 158.8 (H-c/C-e, C-a), 7.53/122.4 (H-b/C-d), 7.43/127.3 (H-7/C-8), 7.20/131.8, 125.6 (H-9/C-5, C-7), 7.20/120.7 (H-d/C-b), 7.06/144.4, 129.5 (H-20/C-22, C-21), 6.87/133.2, 36.0 (H-21/C-19, C-23), 6.75/131.4 (H-13/C-11), 6.75/158.2, 35.3 (H-j/C-l, C-f), 6.58/158.2, 134.8 (H-k/C-l, C-i), 5.23, 5.20/133.2, 129.2, 125.0 (H-18, H-18'/C-19, C-20, C-17), 4.68/144.7, 125 (H-15/C-16, C-17), 2.50/163.3, 130.2, 33.4 (H-h/C-e, C-j, C-g), 2.06/144.4, 129.5, 32.4 (H-23/C-22, C-21, C-24), 1.68/134.8, 37.9 (H-g/C-i, C-h).

[DEJ-PA3CatenaneNet3]

HR-MS [ESI-pos, methanol/water]: m/z = 978.4636 $[M+2H]^{2+}$, calculated 978.4653 for $[C_{125}H_{123}N_{10}O_{10}P]^{2+}$.

7.4 Catalytic Reactions and Kinetic Data from chapter 3

7.4.1 General procedure for catalysis for determination of enantiomeric excess

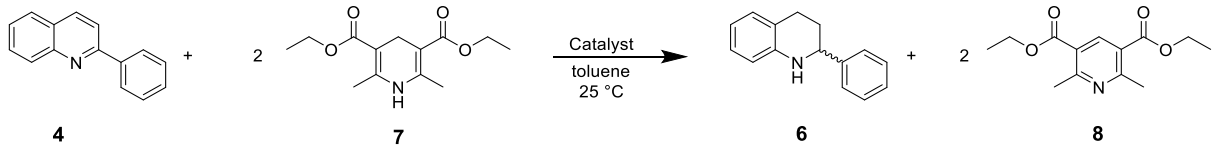

4 **7** **6** **8**

2-Phenylquinoline (4.98 µmol or 25.0 µmol, 1 eq.) and diethyl 1,4-dihydro-2,6-dimethyl-3,5-pyridinedicarboxylate (11.95 µmol or 60.0 µmol, 2.4 eq.) were taken in a Schlenk flask which was evacuated three times and back filled with argon. To that mixture, toluene (3 or 5 ml), followed by the catalyst (*S*,*S*)-**1**/(*S*)-**2**/(*S*)-**3** (stock solution in toluene, 15 mg/ml for (*S*,*S*)-**1a/b/c** and (*S*)-**2a/b/c**, 0.69 mg/ml or 1.75 mg/ml for (*S*)-**3**) were added and the reaction mixture was stirred at room temperature. The reaction was monitored by TLC with cyclohexane/ethyl acetate (10 : 1) mixtures. After full conversion the solvent was evaporated in the rotatory evaporator and the mixture was purified by silica gel flash column chromatography with cyclohexane/ethyl acetate (99 : 1) mixtures. The purified sample was used for the chiral HPLC analysis (Chiralcel OD-H column) to determine the enantiomeric excess (*ee*).

7.4.2 Enantiomeric excess experiments

Table 12: Reaction conditions for the transfer hydrogenation of 2-phenylquinoline catalysed by catenated phosphoric acids (*S*,*S*)-**1a/b/c**, macrocyclic phosphoric acids (*S*)-**2a/b/c** or acyclic phosphoric acid (*S*)-**3.**

Entry	Catalyst	Cat. loading [mol%][(a)]	Quinoline [mM]	Enantiomeric excess[(b)] [%]
0	(S,S)-**1a**	2.5	5	80.9
1	(S,S)-**1b**	2.5	5	79.3
2	(S,S)-**1c**	2.5	5	81.7
3	(S)-**2a**	2.5	5	-16.9
4	(S)-**2b**	2.5	5	-12.2
5	(S)-**2c**	2.5	5	-16.6
6	(S)-**3**	0.1	1.66	-29.5
7	(S)-**3**	0.25	1.66	-20.9
8	(S)-**3**	0.5	1.66	-10.1
9	(S)-**3**	1	1.66	12.8
10	(S)-**3**	1.5	1.66	20.4
11	(S)-**3**	2.5	1.66	36.5
12	(S)-**3**	5	1.66	54.7
13	(S)-**3**	10	1.66	61.2
14	(S)-**3**	20	1.66	67.5
15	(S)-**3**	35	1.66	70.6
16	(S)-**3**	50	1.66	71.6
17	(S)-**3**	0.5	5	-22.8
18	(S)-**3**	1.5	5	14.3
19	(S)-**3**	2.5	5	24.5
20	(S)-**3**	5	5	45.0
21	(S)-**3**	20	5	66.1
22	(S)-**3**	50	5	71.1
23[(c)]	(S)-**3**	1	1.66	9.6

(a) Catalyst loading relative to quinoline. (b) Determined by chiral HPLC (Chiralcel OD-H column). (c) 49 mol% benzoic acid added. All values are given for the excess of (*R*)-enantiomer.

Table 13: Conversion vs. time and enantiomeric excess vs. time data for the catalytic reaction using 1 mol% **3** (1.6 mM **4** in toluene)**.**

Entry	Time [h]	Conversion[(a)] [%]	Enantiomeric excess[(b)] [%]
1	0.5	15.5	9.3
2	1	23.7	8.6
3	2	41.9	8.8
4	3	50.6	9.0
5	4	57.3	9.0
6	5	64.1	8.3
7	6	69.1	8.2
8	7	73.8	8.8
9	24	94.9	8.1

(a) Determined by chiral HPLC, approximated by using identical extinction coefficients for starting materials **4** and product **6**. (b) Determined by chiral HPLC (Chiralcel OD-H column). All values are given for the excess of (*R*)-enantiomer.

Table 14: Reaction conditions for the transfer hydrogenation of 2-phenylquinoline catalysed by acyclic phosphoric acid (S)-**3** in dichloromethane**.**

Entry	Catalyst	Cat. loading [mol%][(a)]	Quinoline [mM]	Enantiomeric excess[(b)] [%]
1	(*S*)-**3**	1	1.66	-33.3
2	(*S*)-**3**	2.5	1.66	-30.3
3	(*S*)-**3**	5	1.66	-29.1
4	(*S*)-**3**	10	1.66	-23.6
5	(*S*)-**3**	20	1.66	-17.7
6	(*S*)-**3**	35	1.66	-5.3
7	(*S*)-**3**	50	1.66	-6.0

(a) Catalyst loading relative to quinoline. (b) Determined by chiral HPLC (Chiralcel OD-H column). All values are given for the excess of (*R*)-enantiomer.

7.4.3 Kinetic results

Table 15: Experimental data and results for kinetic experiments with catenated catalysts **1a**/**b**/**c**.

Experimental setup											Analysis for k_{Obs} and v_0[c]			
		Concentrations									Linear fit	Nonlinear fit		
Exp.-No.	Catalyst	[4][a] (mM)	[4][a] (M)	[7][b] (mM)	[7][b] (M)	[8][c] (mM)	[8][c] (M)	[Cat][b] (mM)	[Cat][b] (M)	[Cat][b] (mol%)	k_{Obs} ($s^{-1} M^{-1}$)	k_{Obs} ($s^{-1} M^{-1}$)	v_0 ($M\ s^{-1}$)	v_0 / [Cat] (s^{-1})
1	**1a**	1.66	1.66E-03	3.87	3.87E-03	-	-	0.161	1.61E-04	9.68	5.67E-02	6.66E-02	3.66E-07	2.27E-03
2	**1b**	1.66	1.66E-03	4.32	4.32E-03	-	-	0.196	1.96E-04	11.79	3.94E-02	4.59E-02	3.12E-07	1.59E-03
3	**1c**	1.66	1.66E-03	4.08	4.08E-03	-	-	0.158	1.58E-04	9.53	2.68E-02	3.03E-02	1.98E-07	1.25E-03

a) Determined by weight of **4** and the volume of solvent. b) Determined by the relative integrals of **4** and **7**/**8**/**Cat**. c) Determined by linear or nonlinear fitting of the respective concentration over time data (see the SI for details).

Table 16: Experimental data and results for kinetic experiments with catenated catalyst **1c**.

Experimental setup											Analysis for k_{Obs} and v_0[c]					
		Concentrations									Linear fit	Nonlinear fit			Double ln plot	
Exp.-No.	Exp.-Type	[4][a] (mM)	[4][a] (M)	[7][b] (mM)	[7][b] (M)	[8][c] (mM)	[8][c] (M)	[Cat][b] (mM)	[Cat][b] (M)	[Cat][b] (mol%)	k_{Obs} ($s^{-1} M^{-1}$)	k_{Obs} ($s^{-1} M^{-1}$)	v_0 ($M\ s^{-1}$)	v_0 / [Cat] (s^{-1})	ln [4]	ln v_0
1	Different excess for [4]	1.66	1.66E-03	3.93	3.93E-03	-	-	0.068	6.84E-05	4.12	1.84E-02	1.88E-02	8.92E-08	1.30E-03	-6.40	-16.2
2		1.26	1.26E-03	3.93	3.93E-03	-	-	0.075	7.47E-05	5.93	1.92E-02	1.98E-02	7.35E-08	9.84E-04	-6.68	-16.4
3		0.84	8.40E-04	3.93	3.93E-03	-	-	0.080	7.98E-05	9.50	2.02E-02	1.94E-02	5.09E-08	6.38E-04	-7.08	-16.8
4		0.63	6.30E-04	3.93	3.93E-03	-	-	0.075	7.51E-05	11.93	1.95E-02	2.21E-02	4.09E-08	5.45E-04	-7.37	-17.0
5	Different excess for [7]	0.83	8.30E-04	3.93	3.93E-03	-	-	0.036	3.59E-05	4.33	1.44E-02	1.50E-02	4.23E-08	1.18E-03	-5.54	-17.0
6		0.83	8.30E-04	3.32	3.32E-03	-	-	0.036	3.58E-05	4.32	1.50E-02	1.54E-02	3.79E-08	1.06E-03	-5.70	-17.1
7		0.83	8.30E-04	2.66	2.66E-03	-	-	0.036	3.62E-05	4.37	1.59E-02	1.62E-02	3.21E-08	8.87E-04	-5.94	-17.3
8		0.83	8.30E-04	1.99	1.99E-03	-	-	0.035	3.53E-05	4.26	1.79E-02	1.86E-02	2.63E-08	7.43E-04	-6.23	-17.5
1	Same excess	1.66	1.66E-03	3.93	3.93E-03	-	-	0.068	6.84E-05	4.12	1.84E-02	1.88E-02	8.92E-08	1.30E-03	-6.40	-16.23
15		1.26	1.26E-03	3.26	3.26E-03	-	-	0.113	1.13E-04	8.94	2.70E-05	2.68E-05	9.81E-05	8.68E-04	-6.68	-9.2
16		1.26	1.26E-03	3.12	3.12E-03	0.90	9.01E-04	0.118	1.18E-04	9.33	2.65E-05	2.69E-05	9.44E-05	8.00E-04	-6.68	-9.3
9	Different excess for [Cat]	1.66	1.66E-03	4.05	4.05E-03	-	-	0.066	6.60E-05	3.98	1.33E-02	1.17E-02	8.79E-08	1.33E-03	-9.63	-16.2
10		1.66	1.66E-03	4.08	4.08E-03	-	-	0.158	1.58E-04	9.53	3.03E-02	2.68E-02	1.98E-07	1.25E-03	-8.75	-15.4
11		1.66	1.66E-03	4.21	4.21E-03	-	-	0.251	2.51E-04	15.13	3.40E-02	3.27E-02	2.28E-07	9.06E-04	-8.29	-15.3
12		1.66	1.66E-03	3.62	3.62E-03	-	-	0.352	3.52E-04	21.19	5.70E-02	4.40E-02	3.20E-07	9.10E-04	-7.95	-15.0
13		1.66	1.66E-03	4.13	4.13E-03	-	-	0.575	5.75E-04	34.65	8.32E-02	7.58E-02	5.15E-07	8.95E-04	-7.46	-14.5
14		1.66	1.66E-03	4.29	4.29E-03	-	-	0.748	7.48E-04	45.06	1.12E-01	1.01E-01	6.95E-07	9.29E-04	-7.20	-14.2

a) Determined by weight of **4** and the volume of solvent. b) Determined by the relative integrals of **4** and **7**/**8**/**Cat**. c) Determined by linear or nonlinear fitting of the respective concentration over time data.

Table 17: Experimental data and results for kinetic experiments with macrocyclic catalyst **2c**.

Experimental setup											Analysis for k_{Obs} and v_0[c]					
		Concentrations									Linear fit	Nonlinear fit			Double ln plot	
Exp.-No.	Exp.-Type	[4][a] (mM)	[4][a] (M)	[7][b] (mM)	[7][b] (M)	[8][c] (mM)	[8][c] (M)	[Cat][b] (mM)	[Cat][b] (M)	[Cat][b] (mol%)	k_{Obs} ($s^{-1} M^{-1}$)	k_{Obs} ($s^{-1} M^{-1}$)	v_0 ($M\ s^{-1}$)	v_0 / [Cat] (s^{-1})	ln [Cat]	ln v_0
2c-1	Different excess for [4]	1.66	1.66E-03	4.00	4.00E-03	-	-	0.077	7.67E-05	4.62	3.32E-05	3.48E-05	2.23E-07	2.90E-03	-	-
2c-3		1.26	1.26E-03	4.02	4.02E-03	-	-	0.078	7.82E-05	6.21	3.06E-05	3.19E-05	1.57E-07	2.00E-03	-	-
2c-2	Different excess for [7]	1.26	1.26E-03	3.24	3.24E-03	-	-	0.078	7.85E-05	6.23	3.26E-05	3.42E-05	1.35E-07	1.73E-03	-	-
2c-3		1.26	1.26E-03	4.02	4.02E-03	-	-	0.078	7.82E-05	6.21	3.06E-05	3.19E-05	1.57E-07	2.00E-03	-	-
2c-1	Same excess	1.66	1.66E-03	4.00	4.00E-03	-	-	0.077	7.67E-05	4.62	3.32E-05	3.48E-05	2.23E-07	2.90E-03	-	-
2c-2		1.26	1.26E-03	3.24	3.24E-03	-	-	0.078	7.85E-05	6.23	3.26E-05	3.42E-05	1.35E-07	1.73E-03	-	-
2c-4		1.26	1.26E-03	3.07	3.07E-03	0.71	7.10E-04	0.081	8.10E-05	6.43	3.23E-05	3.50E-05	1.32E-07	1.62E-03	-	-
2c-5	Different excess for [Cat]	1.66	1.66E-03	4.02	4.02E-03	-	-	0.070	7.00E-05	4.22	2.39E-02	1.17E-02	1.50E-07	2.15E-03	-9.57	-15.7
2c-6		1.66	1.66E-03	4.03	4.03E-03	-	-	0.135	1.35E-04	8.12	4.88E-02	2.68E-02	3.34E-07	2.48E-03	-8.91	-14.9
2c-7		1.66	1.66E-03	3.83	3.83E-03	-	-	0.268	2.68E-04	16.16	9.54E-02	3.27E-02	5.77E-07	2.15E-03	-8.22	-14.4
2c-8		1.66	1.66E-03	4.11	4.11E-03	-	-	0.445	4.45E-04	26.80	1.94E-01	4.40E-02	1.06E-06	2.38E-03	-7.72	-13.8
2c-9		1.66	1.66E-03	4.05	4.05E-03	-	-	0.532	5.32E-04	32.02	1.63E-01	7.58E-02	1.12E-06	2.11E-03	-7.54	-13.7
2c-10		1.66	1.66E-03	4.13	4.13E-03	-	-	0.609	6.09E-04	36.68	2.05E-01	1.01E-01	1.16E-06	1.91E-03	-7.40	-13.7
2c-11		1.66	1.66E-03	4.27	4.27E-03	-	-	0.657	6.57E-04	39.57	2.24E-01	0.00E+00	1.29E-06	1.96E-03	-7.33	-13.6
2c-12		1.66	1.66E-03	3.97	3.97E-03	-	-	0.712	7.12E-04	42.91	2.32E-01	0.00E+00	1.42E-06	1.99E-03	-7.25	-13.5
2c-13		1.66	1.66E-03	4.00	4.00E-03	-	-	0.821	8.21E-04	49.47	2.27E-01	0.00E+00	1.44E-06	1.76E-03	-7.10	-13.4
2c-14		1.66	1.66E-03	3.93	3.93E-03	-	-	0.852	8.52E-04	51.31	2.81E-01	0.00E+00	1.46E-06	1.71E-03	-7.07	-13.4

a) Determined by weight of **4** and the volume of solvent. b) Determined by the relative integrals of **4** and **7**/**8**/**Cat**. c) Determined by linear or nonlinear fitting of the respective concentration over time data.

Table 18: Experimental data and results for kinetic experiments with acyclic catalyst **3**.

Experimental setup											Analysis for k_{Obs} and v_0[c]					
		Concentrations									Linear fit	Nonlinear fit			Double ln plot	
Exp.-No.	Exp.-Type	[4][a] (mM)	[4][a] (M)	[7][b] (mM)	[7][b] (M)	[8][c] (mM)	[8][c] (M)	[Cat][b] (mM)	[Cat][b] (M)	[Cat][b] (mol%)	k_{Obs} ($s^{-1} M^{-1}$)	k_{Obs} ($s^{-1} M^{-1}$)	v_0 ($M s^{-1}$)	v_0 / [Cat] (s^{-1})	ln [Cat]	ln v_0
1	Different excess for [4]	1.66	1.66E-03	4.1203071	4.12E-03	-	-	0.025	2.54E-05	1.53	5.51E-05	5.58E-05	2.86E-04	1.13E-02	-10.58	-8.2
2		1.26	1.26E-03	4.2359206	4.24E-03	-	-	0.021	2.14E-05	1.70	4.36E-05	4.38E-05	1.89E-04	8.81E-03	-10.75	-8.6
2	Different excess for [7]	1.26	1.26E-03	3.3746167	3.37E-03	-	-	0.016	1.64E-05	1.30	6.94E-05	6.94E-05	2.22E-04	1.36E-02	-11.02	-8.4
3		1.26	1.26E-03	4.2359206	4.24E-03	-	-	0.021	2.14E-05	1.70	4.36E-05	4.38E-05	1.89E-04	8.81E-03	-10.75	-8.6
1	Same excess	1.66	1.66E-03	4.1203071	4.12E-03	-	-	0.025	2.54E-05	1.53	5.51E-05	5.58E-05	2.86E-04	1.13E-02	-10.58	-8.2
2		1.26	1.26E-03	3.3746167	3.37E-03	-	-	0.016	1.64E-05	1.30	6.94E-05	6.94E-05	2.22E-04	1.36E-02	-11.02	-8.4
4		1.26	1.26E-03	4.2359206	4.24E-03	0.90	9.00E-04	0.017	1.71E-05	1.36	5.31E-05	5.42E-05	1.82E-04	1.07E-02	-10.98	-8.6
5	Different excess for [Cat]	1.66	1.66E-03	4.44	4.44E-03	-	-	0.041	4.12E-05	2.48	0.10	0.11	7.21E-07	1.75E-02	-10.10	-14.1
6		1.66	1.66E-03	4.03	4.03E-03	-	-	0.074	7.38E-05	4.44	0.38	0.42	1.80E-06	2.44E-02	-9.51	-13.2
7		1.66	1.66E-03	3.83	3.83E-03	-	-	0.115	1.15E-04	6.91	0.61	0.57	2.29E-06	2.00E-02	-9.07	-13.0
8		1.66	1.66E-03	4.11	4.11E-03	-	-	0.227	2.27E-04	13.65	1.28	1.08	3.95E-06	1.74E-02	-8.39	-12.4
9		1.66	1.66E-03	4.05	4.05E-03	-	-	0.402	4.02E-04	24.23	1.52	1.41	4.17E-06	1.04E-02	-7.82	-12.4
10		1.66	1.66E-03	4.13	4.13E-03	-	-	0.406	4.06E-04	24.45	1.43	1.21	3.92E-06	9.66E-03	-7.81	-12.4
11		1.66	1.66E-03	4.27	4.27E-03	-	-	0.625	6.25E-04	37.66	1.55	1.57	5.39E-06	8.62E-03	-7.38	-12.1
12		1.66	1.66E-03	3.97	3.97E-03	-	-	0.649	6.49E-04	39.10	1.50	1.65	5.43E-06	8.36E-03	-7.34	-12.1
13		1.66	1.66E-03	4.00	4.00E-03	-	-	0.783	7.83E-04	47.17	1.98	1.58	4.69E-06	5.99E-03	-7.15	-12.3
14		1.66	1.66E-03	3.93	3.93E-03	-	-	0.863	8.63E-04	51.97	2.22	2.29	5.68E-06	6.58E-03	-7.06	-12.1

a) Determined by weight of **4** and the volume of solvent. b) Determined by the relative integrals of **4** and **7**/**8**/**Cat**. c) Determined by linear or nonlinear fitting of the respective concentration over time data.

Table 19: Experimental data and results for rate fitting using different concentrations of acyclic catalyst **3**.

Experimental setup				Results					
	Concentrations				Calculated		Fitted			
Exp.-No.	[4][a] (mM)	[7][b] (mM)	[Cat][b] (mM)	[Cat][b] (mol%)	v_{max} ($\mathbf{3}_{Mono}$) ($M s^{-1}$)	v_{max} ($\mathbf{3}_{Di}$) ($M s^{-1}$)	x_{Mono}	x_{Di}	v_0 ($\mathbf{3}_{Mono}$) ($M s^{-1}$)	v_0 ($\mathbf{3}_{Di}$) ($M s^{-1}$)
1	1.66	4.03	0.074	4.44	1.94E-06	4.64E-07	0.91	0.09	1.76E-06	4.32E-08
2	1.66	3.83	0.115	6.91	3.02E-06	7.21E-07	0.69	0.31	2.07E-06	2.27E-07
3	1.66	4.11	0.227	13.65	5.96E-06	1.42E-06	0.56	0.44	3.32E-06	6.32E-07
4	1.66	4.05	0.402	24.23	1.06E-05	2.53E-06	0.20	0.80	2.16E-06	2.01E-06
5	1.66	4.27	0.625	37.66	1.64E-05	3.93E-06	0.12	0.88	1.91E-06	3.47E-06
6	1.66	3.97	0.649	39.10	1.71E-05	4.08E-06	0.10	0.90	1.77E-06	3.66E-06
7	1.66	3.93	0.863	51.97	2.27E-05	5.42E-06	0.01	0.99	3.32E-07	5.34E-06

a) Determined by weight of **4** and the volume of solvent. b) Determined by the relative integrals of **4** and **7**/**8**/**Cat**.

Table 20: Results for fitting of stereoselectivity data using different concentrations of acyclic catalyst **3.**

Experimental setup						Results						
		Concentrations				*ee*	Calculated		Fitted			
Exp.-No.	Exp.-Type	[4][a] (mM)	[7][a] (mM)	[3][a] (mM)	[3][a] (mol%)	*ee*[b] (%)	*ee* / *ee* ($\mathbf{3}_{Mono}$) (%)	*ee* / *ee* ($\mathbf{3}_{Di}$) (%)	x_{Mono}	x_{Di}	*ee*_contr. ($\mathbf{3}_{Mono}$) (%)	*ee*_contr. ($\mathbf{3}_{Di}$) (%)
1	Different excess for [3] at 1.66 mM quinoline	1.66	3.93	0.0002	0.01	-[c]	-[c]	-[c]	-[c]	-[c]	-[c]	-[c]
2		1.66	3.93	0.0017	0.10	-29.5	1.19	-2.55	1.00	0.00	-33.2	3.8
3		1.66	3.93	0.0042	0.25	-20.9	1.67	-3.58	0.99	0.01	-30.5	9.6
4		1.66	3.93	0.0083	0.50	-10.1	3.47	-7.43	0.98	0.02	-27.1	17.0
5		1.66	3.93	0.0166	1.00	12.8	-2.72	5.84	0.96	0.04	-19.8	32.6
6		1.66	3.93	0.0249	1.50	20.4	-1.71	3.67	0.95	0.05	-17.4	37.8
7		1.66	3.93	0.0415	2.50	36.5	-0.96	2.05	0.90	0.10	-12.2	48.8
8		1.66	3.93	0.0830	5.00	54.7	-0.64	1.37	0.80	0.20	-6.5	61.2
9		1.66	3.93	0.1660	10.00	61.2	-0.57	1.23	0.72	0.28	-4.4	65.6
10		1.66	3.93	0.3320	20.00	67.5	-0.52	1.11	0.57	0.43	-2.4	69.9
12		1.66	3.93	0.5810	35.00	70.6	-0.50	1.06	0.43	0.57	-1.4	72.0
13		1.66	3.93	0.8300	50.00	71.6	-0.49	1.05	0.36	0.64	-1.1	72.7
12	Different excess for [3] at 5.0 mM quinoline	1.66	3.93	0.0250	0.50	-22.7	1.54	-3.30	0.99	0.01	-31.1	8.4
13		1.66	3.93	0.0750	1.50	14.3	-2.45	5.24	0.96	0.04	-19.3	33.6
14		1.66	3.93	0.1250	2.50	24.5	-1.43	3.06	0.94	0.06	-16.1	40.6
15		1.66	3.93	0.2500	5.00	45.0	-0.78	1.67	0.87	0.13	-9.6	54.5

a) Determined by weight of **4**/**7**/**3** and the volume of solvent. b) Determined by chiral HPLC. Enantiomeric excesses given for the (*R*)-product isomer. [c] No conversion observed.

7.5 Catalytic Reactions from chapter 4

7.5.1 Catalytic reactions with endotopologically bound Lewis acids

General procedure for the asymmetric hydrocyanation using Sc(III)-catalysts

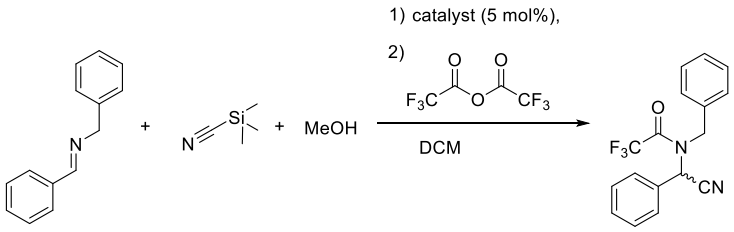

The corresponding catalyst (1 eq.) precursors were dissolved in dichloromethane (1 ml) and $Sc(OTf)_3$ (0.96 eq.) was added. The mixture was stirred for one hour at room temperature, before it was filtered. The solvent was removed under reduced pressure to yield the corresponding Sc(III)-catalysts.

Imine **96** (19.5 mg, 100 µmol, 1 eq.) was placed in a Schlenk tube and evacuated three times with argon. To this the corresponding Sc(III)-catalyst (5.00 µmol, 0.05 eq.) in dry dichloromethane (0.50 ml) was added and the mixture was stirred for 30 minutes at 25 °C or -40 °C. Trimethylsilyl cyanide (24.8 mg, 250 µmol, 2.5 eq.) and methanol (6.41 mg, 200 µmol, 2 eq.) were added and the mixture was further stirred for 24 hours. Trifluoroacetic anhydride (63.0 mg, 300 µmol, 3 eq.) was added and the mixture was stirred for one hour at 25 °C. The solvent was removed under reduced pressure and the crude mixture was purified by silica gel column chromatography with cyclohexane/ethyl acetate (95 : 5) + 2 vol% triethylamine to yield the product as a colorless oil. The purified sample was used for chiral HPLC analysis (Chiralcel AD-H column) to determine the enantiomeric excess.

Table 21: Summarized results for the hydrocyanation of imine **96**.

Entry	Catalyst[(a)]	Temperature [°C]	Enantiomeric excess [%][(b)]
1	**11-Sc**	25	6
2	-	25	-
3	**11-Sc**	-40	3
4	-	-40	-
5	(*S*)-**14-HNEt$_3$-Sc**	-40	0
6	(*S*)-**17-HNEt$_3$-Sc**	-40	0

(a) 5 mol% relative to imine **96**. (b) Determined by chiral HPLC (AD-H column).

7.5.2 Tsuji-Trost reaction

General procedure for the Tsuji-Trost reaction

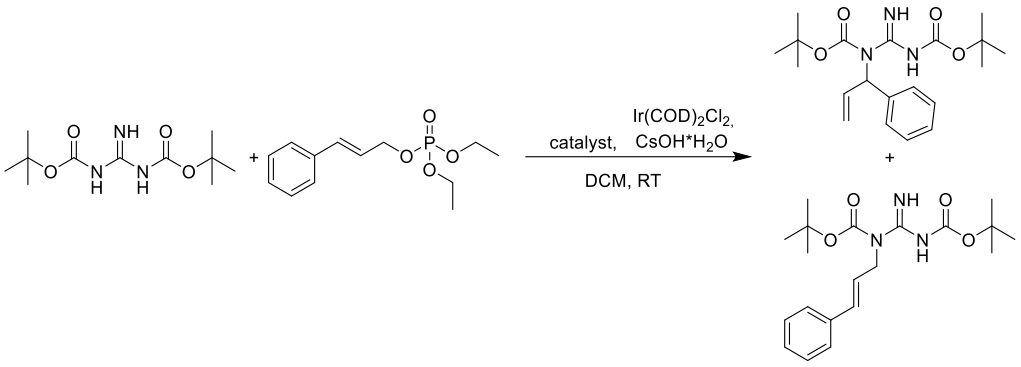

The corresponding catalyst (1 eq.) precursors were dissolved in dichloromethane (1 ml) and cyclooctadiene iridium chloride dimer (0.48 eq.) was added. The mixture was stirred for one hour at room temperature, before it was filtered. The solvent was removed under reduced pressure to yield the corresponding Ir(I)-catalysts.

Guanidine **106** (12.3 mg, 0.0500 mmol, 1 eq.) and caesium hydroxide (8.40 mg, 0.0500 mmol, 1eq.) were placed in a Schlenk tube and dried under high vacuum for three hours. Dry dichloromethane (0.5 ml) was added and the mixture was stirred for 30 minutes. To this, a mixture of the corresponding Ir(I)-cataylst (2.50 µmol, 0.05 eq.) and phosphate **107** (20.3 mg, 0.0750 mmol, 1.5 eq.) dissolved in dry dichloromethane (0.25 ml) was added. The reaction mixture was stirred at room temperature. Conversion was checked by thin layer chromatography with cyclohexane/ethyl acetate (90 : 10) mixtures. After the reaction was complete, the solvent was removed under reduced pressure. Determination of the ratio of products was determined from the crude mixture in the ^{1}H-NMR. The crude mixture was purified chromatographically with a cyclohexane/ethyl acetate (90 : 10) eluent to yield the product as a colourless oil.

Table 22: Summarized results for the Tsuji-Trost reaction.

Entry	Catalyst[(a)]	Ratio (branched/linear)[(b)]	Enantiomeric excess [%][(c)]
1	**110-Ir**	23/77	0
2	**11-Ir**	49/51	3
3	(*S*)-**14-HNEt$_3$-Ir**	63/37	0
4	(*S*)-**17-HNEt$_3$-Sc**	58/42	0

(a) 5 mol% catalyst loading relative to guanidine **106** (b) Determined by ^{1}H-NMR spectroscopy. (c) Determined by chiral HPLC (AD-S column).

7.5.3 Transfer hydrogenation of 2-(4-*tert*-butylphenyl)quinoline 4e

General procedure for the transfer hydrogenation of 2-(4-tert-butylphenyl)quinoline 4e

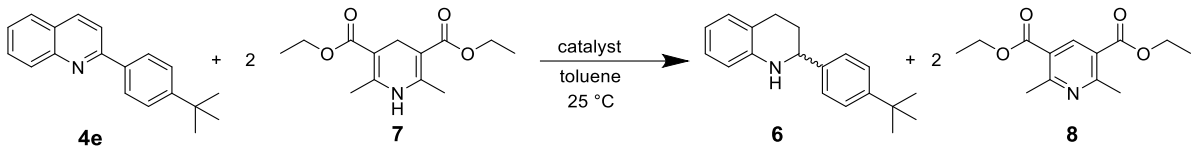

Figure 125: Transfer hydrogenation of 2-(4-*tert*-butylphenyl)quinoline by different catalysts

2-(4-*tert*-butylphenyl)quinoline (4.98 µmol, 1 equiv.) and diethyl 1,4-dihydro-2,6-dimethyl-3,5-pyridinedicarboxylate (11.95 µmol, 2.4 equiv.) were taken in a Schlenk flask which was evacuated three times and back filled with argon. To that mixture, toluene (4 ml), followed by the catalyst (*S*)-**14-HCL**/(*S*)-**14-HC,** (*S*)-**17-HCL**/(*S*)-**17-HC,** (*S*)-**19-HCL**/(*S*)-**19-HC** (solutions in 1 ml toluene; total reaction volume: 5 ml) were added and the reaction mixture was stirred at room temperature. The reaction was monitored by TLC with cyclohexane/ethyl acetate (10 : 1) mixtures. After 24 hours, the solvent was evaporated in the rotatory evaporator and the crude mixture was analyzed by ^{1}H-NMR spectroscopy and purified by silica gel flash column chromatography with cyclohexane/ethyl acetate (99 : 1) mixtures. The purified sample was used for the chiral HPLC analysis (Chiralcel OD-H column) to determine the enantiomeric excess.

Table 23: Summary of catalytic reactions using 2-(4-*tert*-butylphenyl)quinoline.

Entry	Catalyst (5 mol%)[(a)]	Conversion (%)[(b)]	Enantiomeric excess for (*R*)-4e[(c)]
5	(*S*)-**19-HC**	100	75
6	(*S*)-**19-HC**	100	78
7	(*S*)-**19-HCL** + 5 mol% **11**	100	78
8	(*S*)-**14-HCl**	100	33
9	(*S*)-**14-HC**	100	33
10	(*S*)-**17-HC**	20	13
11	(*S*)-**14-HC**[(d)]	n.d.	82
12	(*S*)-**14-HC**[(d)(e)]	n.d.	84
13	(*S*)-**14-HCl**[(d)]	100	33
14	(*S*)-**19-DFA**	100	77
15	(*S*)-**14-DFA**	n.d.	37
16	(*S*)-**17-DFA**	n.d.	8
17	Citric acid	< 5	n.d.
18	Difluoroacetic acid	68	n.d.

(a) Catalyst loading relative to quinoline. (b) After 24 hours. (c) Determined by chiral HPLC (Chiralcel OD-H column). (d) Different catalyst batch. (e) 10 mol% catalyst.

8. Appendix

8.1 NMR spectra of new compounds

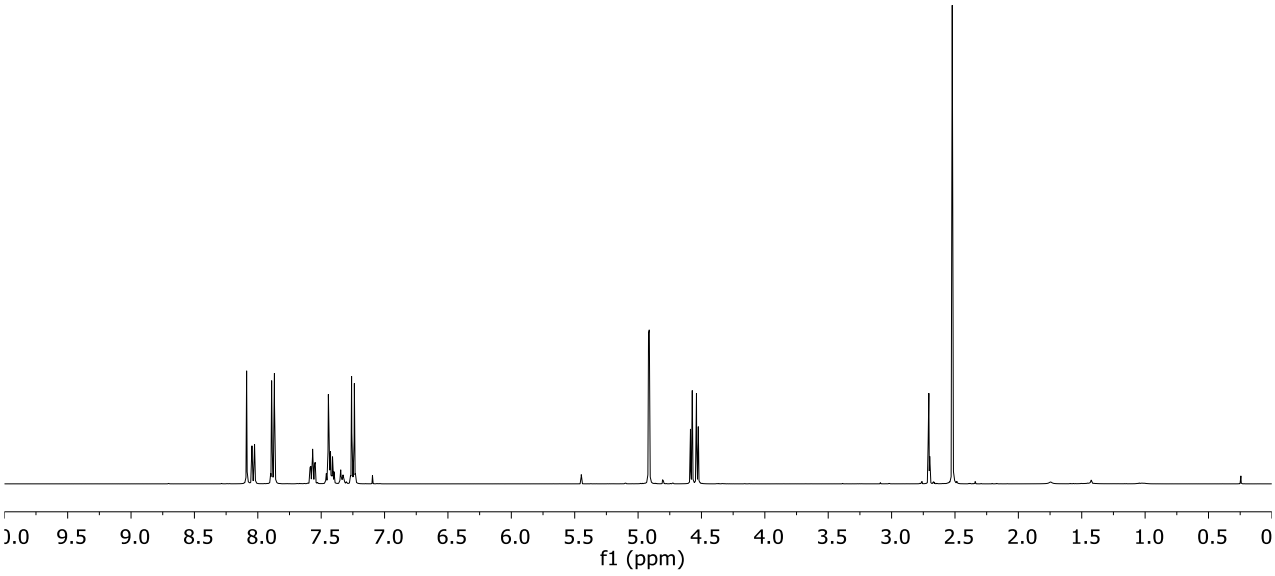

Figure 126: ^{1}H-NMR spectrum of MOM-bisalkyne (*S*)-**9** ([D_1]-chloroform, 400 MHz, 298 K).

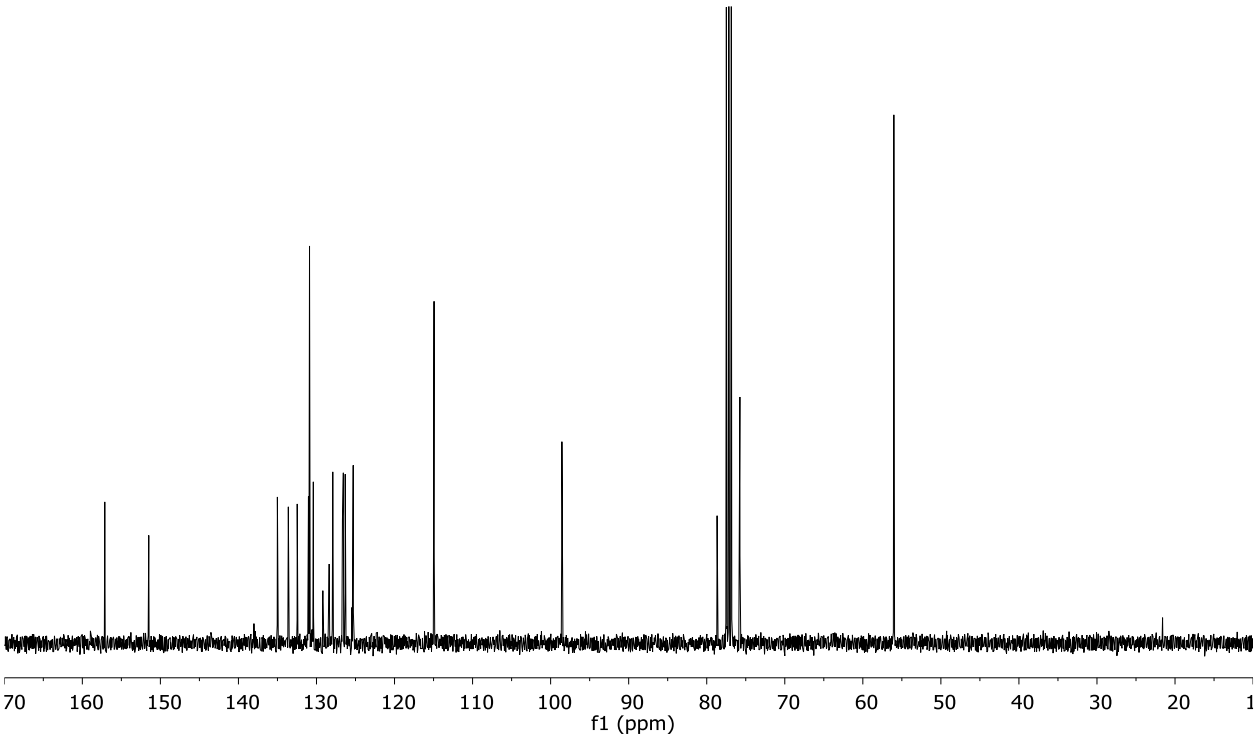

Figure 127*:* ^{13}C-NMR spectrum of MOM-bisalkyne (*S*)-**9** ([D_1]-chloroform, 101 MHz, 298 K).

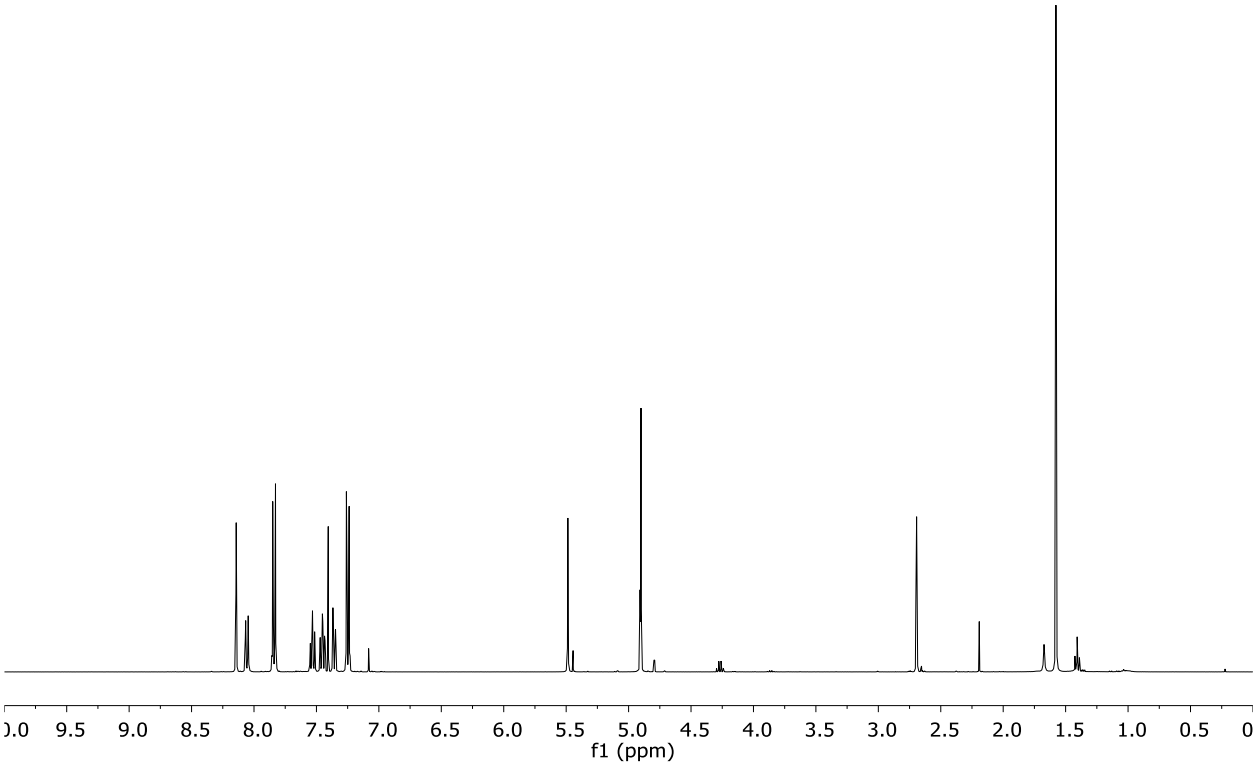

Figure 128: ^{1}H-NMR spectrum of OH-bisalkyne (*S*)-**9** ([D$_1$]-chloroform, 400 MHz, 298 K).

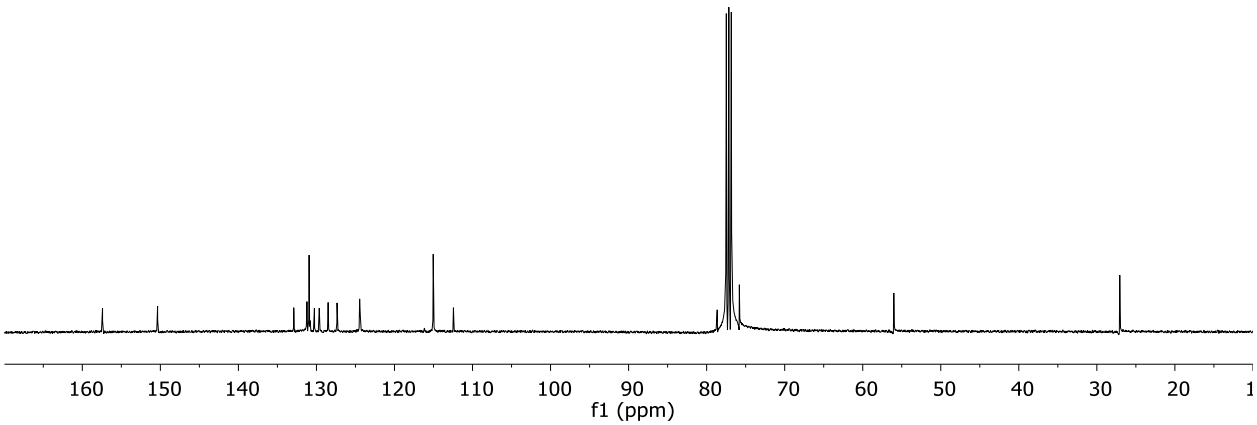

Figure 129: ^{13}C-NMR spectrum of OH-bisalkyne (*S*)-**9** ([D$_1$]-chloroform, 101 MHz, 298 K).

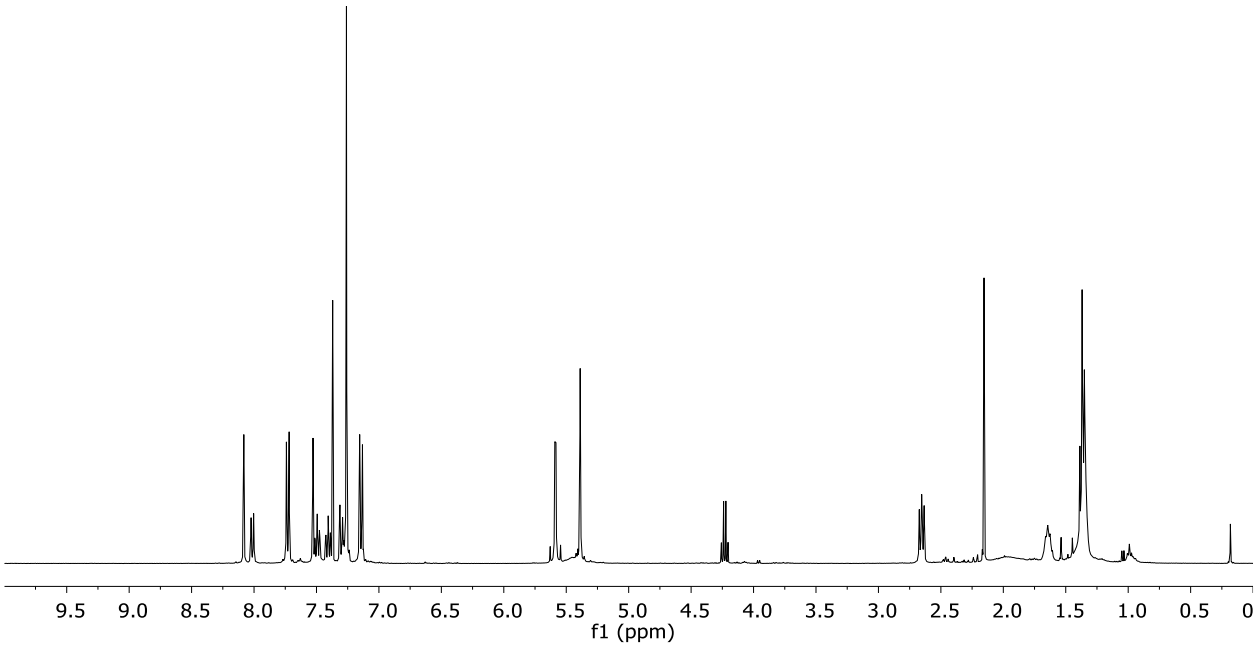

Figure 130: ^{1}H-NMR spectrum of OH-macrocycle (*S*)-**9**5 ([D_1]-chloroform, 400 MHz, 298 K).

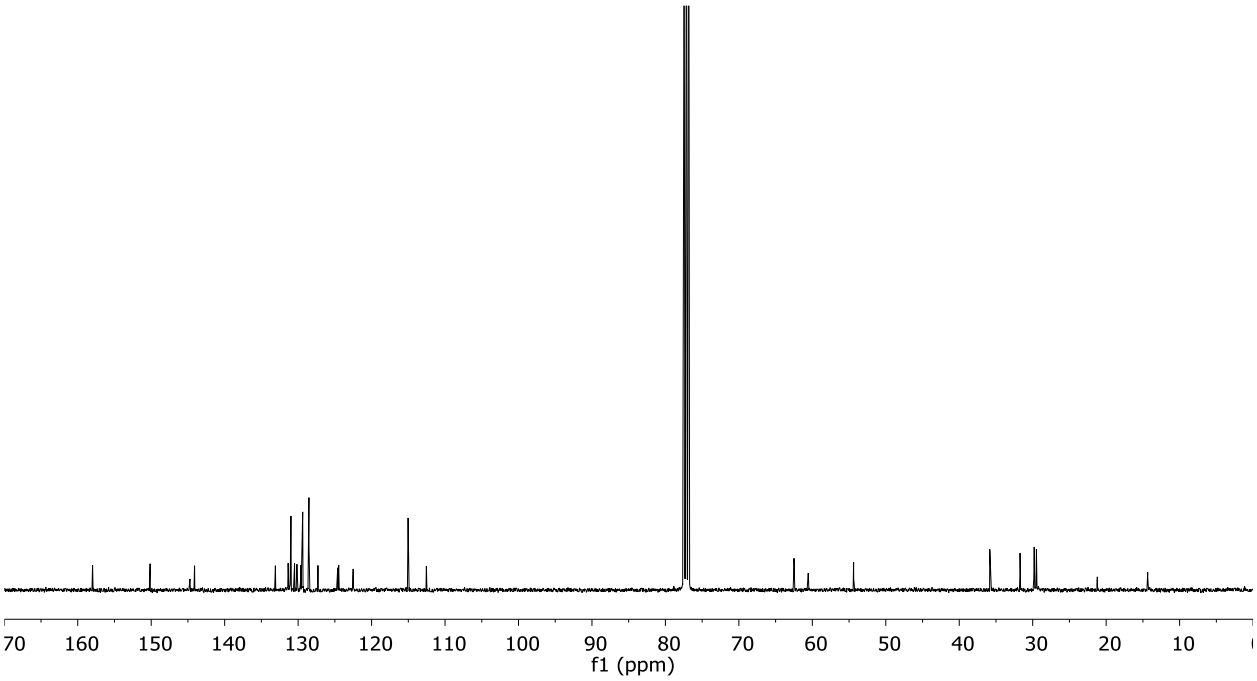

Figure 131: ^{13}C-NMR spectrum of OH-macrocycle (*S*)-**95** ([D_1]-chloroform, 101 MHz, 298 K).

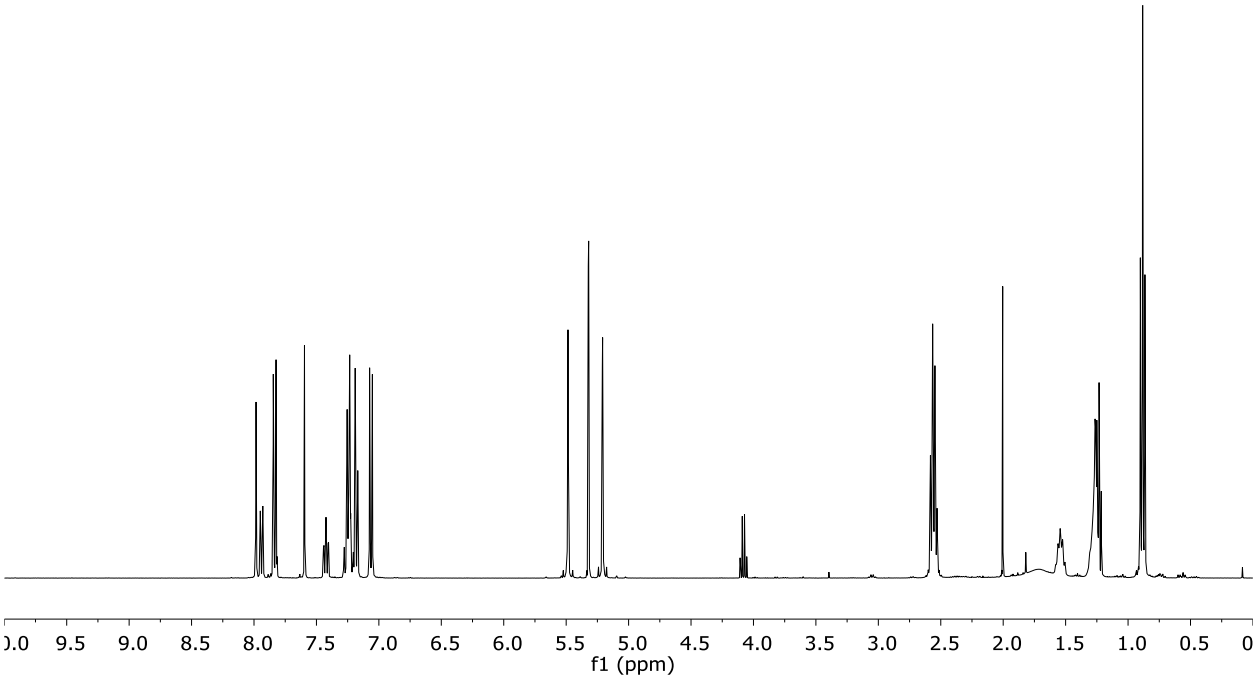

Figure 132: ^{1}H-NMR spectrum of PA-macrocycle (*S*)-1**9-HNEt$_3$** ([D_2]-dichloromethane, 400 MHz, 298 K).

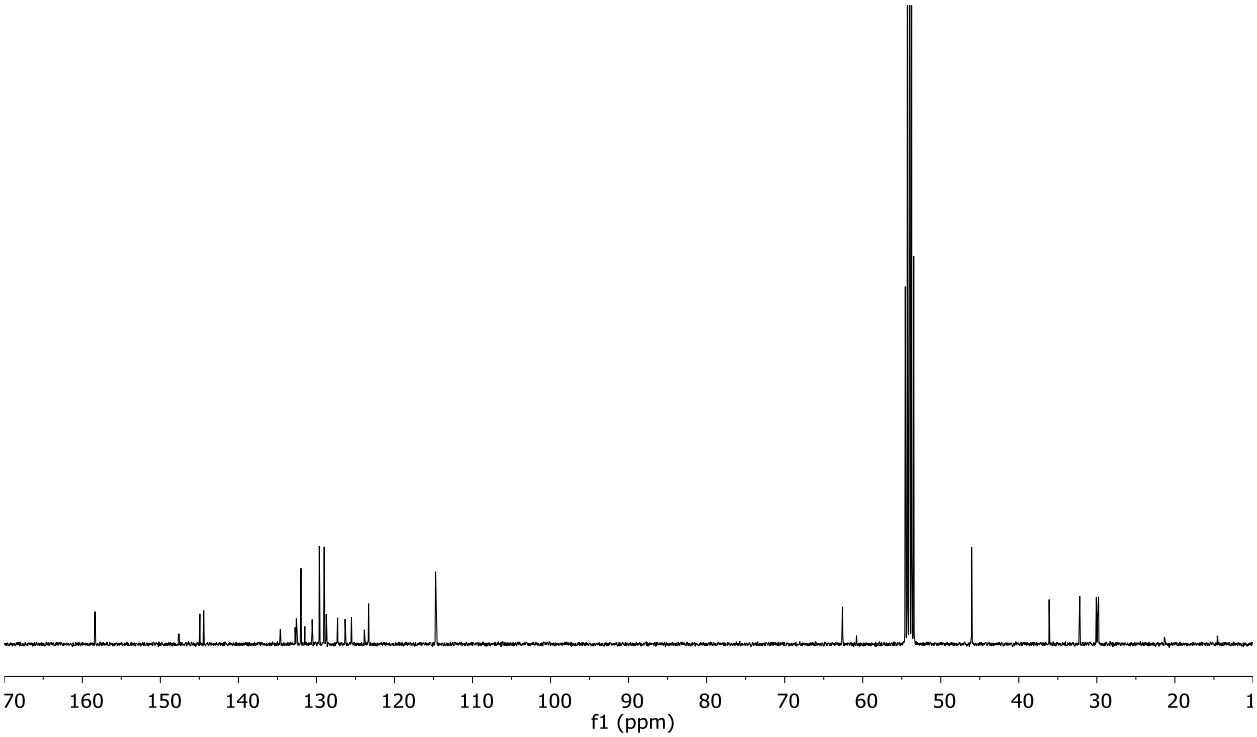

Figure 133: ^{13}C-NMR spectrum of PA-macrocycle (*S*)-1**9-HNEt$_3$** ([D_2]-dichloromethane, 101 MHz, 298 K).

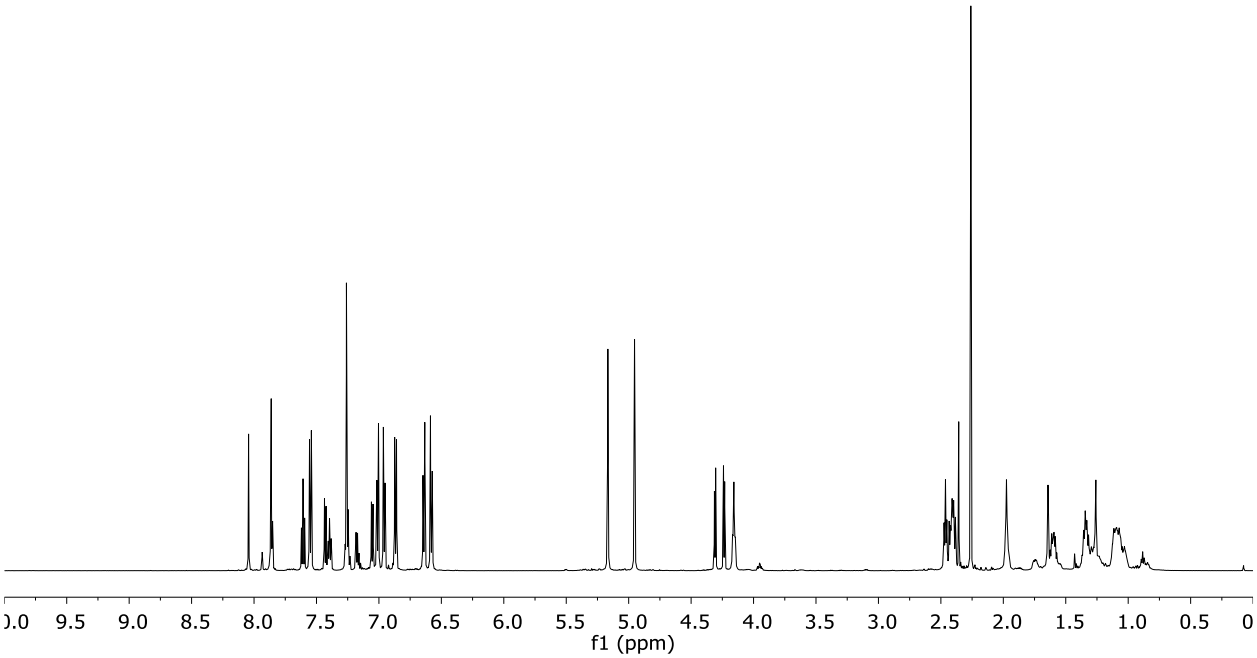

Figure 134: ^{1}H-NMR spectrum of MOM-[2]catenane (*S*)-**12** ([D$_1$]-chloroform, 400 MHz, 298 K).

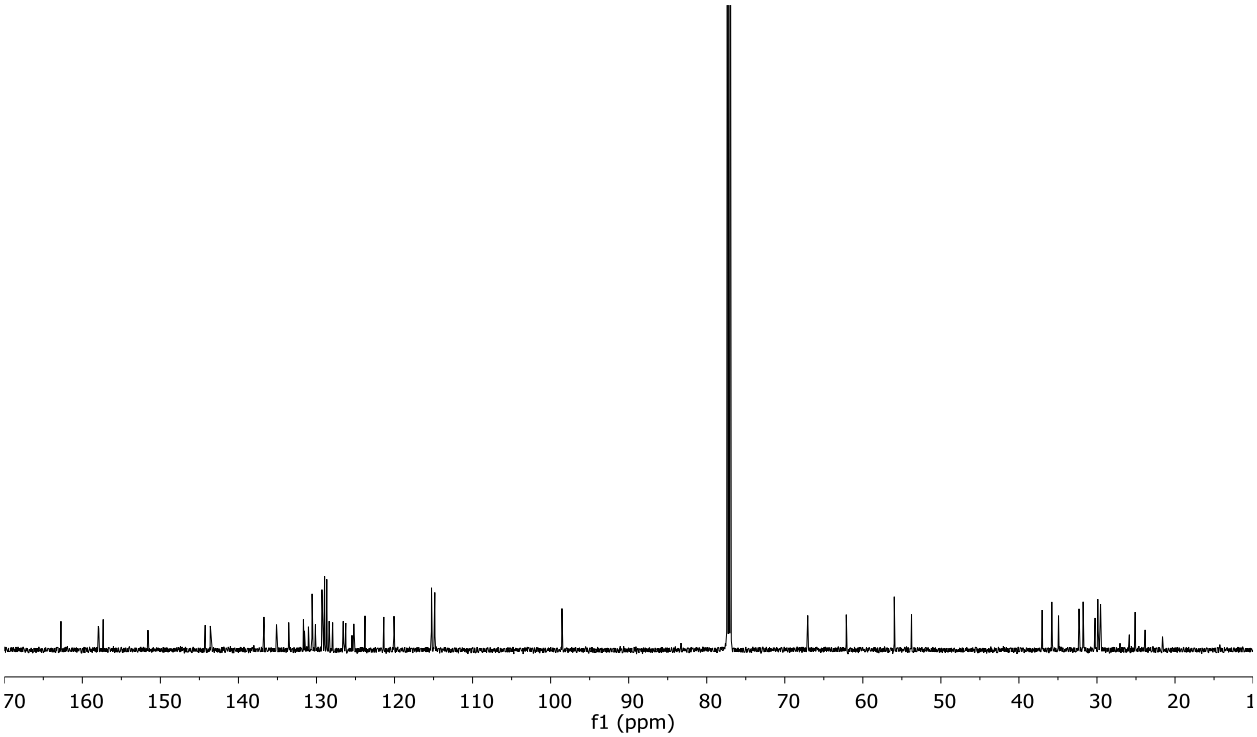

Figure 135: ^{13}C-NMR spectrum of MOM-[2]catenane (*S*)-**12** ([D$_1$]-chloroform, 101 MHz, 298 K).

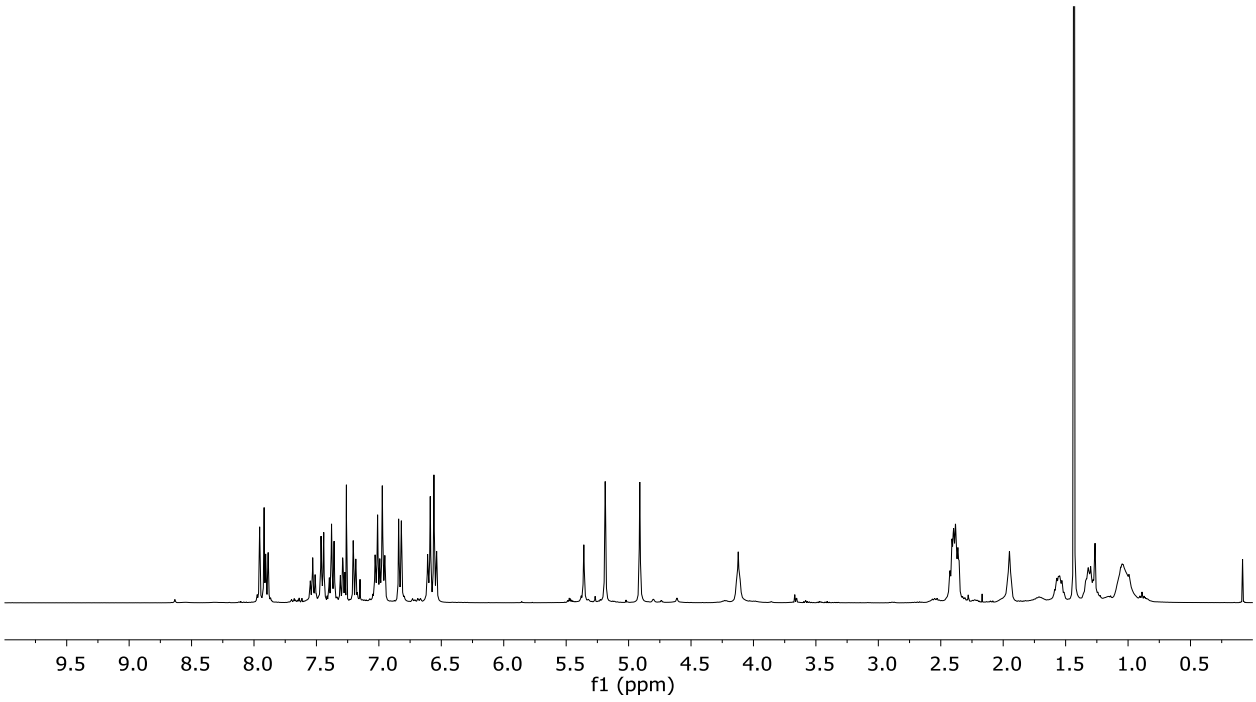

Figure 136: ^{1}H-NMR spectrum of OH-[2]catenane (*S*)-**13** ([D_2]-dichloromethane, 400 MHz, 298 K).

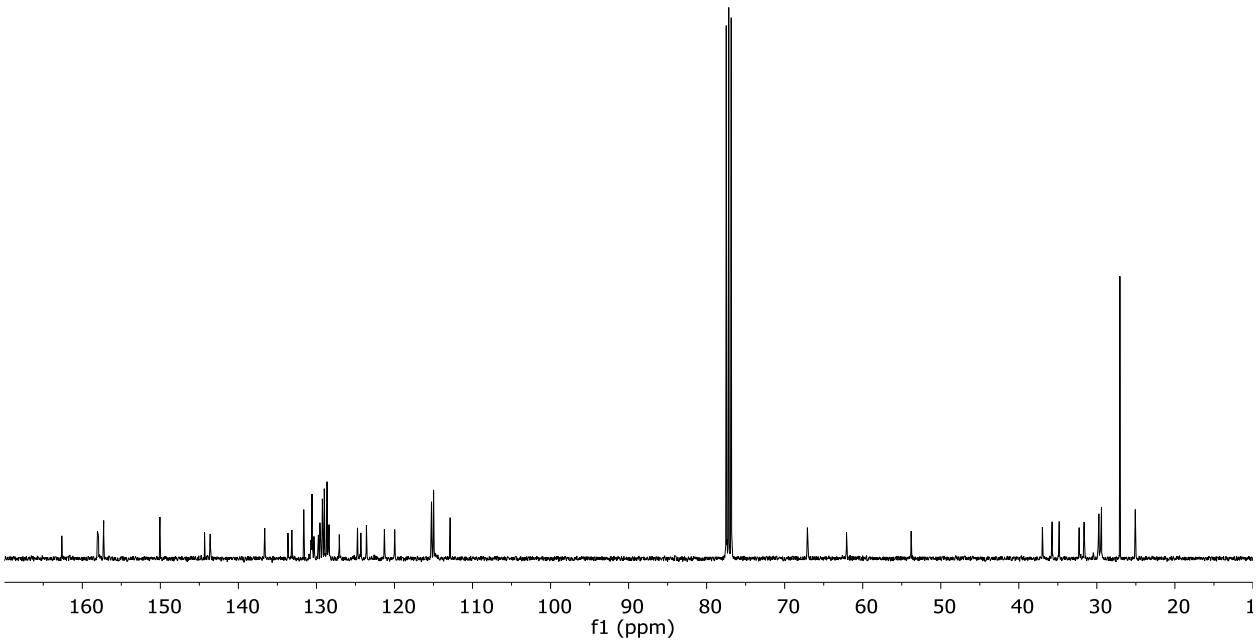

Figure 137: ^{13}C-NMR spectrum of OH-[2]catenane (*S*)-**13** ([D_2]-dichloromethane, 101 MHz, 298 K).

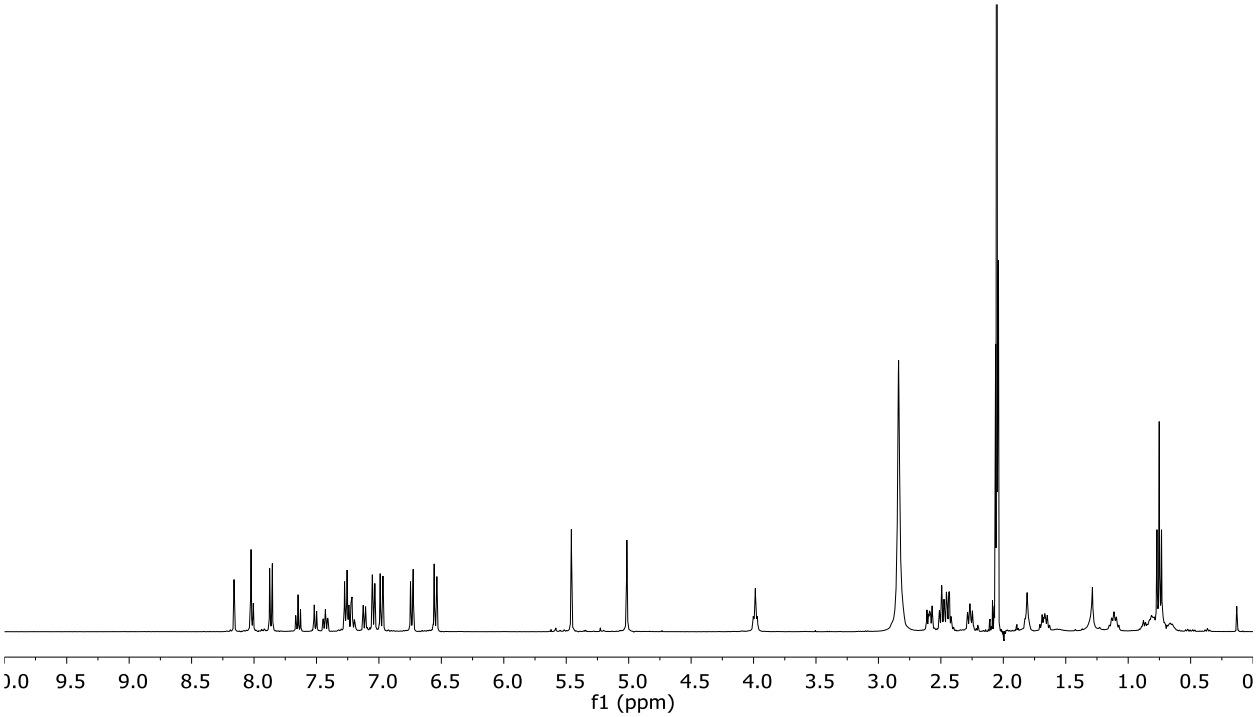

Figure 138: ^{1}H-NMR spectrum of PA-[2]catenane (*S*)-**14-HNEt$_3$** ([D$_6$]-acetone, 400 MHz, 298 K).

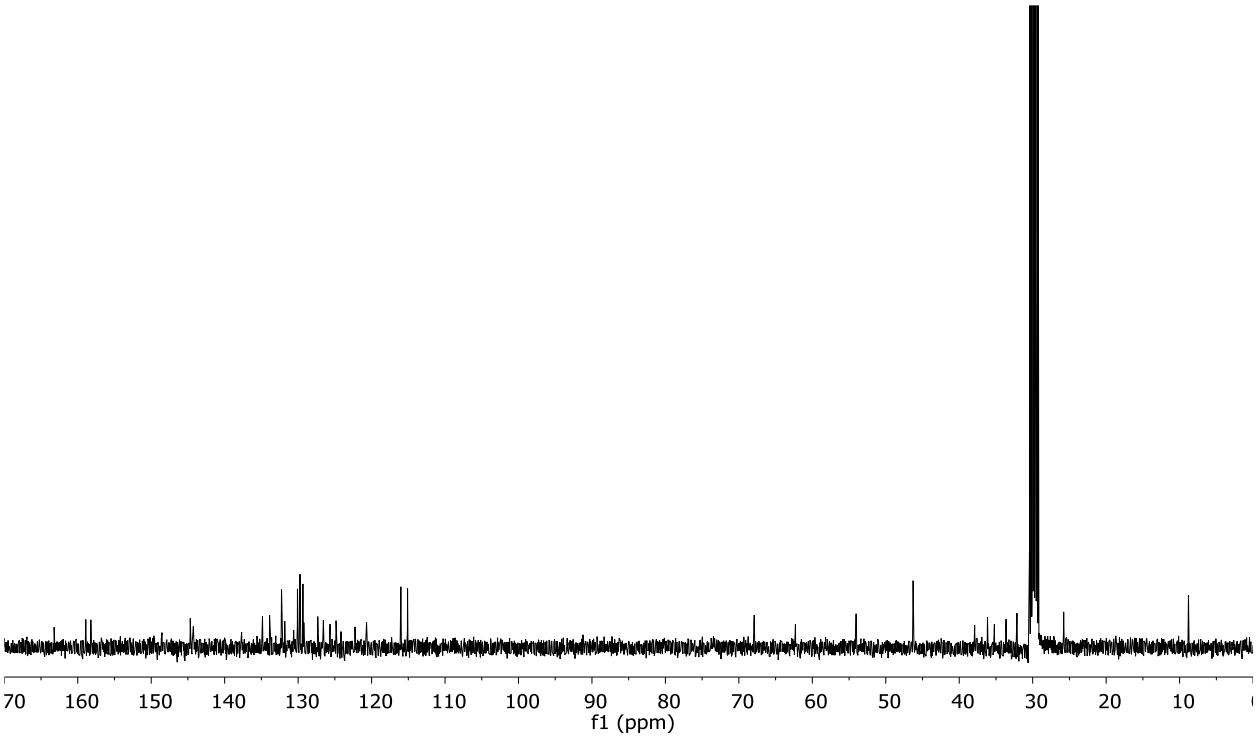

Figure 139: ^{13}C-NMR spectrum of PA-[2]catenane (*S*)-**14-HNEt$_3$** ([D$_6$]-acetone, 101 MHz, 298 K).

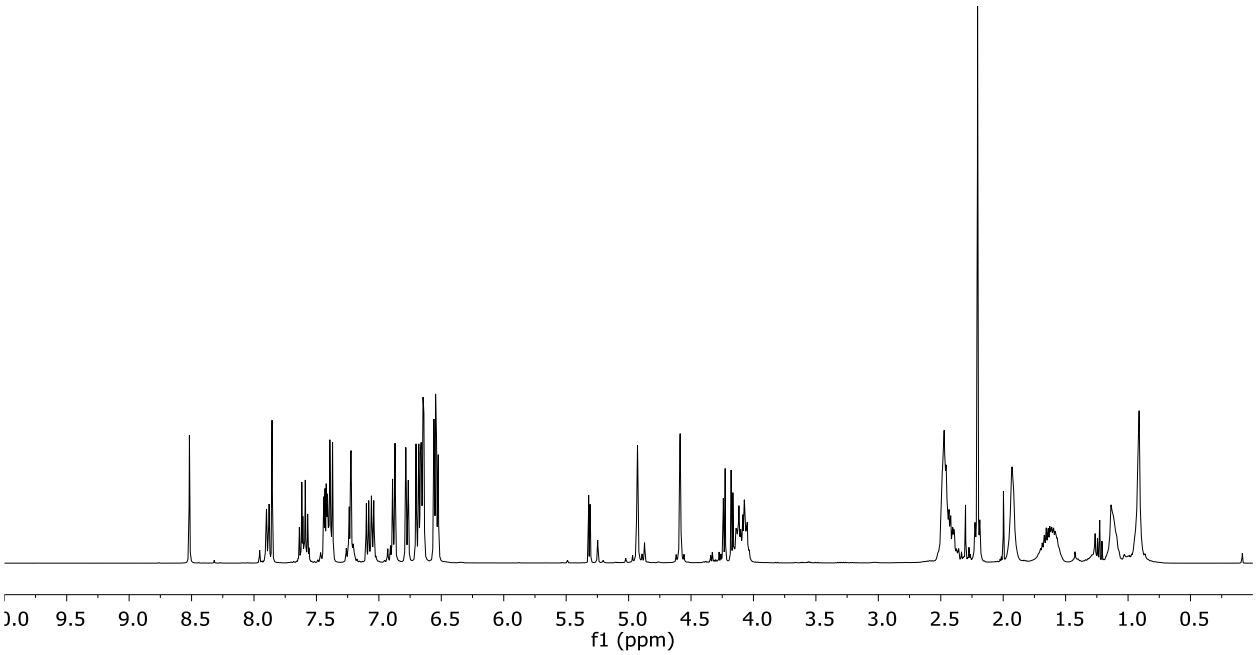

Figure 140: ^{1}H-NMR spectrum of MOM-[3]catenane (*S*)-**15** ([D$_1$]-chloroform, 400 MHz, 298 K).

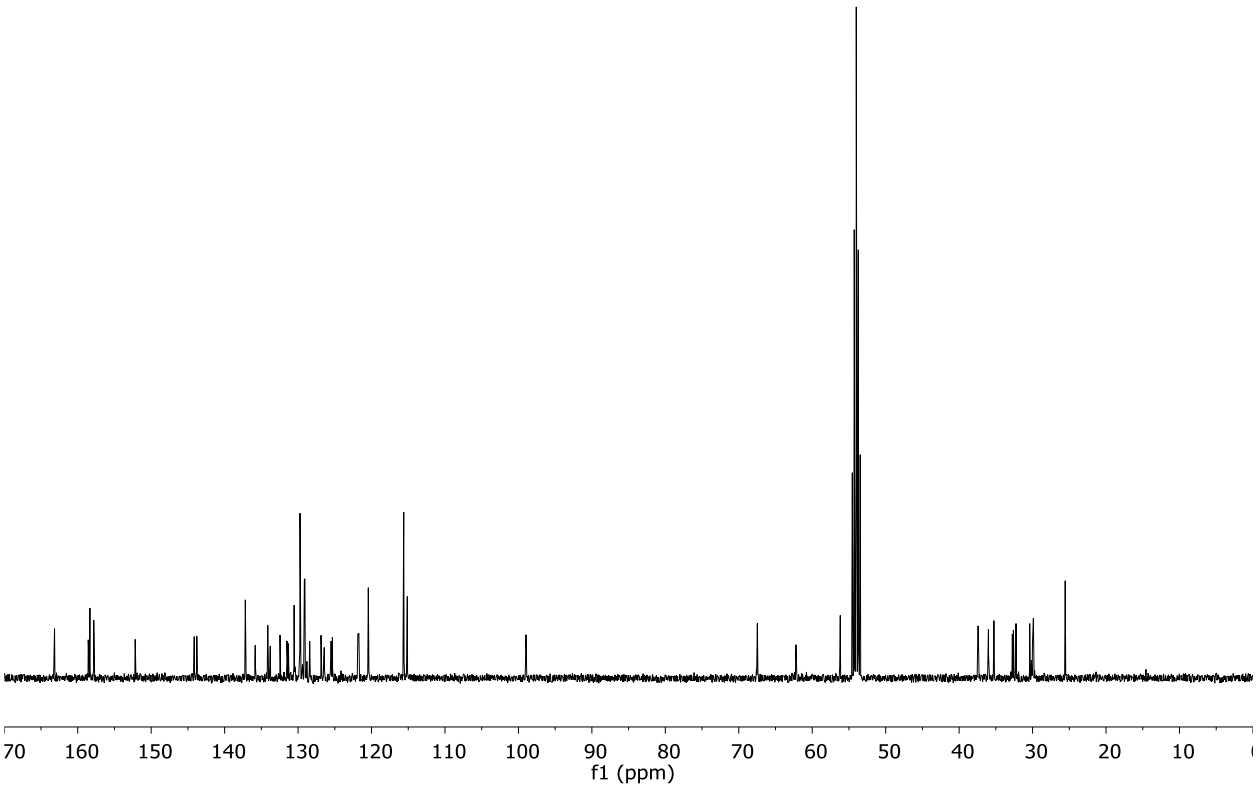

Figure 141: ^{13}C-NMR spectrum of MOM-[3]catenane (*S*)-**15** ([D$_1$]-chloroform, 101 MHz, 298 K).

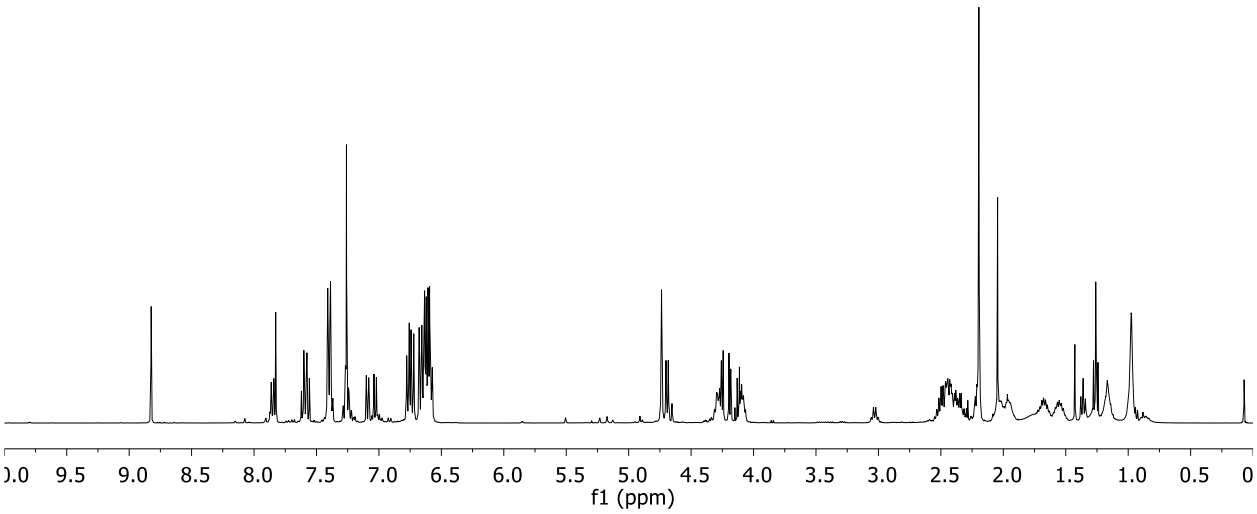

Figure 142: ^{1}H-NMR spectrum of OH-[3]catenane (*S*)-**16** ([D_2]-dichloromethane, 400 MHz, 298 K).

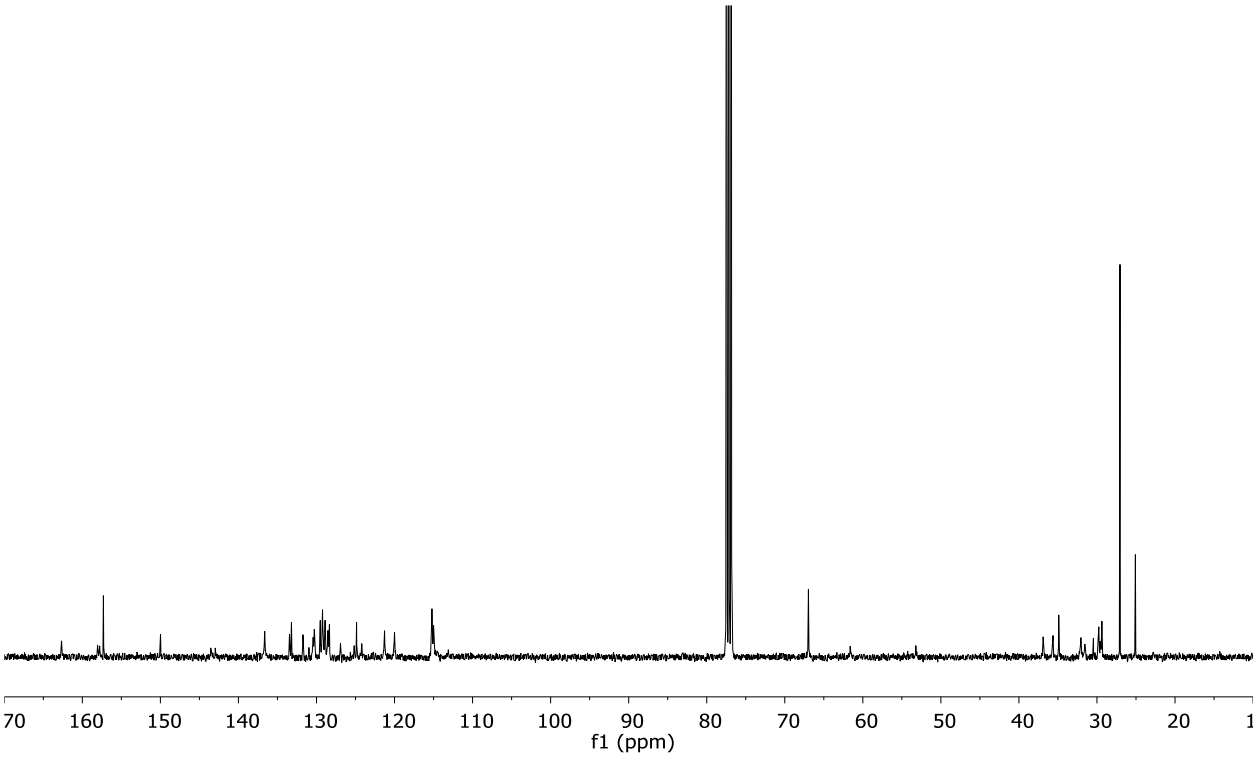

Figure 143: ^{13}C-NMR spectrum of OH-[3]catenane (*S*)-**16** ([D_2]-dichloromethane, 101 MHz, 298 K).

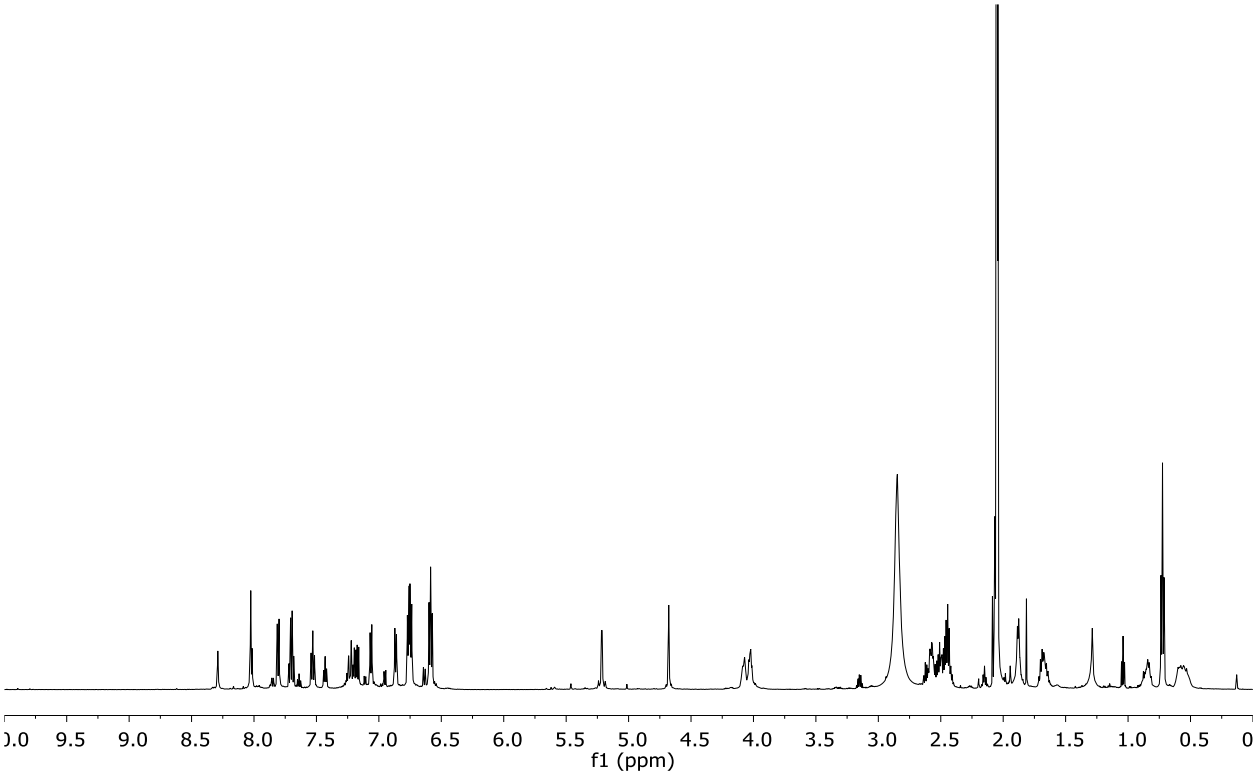

Figure 144: ^{1}H-NMR spectrum of PA-[3]catenane (*S*)-**17-HNEt$_3$** ([D$_2$]-dichloromethane, 400 MHz, 298 K).

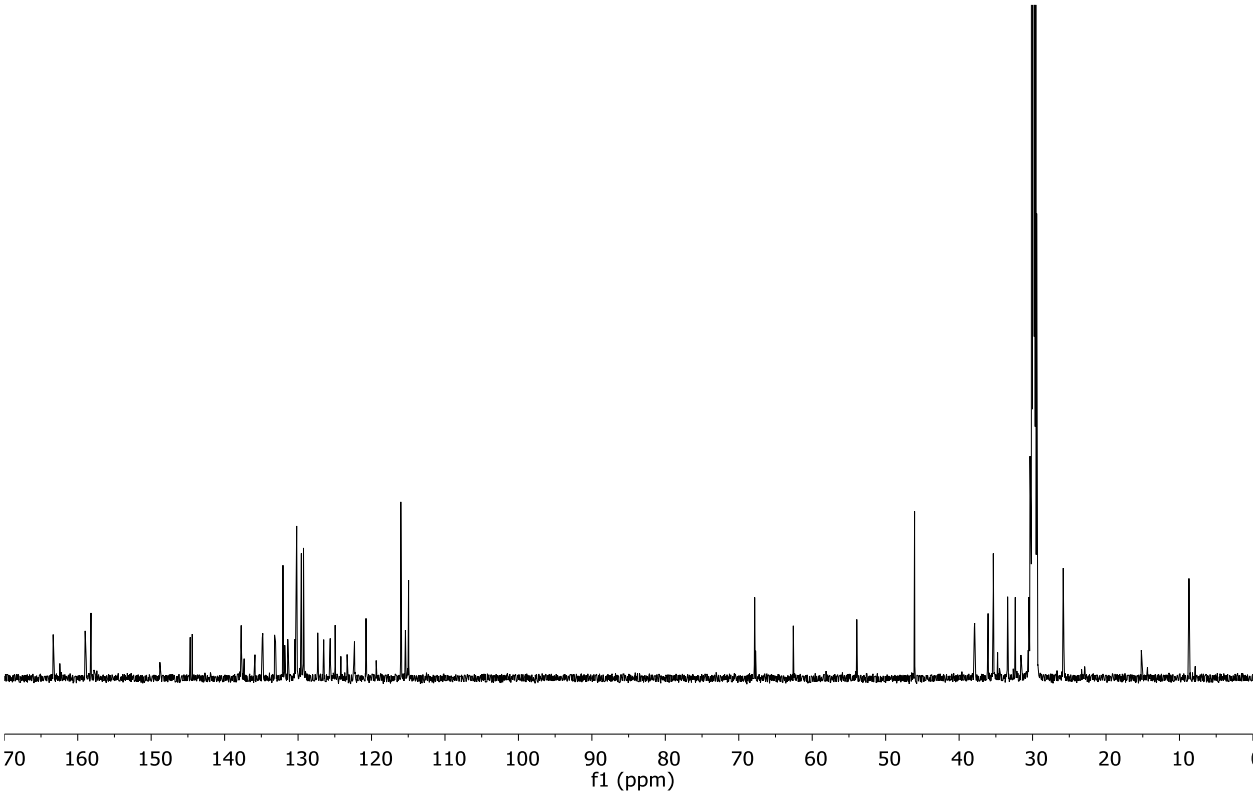

Figure 145: ^{13}C-NMR spectrum of PA-[3]catenane (*S*)-**17-HNEt$_3$** ([D$_2$]-dichloromethane, 101 MHz, 298 K).

8.2 Chiral HPLC chromatograms

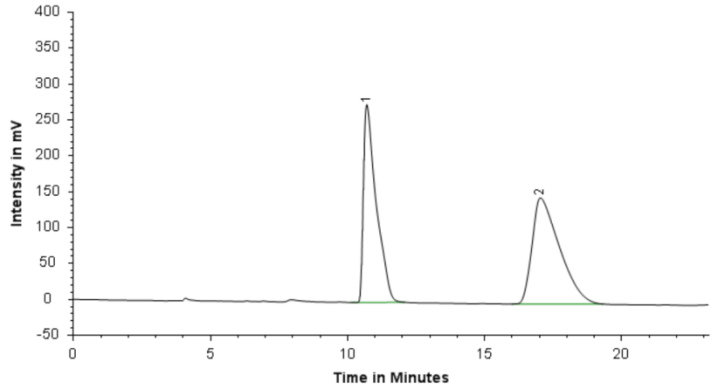

No.	Ret. Time	Height	Area	Percent
1	10.7	275.5193	8962023	46.58001
2	17.03333	147.7024	1.027804E+07	53.41999

Figure 146: HPLC chromatogram of **105** (Table 21 Entry 1).

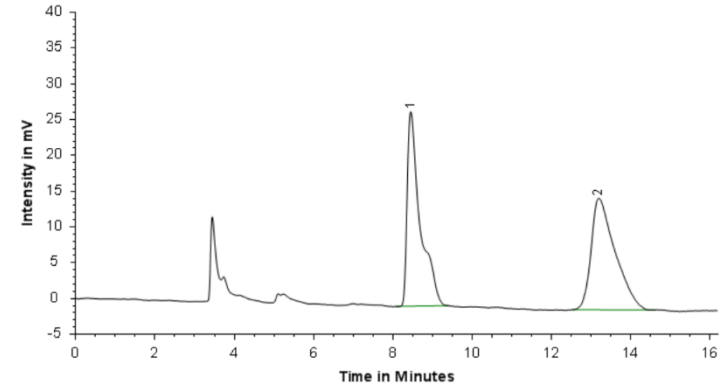

No.	Ret. Time	Height	Area	Percent
1	8.458333	27.1101	617472.4	48.57661
2	13.19167	15.57781	653658.8	51.42339

Figure 147: HPLC chromatogram of **105** (Table 21 Entry 3).

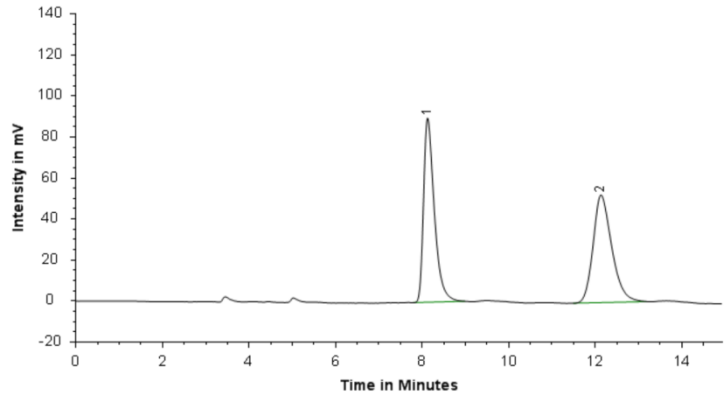

No.	Ret. Time	Height	Area	Percent
1	8.133333	89.53386	1548505	49.71648
2	12.14167	52.3949	1566167	50.28352

Figure 148: HPLC chromatogram of **105** (Table 21 Entry 5).

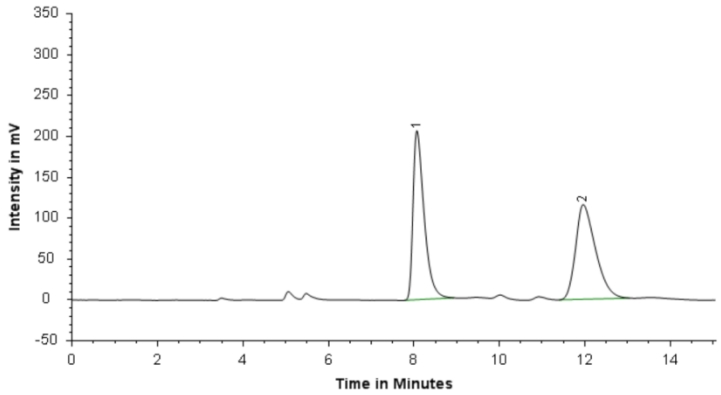

No.	Ret. Time	Height	Area	Percent
1	8.075	206.4806	3720942	49.81484
2	11.95833	115.6589	3748603	50.18516

Figure 149*:* HPLC chromatogram of **105** (Table 21 Entry 6).

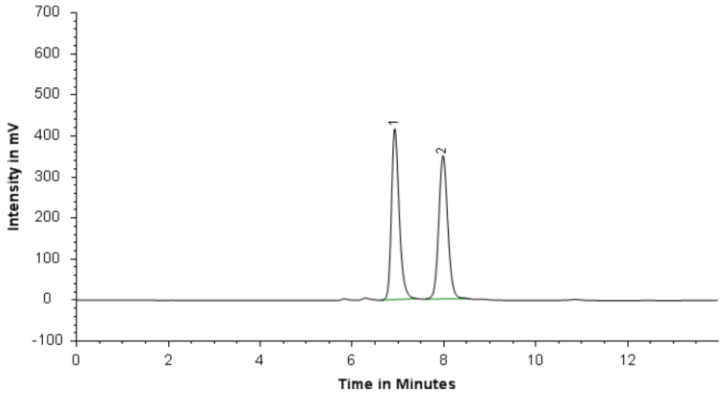

No.	Ret. Time	Height	Area	Percent
1	6.925	415.1252	4866968	50.54369
2	7.975	348.5536	4762262	49.45631

Figure 150: HPLC chromatogram of **108** (**Table 22** Entry 3).

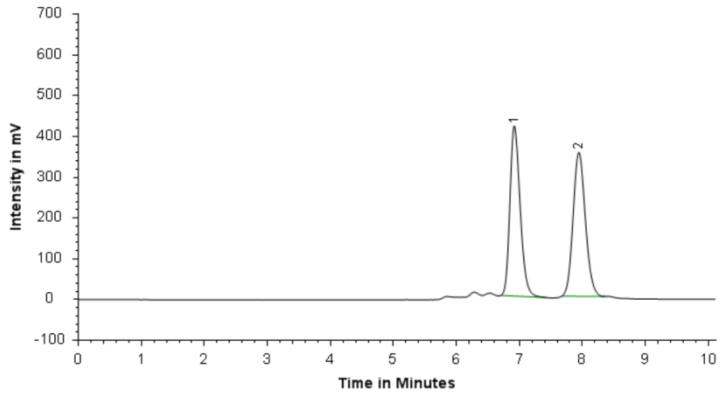

No.	Ret. Time	Height	Area	Percent
1	6.925	416.0429	4700179	49.57781
2	7.95	352.2271	4780229	50.42219

Figure 151: HPLC chromatogram of **108** (**Table 22** Entry 4).

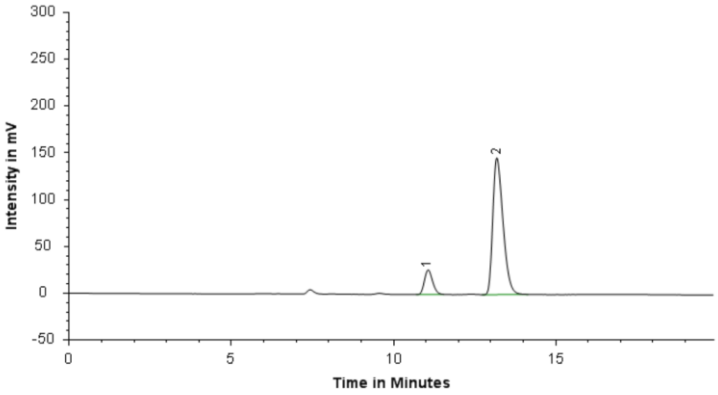

No.	Ret. Time	Height	Area	Percent
1	11.05833	26.13401	460352.3	12.58696
2	13.19167	145.9351	3197023	87.41304

Figure 152: HPLC chromatogram of **4e** (**Table 23** Entry 5).

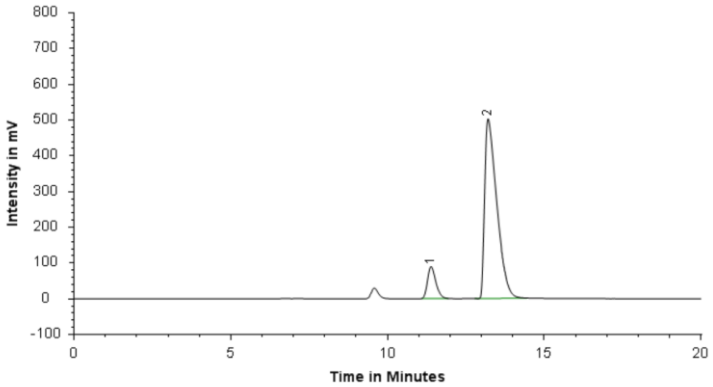

No.	Ret. Time	Height	Area	Percent
1	11.38333	89.01082	1635521	10.80663
2	13.21667	502.3834	1.349889E+07	89.19337

Figure 153: HPLC chromatogram of **4e** (**Table 23** Entry 6).

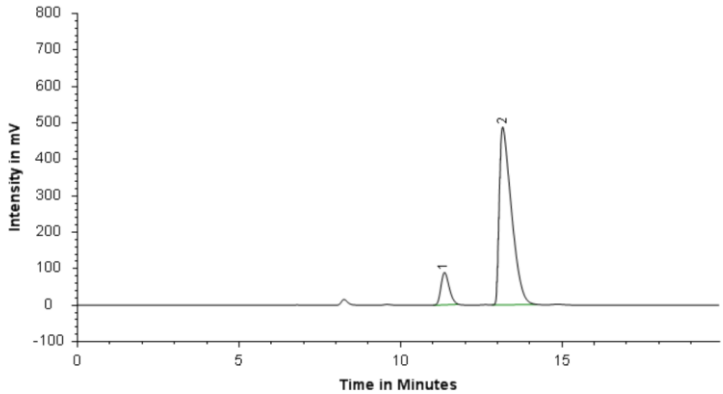

No.	Ret. Time	Height	Area	Percent
1	11.35833	88.84408	1575004	10.97917
2	13.175	486.9286	1.277038E+07	89.02083

Figure 154: HPLC chromatogram of **4e** (**Table 23** Entry 7).

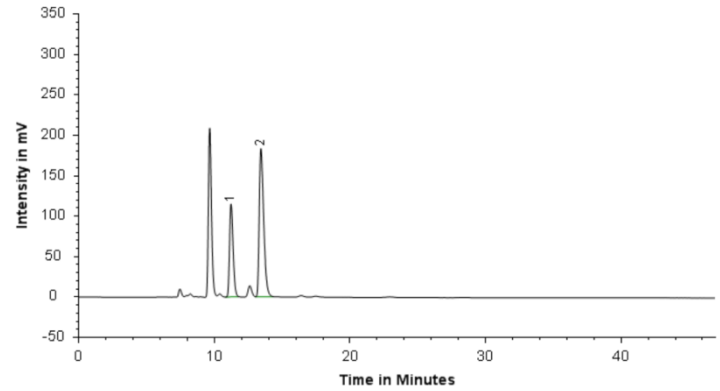

No.	Ret. Time	Height	Area	Percent
1	11.225	114.7718	2095348	33.39141
2	13.41667	183.0712	4179762	66.60858

Figure 155: HPLC chromatogram of **4e** (**Table 23** Entry 8).

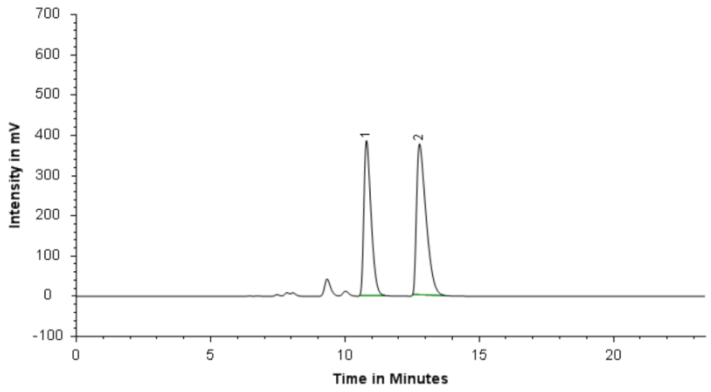

No.	Ret. Time	Height	Area	Percent
1	10.80833	384.4335	126018.5	33.85982
2	12.78333	374.3549	246158.7	66.14018

Figure 156: HPLC chromatogram of **4e** (**Table 23** Entry 9).

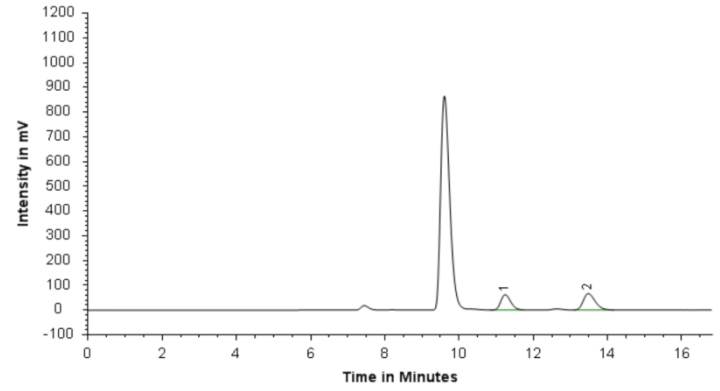

No.	Ret. Time	Height	Area	Percent
1	11.25	61.53311	1136900	43.6574
2	13.49167	66.10756	1467241	56.3426

Figure 157: HPLC chromatogram of **4e** (**Table 23** Entry 10).

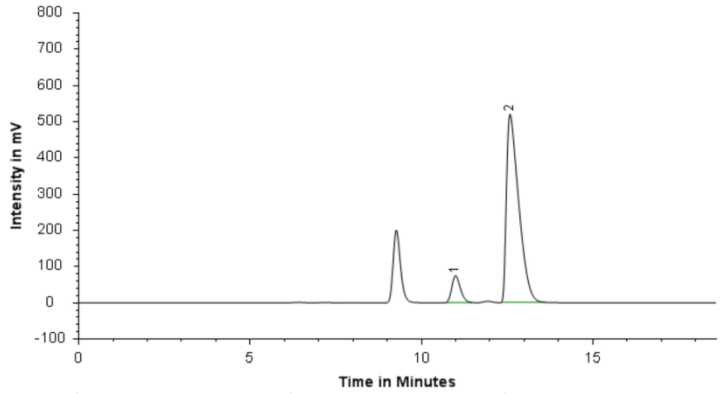

No.	Ret. Time	Height	Area	Percent
1	11	73.98067	1277319	9.032276
2	12.59167	518.3555	1.286439E+07	90.96773

Figure 158: HPLC chromatogram of **4e** (**Table 23** Entry 11).

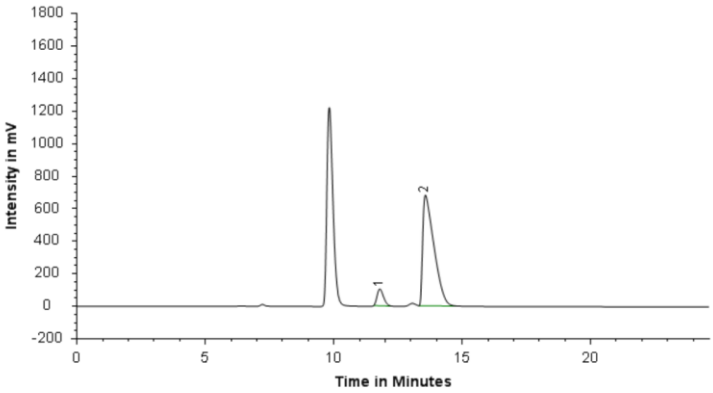

No.	Ret. Time	Height	Area	Percent
1	11.78333	103.1024	1801791	7.984514
2	13.55833	679.8533	2.076427E+07	92.01549

Figure 159: HPLC chromatogram of **4e** (**Table 23** Entry 12).

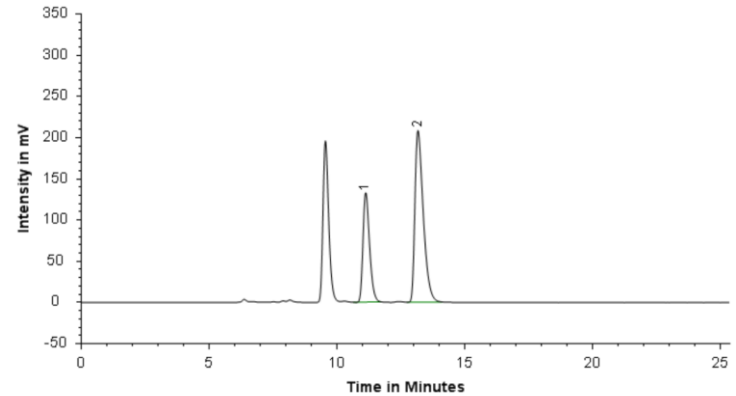

No.	Ret. Time	Height	Area	Percent
1	11.10833	132.4242	2367856	33.30271
2	13.16667	208.0618	4742243	66.69729

Figure 160: HPLC chromatogram of **4e** (**Table 23** Entry 13).

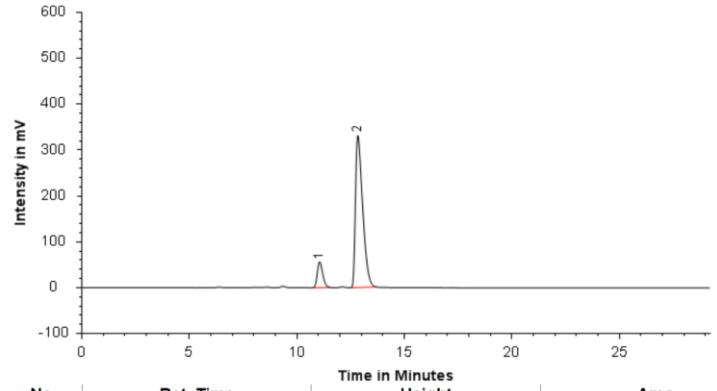

No.	Ret. Time	Height	Area	Percent
1	11.05833	56.28186	984748.2	11.31604
2	12.84167	331.245	7717486	88.68396

Figure 161: HPLC chromatogram of **4e** (**Table 23** Entry 14).

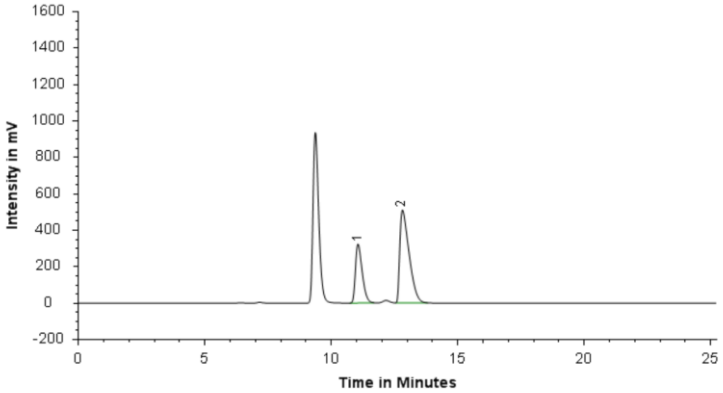

No.	Ret. Time	Height	Area	Percent
1	11.05833	323.006	5995573	31.59949
2	12.80833	509.2811	1.297806E+07	68.40051

Figure 162: HPLC chromatogram of **4e** (**Table 23** Entry 15).

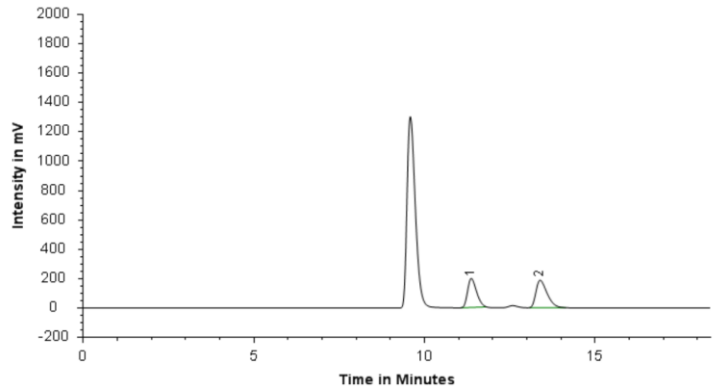

No.	Ret. Time	Height	Area	Percent
1	11.375	197.7838	3594853	45.94231
2	13.38333	187.1645	4229859	54.05769

Figure 163: HPLC chromatogram of **4e** (**Table 23** Entry 16).

8.3 Acknowledgements

Zuallererst bedanke ich mich bei Prof. Dr. Jochen Niemeyer für das spannende Thema und die Möglichkeit meine Promotion unter seiner Leitung anfertigen zu können, sowie für die zahlreichen Tipps und die durchgehende Unterstützung. Ich habe in meiner Zeit in der Arbeitsgruppe extrem viel gelernt und bin extrem dankbar dafür.

In summer 2019 I was able to spend three months in Southampton in the group of Prof. Stephen Goldup. I want to express my gratitude for the very kind hospitality as well as for the great support. I am also sincerely thankful to him for agreeing on being the second reviewer of my PhD work.

Ich danke meinen aktuellen und ehemaligen Kollegen des AK Niemeyers für die schöne Zeit in und außerhalb der Uni. Besonders danke ich Frescilia Octa-Smolin für das herzliche willkommen heißen in der Gruppe, der vielen Unterstützung vor allem zu Beginn meiner Zeit und die coolen Aktivitäten abseits der Arbeit. Additionally, I want to separately thank Noel Pairault for the great support in the lab and the nice time outside.

I also want to thank the members of the Goldup group for the great time in the lab and the nice evenings in the pubs. I thank Florian Modicom also for advising me in the lab.

Ebenfalls danke ich den Vosgieniehäuser- und Schmuck-Kollegen für die angenehme Zeit und die unterhaltsamen Momente. Speziell möchte ich hier Florian Malotke hervorheben, dessen Freundschaft die Zeit auf und neben der Arbeit deutlich unterhaltsamer gemacht hat.

Teile meiner Arbeit wären in dieser Form nicht ohne die Hilfe einiger Personen möglich gewesen. Deshalb möchte ich meinen Kooperationspartnern Johannes Gramüller, Prof. Ruth M. Gschwind, Dr. Hui Zhu und Prof. Stefan Grimme danken. Im gleichen Atemzug möchte ich Dr. Torsten Schaller und Dr. Felix Niemeyer nicht nur für ihren Beitrag, sondern auch für die zahlreichen Hilfen bei spektroskopischen Fragestellungen danken. Außerdem danke ich Gudrun Heinrich und Werner Karow für die massenspektroskopischen Analysen.

Dr. Fabian Lutz, Jan Riebe, Dana Kauerhof und Maike Thiele danke ich für das Korrekturlesen meiner Arbeit.

Außerdem möchte ich mich hier bei meinen Freunden und meiner Familie für die Unterstützung bedanken

Zuletzt danke ich Alana Kenda, die mich in allen Lebenslagen unterstützt hat. Mit deiner Hilfe konnte ich jede noch so schwierige und stressige Phase überwinden.

8.4 Curriculum Vitae

The CV is not included in this online version for reasons of data protection.